

UNIVERSITAT POLITÈCNICA DE VALÈNCIA
DEPARTAMENTO DE MÁQUINAS Y MOTORES TÉRMICOS



UNIVERSITAT
POLITÈCNICA
DE VALÈNCIA

IN-CYLINDER PRESSURE RESONANCE ANALYSIS
FOR TRAPPED MASS ESTIMATION IN
AUTOMOTIVE ENGINES

PHD DISSERTATION
Presented by
Pau Bares
Advised by
Dr. Carlos Guardiola

Valencia, June 2017

Resumen. Esta tesis presenta una nueva aplicación para los sensores de presión en cámara. El nuevo método utiliza el contenido de alta frecuencia de la señal de presión en cámara para estimar la evolución de la velocidad del sonido durante la expansión de los gases de escape y combina esta estimación con el contenido de baja frecuencia de la presión en cámara y el volumen instantáneo de la cámara para obtener una medida de la masa atrapada.

El nuevo método está basado en los estudios de la resonancia en cámaras de combustión cilíndricas y propone tres procedimientos de calibración para estimar la evolución de la frecuencia de resonancia en cámaras de combustión con bowl. La transformada de Fourier ha sido modificada para considerar armónicos con frecuencias que varían en el tiempo, lo que permite una rápida identificación de los modos de resonancia sin necesidad de utilizar un análisis en tiempo frecuencia, como por ejemplo STFT o WD.

La principal limitación del método es la necesidad de excitación suficiente de la resonancia, que puede impedir su uso en condiciones de baja carga como el ralentí. Para solventar este problema se ha diseñado un observador. El observador incluye las dinámicas de los sensores, las dinámicas del colector de admisión, y combina los sensores actuales de flujo con medidas intermitentes (como la medida ofrecida por el nuevo método de la resonancia) para obtener medidas de la masa atrapada, del EGR y de la composición en el escape precisas y robustas.

La medida de la masa atrapada obtenida por el método de la resonancia ha sido comparado con métodos auxiliares en diferentes instalaciones experimentales: en un motor SI, sin EGR, las diferencias con los sensores eran menores del 1 %, en un motor convencional CI la media de las diferencias sobre 808 puntos de operación distintos ha sido de 2.64 %, en un motor de investigación con EGR, con inyección gasolina en el colector y inyección directa de diesel, las diferencias fueron de 2.17 %, y en un motor de investigación de dos tiempos, donde existían grandes cantidades de corto-circuito y gases residuales, las diferencias fueron de 4.36 %. En todos los casos estudiados las diferencias encontradas pueden ser atribuidas a los errores que caracterizan los métodos auxiliares utilizados para obtener la medida de referencia.

Finalmente, para demostrar el potencial del método se han desarrollado cuatro aplicaciones para control y diagnóstico de motores de combustión interna alternativos: la estimación de gases residuales en motores con NVO, la predicción de knock en motores SI, la estimación de la temperatura de los gases de escape, y un modelo de NO_x para motores CI. En las cuatro aplicaciones el método ha sido comparado con los sistemas de medidas actuales y con sensores adicionales, demostrando mejoras importantes en la precisión de la medida y una resolución de un solo ciclo.

Resum. Aquesta tesi presenta una nova aplicació per als sensors de pressió en cambra. El nou mètode utilitza el contingut d'alta freqüència del senyal de pressió en cambra per estimar l'evolució de la velocitat del so durant l'expansió dels gasos d'eixida i combina aquesta estimació amb el contingut de baixa freqüència de la pressió en cambra i el volum instantani de la cambra per obtenir una mesura de la massa atrapada.

El nou mètode està desenvolupat dels estudis de la ressonància en cambres de combustió cilíndriques i proposa tres procediments de calibratge per estimar l'evolució de la freqüència de ressonància en cambres de combustió amb bowl. La transformada de Fourier ha sigut modificada per considerar harmònics amb freqüències que varien en el temps, el que permet una ràpida identificació dels modes de ressonància sense necessitat d'utilitzar una anàlisi en temps-freqüència, com per exemple la STFT o la WD.

La principal limitació del mètode és la necessitat d'excitació suficient de la ressonància, que pot impedir el seu ús en condicions de baixa càrrega, com al ralenti. Per solucionar aquest problema s'ha desenvolupat un observador. L'observador inclou les dinàmiques dels sensors, les dinàmiques del col·lector d'admissió, i combina els sensors actuals de flux amb mesures intermitents (com l'obtinguda pel nou mètode de la ressonància) per obtenir mesures de la massa atrapada, del EGR i de la composició d'eixida precises i robustes.

La mesura de la massa atrapada obtinguda pel mètode de la ressonància ha sigut comparada en mètodes auxiliars en diferents instal·lacions experimentals: a un motor SI, sense EGR, les diferències amb els sensors estaven per davall de l'1 %, a un motor convencional CI la mitja de les diferències sobre 808 punts d'operació diferents ha sigut de 2.64 %, a un motor d'investigació, en EGR, en injecció gasolina en el col·lector i injecció directa de dièsel, les diferències van ser de 2.17 %, i a un motor d'investigació de dos temps, on existien grans quantitats de curtcircuit i residuals, les diferències foren de 4.36 %. En tots els casos estudiats les diferències trobades poden ser atribuïdes als errors que caracteritzen els mètodes auxiliars utilitzats per obtenir la mesura de referència.

Finalment, per demostrar el potencial del mètode s'han desenvolupat quatre aplicacions per al control i diagnòstic de motors de combustió interna alternatius: l'estimació de gasos residuals en motors amb NVO, la predicció de knock en motors SI, l'estimació de la temperatura dels gasos d'eixida, i un model de NO_x per a motors CI. En les quatre aplicacions el mètode ha sigut comparat amb els sistemes de mesures actuals i amb sensors addicionals, demostrant millores importants en la precisió de la mesura i una resolució de solament un cicle.

Abstract. This thesis presents a new application for in-cylinder pressure sensors in internal combustion engines. The new method takes profit of the high-frequency content of the in-cylinder pressure signal to determine the speed of sound evolution during the expansion stroke and combines this estimation with the low-frequency content of the pressure signal and a volume estimation to obtain a measurement of the trapped mass.

The new method is based on the studies of the resonance phenomenon in pent-roof combustion chambers and proposes three calibration procedures to determine the resonant frequency evolution when bowl-in-piston geometries are considered. The Fourier transform has been modified in order to include harmonics with frequency variations, which allows a rapid identification of the resonant modes with no need of time-frequency analysis, e.g. STFT or WD.

The main limitation of the method resides in the resonance excitation, which may be insufficient in low-load conditions, such as idle. An observer is presented to overcome that problem. The observer takes into account the dynamics of the sensors, the dynamics at the intake manifold, and combines current flow sensors with intermittent measurements, such as the trapped mass obtained by the resonance method, to provide the system with accurate and robust measurements of the trapped mass, the EGR, and the composition at the exhaust.

The trapped mass obtained by the resonance method has been compared with auxiliary methods in various experimental facilities: in a SI engine, where no EGR exist, the differences founded were below 1%, in a conventional CI light-duty engine the average of the differences over 808 operating conditions accounted for a 2.64 %, in a research heavy-duty RCCI engine, with EGR, port fuel gasoline, and direct diesel injections, the average difference was 2.17 %, and in a research two-strokes single cylinder engine, where significant short-circuit and residual gases exist, the differences founded were 4.36 %. In all the studied cases the differences founded with the reference estimation can be attributed to the auxiliary method employed and its expected error.

In order to demonstrate the potential of the resonance method four applications for control and diagnosis of internal combustion engines have been proposed: the estimation of residuals in engines with NVO, the prediction of knock in SI engines, the estimation of the exhaust gases temperature, and a NOx model for CI engines. In the four applications the method was compared with current methodologies and with additional sensors, demonstrating the improvement in accuracy and a cycle-to-cycle resolution.

Agradecimientos

Cuando te planteas empezar una tesis doctoral, el primer paso es tener una conversación con los posibles directores de tesis. Recuerdo perfectamente la primera reunión con Carlos Guardiola: despeinado, con un lenguaje informal y directo al grano, sin formalismos, sin protocolos imprecisos que nublan el mensaje. Ese mismo Carlos es el que me ha acompañado durante estos cinco años, quien me ha enseñado a identificar la parte importante y acotar el ruido, a simplificar los modelos y, en definitiva, me ha ensañado cómo resolver cualquier problema, tanto en la ingeniería como en la vida diaria. Carlos es posiblemente la persona más brillante que he conocido y también una de las más modestas y sinceras. A él, sin duda alguna, he de agradecer los resultados de esta tesis.

Querría hacer una mención especial a Alberto Reig por todos sus consejos, por tratar siempre de ayudar, y por hacer más amenos los días en el despacho, a Benjamin Pla, por estar siempre dispuesto a echar una mano, a Javi Mora y Alvin Barbier por todas las bromas y sonrisas de los últimos años, y en definitiva a todos los compañeros de despacho que han compartido conmigo esta etapa de mi vida y de los que siempre guardaré un gran recuerdo: Varun, Marcelo, Vero, Nando, Josep, Pedro, David, Vicent...

Esta tesis no hubiera sido posible sin el apoyo recibido por parte de todas las personas que componen el departamento de Máquinas y Motores Térmicos: A la dirección por confiar en el proyecto, a las personas de secretaria que siempre están atentas a todos los trámites, a los técnicos quienes dedican más horas de las exigibles para que todo funcione, y a todos los profesores e investigadores que me han ayudado con sus consejos y discusiones. Ha sido todo un honor poder formar parte de este equipo de investigación.

Además del departamento de Máquinas y Motores Térmicos me gustaría agradecer la colaboración de Paco Denia quien ha trabajado duramente para poder satisfacer nuestras exigencias de simulaciones de elementos finitos y a todo el equipo de control automático en la ETH de Zurich (C. Onder, Severin, Rafi, Donald, Mauro...) por hacer que fuera tan sencillo y provechoso trabajar con ellos.

Finalmente me gustaría dedicar esta tesis a mi familia y a mis amigos. Sin su apoyo no habría encontrado las fuerzas ni la motivación suficiente para poder realizar esta tesis.

Valencia, a 5 de junio de 2017

Agradecimientos institucionales

El trabajo desarrollado en esta tesis ha sido posible gracias a la financiación del programa de ayudas de investigación y desarrollo (PAID) de la Universitat politècnica de València (FPI-subprograma 1, 2014-2017)

Contents

| | | |
|----------|--|-----------|
| 1 | Introduction | 1 |
| 1.1 | Background | 1 |
| 1.2 | The future of IC engines technology | 8 |
| 1.3 | Scope of the work | 14 |
| 1.4 | Objectives | 15 |
| 1.4.1 | Methodology | 15 |
| 1.A | Publications | 17 |
| | References | 18 |
| 2 | In-cylinder pressure signal: characteristics and applications | 27 |
| 2.1 | Introduction | 27 |
| 2.2 | Applications based on a polytropic evolution | 28 |
| 2.3 | Combustion modelling and control | 31 |
| 2.3.1 | Combustion noise assessment | 32 |
| 2.3.2 | Autoignition prediction | 33 |
| 2.3.3 | Emission models | 35 |
| 2.3.3.1 | Diffusive flame NO_x emissions | 35 |
| 2.4 | Resonance analysis | 37 |
| 2.4.1 | Knock detection and control | 40 |
| 2.5 | Conclusions | 42 |
| 2.A | Instantaneous crankshaft speed models | 43 |
| | References | 43 |

| | | |
|----------|--|-----------|
| 3 | Charge and composition estimation in IC engines | 57 |
| 3.1 | Introduction | 58 |
| 3.2 | Flow and composition sensors | 58 |
| 3.2.1 | Air mass flow sensor | 59 |
| 3.2.2 | Exhaust gas recirculation measurement | 59 |
| 3.2.3 | Oxygen concentration sensors | 61 |
| 3.3 | Models and virtual sensors | 63 |
| 3.3.1 | Speed density method | 63 |
| 3.3.2 | The orifice principle | 64 |
| 3.3.3 | Δp method | 65 |
| 3.3.4 | Residual gas fraction determination | 65 |
| 3.3.5 | Injected fuel mass | 67 |
| 3.4 | Data fusion techniques | 67 |
| 3.4.1 | Sensor dynamics | 68 |
| 3.4.2 | Intake manifold dynamics | 68 |
| 3.4.3 | Observers | 70 |
| 3.4.3.1 | Closed-loop observers | 71 |
| 3.4.3.2 | Unknown input observers | 73 |
| 3.5 | Conclusions | 73 |
| | References | 74 |
| 4 | System setup and in-cylinder pressure acquisition | 85 |
| 4.1 | Introduction | 85 |
| 4.2 | Experimental set-up | 86 |
| 4.2.1 | Acquisition and control system layout | 86 |
| 4.2.2 | In-cylinder pressure acquisition | 88 |
| 4.2.3 | Engines | 90 |
| 4.3 | Engine tests | 94 |
| 4.3.1 | Steady-state tests | 95 |
| 4.3.2 | Transient tests | 101 |

| | | |
|----------|---|------------|
| 4.3.2.1 | Closed-loop knock control | 101 |
| 4.3.2.2 | Steps | 102 |
| 4.3.2.3 | Cycles | 104 |
| 4.4 | Conclusions | 106 |
| 4.A | Time-frequency analysis | 107 |
| | References | 110 |
| 5 | In-cylinder pressure resonance characterisation | 113 |
| 5.1 | Introduction | 113 |
| 5.2 | Resonance theory: the cylindrical assumption | 114 |
| 5.3 | Exceptions to the cylindrical theory | 118 |
| 5.3.1 | Effect of bowl-in-piston geometries | 121 |
| 5.3.2 | Effect of in-cylinder inhomogeneities | 124 |
| 5.4 | Resonance excitation | 127 |
| 5.4.1 | Knock event definition in SI engines | 131 |
| 5.5 | Conclusions | 135 |
| | References | 136 |
| 6 | Trapped mass estimation by using the resonance | 137 |
| 6.1 | Introduction | 137 |
| 6.2 | A trapped mass estimation from resonance | 138 |
| 6.3 | A resonance oriented transform | 142 |
| 6.4 | Analysis of the accuracy | 146 |
| 6.4.1 | Method simplifications | 148 |
| 6.4.2 | Quantification in a real operation | 154 |
| 6.5 | Validation in steady-state conditions | 155 |
| 6.5.1 | SI combustion (Engine A) | 157 |
| 6.5.2 | CI combustion (Engine C) | 157 |
| 6.5.3 | Heavy-duty engine with RCCI combustion (Engine D) | 159 |
| 6.5.4 | Two strokes engine with CAI combustion (Engine F) | 160 |
| 6.5.5 | Summary of results | 162 |

| | | |
|----------|---|------------|
| 6.6 | Conclusions | 163 |
| | References | 164 |
| 7 | Sensor data fusion | 167 |
| 7.1 | Introduction | 167 |
| 7.2 | Model description | 168 |
| | 7.2.1 Sensor and model dynamics | 172 |
| 7.3 | Observer design | 175 |
| | 7.3.1 Identification of outliers | 179 |
| 7.4 | Results | 181 |
| | 7.4.1 Dynamic measurement of trapped mass | 181 |
| | 7.4.2 Suppression of sensors | 182 |
| 7.5 | Conclusions | 184 |
| 7.A | Parameters of the EKF | 184 |
| | References | 186 |
| 8 | Applications of the resonance method | 191 |
| 8.1 | Introduction | 192 |
| 8.2 | Residual gases estimation with NVO strategies | 192 |
| | 8.2.1 Model description | 193 |
| | 8.2.2 Results and discussion | 193 |
| 8.3 | Knock model for SI engines | 197 |
| | 8.3.1 Model description | 199 |
| | 8.3.2 Results and discussion | 203 |
| 8.4 | Exhaust temperature estimation | 205 |
| | 8.4.1 Model description | 206 |
| | 8.4.2 Results and discussion | 210 |
| 8.5 | NO _x model for CI engines | 216 |
| | 8.5.1 Model description | 217 |
| | 8.5.2 Results and discussion | 220 |
| 8.6 | Conclusions | 225 |
| | References | 227 |

| | | |
|----------|--|------------|
| 9 | Conclusions and future work | 229 |
| 9.1 | Main contributions and conclusions | 229 |
| 9.1.1 | Resonance characterization | 230 |
| 9.1.2 | Trapped mass estimation | 232 |
| 9.1.3 | Sensor data fusion | 234 |
| 9.1.4 | Applications for control and diagnosis | 235 |
| 9.2 | Future work | 237 |
| | References | 241 |

Nomenclature

Acronyms

| | |
|-----------------|---|
| ACEA | European automotive manufacturers association |
| ATDC | After top dead center |
| BTDC | Before top dead center |
| CAD | Crank angle degrees |
| CAI | Controlled auto-ignition |
| CFD | Computational fluid dynamics |
| CI | Compression ignition |
| CL | Closed loop |
| CO | Carbon monoxide |
| CO ₂ | Carbon dioxide |
| COPD | Chronic obstructive pulmonary disease |
| DoF | Degree of freedom |
| DOHC | Double overhead camshaft |
| ECU | Electronic control unit |
| EGR | Exhaust gases recirculation |
| EU | European union |
| EV | Electric vehicles |
| EVC | Exhaust valve closing |
| EVO | Exhaust valve opening |
| FFT | Fast fourier transform |
| GHG | Green house gases |
| HCCI | Homogeneous charge compression ignition |
| HEV | Hybrid electric vehicles |
| HRL | Heat release law |
| HRR | Heat release rate |
| ICCT | International council on clean transportation |
| IGR | Internal gas recirculation |
| IVC | Intake valve closing |
| IVO | Intake valve opening |
| KF | Kalman filter |
| KO | Knock onset |

| | |
|-----------------|---|
| LNT | Lean NOx trap |
| LSM | Least square method |
| LTC | Low temperature combustion |
| MAPO | Maximum amplitude pressure oscillation |
| MFB | Mass fraction burnt |
| NA | Naturally aspirated |
| NEDC | New european driving cycle |
| NO | Nitric oxide |
| NO ₂ | Nitric dioxide |
| NOx | Oxides of nitrogen |
| NVO | Negative valve overlap |
| OECD | Organization for economic cooperation and development |
| OL | Open loop |
| OPEC | Organization of the petroleum exporting countries |
| PEMS | Portable emission measurement system |
| PM | Particulate matter |
| PPCI | Partially premixed compression ignited |
| RCCI | Reactivity controlled compression ignited |
| RDE | Real driving emissions |
| RGF | Residual gas fraction |
| SA | Spark advance |
| SACI | Spark assisted compression ignition |
| SCR | Selective catalyst reduction |
| SI | Spark ignition |
| STFT | Short time fourier transform |
| TDC | Top dead center |
| VGT | Variable geometry turbocharged |
| TWC | Three way catalyst |
| US | United states |
| VVT | Variable Valve Timing |
| WD | Wigner Distribution |
| WLTP | World harmonized light duty test procedure |

Variables

| | | |
|-----------|------------------------|--------|
| \dot{m} | Mass flows | kg/h |
| m | Mass per stroke | mg/str |
| p | Pressures | bar |
| T | Temperatures | °C |
| V | Volume | l |
| F | Oxygen concentration | % |
| n | Engine speed | rpm |
| N | Engine torque | Nm |
| R | Gas constant | J/kg/K |
| γ | Heat capacities ratio | - |
| V_m | Intake manifold volume | l |
| V_{dis} | Displaced Volume | l |
| m_{air} | Air mass | mg/str |

| | | |
|------------------|--|--------|
| m_f | Injected fuel mass | mg/str |
| m_{cyl} | Cylinder mass | mg/str |
| m_{int} | Intake mass | mg/str |
| m_{EGR} | EGR mass | mg/str |
| u_{EGR} | EGR control signal | % |
| p_{int} | Boost pressure | bar |
| p_{rail} | Rail pressure | bar |
| T_{air} | Air temperature | °C |
| T_{EGR} | EGR temperature | °C |
| T_{int} | Intake gases temperature | °C |
| F_{air} | Oxygen concentration at air (21%) | °C |
| F_{int} | Oxygen concentration at the intake | °C |
| F_{exh} | Oxygen concentration at the exhaust | °C |
| p_{cyl} | In-cylinder pressure | bar |
| I_q | Quality index of the resonance method | - |
| η_v | Volumetric efficiency | - |
| θ_f | Fuel bias | mg/str |
| θ_η | Volumetric efficiency bias | - |
| α | Crankshaft angle | ° |
| y | Sensor measurements | - |
| x | State-vector | - |
| u | Input | - |
| τ | Sensor delay | s |
| a_S | Discrete time response parameter for a first order filter | - |
| F_s | Sampling frequency | Hz |
| Δt_{cic} | Cycle duration | s |
| t | time | s |
| k | Discrete instant | - |
| s | s transform variable | - |

Chapter 1

Introduction

Contents

| | | |
|------------|--|-----------|
| 1.1 | Background | 1 |
| 1.2 | The future of IC engines technology | 8 |
| 1.3 | Scope of the work | 14 |
| 1.4 | Objectives | 15 |
| | 1.4.1 Methodology | 15 |
| 1.A | Publications | 17 |
| | References | 18 |

1.1 Background

Nowadays, internal combustion (IC) engines are part of our culture: the flexibility that IC engines offer have transformed our mobility, urban planning and our consumption habits [1,2]. In fact, they represented the 84.1% of passengers displacement in 2011 [3] and as shown in Figure 1.1, cars per person already exceed 0.5 units in developed countries: in 2014, in United States the motorization rate reached 808 cars per 1000 habitants and in the European Union 569 [4,5].

In parallel, the number of automotive vehicles in developing countries is rapidly increasing, due to their economic growth and the consequent access to cars [6]. In only 10 years, from 2005 to 2014, the number of cars in China augmented a 450.8%, from 31.6 M of cars in use in 2005 to 142.4 in 2014 [7].

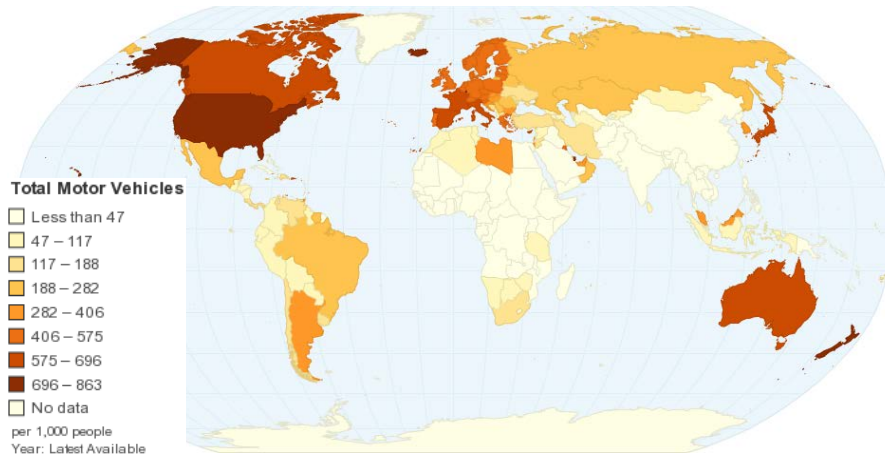


Figure 1.1. Cars per person distribution around the world, adapted from [4].

IC engines problematic. At the end of the last century one of the major concerns about IC engines was the oil depletion risk. However, during the last decades, since mid-1980s, proved oil reserves to production ratio has held relatively constant. New oil reserves, which have increased due to technology advances in oil discovery and recovery, have compensated the fuel demands growth. Although predictions are intrinsically dependent on the oil demands evolution, the probable reserves to production ratio is greater than 130 years [8].

Current studies on IC engines problematic are driven by the negative consequences of their emissions. Locally, because of the exhaust concentration of pollutants which threaten the animal, plant and human life, which are specially harmful in urban areas [9], and globally, because of the impact of anthropogenic CO₂ emissions on climate change [10], which is proportional to the fuel consumption.

Some of the pollutant emissions of IC engines are:

- Nitrogen Oxides (NO_x), namely NO and NO₂, are created at high temperatures and stoichiometric conditions. Although NO is predominant, between 70 and 90%, NO₂ can be significant due to the NO to NO₂ conversion at low temperature and high O₂ concentrations [11]. They are one of the main responsible of acid rain and a potential producer of *smog*; NO₂ can irritate the lung and reduce its resistance to infectious diseases if the level of NO₂ exceeds 600 mg/m³, while NO participates

on the ozone reduction at the stratosphere, reducing the ozone layer and allowing the ultraviolet radiation come inside the earth surface.

- Carbon monoxide (CO) is a sub-product of the combustion at stoichiometric or rich conditions. Although significant quantities can be locally created in compression ignited (CI) engines they oxydize with the excess of oxygen, thus they are more representative in spark ignited (SI) engines. It slowly oxidises at the atmosphere to create CO₂, but before that, it is a colorless, odourless, and tasteless gas, which combines with the blood haemoglobin and reduces its capacity for transporting oxygen. Consequently, it is highly dangerous for the human being and an exposition to 600 ppm during 3 hours can be lethal [12].
- Particulate Matter (PM) is defined as any component at the exhaust products in solid or liquid state. Soot, fine black particles composed of carbon, are one of the main components of PM. They are produced at locally rich conditions and bad fuel injection atomization. Epidemiological studies indicate that PM exposure is associated with risk of lung cancer and more recently has been associated with chronic obstructive pulmonary disease (COPD) mortality [13, 14].
- Hydrocarbons (HC) are a product of an incomplete combustion due to rich conditions and low temperatures. Combustion irregularities, e.g. misfires, wall impingement, or leakage, cause significant concentrations of HC at the exhaust. Prolonged exposure to HC contributes to asthma, liver disease, lung disease, and cancer [13, 14].

Transport accounted for the 28% of all energy-related CO₂ emissions in 2013 and it is the main responsible of the total energy consumption growth in the last decades. Its total consumption grew by more than 90% between 1971 and 2013 [15].

Climate change is causing a global warming on the earth surface, that accounted in 2015 for 0.87°C with respect to 1951-1980 period [16], but this variation would be higher if local surface temperature anomalies were considered, as shown in Figure 1.2. The evidences of climate change, such as the ice core thickness reduction, the sea level variation or the vegetation changes, are today more visible [17], and a major concern is shown by the states while policies are being set for keeping the global warming below 2°C [18]. Indeed, for 2050 a reduction objective of 50% of emissions from 1990 levels has been set for greenhouse gases (GHG), which corresponds to 80-95% reduction for

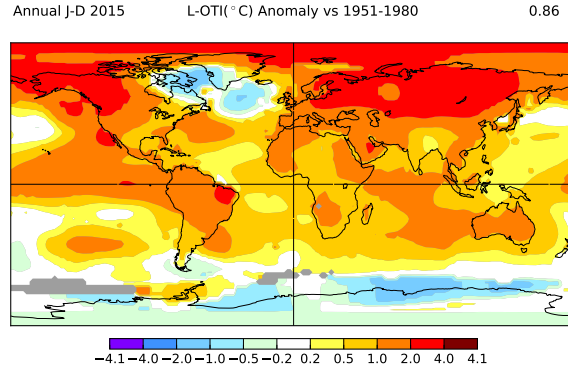


Figure 1.2. 2015 annual mean surface temperature anomaly with respect to 1951-1980 period. Source NASA Goddard Institute for Space studies [16].

many developed countries [19].

IC engines perspective. However, the number of vehicles are not expected to decrease, but on the contrary, growing trends of vehicles sales are predicted. Between 2014 and 2040, the total number of passenger cars will be increased by 125 million in the OECD countries, but in the developing countries (non-OECD) almost 1 billion vehicles are expected. Similarly, 47 and 229 millions of new commercial vehicles are expected in the OECD and in the developing countries, respectively. Future developments on the back of better efficiency will lower the oil use per vehicle in both regions, however, while in the OECD countries the oil demand in the road transportation sector will decrease in 6.7 million barrels of oil equivalent per day (mboe/d), the non-OECD countries will demand 12.6 mboe/d more, globally increasing the total oil demand. Actually, the road transportation sector accounts for one third of oil demand growth between 2014 and 2040 [20].

Media has paid a lot of attention to Electrical Vehicles (EV) as an alternative solution to the IC engine. However, when considering the total energy cycle, and not the direct tailpipe emissions, the benefits in CO₂ emissions of EV depends on the electricity production mix. Although renewables are the world's fastest-growing energy source, fossil fuels still account for 78% of energy use in 2040 and coal still represents an important source of energy [21]. Hence, EV are only a local solution for urban decarbonisation, but globally, they do not have a direct benefit on the CO₂ footprint and they can even in-

crease the particulate matter emissions depending on the national electricity production mix [22]. ACEA expects the new registrations related to electrically chargeable vehicles in the range of 2 to 8% for the next decade [23], while the OPEC considers that, by 2040, only a 6% of passenger cars and a 5.3% of commercial vehicles will be running on non-oil fuels, as shown in Figure 1.3.

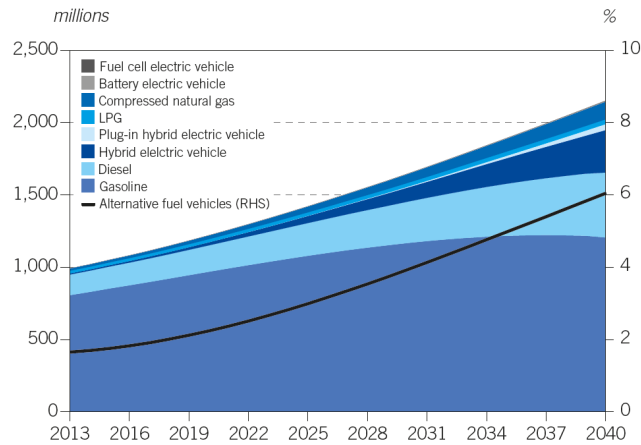


Figure 1.3. Passenger car fleet composition prediction by technology, extracted from [20].

Hybrid-electric vehicles (HEV) is a well-known technology, already in the market since the 90s, which allows decoupling the vehicle torque demand from the actual engine torque [24]. In this way HEV avoid transient efficiency penalties and they can perform a controlled regeneration of the after-treatment systems with no influence in torque [25]. Nevertheless, the market share highly depends on the considered country. In 2014, while in Japan HEV represented more than 20% of all new car sales, in the US and in the EU the share of hybrid-electric passenger cars was around 3% and 1.4%, respectively [26, 27].

Summarizing, even in the worst case scenario, IC engines will be the main technology used for passengers transportation for several decades. The 2020 target (average fleet CO₂ emission of 95 g/km) can be reached with IC engines by including the current technology on the market, and although going beyond 70-80 g/km could require the extension of hybrid electric technology, IC engines are constitutive parts of HEV [28].

The emissions regulation. In order to control transport emissions, the regulations have been tightening the pollutant limits in the last two decades.

Figure 1.4 shows the NO_x and PM emission limits for the consecutive versions of the European legislation standards for light-duty diesel engines [29]. It must be noticed that NO_x emission limits have been lowered from 1.13 g/km in 1992 to 0.08 g/km in 2014, a 93% reduction, while PM from 0.18 to 0.005 g/km in the same period, a 97% reduction.

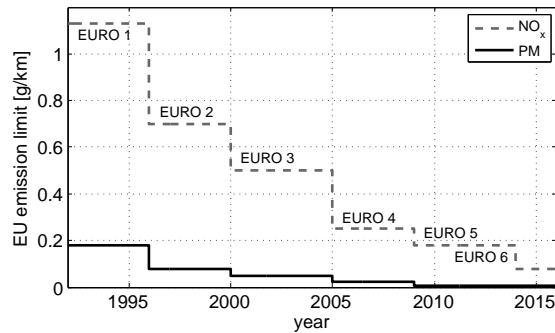


Figure 1.4. Evolution of the NO_x and PM emission limits for light duty diesel engines in Europe.

In addition, new regulations are being revised to be adapted to the new future challenges. On one hand, although CO_2 emission targets were actually being lowered to satisfy customers demand in terms of fuel efficiency, the future regulatory framework will also take into account CO_2 emissions in order to fulfil world Green House Gases (GHG) objectives [30]. Figure 1.5 shows the CO_2 historical records and the emission targets for cars in four countries (EU, US, Japan and China): as an example, EU has set the CO_2 emissions target at 95 g/km for 2020, which represents a 25% reduction.

And on the other hand, current homologation cycles are being discussed because they do not represent all the real-life engine operation [31,32]. Indeed, the International Council on Clean Transportation (ICCT) states that the differences found between the homologation cycle and the real-life consumption have increased from 8% in 2001 to 21% in 2012, with a particularly strong increase since 2007 [33].

Upcoming real-driving emission (RDE) regulation will address this problem by including real-world operation with portable emission measurement systems (PEMS) [34] or by implementing more realistic cycles, e.g. worldwide harmonized light vehicles test procedures (WLTP) [35]. Of interest, in [36] it was reported the average NO_x emissions for three configurations of a EURO

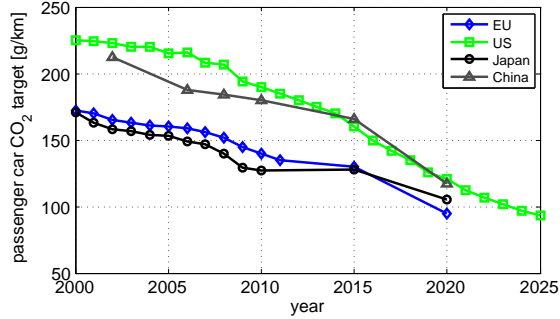


Figure 1.5. Comparison of CO₂ historical records and future emission targets for the NEDC cycle in various countries. Adapted from [30].

6 CI diesel engine: with only EGR, with lean NO_x trap (LNT), and with selective catalytic reduction (SCR) system. Figure 1.6 shows a summary of the final results: the emissions are dramatically higher over the WLTP cycle (EGR-only 0.17 g/km, LNT 0.21 g/km, and SCR 0.13 g/km), than those obtained for the NEDC cycle (EGR-only 0.07 g/km, LNT 0.04 g/km, and SCR 0.05 g/km), similar results were found for thirteen Euro 5 cars, six diesel and five gasoline, in [37].

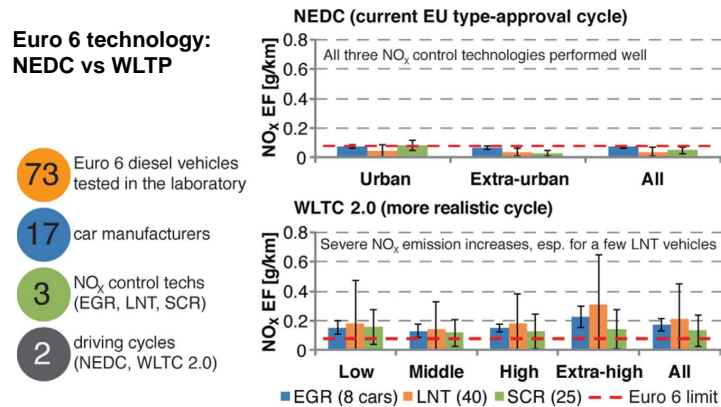


Figure 1.6. NO_x emissions of a Euro 6 diesel engine: NEDC vs WLTP, adapted from [36].

1.2 The future of IC engines technology

Vehicle performance benefits from several developments which are being introduced in parallel and can be applied to conventional IC engines. Between them, one can highlight: downsizing and downspeeding, lightweighting, and waste heat recovery. More detailed reviews can be found in [38,39].

Downsizing and downspeeding are common trends in current engines. In the first case, the size of the engine is minimized to reduce wall heat losses and improve overall engine efficiency, on the latter, friction is reduced by decreasing the engine speed [40]. Both trends, downsizing and downspeeding, require a higher boost pressure and improved injection systems. Although the boosting technology was widespread only in CI engines, it is progressively being included in SI engines, pushed by the need of lowering CO₂ emissions. Figure 1.7 shows the evolution of the boost pressure system in SI engines. Several authors aim to improve current turbocharger in terms of dynamic response, capacity, operation range and complexity, a good review can be found in [41]. Nevertheless, multi-mode system require a complex transition control to keep transitions smooth [42] and downsizing trend is pushing boosting technology to its limits because the high ratios demanded are causing thermal stresses at the intake system and at the turbocharger.

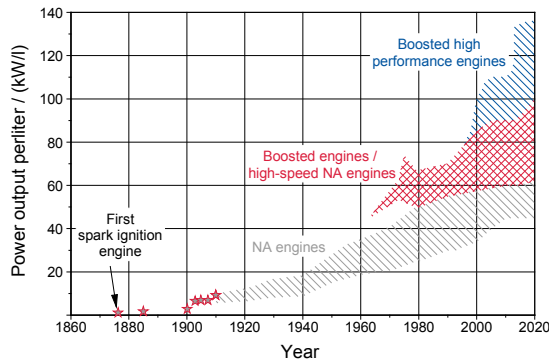


Figure 1.7. Power output per liter evolution in SI engines, extracted from [43].

Regarding the overall vehicle development, lightweighting, i.e. an adequate investment in materials and vehicle design for reducing the total mass, can implicate a sufficient fuel saving for compensating the increase in the vehicle cost [44,45].

Efficiency can be also improved by profiting part of the heat loss at the exhaust. This can be done with turbo-compounding, by using thermoelectric materials or by adding a Rankine cycle. Turbo-compounding needs an additional turbine to extract exhaust power and uses a mechanical gear train to move the crankshaft (mechanical turbo-compounding [46, 47]) or uses that energy for electricity generation (electrical turbo-compounding [48, 49]), thermoelectric materials are installed at the exhaust to provide energy to auxiliary systems [50, 51] and finally the Rankine cycle recovers part of the heat energy with the steam of an external fluid [52–56].

Until now, engine manufacturers have fulfilled emission restrictions by developing emission control strategies, e.g. delayed combustion phasing for controlling NO_x in CI engines. However, these strategies may have significant associated fuel penalties and because of the aforementioned change of paradigm for future emission legislations, car manufacturers are forced to update current technologies for lowering the fuel consumption while keeping the pollutant emissions under the limitations.

After-treatment devices. One of the expected solution for next generation CI engines are the after-treatment systems. These permit reducing the raw emissions of the engine at the expense of some negative effect on the fuel efficiency, mainly caused due to regeneration strategies and the pressure drop losses. Indeed, some authors consider after-treatment devices as the only solution for achieving new legislation emission limits [57].

New systems, such as Selective Catalytic Reduction (SCR) system or lean NO_x trap (LNT), are being implemented on commercial passenger cars to achieve euro 6 NO_x limitations. The first uses an ammonia source, normally urea, which must be precisely controlled to make an efficient NO_x conversion and avoid NH_3 slip [58, 59]. The latter, uses a filter where NO_x are adsorbed and reduced in combination of CO and HC. To create the required exhaust mixture and temperature, the engine must operate in rich conditions by penalising the fuel efficiency [60].

However, the performance of the after-treatment devices is intrinsically related with the exhaust conditions, namely temperature, composition, and emissions. SCR systems need constant information from exhaust NO_x [61], where models [62] and sensors [63, 64] present different capabilities in terms of dynamic response, accuracy and cost. Regeneration events, such as the

aforementioned LNT events or the ones produced in diesel or gasoline particulate filters (DPF or GPF), do also require a complex control of the air to fuel ratio (AFR) to perform the regeneration process [65, 66]. The light-off temperature can be achieved by controlling combustion with the associated fuel penalty, including an intermediate aftertreatment device, e.g. diesel oxidation catalyst (DOC) or SCR, to increase the temperature [67], or by using electric warmers [68].

Conventional SI engines take profit of the stoichiometric conditions at the exhaust by using a three way catalyst to mitigate NO_x , HC and CO at the same time. However, new lean-burn gasoline combustions or stratified gasoline combustions [69], which use a low fuel-to-air ratio would probably require similar after-treatment solutions as CI engines. A summary of the new challenges that after-treatment devices should overcome in order to effectively handle transient operation can be found in [43].

New combustion modes. One of the main handicaps when reaching new legislation limits is intrinsically related with the traditional combustion modes used, compression ignited (CI) and spark ignited (SI) concepts.

The former uses a direct injection of a high reactivity fuel, normally diesel, near the top dead center (TDC) in a previously compressed air charge. CI combustion concept relies in a non-homogeneous diffusive flame, using high intake pressures for achieving high fuel efficiency. However, if combustion is located near the TDC, the diffusive flame layer, with local stoichiometric conditions and high temperatures, propitiates the NO_x formation. But, if combustion is delayed for lowering the flame temperature, soot appears due to incomplete combustion [70].

The latter uses an electric spark to activate the combustion of a premixed charge mixture with stoichiometric conditions. The fuel, normally gasoline with low-reactivity characteristics, is injected far from the TDC; although traditionally gasoline has been port fuel injected, more recently direct injection is used to avoid port fuel delay dynamics [71]. A flame is propagated from the spark to the cylinder head in a controlled scheme. Although this avoids the soot- NO_x trade-off of the diffusive flame, intake pressure cannot be highly increased because of the knock phenomena. Knock occurs when the unburned gases temperature increase during the flame propagation and lead to an uncontrolled autoignition of the end-gas, which lowers the efficiency and

Table 1.1. Comparison of SI, CI and HCCI engines characteristics.

| | SI | CI | HCCI |
|---------------------|------------------------|--------------------------------|---|
| mixture type | Premixed | Non-premixed | Premixed |
| AFR ratio | Stoichiometric | Lean | Typically lean |
| Ignition | Spark ignited | Compression ignited | Compression ignited |
| Combustion | Flame propagation | Diffusive flame | Auto-ignition |
| Emissions | Higher CO ₂ | Soot-NO _x trade-off | Lower NO _x , soot PM, and CO ₂ |

can damage the engine [72].

The basic idea of new combustion modes relies in a homogeneous charge compression ignition (HCCI) combustion [73, 74]. In this way, HCCI engines avoid the soot-NO_x trade-off of the diffusive flame in CI combustion and the knock phenomena due to the flame propagation in SI combustion [75]. Experimental results of HCCI engines show equivalent or higher efficiencies than CI engines with low NO_x and soot emissions. A summary with the characteristics of the SI, CI and HCCI combustions is depicted in Table 1.1. However, HCCI combustion phasing control during transients and off-design conditions is today still challenging. In contrast to CI and SI combustion phasing, which are triggered by the injection and the spark, respectively, HCCI combustion lacks from a direct control and disturbances at the intake temperature or the mixture composition lead to bias and instabilities [76].

From the first HCCI results around 1980 [77, 78], several authors have proposed modifications to the HCCI combustion in order to control the combustion phasing. These are the following:

- Controlled auto-ignition (CAI) engines, developed from SI engines, use direct injection for a stratified charge and, in some cases, negative valve overlap (NVO) to control the internal residual gases for providing sufficient energy for autoignition [79, 80].
- Spark assisted compression ignited (SACI) engines take profit of the flame propagation to control the autoignition of the end-gas [81, 82].
- Premixed-charge compression ignited (PCCI) or partially premixed charge compression ignited (PPCI) engines inject part of the fuel far from the TDC to create a premixed charge and the rest is used for triggering the combustion near the TDC [83, 84].

- Reactivity controlled compression ignition (RCCI) engines modify the reactivity of the final mixture by combining fuels with different characteristics or by adding additives to a base fuel [85–88].

A significant characteristic of these combustion concepts is the possibility of shifting between modes for reaching all the operating range [89]. Some examples can be found in [90] for SI-SACI-HCCI modes, in [91] for CI-HCCI modes and in [92] for SI-HCCI-SI variations.

Air-path control. The air-path loop has been growing in complexity for performing a better and faster control of the charge composition and the intake pressure. A precise estimation of the trapped mass and its composition is crucial for a proper heat transfer analysis [93]. Current IC engines have more degrees of freedom than before: some turbocharger dispose of several modes with combined controls (e.g. VGT and waste-gate), low-pressure EGR loops are being included in conjunction with the traditional high-pressure EGR loops and VVT systems are being used to regulate the internal gas recirculation (IGR).

Low-pressure EGR systems are being introduced, substituting or together with the traditional high-pressure EGR loops [94, 95]. Although, they were not widespread till now due to compressor wheel damaging and acid corrosion problems in the intercooler [96], the implementation of after-treatment devices [97] and the development of more resistant intercoolers [98], has pushed to its use in commercial engines.

Furthermore, variable valve timing (VVT) technology has been adapted for nearly all light-duty and heavy-duty engines [27], and the implementation of new strategies with fully flexible VVT systems, e.g. NVO, are being used to regulate the internal EGR and the admitted air to perform new combustion concepts [99, 100].

Combustion control. In addition to after-treatment demands, such as regeneration events, and new combustion concepts requirements, lowering the GHG by using new biofuels, as some countries like Brasil are already promoting with national laws, would require new IC engines to tolerate fuels with different qualities [101, 102]. Indeed, new fuel composition sensors are being

developed for detecting the fuel properties [103, 104].

These challenges are pushing current combustion control strategies (based on OL look-up tables) to its limits. As a result, the next generation of IC engines will probably require some form of combustion feedback. Although other solutions exist [105], one of the most promising alternatives is the use of in-cylinder pressure sensor for closed-loop combustion control [106, 107]. Piezo-electric pressure sensors have been restricted to research benches, but the lowering cost of new piezo-resistive pressure sensors [108, 109], as well as the diverse applications of in-cylinder pressure signal for combustion feedback, modelling, and on-board diagnosis [110–112] are justifying its nearby implementation in commercial engines.

ECUs evolution. Finally, electronic control units (ECUs) evolution presents an opportunity for implementing new control strategies and models: upcoming multicore ECUs and the increase in computational power [113] promise enough capabilities for implementing more heavy codes, such as crank-angle solved (CAS) combustion models, while the replacement of low-level languages by high-level languages and automated code facilitate the inclusion of new control elements, such as new models and sensors [114].

In fact, models are being progressively included in ECUs [115] to provide sufficient information for an efficient operation, for implementing OBD strategies [116], and also for verification and validation of the final engine control [117]. New models and sensors can significantly alleviate calibration efforts of current ECUs, which have numerous 2D look-up table to calibrate the phenomena, and improve the robustness and off-design accuracy of the measurements.

The attention to the real-life performance of the engine aims to take profit from new sources of information to improve the fuel efficiency and the engine operation. Some examples can be found in [118–120] by profiting location information, in [121–123] by using information from the surroundings, in [124–126] by predicting the driver behaviour, or in [127] by using various calibration for a real emission accomplishment in urban areas.

1.3 Scope of the work

Future technologies in IC engines, focused on reducing harmful IC emissions, will require an accurate estimation of the intake mixture: either for achieving adequate exhaust conditions for after-treatment devices or for controlling the combustion phasing in new combustion concepts. In addition, the combustion feedback of in-cylinder pressure sensors seems mandatory for controlling new combustion concepts.

This dissertation presents a new methodology for in-cylinder trapped mass estimation. The new procedure uses the high-frequency content of the in-cylinder pressure signal to analyse the acoustical response of the cylinder bore, i.e. it provides a cycle-independent trapped mass estimation by relying on the resonant frequencies of the in-cylinder pressure signal of one combustion cycle.

Regarding the future implementation of the method in commercial ECUs, a specific transformation has been created for analysing the in-cylinder pressure resonance without a complex time-frequency analysis. The final transformation allows obtaining trapped mass information even with low resonance excitation. Six engines with different combustion modes (SI, CI, RCCI, CAI and SACI), were used for validation and verification, and the output of the new method shown a good agreement with test bench sensors.

A wide range of possibilities are presented for the future implementation of the method, ranging from using only in-cylinder pressure data to a more complex sensor data fusion with an observer design. A quality indicator of the resonance is used to reject outliers and intake manifold dynamics are also included to improve the transient response of the model. The final transient response was verified in a conventional CI engine by performing TGV and EGR steps at four operating conditions and in a WLTP cycle.

Finally, to illustrate the potential of the method, the trapped mass estimation obtained from in-cylinder pressure resonance is used in conjunction with other models for the determination of various combustion parameters, such as exhaust temperature, NO_x emissions, IGR, and knock. The models not only benefit from an additional input, but their output then matches experimental data better than other available sensors.

1.4 Objectives

The following pages will cover the presentation of a new methodology for trapped mass determination through the analysis of the high-frequency content of one in-cylinder pressure cycle. Particularly, the main objectives of this dissertation are the following:

- The analysis of the in-cylinder pressure resonance characteristics in different combustion modes (Chapter 5).
- The introduction of a novel methodology for trapped mass estimation based on the in-cylinder pressure resonant modes (Chapter 6).
- The design of a new transformation for avoiding computationally expensive time-frequency analysis (Chapter 6).
- A sensor data fusion with different set of sensors for a fast and robust transient response (Chapter 7).
- The use of the methodology to derive various control parameters for automotive applications (Chapter 8).

1.4.1 Methodology

The dissertation is divided in 9 chapters to cover all the aspects of the work presented.

The first chapter has introduced the current situation of IC engines, their emissions concern and the change of paradigm of the regulatory framework. The main future technologies have been also summarized, highlighting the need of a precise measurement of the intake composition and the likely commercialization of in-cylinder pressure sensors.

Next chapter covers the basics of in-cylinder pressure signal. The information that pressure sensors offer is analysed and the main applications developed are commented. Special attention is taken to the pressure based knock and NO_x modelling, as they will be later improved in Chapter 8.

Chapter 3 introduces the challenging problematic of an accurate trapped mass determination. Herein, the main models and sensors for the estimation

of each mass flow (fuel, air, EGR and IGR) are presented and discussed.

Chapter 4 describes the system set-up: the main engine characteristics are summarized and the principal sensors employed are described. In this chapter the mathematical tools for time-frequency analysis are also described, pointing out the advantages and the weaknesses of each one.

Chapter 5 analyses the frequency spectrum of the pressure traces for several combustion modes. Combustion characteristics are shown, not only by computing the traditional heat release law, but also by identifying the high-frequency content. Additionally, an analysis of low knocking cycles in SI engines is also included and a new procedure for knock detection is proposed.

The core of this dissertation is presented in chapter 6. The hypothesis and assumptions taken to develop a trapped mass estimation procedure are listed in this chapter and experimental data is used for verification, validation and illustration purposes.

In the first part of Chapter 6, traditional time-frequency analysis tools, such as short time Fourier transform (STFT) or Wigner distribution (WD), are used to obtain the in-cylinder pressure resonant frequency evolution. The resonant frequency content is used to estimate the speed of sound evolution, and finally, the trapped mass is derived from the speed of sound.

In the second part of the chapter, a modification of the Fourier transform, which considers variable frequency harmonics, is developed. This transformation allows the direct estimation of the trapped mass with an indicator of the resonant excitation, avoiding the computational burden of time-frequency analysis.

Chapter 7 presents some data fusion strategies for a robust and fast estimation. A Kalman filter (KF) is designed capable of combining different set of sensors. Transient tests, such as WLTP or control steps, are used to illustrate the dynamic response of the final implementation.

Afterwards, in chapter 8, the development of some models for automotive applications exemplify the potential of the trapped mass methodology, these are the following:

- IGR determination through a polytropic evolution during the exhaust process in NVO strategies.
- An autoignition model for the knock phenomenon based on an Arrhenius-like function of the temperature of the unburned gasses in SI engines.
- Exhaust temperature estimation by assuming a polytropic expansion through the valves and using a lumped thermal model at the exhaust manifold.
- A NO_x emissions model based on an Arrhenius-like function of the adiabatic flame temperature for diffusive CI combustion.

Finally, chapter 9 concludes the dissertation by highlighting the strengths, pointing out the weaknesses, and suggesting the future work for the commercial implementation of the developments.

1.A Publications

Most of the contents have been published in international journals. Herein, the publications by the author that are directly linked with the dissertation are listed. Together, the chapter which contains the publication information is pointed out in brackets.

Journal papers

1. Broatch A., Guardiola C., Bares P. and Denia F.D. Determination of the resonance response in an engine cylinder with a bowl-in-piston geometry by the finite element method for inferring the trapped mass. *International Journal of Engine Research*, 17(5): 534:542, 2015. [Chapter 5]
2. Luján J. M., Guardiola C., Pla B., and Bares P. Estimation of trapped mass by in-cylinder pressure resonance in HCCI engines. *Mechanical Systems and Signal Processing*, 66-67: 862:874, 2016. [Chapter 6]
3. Broatch A., Guardiola C., Pla B., and Bares P. A direct transform for determining the trapped mass on an internal combustion engine based on the in-cylinder pressure resonance phenomenon. *Mechanical Systems and Signal Processing*, 62: 480-489, 2015. [Chapter 6]
4. Guardiola C., Martín J., Pla B., and Bares P. Cycle by cycle NO_x model for diesel engine control. *Applied Thermal Engineering*, 110: 1011-1020, 2017. [Chapter 8]
5. Guardiola C., Olmeda P., Pla B., and Bares P. In-cylinder pressure based model for exhaust temperature estimation in internal combustion engines. *Applied Thermal Engineering*, 115: 212-220, 2017. [Chapter 8]

6. Bares P., Selmanaj D., Guardiola C. and Onder C. Knock probability estimation through an in-cylinder temperature model with exogenous noise. *Mechanical Systems and Signal Processing*. [Chapter 8]

Conference papers

1. Guardiola C., Pla B., Blanco-Rodriguez D., and Bares P. Cycle by cycle trapped mass estimation for diagnosis and control. *SAE International Journal of Engines*, 7(3), 2014. [Chapter 6]
2. Guardiola C., Pla B., and Bares P. In-Cylinder pressure based determination of cycle-to-cycle air charge. *International Advanced Engine Control Symposium (AECS)*, 2014. [Chapter 6]
3. Guardiola C., Triantopoulos V., Bares P., Bohac S., Stefanopoulou A. Simultaneous estimation of intake and residual mass using in-cylinder pressure in an engine with negative valve overlap. *IFAC-PapersOnLine*, 49(11): 461:468, 2016. [Chapter 8]

References

- [1] Urry J. *Sociology beyond societies: Mobilities for the twenty first century*. Routledge, 2000. (cited in p. 1)
- [2] Carrabine E and Longhurst B. “Consuming the car: anticipation, use and meaning in contemporary youth culture”. *The Sociological Review*, Vol. 50 n° 2, pp. 181–196, 2002. (cited in p. 1)
- [3] EC. *Energy, transport and environment indicators*. Publications Office of the European Union, 2011. (cited in p. 1)
- [4] statistics collector team 2011 ChartsBin. “Worldwide Total Motor Vehicles (per 1,000 people)”. ChartsBin.com. Accessed: 2016-12-02. (cited in pp. 1 and 2)
- [5] Santos A, McGuckin N, Nakamoto HY, Gray D and Liss S. *Summary of travel trends: 2009 National Household Travel Survey*. US Department of Transportation. Federal Highway Administration, 2011. (cited in p. 1)
- [6] Dargay J and Gatley D. “Income’s effect on car and vehicle ownership, worldwide: 1960-2015”. *Transportation Research Part A: Policy and Practice*, Vol. 33 n° 2, pp. 101–138, 1999. (cited in p. 1)
- [7] OICA. “Worldwide Vehicles in use”. <http://www.oica.net/category/vehicles-in-use/>. Accessed: 2016-12-02. (cited in p. 1)
- [8] Johnson TV. “Review of CO₂ Emissions and Technologies in the Road Transportation Sector”. *SAE paper 2010-01-1276*, 2010. (cited in p. 2)
- [9] Straif K., Cohen A. and Samet J. *Air pollution and cancer: IARC scientific publication no. 161*. International Agency for Research on Cancer, 2013. (cited in p. 2)
- [10] IPCC. *The Science of Climate Change*. Joint national science academies’ statement, 2001. (cited in p. 2)
- [11] Hernández López Leonor. *Desarrollo de una metodología para la predicción y optimización de emisiones contaminantes y consumo en motores diesel de automoción mediante redes neuronales artificiales*. PhD Thesis, Universitat Politècnica de València. Departamento de Máquinas y Motores Térmicos, 2004. (cited in p. 2)

- [12] Payri F. and Desantes J.M. *Motores de combustión interna alternativos*. Universitat Politècnica de València, 2011. (cited in p. 3)
- [13] Sheesley R. J., Schauer J. J., Garshick E., Laden F., Smith T. J., Blicharz A. P. and Deminter J. T. “Tracking personal exposure to particulate diesel exhaust in a diesel freight terminal using organic tracer analysis”. *Journal of Exposure Science and Environmental Epidemiology*, Vol. 19 n° 2, pp. 172–186, 2009. (cited in p. 3)
- [14] Adams M and Lükewille A. *The European Environment State and Outlook 2010: Air pollution*. European Environment Agency. Publications Office of the European Union, 2010. (cited in p. 3)
- [15] IEA. *Energy balances of non-OECD countries*. OECD International Energy Agency, 2015. (cited in p. 3)
- [16] NASA. “GISS Surface Temperature Analysis”. <http://data.giss.nasa.gov/gistemp/>. Accessed: 2016-12-05. (cited in pp. 3 and 4)
- [17] Hansen J, Ruedy R, Sato M and Lo K. “Global surface temperature change”. *Reviews of Geophysics*, Vol. 48 n° 4, 2010. (cited in p. 3)
- [18] EEA. *The European environment - state and outlook 2015: synthesis report*. European Environment Agency, Copenhagen, 2015. (cited in p. 3)
- [19] EC. *A Roadmap for moving to a competitive low carbon economy in 2050*. Communication from the Commission to the European Parliament, the Council, the European Economic and Social Committee and the Committee of the Regions, 2011. (cited in p. 4)
- [20] OPEC. *World Oil Outlook*. OPEC Secretariat, 2015. (cited in pp. 4 and 5)
- [21] IEO. *International Energy Outlook 2016*. US Energy Information Administration, 2016. (cited in p. 4)
- [22] IEA. *Energy Technology Perspectives*. OECD International Energy Agency, 2010. (cited in p. 5)
- [23] ACEA. *ACEA position paper on electrically chargeable vehicles*. European Automobile Manufacturers’ Association, 2012. (cited in p. 5)
- [24] Rizzoni G, Guzzella L and Baumann BM. “Unified modeling of hybrid electric vehicle drivetrains”. *IEEE/ASME Transactions on Mechatronics*, Vol. 4 n° 3, pp. 246–257, 1999. (cited in p. 5)
- [25] Lindenkamp N, Stöber-Schmidt C and Eilts P. “Strategies for Reducing NOX- and Particulate Matter Emissions in Diesel Hybrid Electric Vehicles”. *SAE Paper 2009-01-1305*, 2009. (cited in p. 5)
- [26] Mock P. “European Vehicle Market Statistics: Pocketbook 2015/16”. Technical report, The International Council on Clean Transportation, 2016. (cited in p. 5)
- [27] EPA. *Light-duty automotive technology, carbon dioxide emissions, and fuel economy trends: 1975 through 2016*. EPA-420-R-12-001a. Transportation and Climate Division. Office of Transportation and Air Quality. US Environmental Protection Agency, 2016. (cited in pp. 5 and 12)
- [28] Mock P. “EU vehicle technology study: Development of preliminary cost curves for the EU market”. In *27 April 2012 workshop for regulators, manufacturers, and others working on these issues in the EU in the 2020-25 time frame. GHG reduction potential and costs of LDV technologies, II*. The International Council on Clean Transportation, 2012. (cited in p. 5)

- [29] EU. *Regulation (EC) No 443/2009 of the European Parliament and of the Council of 23 April 2009 setting emission performance standards for new passenger cars as part of the Community's integrated approach to reduce CO₂ emissions from light-duty vehicles*. Official Journal of the European Union, 2009. (cited in p. 6)
- [30] Mock P. "European CO₂ Emission Performance Standards for Passenger Cars and Light Commercial Vehicles". Technical report, The International Council on Clean Transportation, 2012. (cited in pp. 6 and 7)
- [31] Galindo J, Climent H, Guardiola C, Tiseira A and Portalier J. "Assessment of a sequentially turbocharged diesel engine on real-life driving cycles". *International Journal of Vehicle Design*, Vol. 49 n° 1-3, pp. 214–234, 2009. (cited in p. 6)
- [32] Rubino L, Bonnel P, Hummel R, Krasenbrink A, Manfredi U and Santi G De. "On-road Emissions and Fuel Economy of Light Duty Vehicles using PEMS: Chase-Testing Experiment". *SAE Paper 2008-01-1824*, 2008. (cited in p. 6)
- [33] Mock P, German J, Bandivadekar A and Riemersma I. "Discrepancies between type-approval and real-world fuel consumption and CO₂ values in 2001-2011 European passenger cars". Technical report, The International Council on Clean Transportation, 2012. (cited in p. 6)
- [34] Daham B, Li H, Andrews GE, Ropkins K, Tate JE and Bell MC. "Comparison of Real World Emissions in Urban Driving for Euro 1-4 Vehicles Using a PEMS". *SAE Paper 2009-01-0941*, 2009. (cited in p. 6)
- [35] ECE. *Proposal for a new UN Global Technical Regulation on Worldwide harmonized Light vehicles Test Procedures (WLTP)*. United Nations. Economic commission for Europe. Inland Transport Committee. World Forum for Harmonization of Vehicle Regulations, ece/trans/wp29/grpe/2013/13 edition, 2013. (cited in p. 6)
- [36] Yang L., Franco V., Mock P., Kolke R., Zhang S., Wu Y. and German J. "Experimental Assessment of NO_x Emissions from 73 Euro 6 Diesel Passenger Cars". *Environmental Science and Technology*, Vol. 49 n° 24, pp. 14409–14415, 2015. (cited in pp. 6 and 7)
- [37] Fontaras G., Franco V., Dilara P., Martini G. and Manfredi U. "Development and review of Euro 5 passenger car emission factors based on experimental results over various driving cycles". *Science of the Total Environment*, Vol. 468-469, pp. 1034–1042, 2014. (cited in p. 7)
- [38] Payri F., Luján J. M., Guardiola C. and Pla B. "A challenging future for the IC engine: New technologies and the control role". *Oil and Gas Science and Technology*, Vol. 70 n° 1, pp. 15–30, 2015. (cited in p. 8)
- [39] Johnson T. "Vehicular Emissions in Review". *SAE International Journal of Engines*, Vol. 7 n° 3, 2014. (cited in p. 8)
- [40] Ostrowski G, Neely GD, Chadwell CJ, Mehta D and Wetzel P. "Downspeeding and Supercharging a Diesel Passenger Car for Increased Fuel Economy". *SAE Paper 2012-01-0704*, 2012. (cited in p. 8)
- [41] Varnier O. *Trends and limits of two-stage boosting systems for automotive diesel engines*. Universitat Politècnica de València. Departamento de Máquinas y Motores Térmicos, 2012. (cited in p. 8)
- [42] Galindo J, Climent H, Guardiola C and Doménech J. "Strategies for improving the mode transition in a sequential parallel turbocharged automotive diesel engine". *International Journal of Automotive Technology*, Vol. 10 n° 2, pp. 141–149, 2009. (cited in p. 8)

- [43] Pischinger S. “Current and Future Challenges for Automotive Catalysis: Engine Technology Trends and Their Impact”. *Topics in Catalysis*, Vol. 59 n° 10-12, pp. 834–844, 2016. (cited in pp. 8 and 10)
- [44] Meszler D, German J, Mock P and Bandivadekar A. “Summary of mass reduction impacts on EU cost curves”. Technical report, The International Council on Clean Transportation, 2013. (cited in p. 8)
- [45] Brooker AD, Ward J and Wang L. “Lightweighting Impacts on Fuel Economy, Cost, and Component Losses”. *SAE paper 2013-01-0381*, 2013. (cited in p. 8)
- [46] Brands M.C., Werner J. and Hoehne J.L. “Vehicle testing of Cummins turbocompound Diesel engine”. *SAE paper 810073*, 1981. (cited in p. 9)
- [47] Hountalas D.T., Katsanos C.O., Kouremenos D.A. and Rogdakis E.D. “Study of available exhaust gas heat recovery technologies for HD Diesel engine applications”. *International Journal of Alternative Propulsion*, Vol. 1, pp. 228–249, 2007. (cited in p. 9)
- [48] Weerasinghea W.M.S.R., Stobarta R.K. and Hounshama S.M. “Thermal efficiency improvement in high output diesel engines a comparison of a Rankine cycle with turbo-compounding”. *Applied Thermal Engineering*, Vol. 30, pp. 2253–2256, 2010. (cited in p. 9)
- [49] Hopmann U. “Diesel engine waste heat recovery utilizing electric turbocompound technology”. *2004 Diesel Engine-Efficiency and Emissions Research (DEER) Conference*, 2004. (cited in p. 9)
- [50] Kushch A.S., Bass J.C., Ghamaty S. and Elsner N.B. “Thermoelectric development at Hi-Z Technology”. *2002 Diesel Engine-Efficiency and Emissions Research (DEER) Conference*, 2002. (cited in p. 9)
- [51] Bass J.C., Kushch A.S. and Elsner N.B. “Thermoelectric Generator (TEG) on Heavy Diesel Trucks”. Technical report, Hi-Z Technology Inc., 2001. (cited in p. 9)
- [52] Boretti A. “Improving the Efficiency of Turbocharged Spark Ignition Engines for Passenger Cars through Waste Heat Recovery”. *SAE Paper 2012-01-0388*, 2012. (cited in p. 9)
- [53] Aly S.E. “Diesel engine waste-heat power cycle”. *Applied Energy*, Vol. 29, pp. 179–189, 1988. (cited in p. 9)
- [54] Bailey M.M. “Comparative Evaluation of Three Alternative Power Cycles for Waste Heat Recovery Form the Exhaust of Adiabatic Diesel Engines”. Technical report, National Aeronautics and Space Administration, 1985. (cited in p. 9)
- [55] Dolz V., Novella R., García A. and Sánchez J. “HD Diesel engine equipped with a bottoming Rankine cycle as a waste heat recovery system. Part 1: Study and analysis of the waste heat energy”. *Applied Thermal Engineering*, Vol. 36, pp. 269–278, 2012. (cited in p. 9)
- [56] Doyle E., Dinanno L. and Kramer S. “Installation of a Diesel Organic-Rankine Compound engine in a class 8 truck for a single-vehicle test”. *SAE paper 790646*, 1979. (cited in p. 9)
- [57] Brijesh P. and Sreedhara S. “Exhaust emissions and its control methods in compression ignition engines: A review”. *International Journal of Automotive Technology*, Vol. 14 n° 2, pp. 195–206, 2013. (cited in pp. 9 and 216)

- [58] Chi J and DaCosta H. “Modeling and Control of a Urea-SCR Aftertreatment System”. *SAE paper 2005-01-0966*, 2005. (cited in pp. 9 and 216)
- [59] Devarakonda M, Parker G, Johnson J and Strots V et al. “Model-Based Estimation and Control System Development in a Urea-SCR Aftertreatment System”. *SAE Int. J. Fuels Lubr.*, Vol. 1 n° 1, pp. 646–661, 2009. (cited in pp. 9 and 216)
- [60] Nakagawa S, Hori T and Nagano M. “A New Feedback Control of a Lean NO_x Trap Catalyst”. *SAE paper 2004-01-0527*, 2004. (cited in p. 9)
- [61] Willems F, Cloudt R, van den Eijnden E and et al. M van Genderen. “Is Closed-Loop SCR Control Required to Meet Future Emission Targets?”. *SAE paper 2007-01-1574*, 2007. (cited in pp. 9 and 35)
- [62] Quérel C, Grondin O and Letellier C. “State of the Art and Analysis of Control Oriented NO_x Models”. *SAE paper 2012-01-0723*, 2012. (cited in pp. 9 and 35)
- [63] Moos R. “A brief overview on automotive exhaust gas sensors based on electroceramics”. *International Journal of Applied Ceramic Technology*, Vol. 2 n° 5, pp. 401–413, 2005. (cited in pp. 9 and 63)
- [64] Riegel J, Neumann H and Wiedenmann H-M. “Exhaust gas sensors for automotive emission control”. *Solid State Ionics*, Vol. 152-153, pp. 783–800, 2002. (cited in pp. 9, 35, 61, and 62)
- [65] Zhan R, Huang Y and Khair M. “Methodologies to Control DPF Uncontrolled Regenerations”. *SAE paper 2006-01-1090*, 2006. (cited in p. 10)
- [66] Hsieh M, Canova M and Wang J. “Model Predictive Control Approach for AFR Control during Lean NO_x Trap Regeneration”. *SAE Int. J. Engines*, Vol. 2 n° 1, pp. 149–157, 2009. (cited in p. 10)
- [67] Song X., Johnson J. H. and Naber J. D. “A review of the literature of selective catalytic reduction catalysts integrated into diesel particulate filters”. *International Journal of Engine Research*, Vol. 16 n° 6, pp. 738–749, 2015. (cited in p. 10)
- [68] Pace L and Presti M. “An Alternative Way to Reduce Fuel Consumption During Cold Start: The Electrically Heated Catalyst”. *SAE paper 2011-24-0178*, 2011. (cited in p. 10)
- [69] Husted HL, Piock W and Ramsay G. “Fuel Efficiency Improvements from Lean, Stratified Combustion with a Solenoid Injector”. *SAE Paper 2009-01-1485*, 2009. (cited in p. 10)
- [70] Reijnders J., Boot M. and de Goey P. “Impact of aromaticity and cetane number on the soot-NO_x trade-off in conventional and low temperature combustion”. *Fuel*, Vol. 186, pp. 24–34, 2016. (cited in p. 10)
- [71] Aquino C. F. “Transient A/F control characteristics of the 5 liter central fuel injection engine”. *SAE Technical Papers*, 1981. (cited in p. 10)
- [72] Zhen X., Wang Y., Xu S., Zhu Y., Tao C., Xu T. and Song M. “The engine knock analysis - An overview”. *Applied Energy*, Vol. 92, pp. 628–636, 2012. (cited in pp. 11, 40, and 41)
- [73] Stanglmaier R. H. and Roberts C. E. “Homogeneous charge compression ignition (HCCI): Benefits, compromises, and future engine applications”. *SAE Technical Papers*, 1999. (cited in p. 11)
- [74] Lu X., Han D. and Huang Z. “Fuel design and management for the control of advanced compression-ignition combustion modes”. *Progress in Energy and Combustion Science*, Vol. 37 n° 6, pp. 741–783, 2011. (cited in p. 11)

- [75] Gan S., Ng H. K. and Pang K. M. “Homogeneous Charge Compression Ignition (HCCI) combustion: Implementation and effects on pollutants in direct injection diesel engines”. *Applied Energy*, Vol. 88 n° 3, pp. 559–567, 2011. (cited in p. 11)
- [76] Chiang CJ and Stefanopoulou AG. “Stability analysis in homogeneous charge compression ignition (HCCI) engines with high dilution”. *IEEE Trans. Control Syst. Technol.*, Vol. 15, pp. 209–219, 2007. (cited in p. 11)
- [77] Onishi S., Jo S. H., Shoda K., Jo P. D. and Kato S. “Active Thermo-Atmosphere Combustion (ATAC) - A new combustion process for internal combustion engines”. *SAE Technical Papers*, 1979. (cited in p. 11)
- [78] Najt P. M. and Foster D. E. “Compression-ignited homogeneous charge combustion”. *SAE Technical Papers*, 1983. (cited in p. 11)
- [79] Hunicz J. and Kordos P. “An experimental study of fuel injection strategies in CAI gasoline engine”. *Experimental Thermal and Fluid Science*, Vol. 35 n° 1, pp. 243–252, 2011. (cited in p. 11)
- [80] Adomeit P., Sehr A., Weinowski R., Stapf K. G., Seebach D., Pischinger S., Hoffmann K., Abel D., Fricke F., Kleeberg H. and Tomazic D. “Operation strategies for controlled auto ignition gasoline engines”. *SAE International Journal of Engines*, Vol. 2 n° 1, pp. 164–172, 2009. (cited in p. 11)
- [81] Lin W., Sterniak J. and Bohac S. V. “NO_x emissions characterization during transient spark assisted compression ignition (SACI) engine operation”. In *ASME 2013 Internal Combustion Engine Division Fall Technical Conference, ICEF 2013*, volume 1, 2013. (cited in p. 11)
- [82] Manofsky L., Vavra J., Assanis D. and Babajimopoulos A. “Bridging the gap between HCCI and SI: Spark-assisted compression ignition”. *SAE Technical Papers*, 2011. (cited in p. 11)
- [83] D’Ambrosio S. and Ferrari A. “Effects of exhaust gas recirculation in diesel engines featuring late PCCI type combustion strategies”. *Energy Conversion and Management*, Vol. 105, pp. 1269–1280, 2015. (cited in p. 11)
- [84] Zehni A., Khoshbakhti Saray R. and Poorghasemi K. “Numerical comparison of PCCI combustion and emission of diesel and biodiesel fuels at low load conditions using 3D-CFD models coupled with chemical kinetics”. *Applied Thermal Engineering*, Vol. 110, pp. 1483–1499, 2017. (cited in p. 11)
- [85] Kokjohn S. L., Hanson R. M., Splitter D. A. and Reitz R. D. “Fuel reactivity controlled compression ignition (RCCI): A pathway to controlled high-efficiency clean combustion”. *International Journal of Engine Research*, Vol. 12 n° 3, pp. 209–226, 2011. (cited in p. 12)
- [86] Reitz R. D. and Duraisamy G. “Review of high efficiency and clean reactivity controlled compression ignition (RCCI) combustion in internal combustion engines”. *Progress in Energy and Combustion Science*, Vol. 46, pp. 12–71, 2015. (cited in p. 12)
- [87] Paykani A., Kakaee A., Rahnama P. and Reitz R. D. “Progress and recent trends in reactivity-controlled compression ignition engines”. *International Journal of Engine Research*, Vol. 17 n° 5, pp. 481–524, 2016. (cited in p. 12)
- [88] Li J., Yang W. and Zhou D. “Review on the management of RCCI engines”. *Renewable and Sustainable Energy Reviews*, Vol. 69, pp. 65–79, 2017. (cited in p. 12)

- [89] Saxena S. and Bedoya I. D. “Fundamental phenomena affecting low temperature combustion and HCCI engines, high load limits and strategies for extending these limits”. *Progress in Energy and Combustion Science*, Vol. 39 n° 5, pp. 457–488, 2013. (cited in p. 12)
- [90] Núesch S., Hellström E., Jiang L. and Stefanopoulou A. G. “Mode switches among SI, SACI, and HCCI combustion and their influence on drive cycle fuel economy”. In *Proceedings of the American Control Conference*, pp. 849–854, 2014. (cited in p. 12)
- [91] Asad U, Divekar P, Chen X and Zheng M et al. “Mode Switching Control for Diesel Low Temperature Combustion with Fast Feedback Algorithms”. *SAE Int. J. Engines*, Vol. 5 n° 3, pp. 850–863, 2012. (cited in p. 12)
- [92] Milovanovic N, Blundell D, Gedge S and Turner J. “SI-HCCI-SI Mode Transition at Different Engine Operating Conditions”. *SAE paper 2005-01-0156*, 2005. (cited in p. 12)
- [93] Armas O., Rodríguez J., Payri F., Martín J. and Agudelo J. R. “Effect of the trapped mass and its composition on the heat transfer in the compression cycle of a reciprocating engine”. *Applied Thermal Engineering*, Vol. 25 n° 17-18, pp. 2842–2853, 2005. (cited in p. 12)
- [94] Baert RSG, Beckman DE and Veen A. “Efficient EGR Technology for Future HD Diesel Engine Emission Targets”. *SAE paper 1999-01-0837*, 1999. (cited in p. 12)
- [95] Luján J. M., Guardiola C., Pla B. and Cabrera P. “Considerations on the low-pressure exhaust gas recirculation system control in turbocharged diesel engines”. *International Journal of Engine Research*, Vol. 15 n° 2, pp. 250–260, 2014. (cited in pp. 12 and 61)
- [96] Moroz S, Bourgoïn G, Luján JM and Pla B. “A 2.0 litre Diesel Engine with Low Pressure Exhaust Gas Recirculation and Advanced Cooling System”. *The Diesel Engine Conference, Proceedings of the SIA 2008 Conference, Rouen, France*, 2008. (cited in p. 12)
- [97] Walker AP. “Controlling particulate emissions from diesel vehicles”. *Topics in Catalysis*, Vol. 28, pp. 165–170, 2004. (cited in p. 12)
- [98] Krüger U, Edwards S, Pantow E, Lutz R, Dreisbach R and Glensvig M. “High Performance Cooling and EGR Systems as a Contribution to Meeting Future Emission Standards”. *SAE paper 2008-01-1199*, 2008. (cited in p. 12)
- [99] Gerow M. S., Shingne P. S., Triantopoulos V., Bohac S. V. and Martz J. B. “A comparison of valving strategies appropriate for multi-Mode combustion within a downsized boosted automotive engine part b: Mid load operation within the SACI combustion regime”. In *ASME 2013 Internal Combustion Engine Division Fall Technical Conference, ICEF 2013*, volume 1, 2013. (cited in p. 12)
- [100] Palma A, D Del Core and Esposito C. “The HCCI Concept and Control, Performed with MultiAir Technology on Gasoline Engines”. *SAE paper 2011-24-0026*, 2011. (cited in p. 12)
- [101] Lamping M, Körfer T, Schnorbus T, Pischinger S and Chen Y. “Tomorrows Diesel Fuel Diversity - Challenges and Solutions”. *SAE Paper 2008-01-1731*, 2008. (cited in pp. 12 and 27)
- [102] Luján JM, Bermúdez V, Tormos B and Pla B. “Comparative analysis of a DI diesel engine fuelled with biodiesel blends during the European MVEG-A cycle: Performance and emissions (II)”. *Biomass and Bioenergy*, Vol. 33 n° 6-7, pp. 948–956, 2009. (cited in p. 12)

- [103] Continental. *Fuel quality sensor helps to protect the engine and the environment*. Continental, press release, 2011. (cited in p. 13)
- [104] Vanzuilen D, Mouaici G, Bernard F and McKenzie I. “Fuel sensor”. *US patent 7170303*, 2007. (cited in p. 13)
- [105] Jia L., Naber J. D. and Blough J. R. “Review of Sensing Methodologies for Estimation of Combustion Metrics”. *Journal of Combustion*, Vol. 2016, 2016. (cited in pp. 13 and 27)
- [106] Saracino R., Gaballo M. R., Mannal S., Motz S., Carlucci A. and Benegiamo M. “Cylinder Pressure-Based Closed Loop Combustion Control: A Valid Support to Fulfill Current and Future Requirements of Diesel Powertrain Systems”. *SAE Technical Papers*, Vol. 2015, 2015. (cited in pp. 13 and 31)
- [107] Yoon P, Park S, Sunwoo M, Ohm I and Yoon KJ. “Closed-loop Control of Spark Advance and Air-fuel Ratio in SI Engines using Cylinder Pressure”. *SAE Paper 2000-01-0933*, 2000. (cited in pp. 13 and 31)
- [108] Von Berg J., Ziermann R., Reichert W., Obermeier E., Eickhoff M., Krötz G., Thoma U., Boltshauser Th, Cavalloni C. and Nendza J. P. “High temperature piezoresistive B-SiC-on-SOI pressure sensor for combustion engines”. *Materials Science Forum*, Vol. 264-268 n° PART 2, pp. 1101–1104, 1998. (cited in pp. 13 and 88)
- [109] Chen L. and Mehregany M. “A silicon carbide capacitive pressure sensor for in-cylinder pressure measurement”. *Sensors and Actuators, A: Physical*, Vol. 145-146 n° 1-2, pp. 2–8, 2008. (cited in pp. 13 and 88)
- [110] Powell J. D. “Engine control using cylinder pressure: Past, present, and future”. *Journal of Dynamic Systems, Measurement and Control, Transactions of the ASME*, Vol. 115 n° 2 B, pp. 343–350, 1993. (cited in p. 13)
- [111] Leonhardt S, Müller N and Isermann R. “Methods for engine supervision and control based on cylinder pressure information”. *IEEE/ASME Transactions on Mechatronics*, Vol. 4 n° 3, pp. 235–245, 1999. (cited in pp. 13 and 30)
- [112] Muller R, Hart M, Truscott A, Noble A, Krotz G, Eickhoff M, Cavalloni C and Gnielka M. “Combustion Pressure Based Engine Management System”. *SAE Paper 2000-01-0928*, 2000. (cited in p. 13)
- [113] Negrean M., Schliecker S. and Ernst R. “Timing implications of sharing resources in multicore real-time automotive systems”. *SAE International Journal of Passenger Cars - Electronic and Electrical Systems*, Vol. 3 n° 1, pp. 27–40, 2010. (cited in p. 13)
- [114] Xie H, Stobart R, Tunestal P, Eriksson L, and Leteinturier Y Huangand P. “Future Engine Control Enabling Environment Friendly Vehicle”. *SAE paper 2011-01-0697*, 2011. (cited in p. 13)
- [115] Potter MA. “The Road to Math: The General Motors Approach to an Efficient Diesel Engine Technology Development”. In *Thiesel Conference*, 2012. (cited in p. 13)
- [116] Vitale G, Siebenbrunner P, Hülser H, Bachler J and Pfahl U. “OBd Algorithms: Model-based Development and Calibration”. *SAE Paper 2007-01-4222*, 2007. (cited in p. 13)
- [117] Butts K and Jaikamal V. “Model-Based Verification and Validation of Electronic Engine Controls”. *SAE paper 2012-01-0961*, 2012. (cited in p. 13)

- [118] Alsabaan M., Naik K., Khalifa T. and Nayak A. “Optimization of fuel cost and emissions with vehicular networks at traffic intersections”. *IEEE Conference on Intelligent Transportation Systems, Proceedings, ITSC*, pp. 613–619, 2012. (cited in p. 13)
- [119] Iglesias I, Isasi L, Larburu M and Martin A et al. “Networked Clean Vehicles, How the Environment Information will Improve Fuel Efficiency and CO₂ Emissions”. *SAE Int. J. Fuels Lubr.*, Vol. 2 n° 1, pp. 167–171, 2009. (cited in p. 13)
- [120] Lang D., Stanger T. and Del Re L. “Opportunities on fuel economy utilizing V2V based drive systems”. *SAE paper 2013-01-0985*, 2013. (cited in p. 13)
- [121] Kamalanathsharma R.K. and Rakha H. “Agent-based modeling of eco-cooperative adaptive cruise control systems in the vicinity of intersections”. *IEEE Conference on Intelligent Transportation Systems, Proceedings, ITSC*, pp. 840–845, 2012. (cited in p. 13)
- [122] Tsugawa S. “An overview on an automated truck platoon within the energy ITS project”. *IFAC Proceedings Volumes (IFAC-PapersOnline)*, Vol. 7, pp. 41–46, 2013. (cited in p. 13)
- [123] Kato S., Tsugawa S., Tokuda K., Matsui T. and Fujii H. “Vehicle Control Algorithms for Cooperative Driving with Automated Vehicles and Intervehicle Communications”. *IEEE Transactions on Intelligent Transportation Systems*, Vol. 3 n° 3, pp. 155–160, 2002. (cited in p. 13)
- [124] Ferrari A, Chiodi M, Bargende M and Roberti P et al. “Virtual Set-up of a Racing Engine for the Optimization of Lap Performance through a Comprehensive Engine-Vehicle-Driver Model”. *SAE paper 2011-24-0141*, 2011. (cited in p. 13)
- [125] Guardiola C, Pla B, Blanco-Rodriguez D and Reig A. “Modelling driving behaviour and its impact on the energy management problem in hybrid electric vehicles”. *International Journal of Computer Mathematics*, 2013. (cited in p. 13)
- [126] Malikopoulos A.A. and Aguilar J.P. “Optimization of driving styles for fuel economy improvement”. *IEEE Conference on Intelligent Transportation Systems, Proceedings, ITSC*, pp. 194–199, 2012. (cited in p. 13)
- [127] Guardiola C., Pla B., Bares P. and Waschl H. “Adaptive calibration for reduced fuel consumption and emissions”. *Proceedings of the Institution of Mechanical Engineers, Part D: Journal of Automobile Engineering*, Vol. 230 n° 14, pp. 2002–2014, 2016. (cited in p. 13)

Chapter 2

In-cylinder pressure signal: characteristics and applications

Contents

| | | |
|------------|---|-----------|
| 2.1 | Introduction | 27 |
| 2.2 | Applications based on a polytropic evolution | 28 |
| 2.3 | Combustion modelling and control | 31 |
| 2.3.1 | Combustion noise assessment | 32 |
| 2.3.2 | Autoignition prediction | 33 |
| 2.3.3 | Emission models | 35 |
| 2.4 | Resonance analysis | 37 |
| 2.4.1 | Knock detection and control | 40 |
| 2.5 | Conclusions | 42 |
| 2.A | Instantaneous crankshaft speed models | 43 |
| | References | 43 |

2.1 Introduction

Between all the available signals for combustion feedback [1], in-cylinder pressure is the most precise measurement and it is used in all validation and research applications. In-cylinder pressure sensors offer a direct measurement of the combustion process, and a wide range of applications exist for its use: combustion detection [2], knock detection [3, 4], noise control [5, 6], fuel tolerance diagnostics [7], combustion control in both, next cycle [8] and same cycle

approach [9], emissions dispersion [10], mass composition estimation [11], TDC determination [12, 13], EOC detection [14], among others.

In-cylinder pressure signal gathers information in three frequency bands, corresponding to different IC phenomena [15], namely compression or expansion, combustion, and resonance. The compression and expansion is associated with the piston movement and its energy depends mainly on engine operating conditions, i.e. load and engine speed, combustion features are also affected by injection settings, and resonance depends on the resonant modes excitation and the cylinder damping characteristics.

Figure 2.1 shows the frequency components of the in-cylinder pressure signal in three zones, namely compression, combustion, and expansion, by using a Fourier transform and three windows. The analysis was performed in a single in-cylinder pressure trace, collected from a RCCI engine working at 1200 rpm and 50% load. The first window (compression) is located before combustion starts, the second one (combustion) is centred at the maximum heat released, and the third one (expansion) is located after combustion has ended. The characteristic bandwidth of each phenomena can be easily distinguished: In the compression and expansion the frequency components above 200 Hz fall down rapidly, but in combustion, all harmonics below 2 kHz are representative. The third phenomenon, resonance, is created by combustion, and it is represented by a peak in the frequency spectrum, which corresponds with punctual resonance modes, the most representative between 4 and 20 kHz. The rest of the signal can be considered sensor and background noise.

In this chapter an overview of the utility of the in-cylinder pressure signal for engine control and diagnosis is presented. The content of the chapter is divided by the different phenomena studied: Compression and expansion, combustion, and resonance, and an additional appendix is included to mention the combination of the crankshaft signal for in-cylinder pressure reconstruction.

2.2 Applications based on a polytropic evolution

The compression and expansion can be represented by a polytropic evolution, which assumes an adiabatic process, and where the pressure p and the volume V can be related by:

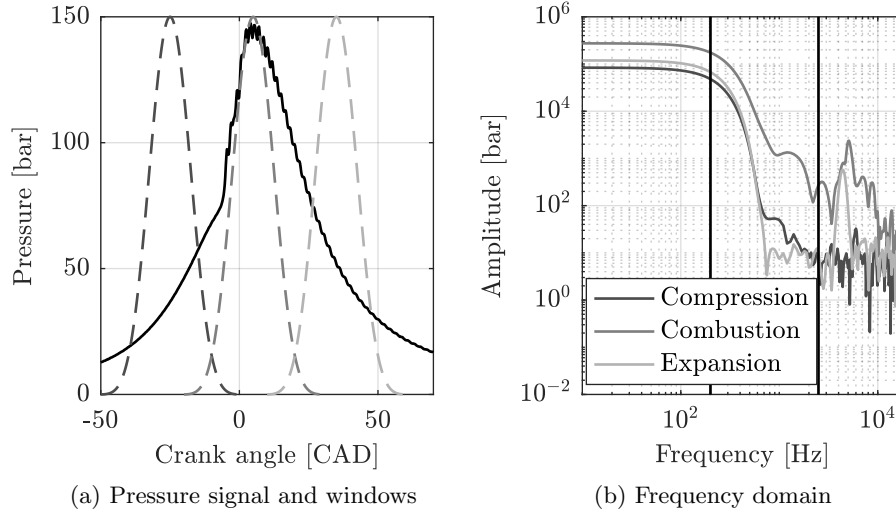


Figure 2.1. In-cylinder pressure signal: in time domain (left plot) and in frequency domain (right plot) by using three windows in different zones, namely compression, combustion, and expansion.

$$pV^\kappa = C \quad (2.1)$$

where κ is the polytropic coefficient and C is a constant.

The coefficient κ is similar to the specific heat capacities ratio γ , but κ accounts for the discrepancies with the adiabatic assumption, i.e. wall heat transfer. Some authors have worked on semi-empirical functions for wall heat transfer modelling [16], e.g. Woschni correlation [17]. But these correlations require calibration procedures where some parameters, such as the cylinder wall temperature in the Woschni expression, must be inferred. Therefore, for most control applications, a constant value or two values, one value for compression and another for expansion, are assumed. Some authors propose self-tuning algorithms, where κ is tuned at compression and expansion [18].

The instantaneous volume evolution V can be computed from the rod L_r , bore D and crank L_c lengths, and the minimum combustion chamber volume V_{cc} , by neglecting pressure deformations, such as:

$$V(\alpha) = V_{cc} + \frac{\pi D^2}{4} [L_c + L_r (1 - \cos(\alpha)) - \sqrt{L_c^2 - L_r^2 \sin^2(\alpha)}] \quad (2.2)$$

These assumptions allow a simple description of the compression and expansion process which can be used in many practical applications in combination of the ideal gas law ($pV = mRT$).

For example, one of the inconveniences of piezo-electric pressure sensors, such as the ones commonly used in research and validation applications [19], is the measurement of the in-cylinder pressure derivative (dp), and not the pressure value. Normally, an additional piezo-resistive sensor is used at the intake in order to set the pressure level at the intake valve closing (IVC) [20]. The procedure for referencing the piezo-electric pressure measurement is named *pegging*. However, turbulence and transient effects on the valve closing can lead to significant errors when using intake pressure as reference. Several authors propose fitting Equation (2.3) by an iterative method, e.g. least square method (LSM), to obtain κ and the pressure offset p_0 during compression [21–23].

$$(p + p_0) V^\kappa = cnt \quad (2.3)$$

Similar approaches can be found in [12, 13] for determining the TDC by referencing an offset in the location of the TDC instead of an offset in the pressure level.

Once κ is determined, either by iteration at the compression or by assuming an adequate value (commonly 1.35), the motored pressure p_m can be modelled through:

$$p_m(\alpha) = p_{IVC} \left(\frac{V_{IVC}}{V(\alpha)} \right)^\kappa \quad (2.4)$$

And the pressure variations due to the piston movement dp_m can be obtained by derivation over Equation (2.1), which yields:

$$dp_m = -\kappa \frac{p}{V} dV \quad (2.5)$$

This equation can be directly compared with the actual pressure derivative for a fast combustion detection, named the pressure difference method [24, 25].

Other common applications assume a polytropic evolution during the compression or expansion process in order to obtain control parameters, such as exhaust temperature estimation by modelling the engine-out temperature from the in-cylinder pressure evolution [26, 27], the intake air charge in the Δp method, or the residual mass estimation by modelling the expansion process.

2.3 Combustion modelling and control

A precise combustion feedback is the main advantage of in-cylinder pressure sensors. While in-cylinder pressure sensing is mandatory for combustion analysis in research and calibration, it also has potential to reduce emission and to improve the efficiency by closed-loop (CL) combustion control. CL combustion control would replace the current OL look-up tables control strategy [28]. In this scenario, calibration efforts would be reduced and the final control system would present many advantages in off-design conditions.

The benefits of introducing a CL control in conventional combustion engines is already in discussion, here some examples for CI [29–31] and for SI [32, 33] combustion strategies. But HCCI combustion, with a more complex combustion phasing prediction, would probably require combustion feedback for normal operation [34–38].

Although the representative information of the combustion evolution is at low frequencies, below 500 Hz [39, 40], if the pressure signal were low-pass filtered with such low limit with a high order filter, higher frequency content, relevant for the maximum pressure derivative estimation, could be missed. Therefore, in-cylinder pressure signal is filtered to avoid the pressure oscillations caused by resonance, which first modes are located at frequencies between 4 and 10 kHz.

The heat release law (HRL) is the main tool for analysing the combustion evolution [41, 42]. The HRL offers a simple equation which expresses the instantaneous heat released as a function of the in-cylinder pressure and Volume evolution. It assumes negligible mass transfer and constant composition when the valves are closed, i.e. the change in enthalpy of formation due to combustion is modelled as heat [43]. It starts from the first law of thermodynamics, namely:

$$dU = dQ - dW \quad (2.6)$$

by substituting dQ and dW by the change in internal energy and the work performed by the system respectively, obtaining:

$$mC_v dT = \frac{C_v}{R} d(pV) = dQ - pdV \quad (2.7)$$

where the gas law was derived for replacing mdT .

Finally, Equation (2.7) can be rearranged, the heat transfer to the system can be divided into the heat released by the fuel HRR and the wall heat transfer dQ_w , and the expressions of the specific heat ratio ($\gamma = c_p/c_v$) and the standard relation $R = C_p - c_v$ can be introduced, following:

$$HRR = \frac{\gamma}{\gamma - 1} pdV + \frac{1}{\gamma - 1} V dp + dQ_w \quad (2.8)$$

Some works have been devoted to develop polynomial correlations to express the specific heat ratio as a function of the temperature and the composition [44, 45], while others have worked on semi-empirical functions for wall heat transfer modelling [16]. As in the compression and expansion modelling, for most control applications, the wall heat transfer is included in a constant polytropic coefficient κ . When κ is used, the HRL is named the apparent HRL, and it is described by:

$$HRR = \frac{\kappa}{\kappa - 1} pdV + \frac{1}{\kappa - 1} V dp \quad (2.9)$$

An alternative to the HRL is the pressure ratio procedure [46–48]. Here, the mass fraction burnt MFB is computed by comparing the actual pressure with the motored one, as follows:

$$MFB = \frac{\frac{p(\alpha)}{p_m(\alpha)} - 1}{\max\left(\frac{p}{p_m}\right) - 1} \quad (2.10)$$

2.3.1 Combustion noise assessment

Traditionally, in CI diesel engines, combustion noise has been one of the major concerns that need to be addressed to satisfy legislation and customer demands [49]. Although the problem was solved by specific injection strategies, e.g. additional pilot injections [50, 51], next generation of IC engines can

represent a challenge for noise control, where pressure-based CL control is one of the solutions.

Figure 2.2 illustrates the basic mechanisms of combustion noise emission. Noise is a direct consequence of the bloc vibration, which is a cause of two type of forces: pressure and mechanical forces [52]. The former, beyond the low-frequency contribution of the piston movement, are caused by combustion. The latter are propagated through the mechanical systems in the cylinder and can excite several range of frequencies depending on the phenomena (piston slap, bearing clearances, element deformation, friction) [53]. Therefore, in-cylinder pressure signal does actually characterizes these two contributions.

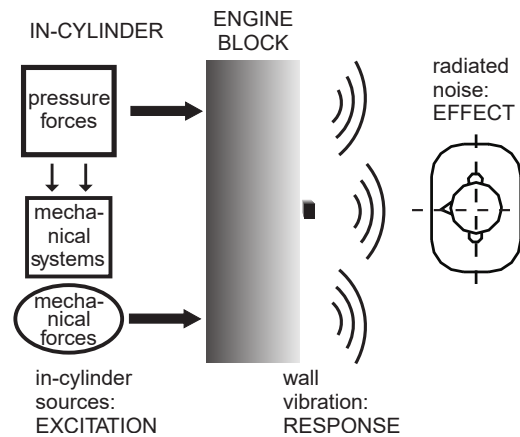


Figure 2.2. Basic mechanisms of combustion noise emission, adapted from [52].

The block attenuation method, is the most extended for noise level assessment. It consists on comparing the in-cylinder pressure with the radiated noise spectrum [54,55]. The final attenuation curve does typically show a valley between 1 and 6 kHz, after which the attenuation increases [56]. Figure 2.3 shows the attenuation curves found in three different experiments.

2.3.2 Autoignition prediction

Autoignition consists in a spontaneous combustion of an air-fuel mixture when it reaches some certain thermodynamic conditions [57]. Autoignition

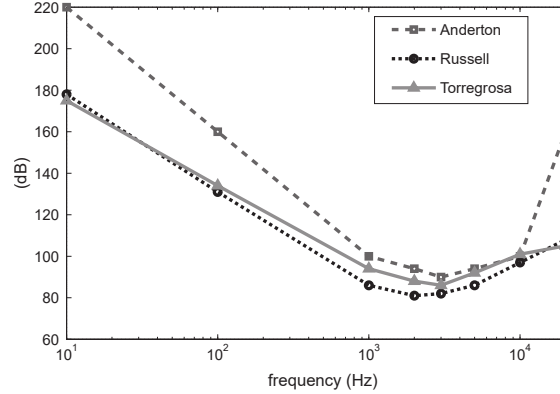


Figure 2.3. Standard attenuation curves, adapted from [56].

has been always a relevant topic as it characterizes the pre-mixed combustion before the diffusive flame in CI engines and the knock phenomenon in SI engines. Currently, many efforts are being made in its study and definition as new combustion concepts are driven by the chemical kinetics of autoignition [58, 59].

Autoignition can be modelled from in-cylinder pressure signal by modelling the combustion process with a single reaction model. The most widespread model is the integral method, presented by Livengood & Wu in 1955 [60, 61]. This methodology estimates the ignition delay for an autoignition event t_i in transient conditions by using the ignition delay under constant conditions of pressure and temperature τ . τ is computed from the in-cylinder conditions, namely pressure p and temperature of the unburned gases T_{ub} , as follows:

$$\tau = C_1 e^{\frac{C_3}{T_{ub}}} p^{C_2} \quad (2.11)$$

where C_1 , C_2 and C_3 are constants defining the autoignition process.

And the integral method is based on:

$$\int_{IVC}^{t_i} \frac{1}{\tau} d\alpha = 1 \quad (2.12)$$

Although this expression is used by several authors to model and control HCCI combustion timing [62–64] and to predict knock in SI engines [65, 66],

the validity of a single reaction assumption when a two-stage ignition occurs, such as cool flames, is discussed by several authors [67–69].

2.3.3 Emission models

Emission models provide an estimation of the combustion emissions from the in-cylinder conditions. They can be divided between those which are made by only looking at the output-input response [70–72] (black-box models) and those which are based on phenomenological studies [73–77].

Black-box models are used for complex phenomena where the physics are too complicated for a real-time application. On the one hand they have sufficient flexibility to offer a good accuracy on the training range, but on the other hand, if they were extrapolated out of this range, they would have significant deviations.

Regarding phenomenological models, there is a trade-off between complexity and physics fidelity [78]. For real-time applications, 0-D phenomenological models, where only equilibrium chemistry is considered, can be applied in conventional ECUs and provide a robust and accurate measurement [79].

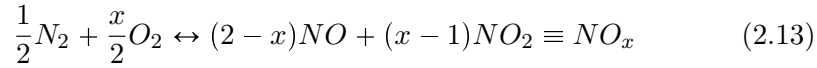
2.3.3.1 Diffusive flame NO_x emissions

NO_x models are of high interest due to the relevance of these contaminants during a diffusive flame combustion, such as in CI engines. A fast and precise NO_x measurement is required to regulate urea dosing in SCR devices [80] and models could be used for CL combustion control [81] to improve soot emissions and fuel efficiency.

Although online NO_x sensors are already in production [82], the dynamic response of the sensors is around 750 ms [83, 84] and hence, it is not sufficient to measure instantaneous NO_x emission in some specific cycles, such as WLTP. Some authors are proposing the use of virtual sensors, i.e. models, for on-board diagnosis (OBD) or to directly replace physical sensors, while others suggest a combination of models and sensors by a proper sensor fusion strategy in order to combine sensors static precision with models time response [85].

There are many control-oriented NO_x models with a variety of complexity and requirement inputs, some reviews can be found in [86–88].

Thermal NO_x formation. All the pressure-based models are based on the thermal NO_x formation mechanism. The reactions that take part on this mechanism were described firstly by Zeldovich [89] and later extended in what is named extended or modified Zeldovich mechanism [90]. This process can be reduced to one single global reaction in order to simplify the physics and reduce the calibration efforts [91], such as:



Which is governed by the net reaction rate of the reactions, forward k_{fw} and backward k_{bw} , and the total volume participating in the reaction V_r . NO_x are finally obtained by integrating over combustion, following:

$$\text{NO}_x = \int_{SOC}^{EOC} V_r \left(k_{fw}[\text{N}_2]^{\frac{1}{2}}[\text{O}_2]^{\frac{x}{2}} - k_{bw}[\text{NO}_x] \right) d\alpha \quad (2.14)$$

where the net reaction rate can be modelled by an Arrhenius function with the temperature of the reaction T_r and a constant that characterizes the activation temperature k_{act} , such as:

$$k_{fw} = e^{\frac{k_{act}}{T_r}} \quad (2.15)$$

Various approximations exist in literature [91–95]. As an example, in [92] the adiabatic flame temperature is considered the reaction temperature while the total volume of the reaction is assumed proportional to the heat release rate.

Reduction mechanism. In [96] a NO_x reduction mechanism was verified by artificial NO insertion at the intake. This NO_x reduction is explained by the NO_x passing through the diffusive flame combustion, either from EGR and IGR at the beginning of the combustion or from the current burnt gases that can be re-entrained into the flame. The conditions created around a diffusive flame [97] represent a reducing atmosphere where most of the NO_x should be eliminated [98,99]. An scheme of the reduction mechanism is shown in figure 2.4.

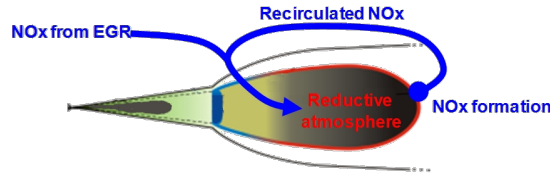


Figure 2.4. NO_x reduction scheme in a diffusive flame combustion.

Other NO_x formation reactions. Although thermal formation mechanism is the most representative of NO_x formation in conventional CI combustion, it is not the only one [100]. Prompt [101] and via N₂O mechanisms [102] are also important mechanisms that can be significant in low temperature combustions (LTC). In [103] the relevance of these mechanisms was investigated through thousands of simulations with different flame conditions, the main NO_x formation mechanisms are collected in Table 2.1.

Table 2.1. Main NO_x formation mechanisms.

| Reactions | name | References | Benefited from |
|--|----------------------|------------|--------------------------------------|
| $N_2 + O \leftrightarrow NO + N$ $N + O_2 \leftrightarrow NO + O$ $N + OH \leftrightarrow NO + H$ | Thermal | [89,90] | diffusive flame |
| $CH + N_2 \leftrightarrow HCN + N$ $HCN \rightarrow CN \rightarrow NCO \rightarrow NH \rightarrow N \rightarrow NO$ | Prompt | [101] | LTC |
| $N_2 + O + M \rightarrow N_2O + M$ $N_2O + O \rightarrow N_2 + O_2$ $N_2O + O \rightarrow 2NO$ | via N ₂ O | [101] | lean conditions and high pressure |

2.4 Resonance analysis

In-cylinder pressure waves are initiated by combustion and resonate along the combustion chamber during the expansion stroke. Figure 2.5 shows the pressure oscillations caused by the resonance in a heavy-duty engine where the resonance was heavily excited.

The acoustical response of a combustion chamber was studied for first time in 1938 by Draper [104]. He determined the resonant modes by applying cylindrical contour conditions to the pressure wave equation and solving the differential equation system by using Bessel functions. Finally, he obtained a proportional relation between the speed of sound a and the resonant frequencies f_{res} as a function of the bore D and a Bessel constant $B_{i,j}$, following:

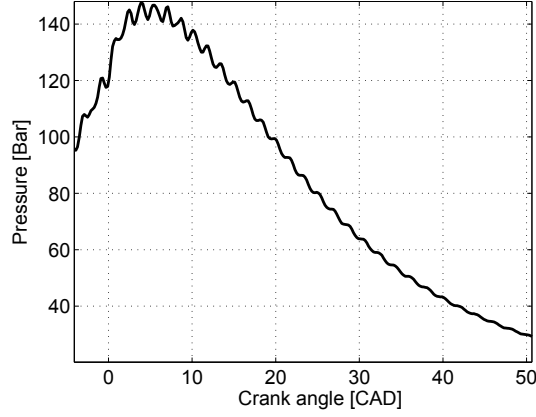


Figure 2.5. In-cylinder pressure resonance in a RCCI combustion cycle.

$$f_{res} = \frac{aB_{i,j}}{\pi D} \quad (2.16)$$

This expression is only valid for the radial modes. However, when combustion occurs (near TDC) resonant frequencies of axial modes are too high and can be neglected. The values of $B_{i,j}$ for the first resonant radial modes are collected in Table 2.2.

Table 2.2. First radial modes for a cylindrical chamber, collected from [104].

| | $B_{i,0}$ | $B_{i,1}$ |
|-----------|-----------|-----------|
| $B_{0,j}$ | 3.832 | 7.016 |
| $B_{1,j}$ | 1.841 | 5.332 |
| $B_{2,j}$ | 3 | 6.75 |

Because of the time-varying evolution of the resonant frequencies, a time-frequency analysis is required for a proper resonance characterization. Some examples can be found in [105, 106] by using short time Fourier transform (STFT), in [107, 108] by performing a Wigner-Ville spectral analysis, in [109] with the S-method (a combination of the STFT and the Wigner distribution) and in [110] through discrete wavelet transformation.

It must be highlighted some experimental and computational fluid dynamic (CFD) studies that found a different resonant frequency evolution when

a piston-in-bowl is used [111, 112]. Figure 2.6 shows CFD results where the resonant frequencies in the piston with bowl are slightly different than those found for a cylindrical assumption.

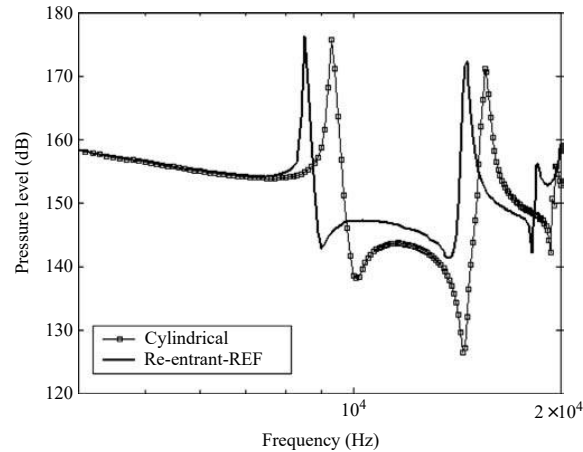


Figure 2.6. Influence of the bowl geometry on the frequency response with a single excitation source using a CFD approach [112].

Resonance can have undesirable consequences in the engine functionality. Although the block strongly attenuates the resonant frequencies above 6 kHz [56], the perception of the noise could be affected by higher resonant modes [52, 113, 114]. Furthermore, when resonance is heavily excited, it can cause significant engine damage. An analysis of the engine damage mechanisms of the resonance in SI engines was presented by Nates and Yates in [115].

Only a pair of works dealt with the inverse problem, i.e. detecting the resonant frequencies to estimate the speed of sound. Hickling et al., in the early 80's, proposed using in-cylinder pressure resonance to estimate the bulk gas temperature [116, 117], and Bodisco et al. in 2012, when modelling in-cylinder resonance evolution, suggested the estimation of the trapped mass [118]. Nevertheless, none of them developed the sufficient mathematical tools for its implementation and the little experimental data used was not sufficient for a validation, they were just suggestions about possible applications of the resonance.

2.4.1 Knock detection and control

Knock is an abnormal phenomenon in SI engines caused by the spontaneous combustion of the end gas. Knock is produced when the unburned gas temperature reaches sufficient energy for autoignition. This rapid combustion, heavily excites the cylinder resonant modes and consequently can damage the engine in certain conditions [119–121].

In [122–124] the knock phenomenon was studied by analysing experimental data. These studies conclude that knock has a random nature which can be fitted by statistical models but not with deterministic ones. Part of this randomness is due to cycle-by-cycle fluctuations in the SI combustion process. In [125] Galloni studied the influence of the main parameters that affect cyclic variation in SI engines. But even analysing cycle by cycle the information, knock still has a statistical response. The answer of unexpected knock occurrences is explained by temperature hot-spots and residual mass variations. The existence of temperature hot-spots where knock is initiated was demonstrated by optical measurement techniques, such as high speed direct light photography and laser schlieren filming, by several authors [126–129].

Knock control. Although several stochastic controllers have been recently proposed [130–132], the classical knock control strategy is the most common technique for knock control in SI engines. Classical knock control consists on advancing the spark angle by an amount k_{adv} to improve engine efficiency, while retarding a higher amount k_{ret} when a knocking cycle is detected in order to avoid engine damage [133, 134], that is:

$$SA(j) = \begin{cases} SA(j-1) - K_{ret} & \text{if knock,} \\ SA(j-1) + K_{adv} & \text{otherwise,} \end{cases} \quad (2.17)$$

Although this controller is actually deterministic in form, the response of the controller is stochastic. It is useful for a closed loop control of the knocking events, however it implies a spark advance (SA) variability even when the controller is performing the desired control for a borderline knock conditions. Figure 2.7 shows a typical SA output for a conventional knock controller.

Knock detection. Knock detection in SI engines is based on determining whether the end gas was autoignited or not [135]. Knock detection plays an

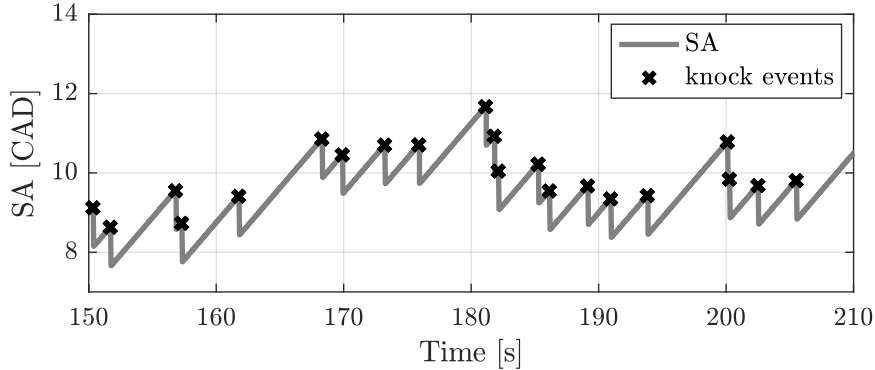


Figure 2.7. SA evolution when using the conventional controller strategy with $K_{ret} = 1.5$ CAD and $K_{adv} = 0.015$ CAD.

important role in any control strategy: a false detection of knocking cycles lowers the engine efficiency, while any detection failure can lead to engine damage.

The most obvious symptom when knock occurs is the oscillation of the in-cylinder pressure signal due to the autoignition [136], thus, knock detection algorithms for research and validation use in-cylinder pressure sensors [119,137]. Although knock can be detected by analysing the HRL evolution [121,138] or by more sophisticated signal processing techniques [105,139], most of the knock detection techniques are based on the analysis of the pressure trace in the time domain [140–143]. The most commonly used detection method is the maximum amplitude pressure oscillation (MAPO). It is based on quantifying the maximum value of the pass-band filtered pressure signal and considering a threshold for a knock evaluation. The frequency band for the filter is normally set between 4 and 20 kHz, which corresponds to the first modes of resonance. That is:

$$MAPO = \max p_{filt}^{4-20kHz} \quad (2.18)$$

In [144] the relevance of detecting low-knocking cycles is highlighted: if only heavy-knocking cycles were detected the control described in Equation (2.17) would dispose from less information and consequently has to perform a sharper control. In [145,146] a dynamic threshold is proposed, nevertheless, transient tests with varying operating conditions would not permit a fast

adaptation and low-knocking cycles would remain undetected. In commercial SI engines, which are not provided with an in-cylinder pressure sensor, knock detection is made with a block vibration sensor [147, 148].

Resonance evaluation. In contrast to SI engines with knock, the autoignition in HCCI engines is provoked. If this autoignition is not properly controlled, the combustion rate can lead to unacceptable pressure oscillations. Although some works directly contemplate the maximum pressure rate or the maximum combustion rate as constraints [149, 150], others use a quantification of the wave intensity. The most extended parameter is the ringing intensity (RI) [151, 152], defined as:

$$RI = \frac{1}{2\gamma} \frac{(\Delta p)^2 \sqrt{\gamma RT}}{p} \quad (2.19)$$

where Δp is the total pressure amplitude of the wave, i.e. the amplitude of the pressure signal band-pass filtered at the resonance band.

This index was simplified to a simpler function in [153–155], following:

$$RI_{red} = 2.88 \times 10^{-8} \frac{(n \max dp)^2}{\max p} \quad (2.20)$$

2.5 Conclusions

The instantaneous volume, which can be estimated from the crank angle evolution, is combined with the in-cylinder pressure signal to obtain a wide range of information, e.g. the evolution of the combustion, i.e. the heat release rate (HRR), or the bulk temperature, if an accurate estimation of the trapped mass is available.

This sort of information is a valuable input for several models for obtaining control parameters that might be mandatory for the next generation of IC engines, such as noise assessment in CI engines, knock detection and prediction in SI engines, NOx emissions for optimizing the soot-NOx trade off in CI conventional combustion or for closed-loop controlling the urea dosing in the after-treatment devices, or autoignition timing and combustion evolution for closed-loop control of the combustion phasing in new combustion concepts.

2.A Instantaneous crankshaft speed models

Instantaneous engine speed encoders are mandatory for injection control in current IC engines. Furthermore, they also give information about the combustion process as the crankshaft mechanism is directly affected by the pressure forces of the piston. Consequently the use of its signals in models and estimators are of high interest for commercial applications.

As it is described in [156], the movement of the crankshaft mechanism can be described by a second order differential equation, following:

$$T = I(\alpha)\ddot{\alpha} + \frac{1}{2} \frac{dI(\alpha)}{d\alpha} \dot{\alpha}^2 + g(\alpha) + Q(\alpha)F_p \quad (2.21)$$

where T is the constant torque of the engine that can be estimated through the brake mean effective pressure (BMEP), $I(\alpha)$ and its derivative are the inertial characteristics and $g(\alpha)$ the gravity forces, both can be determined from the description of the components, and finally $Q(\alpha)F_p$ represents the effect of the pressure forces.

The evolution of the crankshaft angular position can be profited for revealing important information on engine operation. Some authors propose the use of the Fourier transform for detect torque, misfires or fuel injection unbalance [157–160], others suggest to use it together with a crankshaft dynamic model to reconstruct the pressure signal [161–163], in conjunction with an observer [164, 165], or with neural networks (NN) [166–168].

Other possibility is reconstructing all in-cylinder pressure signals from a single cylinder pressure sensor and the crankshaft signal [169]. This is named as the key cylinder approach and seems a likely implementation in commercial engines to combine low costs and a good accuracy.

References

- [1] Jia L., Naber J. D. and Blough J. R. “Review of Sensing Methodologies for Estimation of Combustion Metrics”. *Journal of Combustion*, Vol. 2016, 2016.
(cited in pp. 13 and 27)
- [2] Luján J. M., Bermúdez V., Guardiola C. and Abbad A. “A methodology for combustion detection in diesel engines through in-cylinder pressure derivative signal”. *Mechanical Systems and Signal Processing*, Vol. 24 n° 7, pp. 2261–2275, 2010.
(cited in p. 27)

- [3] Samimy B. and Rizzoni G. “Engine knock analysis and detection using time-frequency analysis”. *SAE Technical Papers*, 1996. (cited in p. 27)
- [4] Kirsten M., Pirker G., Redtenbacher C., Wimmer A. and Chmela F. “Advanced Knock Detection for Diesel/Natural Gas Engine Operation”. *SAE International Journal of Engines*, Vol. 9 n° 3, 2016. (cited in p. 27)
- [5] Jung I., Jin J., Lee D., Lee S., Yang S. and Min K. “Closed-Loop Control Method for Monitoring and Improving the Diesel Combustion Noise”. *SAE Technical Papers*, Vol. 2016-June n° June, 2016. (cited in p. 27)
- [6] Haskara I. and Wang Y. . “Closed-loop combustion noise limit control for modern diesel combustion modes”. *IEEE Transactions on Control Systems Technology*, Vol. PP n° 99, 2016. (cited in p. 27)
- [7] Lamping M, Körfer T, Schnorbus T, Pischinger S and Chen Y. “Tomorrows Diesel Fuel Diversity - Challenges and Solutions”. *SAE Paper 2008-01-1731*, 2008. (cited in pp. 12 and 27)
- [8] Cains T., Pates D. and Warth M. “Improving speed and accuracy of gasoline and diesel engine testing via closed-loop combustion control”. *SAE Technical Papers*, 2012. (cited in p. 27)
- [9] Liu Y., Li L., Lu H., Deng J. and Hu Z. “In-Cycle Knocking Detection and Feedback Control Based on In-Cylinder Pressure and Ion Current Signal in a GDI Engine”. *SAE Technical Papers*, Vol. 2016-April n° April, 2016. (cited in p. 28)
- [10] Beasley M., Cornwell R., Fussey P., King R., Noble A., Salamon T., Truscott A. and Landsmann G. “Reducing diesel emissions dispersion by coordinated combustion feedback control”. *SAE Technical Papers*, 2006. (cited in p. 28)
- [11] Müller N. and Isermann R. “Control of mixture composition using cylinder pressure sensors”. *SAE Technical Papers*, 2001. (cited in p. 28)
- [12] Pipitone E. and Beccari A. “Determination of TDC in internal combustion engines by a newly developed thermodynamic approach”. *Applied Thermal Engineering*, Vol. 30 n° 14-15, pp. 1914–1926, 2010. (cited in pp. 28 and 30)
- [13] Staś M. J. “An universally applicable thermodynamic method for TDC determination”. *SAE Technical Papers*, 2000. (cited in pp. 28 and 30)
- [14] Baratta M. and Misul D. “Development and assessment of a new methodology for end of combustion detection and its application to cycle resolved heat release analysis in IC engines”. *Applied Energy*, Vol. 98, pp. 174–189, 2012. (cited in p. 28)
- [15] Payri F., Broatch A., Tormos B. and Marant V. “New methodology for in-cylinder pressure analysis in direct injection diesel engines - Application to combustion noise”. *Measurement Science and Technology*, Vol. 16 n° 2, pp. 540–547, 2005. (cited in p. 28)
- [16] Komninos N. P. and Rakopoulos C. D. “Heat transfer in HCCI phenomenological simulation models: A review”. *Applied Energy*, Vol. 181, pp. 179–209, 2016. (cited in pp. 29 and 32)
- [17] Woschni G. “A universally applicable equation for the instantaneous heat transfer coefficient in the internal combustion engine”. *SAE Technical Papers*, 1967. (cited in p. 29)
- [18] Tunestål P. “Self-tuning gross heat release computation for internal combustion engines”. *Control Engineering Practice*, Vol. 17 n° 4, pp. 518–524, 2009. (cited in p. 29)

- [19] Lancaster David R., Krieger Roger B. and Lienesch John H. "Measurement and analysis of engine pressure data". *SAE Prepr*, n° 750026, 1975. (cited in p. 30)
- [20] Homsy S. C. and Atreya A. "An experimental heat release rate analysis of a diesel engine operating under steady state conditions". *SAE Technical Papers*, 1997. (cited in p. 30)
- [21] Brunt M. F. J. and Pond C. R. "Evaluation of techniques for absolute cylinder pressure correction". *SAE Technical Papers*, 1997. (cited in pp. 30, 168, and 183)
- [22] Lee K., Yoon M. and Sunwoo M. "A study on pegging methods for noisy cylinder pressure signal". *Control Engineering Practice*, Vol. 16 n° 8, pp. 922–929, 2008. (cited in pp. 30, 168, and 183)
- [23] Fanelli I., Camporeale S. M. and Fortunato B. "Efficient On-Board Pegging Calculation from Piezo-Electric Sensor Signal for Real Time In-Cylinder Pressure Offset Compensation". *SAE International Journal of Engines*, Vol. 5 n° 2, pp. 672–682, 2012. (cited in pp. 30, 168, and 183)
- [24] Leonhardt S, Müller N and Isermann R. "Methods for engine supervision and control based on cylinder pressure information". *IEEE/ASME Transactions on Mechatronics*, Vol. 4 n° 3, pp. 235–245, 1999. (cited in pp. 13 and 30)
- [25] Chung J., Oh S., Min K. and Sunwoo M. "Real-time combustion parameter estimation algorithm for light-duty diesel engines using in-cylinder pressure measurement". *Applied Thermal Engineering*, Vol. 60 n° 1-2, pp. 33–43, 2013. (cited in p. 30)
- [26] Eriksson L. "Mean value models for exhaust system temperatures". *SAE Technical Papers*, 2002. (cited in pp. 31 and 208)
- [27] Mladek M. and Onder C. H. "A model for the estimation of inducted air mass and the residual gas fraction using cylinder pressure measurements". *SAE Technical Papers*, 2000. (cited in p. 31)
- [28] Schaub J., Koerfer T., Pischinger S. and Schnorbus T. "Cylinder Pressure Based Fuel Path Control for Non-Conventional Combustion Modes". *SAE International Journal of Engines*, Vol. 8 n° 5, 2015. (cited in p. 31)
- [29] Schnorbus T., Pischinger S., Körfer T., Lamping M., Tomazic D. and Tatur M. "Diesel combustion control with closed-loop control of the injection strategy". *SAE Technical Papers*, 2008. (cited in p. 31)
- [30] Saracino R., Gaballo M. R., Mammal S., Motz S., Carlucci A. and Benegiamo M. "Cylinder Pressure-Based Closed Loop Combustion Control: A Valid Support to Fulfill Current and Future Requirements of Diesel Powertrain Systems". *SAE Technical Papers*, Vol. 2015, 2015. (cited in pp. 13 and 31)
- [31] Schiefer D., Maennel R. and Nardoni W. "Advantages of diesel engine control using in-cylinder pressure information for closed loop control". *SAE Technical Papers*, 2003. (cited in p. 31)
- [32] Yoon P, Park S, Sunwoo M, Ohm I and Yoon KJ. "Closed-loop Control of Spark Advance and Air-fuel Ratio in SI Engines using Cylinder Pressure". *SAE Paper 2000-01-0933*, 2000. (cited in pp. 13 and 31)
- [33] Emiliano P. "Spark ignition feedback control by means of combustion phase indicators on steady and transient operation". *Journal of Dynamic Systems, Measurement and Control, Transactions of the ASME*, Vol. 136 n° 5, 2014. (cited in p. 31)

- [34] Jung D. and Iida N. "Closed-loop control of HCCI combustion for DME using external EGR and rebreathed EGR to reduce pressure-rise rate with combustion-phasing retard". *Applied Energy*, Vol. 138, pp. 315–330, 2015. (cited in p. 31)
- [35] Shaver G. M. and Gerdes J. C. "Cycle-to-cycle control of HCCI engines". In *American Society of Mechanical Engineers, Dynamic Systems and Control Division (Publication) DSC*, volume 72, pp. 403–412, 2003. (cited in p. 31)
- [36] Strandh P., Bengtsson J., Johansson R., Tunestål P. and Johansson B. "Cycle-to-cycle control of a dual-fuel HCCI engine". *SAE Technical Papers*, 2004. (cited in p. 31)
- [37] Karthikeya Sharma T., Amba Prasad Rao G. and Madhu Murthy K. "Control of peak pressures of an HCCI engine under varying swirl and operating parameters". *Frontiers in Energy*, Vol. 10 n° 3, pp. 337–346, 2016. (cited in p. 31)
- [38] Dempsey A. B., Walker N. R., Gingrich E. and Reitz R. D. "Comparison of low temperature combustion strategies for advanced compression ignition engines with a focus on controllability". *Combustion Science and Technology*, Vol. 186 n° 2, pp. 210–241, 2014. (cited in p. 31)
- [39] Tan C., Xu H., Ma H., Tian J. and Ghafourian A. "A Study of Methodology for the Investigation of Engine Transient Performance". *SAE Technical Papers*, Vol. 2014-October, 2014. (cited in p. 31)
- [40] Alberts T. E., Liu S. and Lally R. W. "Investigation of an inexpensive piezoelectric pressure sensor for internal combustion engine spark timing control". *SAE Technical Papers*, 2006. (cited in p. 31)
- [41] Martín Jaime. *Aportación al diagnóstico de la combustión en motores Diesel de inyección directa*. PhD Thesis, Universitat Politècnica de València. Departamento de Máquinas y Motores Térmicos - Departament de Màquines i Motors Tèrmics, 2007. (cited in p. 31)
- [42] Armas O. *Diagnostico experimental del proceso de combustión en motores Diesel de inyección directa*. PhD Thesis, Universitat Politècnica de València. Departamento de Máquinas y Motores Térmicos - Departament de Màquines i Motors Tèrmics, 1998. (cited in p. 31)
- [43] Gatowski J. A., Balles E. N., Chun K. M., Nelson F. E., Ekchian J. A. and Heywood J. B. "Heat release analysis of engine pressure data". *SAE Technical Papers*, 1984. (cited in p. 31)
- [44] Lapuerta M., Armas O. and Hernández J. J. "Diagnosis of DI Diesel combustion from in-cylinder pressure signal by estimation of mean thermodynamic properties of the gas". *Applied Thermal Engineering*, Vol. 19 n° 5, pp. 513–529, 1999. (cited in pp. 32, 116, 117, 147, 149, and 209)
- [45] Klein M. *A Specific Heat Ratio Model and Compression Ratio Estimation*. PhD Thesis, Linköping University, 2004. (cited in p. 32)
- [46] Giglio V., Iorio B., Police G. and Rispoli N. "In-cylinder Pressure Measurement for Control and Diagnostics in Spark Ignition Engines". *SAE Technical Papers*, 2005. (cited in p. 32)
- [47] Brunt M. F. J. and Emtage A. L. "Evaluation of burn rate routines and analysis errors". *SAE Technical Papers*, 1997. (cited in p. 32)
- [48] Przybyla G., Szlek A., Haggith D. and Sobiesiak A. "Fuelling of spark ignition and homogenous charge compression ignition engines with low calorific value producer gas". *Energy*, Vol. 116, pp. 1464–1478, 2016. (cited in p. 32)

- [49] Parizet E., Brocard J. and Piquet B. “Influence of noise and vibration to comfort in diesel engine cars running at idle”. *Acta Acustica united with Acustica*, Vol. 90 n° 5, pp. 987–993, 2004. (cited in p. 32)
- [50] Win Z., Gakkhar R. P., Jain S. C. and Bhattacharya M. “Investigation of diesel engine operating and injection system parameters for low noise, emissions, and fuel consumption using Taguchi methods”. *Proceedings of the Institution of Mechanical Engineers, Part D: Journal of Automobile Engineering*, Vol. 219 n° 10, pp. 1237–1251, 2005. (cited in p. 32)
- [51] Ghaffarpour M. R. and Noorpoor A. R. “A numerical study of the use of pilot or split rate injection to reduce diesel engine noise”. *Proceedings of the Institution of Mechanical Engineers, Part D: Journal of Automobile Engineering*, Vol. 221 n° 4, pp. 457–464, 2007. (cited in p. 32)
- [52] Payri F., Broatch A., Margot X. and Monelletta L. “Sound quality assessment of Diesel combustion noise using in-cylinder pressure components”. *Measurement Science and Technology*, Vol. 20 n° 1, 2009. (cited in pp. 33, 39, 65, 66, and 159)
- [53] Anderton D. “Relation between combustion system and engine noise”. *SAE Technical Papers*, 1979. (cited in p. 33)
- [54] Austen A. E. W. and Priede T. “Origins of diesel engine noise”. *SAE Technical Papers*, 1959. (cited in p. 33)
- [55] Russell M. F. and Haworth R. “Combustion noise from high speed direct injection diesel engines”. *SAE Technical Papers*, 1985. (cited in p. 33)
- [56] Torregrosa A. J., Broatch A., Martín J. and Monelletta L. “Combustion noise level assessment in direct injection Diesel engines by means of in-cylinder pressure components”. *Measurement Science and Technology*, Vol. 18 n° 7, pp. 2131–2142, 2007. (cited in pp. 33, 34, and 39)
- [57] Bradley D. “Autoignitions and detonations in engines and ducts”. *Philosophical Transactions of the Royal Society A: Mathematical, Physical and Engineering Sciences*, Vol. 370 n° 1960, pp. 689–714, 2012. (cited in p. 33)
- [58] Desantes J. M., Bermúdez V., López J. J. and López-Pintor D. “Experimental validation of an alternative method to predict high and low-temperature ignition delays under transient thermodynamic conditions for PRF mixtures using a Rapid Compression-Expansion Machine”. *Energy Conversion and Management*, Vol. 129, pp. 23–33, 2016. (cited in p. 34)
- [59] Desantes J. M., López J. J., Molina S. and López-Pintor D. “Theoretical development of a new procedure to predict ignition delays under transient thermodynamic conditions and validation using a Rapid Compression-Expansion Machine”. *Energy Conversion and Management*, Vol. 108, pp. 132–143, 2016. (cited in p. 34)
- [60] Livengood J. C. and Wu P. C. “Correlation of autoignition phenomena in internal combustion engines and rapid compression machines”. *Symposium (International) on Combustion*, Vol. 5 n° 1, pp. 347–356, 1955. (cited in pp. 34, 131, and 199)
- [61] Desantes J. M., López J. J., Molina S. and López-Pintor D. “Validity of the Livengood & Wu correlation and theoretical development of an alternative procedure to predict ignition delays under variable thermodynamic conditions”. *Energy Conversion and Management*, Vol. 105, pp. 836–847, 2015. (cited in p. 34)
- [62] Ohyama Y. “Engine control using combustion model”. *International Journal of Automotive Technology*, Vol. 2 n° 2, pp. 53–62, 2001. (cited in p. 34)

- [63] Rausen D. J., Stefanopoulou A. G., Kang J., Eng J. A. and Kuo T. “A mean-value model for control of Homogeneous Charge Compression Ignition (HCCI) engines”. *Journal of Dynamic Systems, Measurement and Control, Transactions of the ASME*, Vol. 127 n° 3, pp. 355–362, 2005. (cited in p. 34)
- [64] Choi Y. and Chen J. . “Fast prediction of start-of-combustion in HCCI with combined artificial neural networks and ignition delay model”. *Proceedings of the Combustion Institute*, Vol. 30 II, pp. 2711–2718, 2005. (cited in p. 34)
- [65] Chen L., Li T., Yin T. and Zheng B. “A predictive model for knock onset in spark-ignition engines with cooled EGR”. *Energy Conversion and Management*, Vol. 87, pp. 946–955, 2014. (cited in pp. 34 and 199)
- [66] Douaud A. M. and Eyzat P. “Four-octane-number method for predicting the anti-knock behavior of fuels and engines”. *SAE Technical Papers*, 1978. (cited in pp. 34, 199, and 204)
- [67] Yates A. D. B., Swarts A. and Viljoen C. L. “Correlating auto-ignition delays and knock-limited spark-advance data for different types of fuel”. *SAE Technical Papers*, 2005. (cited in p. 35)
- [68] Liang L. and Reitz R. D. “Spark Ignition engine combustion modeling using a level set method with detailed chemistry”. *SAE Technical Papers*, 2006. (cited in p. 35)
- [69] Edenhofer R., Lucka K. and Köhne H. “Low temperature oxidation of diesel-air mixtures at atmospheric pressure”. *Proceedings of the Combustion Institute*, Vol. 31 II, pp. 2947–2954, 2007. (cited in p. 35)
- [70] Tschanz F., Amstutz A., Onder C. H. and Guzzella L. “A real-time soot model for emission control of a diesel engine”. In *IFAC Proceedings Volumes (IFAC-PapersOnline)*, pp. 222–227, 2010. (cited in p. 35)
- [71] Johri R., Salvi A. and Filipi Z. “Real-time transient soot and NOx virtual sensors for diesel engine using neuro-fuzzy model tree and orthogonal least squares”. *Journal of Engineering for Gas Turbines and Power*, Vol. 134 n° 9, 2012. (cited in p. 35)
- [72] Asad U. and Zheng M. “Exhaust gas recirculation for advanced diesel combustion cycles”. *Applied Energy*, Vol. 123, pp. 242–252, 2014. (cited in pp. 35, 58, and 60)
- [73] Hiroyasu H., Kadota T. and Arai M. “Development and use of a spray modelling to predict diesel engine efficiency and pollutant emissions (part 1 combustion modelling)”. *Bulletin of the JSME*, Vol. 26 n° 214, pp. 569–575, 1983. (cited in p. 35)
- [74] Kirchen P. *Steady-State and Transient Diesel Soot Emissions: Development of a Mean Value Soot Model and Exhaust-Stream and In-Cylinder Measurements*. PhD Thesis, ETH Zurich, 2008. (cited in p. 35)
- [75] Rezaei R., Dinkelacker F., Tilch B., Delebinski T. and Brauer M. “Phenomenological modeling of combustion and NOx emissions using detailed tabulated chemistry methods in diesel engines”. *International Journal of Engine Research*, Vol. 17 n° 8, pp. 846–856, 2016. (cited in p. 35)
- [76] Egnell R. *On Zero-dimensional Modelling of Combustion and NOx Formation in Diesel Engines*. PhD Thesis, Lund Institute of Technology, 2001. (cited in p. 35)
- [77] Westlund A., Lindström M. and Ångström H. “A one-dimensional model for heat release rate and emission formation in diesel engines based on correlations for entrainment rate, lift-off length and ignition delay: Validation for transient conditions”. *Proceedings of the Institution of Mechanical Engineers, Part D: Journal of Automobile Engineering*, Vol. 226 n° 9, pp. 1243–1258, 2012. (cited in p. 35)

- [78] Westlund A. *Simplified models for emission formation in diesel engines during transient operation*. PhD Thesis, Kungliga Tekniska Högskolan (KTH), 1998. (cited in p. 35)
- [79] Nelson-Gruel D., Chamaillard Y. and Aljarbouh A. “Modeling and estimation of the pollutants emissions in the Compression Ignition diesel engine”. In *2016 IEEE Conference on Control Applications, CCA 2016*, pp. 317–322, 2016. (cited in p. 35)
- [80] Willems F, Cloudt R, van den Eijnden E and et al. M van Genderen. “Is Closed-Loop SCR Control Required to Meet Future Emission Targets?”. *SAE paper 2007-01-1574*, 2007. (cited in pp. 9 and 35)
- [81] Tschanz F., Amstutz A., Onder C. H. and Guzzella L. “Feedback control of particulate matter and nitrogen oxide emissions in diesel engines”. *Control Engineering Practice*, Vol. 21 n° 12, pp. 1809–1820, 2013. (cited in p. 35)
- [82] Riegel J, Neumann H and Wiedenmann H-M. “Exhaust gas sensors for automotive emission control”. *Solid State Ionics*, Vol. 152-153, pp. 783–800, 2002. (cited in pp. 9, 35, 61, and 62)
- [83] Mrosek M., Sequenz H. and Isermann R. “Identification of emission measurement dynamics for Diesel engines”. In *IFAC Proceedings Volumes (IFAC-PapersOnline)*, volume 18, pp. 11839–11844, 2011. (cited in pp. 35 and 68)
- [84] Manchur T. B. and Checkel M. D. “Time resolution effects on accuracy of real-time NOx emissions measurements”. *SAE Technical Papers*, 2005. (cited in pp. 35 and 63)
- [85] Guardiola C., Climent H., Pla B. and Blanco-Rodriguez D. “ECU-oriented models for NOx prediction. Part 2: Adaptive estimation by using an NOx sensor”. *Proceedings of the Institution of Mechanical Engineers, Part D: Journal of Automobile Engineering*, Vol. 229 n° 10, pp. 1345–1360, 2015. (cited in p. 35)
- [86] Guardiola C., Pla B., Blanco-Rodriguez D. and Calendini P. O. “ECU-oriented models for NOx prediction. Part 1: A mean value engine model for NOx prediction”. *Proceedings of the Institution of Mechanical Engineers, Part D: Journal of Automobile Engineering*, Vol. 229 n° 8, pp. 992–1015, 2015. (cited in p. 35)
- [87] Quérel C, Grondin O and Letellier C. “State of the Art and Analysis of Control Oriented NOx Models”. *SAE paper 2012-01-0723*, 2012. (cited in pp. 9 and 35)
- [88] Kihás D. and Uchanski M. R. “Engine-Out NOx Models for on-ECU Implementation: A Brief Overview”. *SAE Technical Papers*, Vol. 2015-April n° April, 2015. (cited in p. 35)
- [89] Zeldovich Y.B. “The oxidation of nitrogen on combustion and explosions”. *Acta Physicochim URSS*, 1946. (cited in pp. 36 and 37)
- [90] Bowman C. T. “Kinetics of pollutant formation and destruction in combustion”. *Progress in Energy and Combustion Science*, Vol. 1 n° 1, pp. 33–45, 1975. (cited in pp. 36 and 37)
- [91] Asprion J., Chinellato O. and Guzzella L. “A fast and accurate physics-based model for the NOx emissions of Diesel engines”. *Applied Energy*, Vol. 103, pp. 221–233, 2013. (cited in p. 36)
- [92] Guardiola C., López J. J., Martín J. and García-Sarmiento D. “Semiempirical in-cylinder pressure based model for NOx prediction oriented to control applications”. *Applied Thermal Engineering*, Vol. 31 n° 16, pp. 3275–3286, 2011. (cited in pp. 36, 217, 219, and 220)

- [93] Karaky H., Mauviot G., Tauzia X. and Maiboom A. “Development and Validation of a New Zero-Dimensional Semi-Physical NOx Emission Model for a D.I. Diesel Engine Using Simulated Combustion Process”. *SAE International Journal of Engines*, Vol. 8 n° 4, 2015. (cited in p. 36)
- [94] Quérel C., Grondin O. and Letellier C. “Semi-physical mean-value NOx model for diesel engine control”. *Control Engineering Practice*, Vol. 40, pp. 27–44, 2015. (cited in p. 36)
- [95] Lee J., Lee S., Park W., Min K., Song H. H., Choi H., Yu J. and Cho S. H. “The development of real-time NOx estimation model and its application”. *SAE Technical Papers*, Vol. 2, 2013. (cited in p. 36)
- [96] Payri F., Arrègle J., Javier López J. and Mocholí E. “Diesel NOx modeling with a reduction mechanism for the initial NOx coming from EGR or re-entrained burned gases”. *SAE Technical Papers*, 2008. (cited in p. 36)
- [97] Dec J. E. “A conceptual model of DI diesel combustion based on laser-sheet imaging”. *SAE Technical Papers*, 1997. (cited in p. 36)
- [98] Krutzsch B., Wenninger G., Weibel M., Stapf P., Funk A., Webster D. E., Chaize E., Kasemo B., Martens J. and Kiennemann A. “Reduction of NOx in lean exhaust by selective NOx-Recirculation (SNR-Technique) Part I: System and decomposition process”. *SAE Technical Papers*, 1998. (cited in p. 36)
- [99] Chaize E., Webster D. E., Krutzsch B., Wenninger G., Weibel M., Hodjati S., Petit C., Pitchon V., Kiennemann A., Loenders R., Monticelli O., Jacobs P. A., Martens J. A. and Kasemo B. “Reduction of NOx in lean exhaust by selective NOx-Recirculation (SNR-Technique) part II: NOx storage materials”. *SAE Technical Papers*, 1998. (cited in p. 36)
- [100] Hernández J. J., Pérez-Collado J. and Sanz-Argent J. “Role of the chemical kinetics on modeling NOx emissions in diesel engines”. *Energy and Fuels*, Vol. 22 n° 1, pp. 262–272, 2008. (cited in p. 37)
- [101] Fenimore C. P. “Formation of nitric oxide in premixed hydrocarbon flames”. *Symposium (International) on Combustion*, Vol. 13 n° 1, pp. 373–380, 1971. (cited in p. 37)
- [102] Malte P. C. and Pratt D. T. “Measurement of atomic oxygen and nitrogen oxides in jet-stirred combustion”. *Symposium (International) on Combustion*, Vol. 15 n° 1, pp. 1061–1070, 1975. (cited in p. 37)
- [103] Desantes J. M., López J. J., Redón P. and Arrègle J. “Evaluation of the thermal NO formation mechanism under lowtemperature diesel combustion conditions”. *International Journal of Engine Research*, Vol. 13 n° 6, pp. 531–539, 2012. (cited in p. 37)
- [104] Draper C. S. “The physical effects of detonation in a closed cylindrical chamber”. Technical report, National Advisory Committee for Aeronautics, 1938. (cited in pp. 37, 38, and 114)
- [105] Akimoto K., Komatsu H. and Kurauchi A. “Development of pattern recognition knock detection system using short-time fourier transform”. In *IFAC Proceedings Volumes (IFAC-PapersOnline)*, volume 7, pp. 366–371, 2013. (cited in pp. 38 and 41)
- [106] Scholl D., Davis C., Russ S. and Barash T. “The volume acoustic modes of spark-ignited internal combustion chambers”. *SAE Technical Papers*, 1998. (cited in pp. 38 and 120)

- [107] König D. and Böhme J. F. “Wigner-Ville spectral analysis of automotive signals captured at knock”. *Applied Signal Processing*, Vol. 3 n° 1, pp. 54–64, 1996.
(cited in p. 38)
- [108] Samimy B. and Rizzoni G. “Mechanical Signature Analysis Using Time-Frequency Signal Processing: Application to Internal Combustion Engine Knock Detection”. *Proceedings of the IEEE*, Vol. 84 n° 9, pp. 1330–1343, 1996.
(cited in p. 38)
- [109] Stanković L. and Böhme J. F. “Time-frequency analysis of multiple resonances in combustion engine signals”. *Signal Processing*, Vol. 79 n° 1, pp. 15–28, 1999.
(cited in p. 38)
- [110] Gerardin R. C., Huallpa B. R. N., Alves M. A. F. and De França Arruda J. R. “Analysis of spark ignition engine knock signals using fourier and discrete wavelet transform”. *SAE Technical Papers*, 2009.
(cited in p. 38)
- [111] Torregrosa A. J., Broatch A., Margot X., Marant V. and Beauge Y. “Combustion chamber resonances in direct injection automotive diesel engines: A numerical approach”. *International Journal of Engine Research*, Vol. 5 n° 1, pp. 83–91, 2004.
(cited in pp. 39 and 119)
- [112] Broatch A., Margot X., Gil A. and Donayre C. “Computational study of the sensitivity to ignition characteristics of the resonance in di diesel engine combustion chambers”. *Engineering Computations (Swansea, Wales)*, Vol. 24 n° 1, pp. 77–96, 2007.
(cited in pp. 39 and 119)
- [113] Pflueger M., Hoeldrich R., Brandl F. K. and Biermayer W. “Subjective assessment of roughness as a basis for objective vehicle interior noise quality evaluation”. *SAE Technical Papers*, 1999.
(cited in p. 39)
- [114] Liu H., Zhang J., Guo P., Bi F., Yu H. and Ni G. “Sound quality prediction for engine-radiated noise”. *Mechanical Systems and Signal Processing*, Vol. 56, pp. 277–287, 2015.
(cited in p. 39)
- [115] Nates R. J. and Yates A. D. B. “Knock damage mechanisms in spark-ignition engines”. *SAE Technical Papers*, 1994.
(cited in p. 39)
- [116] Hickling R., Hamburg J. A., Feldmaier D. A. and Chung J. “Method of measurement of bulk temperatures of gas in engine cylinders”, 1979.
(cited in p. 39)
- [117] Hickling R., Feldmaier D. A., Chen F. H. and Morel J. S. “Cavity resonances in engine combustion chambers and some applications”. *Journal of the Acoustical Society of America*, Vol. 73 n° 4, pp. 1170–1178, 1983.
(cited in p. 39)
- [118] Bodisco T., Reeves R., Situ R. and Brown R. “Bayesian models for the determination of resonant frequencies in a di diesel engine”. *Mechanical Systems and Signal Processing*, Vol. 26 n° 1, pp. 305–314, 2012.
(cited in p. 39)
- [119] Zhen X., Wang Y., Xu S., Zhu Y., Tao C., Xu T. and Song M. “The engine knock analysis - An overview”. *Applied Energy*, Vol. 92, pp. 628–636, 2012.
(cited in pp. 11, 40, and 41)
- [120] McKenzie J. and Cheng W. K. “The Anatomy of Knock”. *SAE Technical Papers*, Vol. 2016-April, 2016.
(cited in p. 40)
- [121] Forte C., Corti E. and Bianchi G. M. “Combined experimental and numerical analysis of knock in spark ignition engines”. In *Proceedings of the ASME Internal Combustion Engine Division Fall Technical Conference 2009*, pp. 473–488, 2009.
(cited in pp. 40 and 41)

- [122] Spelina J. M., Peyton Jones J. C. and Frey J. “Characterization of knock intensity distributions: Part 1: Statistical independence and scalar measures”. *Proceedings of the Institution of Mechanical Engineers, Part D: Journal of Automobile Engineering*, Vol. 228 n° 2, pp. 117–128, 2014. (cited in pp. 40 and 197)
- [123] Spelina J. M., Peyton Jones J. C. and Frey J. “Characterization of knock intensity distributions: Part 2: Parametric models”. *Proceedings of the Institution of Mechanical Engineers, Part D: Journal of Automobile Engineering*, Vol. 227 n° 12, pp. 1650–1660, 2013. (cited in p. 40)
- [124] Leppard W. R. “Individual-cylinder knock occurrence and intensity in multicylinder engines”. *SAE Technical Papers*, 1982. (cited in p. 40)
- [125] Galloni E. “Analyses about parameters that affect cyclic variation in a spark ignition engine”. *Applied Thermal Engineering*, Vol. 29 n° 5-6, pp. 1131–1137, 2009. (cited in p. 40)
- [126] König G., Maly R. R., Bradley D., Lau A. K. C. and Sheppard C. G. W. “Role of exothermic centres on knock initiation and knock damage”. *SAE Technical Papers*, 1990. (cited in p. 40)
- [127] Schießl R. and Maas U. “Analysis of endgas temperature fluctuations in an SI engine by laser-induced fluorescence”. *Combustion and Flame*, Vol. 133 n° 1-2, pp. 19–27, 2003. (cited in p. 40)
- [128] Kawahara N., Tomita E. and Sakata Y. “Auto-ignited kernels during knocking combustion in a spark-ignition engine”. *Proceedings of the Combustion Institute*, Vol. 31 II, pp. 2999–3006, 2007. (cited in pp. 40 and 197)
- [129] Pöschl M. and Sattelmayer T. “Influence of temperature inhomogeneities on knocking combustion”. *Combustion and Flame*, Vol. 153 n° 4, pp. 562–573, 2008. (cited in p. 40)
- [130] Peyton Jones J. C., Spelina J. M. and Frey J. “An optimal cumsum-based knock controller”. In *IFAC Proceedings Volumes (IFAC-PapersOnline)*, volume 7, pp. 372–377, 2013. (cited in p. 40)
- [131] Peyton Jones J. C., Spelina J. M. and Frey J. “Likelihood-based control of engine knock”. *IEEE Transactions on Control Systems Technology*, Vol. 21 n° 6, pp. 2169–2180, 2013. (cited in p. 40)
- [132] Thomasson A., Shi H., Lindell T., Eriksson L., Shen T. and Peyton Jones J. C. “Experimental Validation of a Likelihood-Based Stochastic Knock Controller”. *IEEE Transactions on Control Systems Technology*, Vol. 24 n° 4, pp. 1407–1418, 2016. (cited in p. 40)
- [133] Peyton Jones J. C., Frey J. and Shayestehmanesh S. “Stochastic Simulation and Performance Analysis of Classical Knock Control Algorithms”. *IEEE Transactions on Control Systems Technology*, Vol. PP n° 99, 2016. (cited in pp. 40 and 197)
- [134] Kiencke U. and Nielsen L. *Automotive control system for engine, driveline, and vehicle*. New York: Springer, 2005. (cited in p. 40)
- [135] Worret R., Bernhardt S., Schwarz F. and Spicher U. “Application of different cylinder pressure based knock detection methods in spark ignition engines”. *SAE Technical Papers*, 2002. (cited in p. 40)
- [136] König G. and Sheppard C. G. W. “End gas autoignition and knock in a spark ignition engine”. *SAE Technical Papers*, 1990. (cited in p. 41)

- [137] Millo F. and Ferraro C. V. “Knock in S.I. Engines: A comparison between different techniques for detection and control”. *SAE Technical Papers*, 1998. (cited in p. 41)
- [138] Borg J. M. and Alkidas A. C. “Characterization of autoignition in a knocking si engine using heat release analysis”. *SAE Technical Papers*, 2006. (cited in p. 41)
- [139] Witwit A.R., Yasinb A., Abasc M.A. and Gitanod H. “Modern Methods in Engine Knock Signal Detection”. *Procedia Technology (ICEEI 2013)*, Vol. 11, pp. 40–50, 2013. (cited in p. 41)
- [140] Brecq G. and Le Corre O. “Modeling of in-cylinder pressure oscillations under knocking conditions: Introduction to pressure envelope curve”. *SAE Technical Papers*, 2005. (cited in p. 41)
- [141] Brecq G., Bellettre J. and Tazerout M. “A new indicator for knock detection in gas SI engines”. *International Journal of Thermal Sciences*, Vol. 42 n° 5, pp. 523–532, 2003. (cited in p. 41)
- [142] Cavina N., Corti E., Minelli G., Moro D. and Solieri L. “Knock indexes normalization methodologies”. *SAE Technical Papers*, 2006. (cited in p. 41)
- [143] Lee J., Hwang S., Lim J., Jeon D. and Cho Y. “A new knock-detection method using cylinder pressure, block vibration and sound pressure signals from a SI engine”. *SAE Technical Papers*, 1998. (cited in p. 41)
- [144] Peyton Jones J. C., Spelina J. M. and Frey J. “Optimizing knock thresholds for improved knock control”. *International Journal of Engine Research*, Vol. 15 n° 1, pp. 123–132, 2014. (cited in p. 41)
- [145] Galloni E. “Dynamic knock detection and quantification in a spark ignition engine by means of a pressure based method”. *Energy Conversion and Management*, Vol. 64, pp. 256–262, 2012. (cited in p. 41)
- [146] Galloni E. “Knock-limited spark angle setting by means of statistical or dynamic pressure based methods”. *Energy Conversion and Management*, Vol. 116, pp. 11–17, 2016. (cited in p. 41)
- [147] Xiaofeng G., Stone R., Hudson C. and Bradbury I. “The detection and quantification of knock in spark ignition engines”. *SAE Technical Papers*, 1993. (cited in p. 42)
- [148] Etefagh M. M., Sadeghi M. H., Pirouzpanah V. and Arjmandi Tash H. “Knock detection in spark ignition engines by vibration analysis of cylinder block: A parametric modeling approach”. *Mechanical Systems and Signal Processing*, Vol. 22 n° 6, pp. 1495–1514, 2008. (cited in p. 42)
- [149] Benajes J., Pastor J. V., García A. and Monsalve-Serrano J. “The potential of RCCI concept to meet EURO VI NOx limitation and ultra-low soot emissions in a heavy-duty engine over the whole engine map”. *Fuel*, Vol. 159, pp. 952–961, 2015. (cited in pp. 42 and 92)
- [150] Benajes J., Pastor J. V., García A. and Boronat V. “A RCCI operational limits assessment in a medium duty compression ignition engine using an adapted compression ratio”. *Energy Conversion and Management*, Vol. 126, pp. 497–508, 2016. (cited in pp. 42 and 92)
- [151] Eng J. A. “Characterization of pressure waves in HCCI combustion”. *SAE Technical Papers*, 2002. (cited in pp. 42 and 116)
- [152] Sjöberg M. and Dec J. E. “Effects of engine speed, fueling rate, and combustion phasing on the thermal stratification required to limit HCCI knocking intensity”. *SAE Technical Papers*, 2005. (cited in p. 42)

- [153] Das P., Subbarao P. M. V. and Subrahmanyam J. P. “Study of Combustion Behavior and Combustion Stability of HCCI-DI Combustion for a Wide Operating Range using a Low Cost Novel Experimental Technique”. *SAE Technical Papers*, Vol. 2014-October, 2014. (cited in p. 42)
- [154] Yun H., Wermuth N. and Najt P. “Extending the high load operating limit of a naturally-aspirated gasoline HCCI combustion engine”. *SAE Technical Papers*, pp. 681–699, 2010. (cited in p. 42)
- [155] Szybist J. P., Dean Edwards K., Foster M., Confer K. and Moore W. “Characterization of engine control authority on HCCI combustion as the high load limit is approached”. *SAE International Journal of Engines*, Vol. 6 n° 1, pp. 553–568, 2013. (cited in p. 42)
- [156] Li H. and Stone B. J. “Time domain modelling of a reciprocating engine”. *Mechanical Systems and Signal Processing*, Vol. 13 n° 1, pp. 169–178, 1999. (cited in pp. 43 and 90)
- [157] Ali S. A. and Saraswati S. “Cycle-by-cycle estimation of IMEP and peak pressure using crankshaft speed measurements”. *Journal of Intelligent and Fuzzy Systems*, Vol. 28 n° 6, pp. 2761–2770, 2015. (cited in p. 43)
- [158] Ma X., Xia Z., Wu H. and Huang X. “Combined Frequency Domain Analysis and Fuzzy Logic for Engine Misfire Diagnosis”. *SAE Technical Papers*, Vol. 2015-April n° April, 2015. (cited in p. 43)
- [159] Liu Y. and Zhangsaifei. “Measurement and diagnostic system for crankshaft of diesel engine”. In *ICCCASM 2010 - 2010 International Conference on Computer Application and System Modeling, Proceedings*, volume 13, pp. V13370–V13371, 2010. (cited in p. 43)
- [160] Macián V., Luján J. M., Guardiola C. and Yuste P. “DFT-based controller for fuel injection unevenness correction in turbocharged diesel engines”. *IEEE Transactions on Control Systems Technology*, Vol. 14 n° 5, pp. 819–827, 2006. (cited in p. 43)
- [161] Johnsson R. and Ågren A. “Cylinder pressure reconstruction from vibration and speed measurements on IC engines”. In *Proceedings of the 2004 International Conference on Noise and Vibration Engineering, ISMA*, pp. 965–974, 2004. (cited in p. 43)
- [162] Mocanu F. and Taraza D. “Estimation of main combustion parameters from the measured instantaneous crankshaft speed”. *SAE Technical Papers*, Vol. 2, 2013. (cited in p. 43)
- [163] Chen S. K. and Chen S. “Engine diagnostics by dynamic shaft measurement: A progress report”. *SAE Technical Papers*, 1993. (cited in p. 43)
- [164] Zweiri Y. H. and Seneviratne L. D. “Diesel engine indicated and load torque estimation using a non-linear observer”. *Proceedings of the Institution of Mechanical Engineers, Part D: Journal of Automobile Engineering*, Vol. 220 n° 6, pp. 775–785, 2006. (cited in p. 43)
- [165] Al-Durra A., Fiorentini L., Canova M. and Yurkovich S. “A model-based estimator of engine cylinder pressure imbalance for combustion feedback control applications”. In *Proceedings of the American Control Conference*, pp. 991–996, 2011. (cited in p. 43)
- [166] Saraswati S. and Chand S. “Reconstruction of cylinder pressure for SI engine using recurrent neural network”. *Neural Computing and Applications*, Vol. 19 n° 6, pp. 935–944, 2010. (cited in p. 43)

-
- [167] Taglialatela F., Lavorgna M., Mancaruso E. and Vaglieco B. M. “Determination of combustion parameters using engine crankshaft speed”. *Mechanical Systems and Signal Processing*, Vol. 38 n° 2, pp. 628–633, 2013. (cited in p. 43)
- [168] Gu F., Jacob P. J. and Ball A. D. “RBF neural network model for cylinder pressure reconstruction in internal combustion engines”. In *IEE Colloquium (Digest)*, pp. 4/1–4/11, 1996. (cited in p. 43)
- [169] Hamedović H., Raichle F. and Böhme J. F. “In-cylinder pressure reconstruction for multicylinder SI-engine by combined processing of engine speed and one cylinder pressure”. In *ICASSP, IEEE International Conference on Acoustics, Speech and Signal Processing - Proceedings*, volume V, pp. V677–V680, 2005. (cited in p. 43)

Chapter 3

Charge and composition estimation in IC engines

Contents

| | | |
|------------|---------------------------------------|-----------|
| 3.1 | Introduction | 58 |
| 3.2 | Flow and composition sensors | 58 |
| 3.2.1 | Air mass flow sensor | 59 |
| 3.2.2 | Exhaust gas recirculation measurement | 59 |
| 3.2.3 | Oxygen concentration sensors | 61 |
| 3.3 | Models and virtual sensors | 63 |
| 3.3.1 | Speed density method | 63 |
| 3.3.2 | The orifice principle | 64 |
| 3.3.3 | Δp method | 65 |
| 3.3.4 | Residual gas fraction determination | 65 |
| 3.3.5 | Injected fuel mass | 67 |
| 3.4 | Data fusion techniques | 67 |
| 3.4.1 | Sensor dynamics | 68 |
| 3.4.2 | Intake manifold dynamics | 68 |
| 3.4.3 | Observers | 70 |
| 3.5 | Conclusions | 73 |
| | References | 74 |

3.1 Introduction

The estimation and control of the intake charge and composition is already crucial in conventional combustion modes: the composition in SI engines must be maintained in stoichiometric conditions in order to properly operate the three way catalyst (TWC) [1–5], and the soot-NO_x trade-off in CI engines is highly affected by EGR [6–11]. However, an accurate intake composition estimation in engines working with new combustion concepts will be necessary not only for emissions control, but also for combustion stability [12–17].

An accurate and fast composition estimation is a big challenge for the current set of sensors included in commercial ECUs. Most of the models and sensors estimate the intake charge composition and assume an equal distribution in the cylinders. Nevertheless, cylinder-to-cylinder dispersion exists, and several authors have pointed out that estimating the charge and controlling the injection at each cylinder individually could significantly improve the performance of the engine [18–21]. In addition, as commented in the first chapter, the air-path loop has been growing in complexity: low-pressure EGR loops are being included in conjunction or replacing high-pressure EGR loops [22] and new VVT strategies are being used to modify in-cylinder charge [23, 24].

In the following lines an overview of the state of the art in models, sensors, and observers for composition and charge estimation is presented.

3.2 Flow and composition sensors

Modern sensing technologies are providing IC engines with new sensors, which can be used for real-time control purposes or off-line combustion analysis [25–27]. Concurrently, advanced combustion strategies demand additional information to efficiently control the combustion. As an example, the implantation of new after-treatment devices have benefited the inclusion of extra sensors, such as smart NO_x and exhaust temperature sensors, which can be combined by models and observers to estimate control parameters [28]. However, the cost, durability, and dimensions of many sensors preclude its applicability in commercial applications dividing those between on-board and test bench sensors. The former are characterized by small dimensions and low costs while the latter are used for high precision and accuracy.

3.2.1 Air mass flow sensor

From 1973 to the 90s, most of air measurement systems were based on vane-type sensors, which consists in a sensor flap or vane located in the flow duct and restrained by a spring. Vane-type sensors have been replaced by hot wire/film anemometers, which is the current technology used in the automotive industry [29–31]. The principle of these sensors is sketched in Figure 3.1. Two temperature dependent metal film resistors are located in a sensor flow channel. A first element R_T provides bridge tracking to maintain a fixed temperature in R_S . The electrical current required is a measurement of the air mass flow [32].

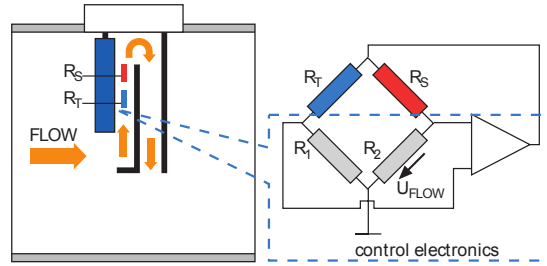


Figure 3.1. Operating principle scheme of a hot-film anemometer, adapted from [32].

Hot wire anemometers can present a faster response, but dust and particles which are not filtered by the air filter can damage the thin hot-wire (around $70\mu\text{m}$). More robust hot-film anemometers are a compromise solution between durability and time response. Commercial hot film anemometers have a time response of some ms (30-50 ms) and can present a non-linear time-response [33–35]. However, hot-film anemometers are subjected to severe ageing due to the accumulation of dust on the sensing element, which causes a bias that can reach 20% of the measured value [36–38].

3.2.2 Exhaust gas recirculation measurement

EGR is defined as the ratio between the burnt gases recirculated into the cylinder and the total mass. Following:

$$r_{EGR} = \frac{m_{EGR}}{m_{air} + m_{EGR} + m_{fuel}} \quad (3.1)$$

Nevertheless, because fuel mass is at least 14.5 times lower than the air charge, much less in CI engines, EGR ratio is commonly expressed by:

$$r_{EGR} \approx \frac{m_{EGR}}{m_{air} + m_{EGR}} \quad (3.2)$$

The ratio of EGR r_{EGR} is difficult to measure on-board. Common on-board flow rate meters can not be used at the extreme exhaust conditions, namely temperature and particles concentration [10, 39]. The EGR is only measured in test benches by including two gas analyser probes at the intake and exhaust manifolds, by following:

$$r_{EGR} = \frac{[CO_2]_{int} - [CO_2]_{amb}}{[CO_2]_{exh} - [CO_2]_{amb}} \quad (3.3)$$

Or by:

$$r_{EGR} = \frac{[O_2]_{amb} - [O_2]_{int}}{[O_2]_{amb} - [O_2]_{exh}} \quad (3.4)$$

if O_2 is used instead of CO_2 .

Despite its extended use in combustion analysis [40–42], CO_2 balance methodology suffers from two significant drawbacks. On the one hand, the transient response of this measurement technique highly depends on the gas analyser system response and on the intake and exhaust manifold dynamics, leading to significant errors when transients are considered [43]. On the other hand, several authors have pointed out the relevance of the probe location in high-pressure EGR loops: because of incomplete mixing, high-pressure loops create a notable cylinder-to-cylinder dispersion, which may lead to a non-representative EGR measurement if the probe locations are in a wrong place [44–46].

In [47, 48] various probe locations were placed in the same intake manifold. The engine was equipped with low-pressure and high-pressure EGR loops. A scheme of the intake with the probe locations is shown in Figure 3.2.

The results of the CO_2 measured at each probe are shown in Figure 3.3 for two tests performed, where high-pressure and low-pressure EGR loops were separately activated. Note that in the low-pressure EGR loop cylinder-to-cylinder dispersion is negligible, but in when high-pressure EGR loop is used significant dispersion exist (cylinder-to cylinder and at the same duct during

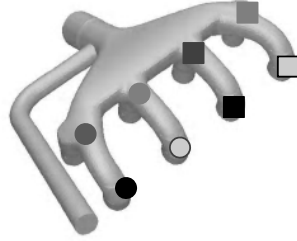


Figure 3.2. Location of the intake manifold probes for the experiment performed in [49].

the length of the intake).

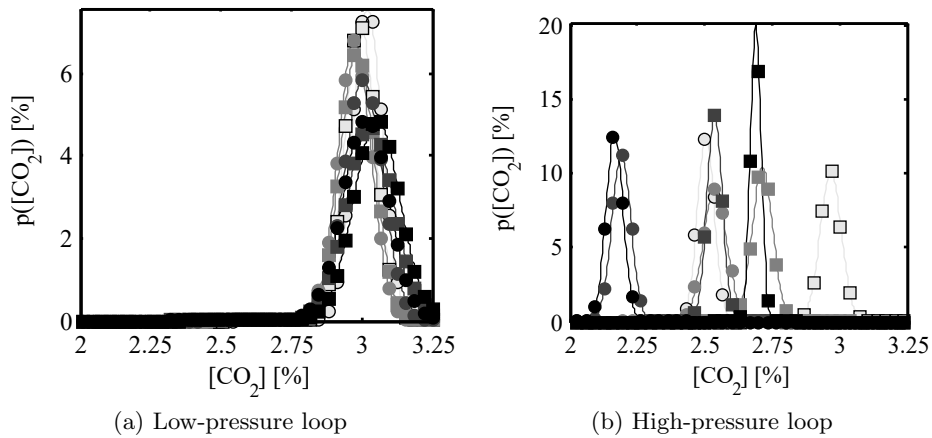


Figure 3.3. Probability distribution of the CO_2 concentration in the eight probes shown in Figure 3.2, in a CI engine running at 1200 rpm and 10 mg/str of injected fuel.

3.2.3 Oxygen concentration sensors

Oxygen sensors are based on the Nernst principle of a ZrO_2 electrochemical cell. This principle relies on the voltage generated of a ZrO_2 cell when different partial pressure of oxygen exist at the platinum electrodes of both sides [50]. These sensors are also named as λ sensors due to the voltage output response of a Nernst cell, which similar to that Greek letter. λ , or normalized A/F ratio, is defined as:

$$\lambda = \frac{(A/F)_{real}}{(A/F)_{stoich}} \quad (3.5)$$

The use of exhaust gas oxygen (EGO) sensors was extended in 1970, when legislation limits pushed manufacturers to use this type of sensors, in conjunction with TWC, to control SI engine emissions [51, 52]. These sensors offer a binary oxygen measurement, rich or lean, which was employed to control the injection settings in order to achieve stoichiometric conditions [53, 54]. A typical response of an EGO sensor is shown in Figure 3.4 where the characteristic binary output is clear.

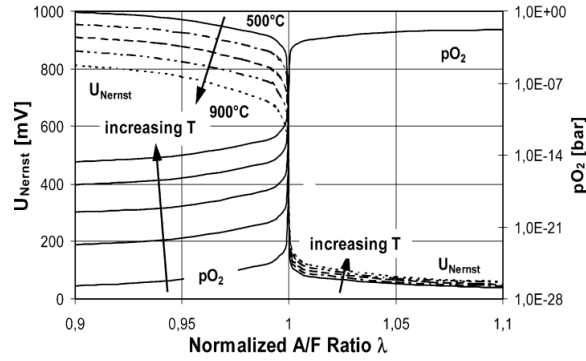


Figure 3.4. Oxygen partial pressure pO_2 and Nerst voltage U_{Nerst} as a function of λ , extracted from [50].

Since 1970, many developments were focused on improving oxygen sensors capabilities, e.g. time response, oxygen resolution or warming time. The development of multilayer sensors and the inclusion of the limiting current principle, which consists on applying a voltage to the ZrO_2 cell to obtain a wide range A/F sensor output, was translated in a second generation of oxygen sensors. These new sensors, also named as universal exhaust oxygen sensors UEGO or directly λ sensors, permit a linear resolution of oxygen over a wide range [55, 56]. Although the response time of λ sensors is quite fast (around 70 ms), Schilling [57], when ageing UEGO sensors during 3000 working hours, reported a 5% error when $\lambda < 0.8$ and a 8.8% when $\lambda > 1.7$.

Theoretically oxygen sensors could be placed at the intake manifold to estimate the actual O_2 available for combustion, but because of the working principle, they would have some significant penalties in the measurement ac-

curacy: on the one hand, oxygen sensors detect the oxygen partial pressure, and not oxygen concentration, so one dimension (the intake pressure) should be added to the calibration procedure, and on the other hand, when using this sensor to measure high-pressure EGR, the O_2 measurement could be erratic if the air has not been properly mixed with the burnt products of the EGR at the location of the λ sensor. Furthermore, the cross-sensitivity of that type of sensors with others gas components than O_2 , at the intake and at the exhaust, specially with H_2 and CO , may result in biased measurements [58].

From the limiting current principle, and profiting that NO_x is reduced in the cathode and the pumped oxygen is also a measurement of the existing NO_x , new on-board NO_x sensors have been developed [59–62]. ZrO_2 based NO_x sensors provide three measurements: a fast binary λ (around 100 ms), a slower full resolution λ (around 500 ms) and a NO_x estimation (between 750 ms–2 s) [63–65]. These sensors have been evolving together with UEGO sensors to improve its capabilities, and today they can be part of the set of sensors included in commercial vehicles [66, 67]. Concretely NO_x sensors are required to provide feedback control for an efficient performance of SCR devices [68, 69], although its cross-sensitivity to urea and other nitrogenous species in SCR operation must be taken into account [70].

3.3 Models and virtual sensors

Despite the relevance of sensors information for diagnostics and control, some parameters cannot be directly measured on-board, e.g. recirculated gases and injected fuel, some sensors suffer from ageing, and some measurements require highest sampling frequency than the response time of the sensors. In order to cope with these issues, models are used in combination of sensors in on-board ECUs, but also in test benches. Herein, some of the most relevant models used for charge estimation will be presented.

3.3.1 Speed density method

The speed density approach, also known as volumetric efficiency method, provides an estimation of the in-cylinder trapped mass by assuming ideal gas conditions ($pV = mRT$) and includes a volumetric efficiency η_v to cope with

other effects [71, 72]. The in-cylinder trapped mass can be computed through:

$$\dot{m} = \eta_v \frac{np_{int}V_d}{120RT_{int}} \quad (3.6)$$

where the mass flow into the cylinder \dot{m} is function of the engine speed n in rpm, the displaced volume V_d , the pressure and temperature manifold, p_{int} and T_{int} , the constant gas R , and the volumetric efficiency η_v .

Traditionally, the volumetric efficiency is calibrated as a function of the engine speed n and intake manifold pressure p_{int} with a 2D table [73]. However, new VVT strategies for intake charge control increase the degrees of freedom (DoF) for the volumetric efficiency estimation and it cannot be stored as a simple 2D table [74]. Some solutions for modelling the volumetric efficiency can be found in [75–77] by using neural networks, or in [78, 79] by using physical-based models for η_v in engines with VVT.

Although the time response of speed-density approaches is sufficient, variations in the operating conditions, such as wall heat transfer or friction losses, can lead to significant model errors in transient operation [80, 81].

3.3.2 The orifice principle

The orifice principle is used to characterize the flow over a restricted area, e.g. a valve [71, 72]. Herein, the process of the valve flow is considered isentropic, adiabatic and following the ideal gas law, thus the flow is function of the conditions at the inlet and outlet of the valve, following:

$$\dot{m}(t) = C_d A_v(t) \frac{p_i(t)}{\sqrt{RT_i(t)}} \Psi \left(\frac{p_i(t)}{p_o(t)} \right) \quad (3.7)$$

where C_d is the discharge coefficient, A_v is the effective flow area, p_i and T_i are the pressure and temperature at the inlet side, p_o is the pressure at the outlet, and Ψ is a function of the pressure ratio defined by:

$$\Psi \left(\frac{p_i(t)}{p_o(t)} \right) = \begin{cases} \sqrt{\gamma \left(\frac{2}{\gamma+1} \right)^{\frac{\gamma+1}{\gamma-1}}} & \text{if } p_o < p_i \left(\frac{2}{\gamma+1} \right)^{\frac{\gamma}{\gamma-1}} \\ \left(\frac{p_i(t)}{p_o(t)} \right)^{\frac{1}{\gamma}} \sqrt{\frac{2\gamma}{\gamma-1} \left[1 - \left(\frac{p_i(t)}{p_o(t)} \right)^{\frac{\gamma-1}{\gamma}} \right]} & \text{if } p_o \geq p_i \left(\frac{2}{\gamma+1} \right)^{\frac{\gamma}{\gamma-1}} \end{cases} \quad (3.8)$$

This equation has been proposed to estimate the flow over the throttle valve in SI engines [82–84], to estimate the residual trapped mass by modelling the exhaust valve flow [85–87], and also to calculate the EGR flow [88–91]. However, these equations require a detailed knowledge of the valve flow process, i.e. the instantaneous effective area and the conditions at the inlet and outlet of the valves, which may be not available in on-board applications.

3.3.3 Δp method

The Δp method [92, 93], is an alternative method for intake charge determination which relies on a polytropic process between two points of the compression stroke, a and b . If Equation (2.1) and the ideal gas law are combined, it yields:

$$\Delta p = p_b - p_a = p_a \left(\left(\frac{V_b}{V_a} \right)^\kappa - 1 \right) = \frac{mRT_a}{V_a} \left(\left(\frac{V_b}{V_a} \right)^\kappa - 1 \right) \quad (3.9)$$

where the trapped mass m can be expressed as a function of the in-cylinder pressure and Volume variation in two points, and the temperature in one of them. Herein, the only unknown is the temperature in point a which must be provided.

Although this methodology rejects pressure *pegging* errors, the temperature at some point of the compression stroke must be known. The estimation of the in-cylinder intake temperature is affected by nonlinear effects, such as flow turbulence at the valves, and even when using intake temperature sensors there are significant uncertainties. Hence, it can be used in some operating conditions where in-cylinder temperature at the IVC does not change a lot, but if high variations of EGR and intake boost pressure are considered the method suffers from significant bias.

3.3.4 Residual gas fraction determination

The residual mass estimation becomes critical when VVT strategies, such as NVO, or 2 stroke engines are contemplated. In this cases the residual mass can account for a significant percentage of the total trapped mass and cycle-to-cycle variations must be measured [94].

In test benches the residual mass can be estimated by measuring the emissions of the engine and tracing the species of the combustion [95, 96]. Another

possibility is the orifice principle, as commented in Section 3.3.2, which can be used to estimate the residual mass by modelling the instantaneous flow through the valves, such as suggested in [85–87]; however, because of the complexity and the required calibration effort, it is avoided in real-time applications.

Other methodologies try to avoid modelling the instantaneous flow evolution through the valves and alleviate the computational burden by using the ideal gas law. Herein, four control-based methodologies are collected and explained. A more detailed explanation and a comparison of three of them, namely the state equation, the Mirsky, and the Fitzgerald methods can be found in [97].

State equation method. This method consists on identifying the residual mass by using the in-cylinder properties at the EVC, namely volume, pressure, and temperature. As normally there is no direct measurement of the in-cylinder temperature, the mean exhaust temperature is typically used. As follows:

$$m_{res} = \frac{p_{EVC} V_{EVC}}{RT_{EVC}} \approx \frac{p_{EVC} V_{EVC}}{RT_{exh}} \quad (3.10)$$

Mirsky method. Yun and Mirsky assumed an isentropic process during the exhaust in order to model the in-cylinder temperature evolution [98]. The residual mass, derived from the isentropic relations of the ideal gas law, can be computed by:

$$m_{res} = m_{EVO} \left(\frac{V_{EVC}}{V_{EVO}} \right) \left(\frac{p_{EVC}}{p_{EVO}} \right)^{\frac{1}{\gamma}} \quad (3.11)$$

Fitzgerald method. In this case the wall heat losses during the exhaust process are modelled and taken into account to calculate T_{EVC} . The evolution of the in-cylinder temperature is modelled from EVO to EVC, by using the measured exhaust temperature and the in-cylinder pressure evolution. The heat transfer coefficient is calculated using the Woschni correlation.

Wang method. Wang et al. proposed the utilization of the state equation method but including a term for the backflow mass in the valve overlap period [99]. The backflow mass m_{bf} is modelled according to Bernoulli's principle, by assuming incompressible flow assumptions during the valve overlap, such as:

$$m_{bf} = \frac{C_1 A_{flow} (V_{EVC} - V_{IVO})}{n} \sqrt{\rho (p_{exh} - p_{int})} \quad (3.12)$$

3.3.5 Injected fuel mass

For an accurate steady precision, in test benches a fuel balance is used. In conventional ECUs the injected fuel mass is controlled by 2D feed forward tables, where the injected fuel quantity is modelled as a function of the energizing time or time of injection (TOI) and the pressure differences at the injector nozzle, following:

$$m_{fuel} = f(\Delta p_{inj}, TOI) \quad (3.13)$$

In CI engines, where the rail pressure can reach values above 2000 bar, the differences between the rail pressure and the in-cylinder pressure can be tabbed by the rail pressure $f(p_{rail}, TOI)$, while in port fuel injection in SI engines, where the injection pressure is kept constant at low values (5-10 bar), the injected fuel can be tabbed with the intake manifold pressure $f(p_{int}, TOI)$.

However, common rail systems have cylinder-to-cylinder dispersion due to minor errors in hole diameter, unavoidable owing to manufacturing variation and to the accumulation of deposits [100, 101]. Furthermore, the use of multi-injection strategies in common rail systems also augments the uncertainties in the final measurement due to pressure waves in the injection line [102, 103]. Other solutions have been proposed in [104, 105] by measuring hydraulic variables in the injection system for modelling the actual injector rate and in [106] by deriving the real fuel injected mass from the heat release rate.

3.4 Data fusion techniques

On one hand, models usually have a good time-response, which is sufficient to represent the dynamics of the phenomena modelled, while sensors use to

have a non-linear time response, which depends on the physics of the sensing phenomenon. On the other hand, most of the models in automotive applications, such as the ones presented above, are based on calibrated parameters which suffer from significant deviations from the real behaviour of the engine, caused by off-design conditions, manufacturer discrepancies, and ageing.

Data fusion techniques permit a combination of models and sensors to have profit of the main strengths of both, and provide the control system with a final measurement with the adequate properties, i.e. time response and precision [107–109]. In automotive applications, sensors placed at various locations can be combined to determine the charge and the composition at the intake. However, when this is the case, specific dynamic models of sensors and transport equations must be included.

3.4.1 Sensor dynamics

The sensors time response depends on the characteristics of the sensing phenomenon and material, e.g. thermocouples time response depends on the sheath diameter [110], but also depends on the digital and analog processing of the signal. Some authors, such as in [111, 112], propose a detailed analysis of the physics of the sensing phenomenon to determine the actual time response of the sensor, while others, as [113], use non-causal deconvolution techniques for off-line procedures. The time response of most of automotive sensors can be described by a first order system with a time delay [114–116], following:

$$G(s) = \frac{A}{1 + \tau s} e^{-s\tau_d} \quad (3.14)$$

where A is the gain of system, τ is the time response of the sensor and τ_d is the pure delay, i.e. transport delay.

A wide variety of sensors can be found in an automotive engine control system. As an example, Table 3.1 collects data from sensors reported by other authors to show the variety of sensor time response.

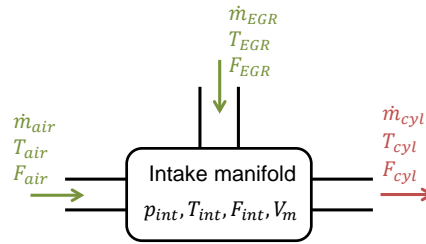
3.4.2 Intake manifold dynamics

The dynamics at the intake process can be represented by an emptying and filling model. These models analyse a control volume with the mass and

Table 3.1. Sensor time response of various sensors used in automotive applications.

| Sensor | Magnitude | Time response | Reference |
|--|-----------------|---------------|-----------|
| NTC | Temperature | 20-100s | [117] |
| Thermocouple | Temperature | 500 ms-10 s | [110] |
| ZrO ₂ NO _x sensors | NO _x | 750 ms-2 s | [64] |
| UEGO | λ | 70 ms | [57] |
| Hot film anemometer | mass air flow | 30 ms | [32] |
| In-cylinder pressure sensor | pressure | 0.5-50 μ s | [118] |

energy conservation equations, by assuming no wall heat transfer and perfect gas mixture composition [119–121]. Figure 3.5 shows a scheme of the intake manifold, where the main mass and energy fluxes are drawn.

**Figure 3.5.** Main energy and mass fluxes in the intake manifold.

The gas properties evolution are modelled from derivation of the ideal gas law, following:

$$\dot{p}_{int}V_m = \dot{m}RT_{int} + mR\dot{T}_{int} \quad (3.15)$$

Two solutions are taken:

- Some authors consider the temperature variations at the intake manifold negligible ($\dot{T}_2 = 0$), in the so named isothermal model, which is developed from the mass conservation principle ($\dot{m} = \dot{m}_{air} + \dot{m}_{EGR} - \dot{m}_{cyl}$), which yields:

$$\dot{p}_{int} = \frac{RT_{int}}{V_m} (\dot{m}_{air} + \dot{m}_{EGR} - \dot{m}_{cyl}) \quad (3.16)$$

- Others prefer a more detailed thermal analysis by including temperature variations and assuming an adiabatic response of the intake manifold,

in the so named adiabatic model [122]. It is developed from the energy conservation principle, which can be defined as:

$$\sum \dot{m}_i h_i = \dot{m} C_v T_{int} + m C_v \dot{T}_{int} \quad (3.17)$$

And including the definition of the specific heat ratio, enthalpy and gas constant, and substituting $\dot{m} T_{int} + m \dot{T}_{int}$ in Equation (3.15), it yields:

$$\dot{p}_{int} = \frac{\gamma R}{V_m} (\dot{m}_{air} T_{air} + \dot{m}_{EGR} T_{EGR} - \dot{m}_{cyl} T_{int}) \quad (3.18)$$

Transport equations can be also applied to composition concentration at the intake, such as proposed in [88, 123, 124], following:

$$\dot{F}_{int} = \frac{RT_{int}}{p_{int} V_m} (\dot{m}_{air} F_{air} + \dot{m}_{EGR} F_{EGR} - \dot{m}_{cyl} F_{cyl}) \quad (3.19)$$

where if F_{int} is the fraction of burnt gases in the intake manifold, $\dot{m}_{air} F_{air}$ can be suppressed from the equation ($F_{air} = 0$).

3.4.3 Observers

A dynamic system can be defined in a general form by:

$$\dot{x} = f(x, u) \quad (3.20)$$

$$y = g(x, u) \quad (3.21)$$

where x are the system states, y the outputs, and u the inputs of the dynamic system.

Normally, observers are defined in control theory as a system that provides an estimation of the internal states by processing measurements from the inputs and outputs of the system.

3.4.3.1 Closed-loop observers

Closed loop observers are designed to give an estimation of the states \hat{x} , to make the measured error $e = y - \hat{y}$ converge to 0. To do so, a feedback control is designed with calibrated observer gains L , as follows:

$$\dot{\hat{x}} = f(x, u) + L(y - \hat{y}) \quad (3.22)$$

Commonly, in automotive applications, in order to use sensor information located at the intake manifold, such as MAF, the isothermal model is used due to its simplicity, the manifold air mass flow m_{air} is considered an input, the intake pressure p_{int} the system state, and unknown parameters can be included in the state equations by assuming no variations. As a representative example, in [125], a volumetric efficiency correction ($\eta_v = \eta_{v,o} + \Delta\eta_v$) was included with the following set of equations:

$$\dot{p}_{int} = \frac{RT_{int}}{p_{int}} \left(\dot{m}_{air} - (\eta_{v,o} + \Delta\eta_v) \frac{np_{int}V_d}{120RT_{int}} \right) \quad (3.23)$$

$$\Delta\dot{\eta}_v = 0 \quad (3.24)$$

$$y = p_{int} \quad (3.25)$$

Where the states are $\Delta\eta$ and p_{int} and the measurement is p_{int} .

More examples of Luenberg-like observers can be found in [126,127] for air-charge estimation in SI engines, in [89,90,128] for EGR estimation by using isothermal intake model dynamics and in [88,123,124] by using the transport equations at the intake for the burnt gases concentration.

Kalman Filters. Kalman filters (KF) are a concrete type of closed-loop observers where the observer gains are continuously adapted to improve the convergence and accuracy of the observer [129,130].

The KF harnesses knowledge of model errors w and sensor noise statistics v , following:

$$x_k = f(x_{k-1}, u_k) + w_k \quad (3.26)$$

$$y_k = g(x_k, u_k) + v_k \quad (3.27)$$

where the system described in Equations (3.20) and (3.21) has been rewritten in the discrete form and the model and sensor errors have been included. w and v are modelled as a Gaussian distribution with zero mean and covariance matrices Q_k and R_k , respectively. Although various approximations exist, in most of the applications Q_k and R_k are chosen to be constant and diagonal.

The observation of the state vector is defined as other observers, by:

$$\hat{x}_{k|k-1} = f(\hat{x}_{k-1}, u_k) \quad (3.28)$$

$$e_k = y_k - g(\hat{x}_{k|k-1}, u_k) \quad (3.29)$$

$$\hat{x}_k = \hat{x}_{k|k-1} + K_k e_k \quad (3.30)$$

The KF is characterized for minimizing the expected estimation error by solving an iterative Riccati matrix equation and updating the value of the Kalman gain (K). Following:

$$P_{k|k-1} = (F_k P_{k-1} F_k^T + Q_k) \quad (3.31)$$

$$K_k = P_{k|k-1} H_k^T (H_k P_{k|k-1} H_k^T + R_k)^{-1} \quad (3.32)$$

$$P_k = (I - K_k H_k) P_{k|k-1} \quad (3.33)$$

where F_k and H_k are the linear state matrices of Equations (3.26) and (3.27). If these equations were non-linear, they could be linearised by:

$$F_{k,ij} = \left. \frac{\delta f_i}{\delta x_j} \right|_{x=\hat{x}_k} \quad (3.34)$$

$$H_{k,ij} = \left. \frac{\delta g_i}{\delta x_j} \right|_{x=\hat{x}_k} \quad (3.35)$$

In this case, the observer is named extended Kalman filter (EKF). Another possibility when dealing with highly non-linear systems is the unscented kalman filter (UKF). It uses the deterministic sampling approach for improving the propagation of the Gaussian random variable [131, 132].

Several examples can be found in literature for automotive applications. In [133], an extended Kalman filter is proposed for air-charge estimation improvements in SI engines. In [134] the complete adiabatic manifold model is used in combination of a throttle model and a first order system modelling the temperature sensor dynamics for predicting the actual in-cylinder air flow. And in [135] an intake manifold model of a CI engine with EGR is used to calculate all the mass flows.

3.4.3.2 Unknown input observers

Input estimation techniques, also named as unknown input observers, are a special case of observers where all the states can be measured but some inputs not. Therefore the system could be rewritten in a single equation such as:

$$\dot{x} = z + u \quad (3.36)$$

where x are the measured states, u unknown inputs, and z a combination of states and inputs that can be measured.

Although theoretically the inputs could be directly computed by derivation of the states, such as in dirty differentiation observers [136], noise would be highly amplified and other techniques are preferred. The main issue of that type of problems is the method for estimating \dot{x} with a noise measurements of x . Various observers can be found in the literature [136, 137], some examples are high gain observers [138], slide mode observers [139, 140], and interpolation observers [141].

Regarding the applicability of input estimation techniques in automotive applications, in SI engines with no EGR loops, input estimation techniques can be used for determining the actual in-cylinder air charge by adding an error to the volumetric efficiency estimation [137] ($\eta_v = \eta_{v,0} + \Delta\eta_v$), while in CI engines, or SI engines with exhaust gases recirculation, the main goal use to be the identification of the unmeasured EGR quantity [142].

3.5 Conclusions

Composition and charge estimation is currently a major research topic, since it is mandatory for combustion control and optimization. This chapter has reviewed several models and sensors used to estimate the air charge, the exhaust gasses recirculation, the trapped mass, and the oxygen concentration.

Models are characterized by an adequate time response but suffer from bias and need from sensor feedback to be updated. Observers and data fusion algorithms permit a combination of sensors and models by taking into account the dynamics of the system. Some examples of closed-loop observers and unknown-input observers applied to automotive applications have been

presented to illustrate the potential of such observers in terms of transient response and accuracy.

References

- [1] Al-Himyari B.A., Yasin A. and Gitano H. “Review of Air-Fuel Ratio Prediction and Control Methods”. *Asian Journal of Applied Sciences*, 2014. (cited in p. 58)
- [2] Zhao Y., Shen T. and Jiao X. “Air-fuel ratio transient control design for gasoline engines based on individual cylinder air charge estimation”. *SAE Technical Papers*, Vol. 1, 2013. (cited in p. 58)
- [3] Yar A. and Bhatti A. I. “Control of Air-to-Fuel ratio of spark ignited engine using super twisting algorithm”. In *Proceedings - 2012 International Conference on Emerging Technologies, ICET 2012*, pp. 71–75, 2012. (cited in p. 58)
- [4] Chang C., Amstutz A. and Powell J. D. “Air-Fuel Ratio Control in Spark-Ignition Engines Using Estimation Theory”. *IEEE Transactions on Control Systems Technology*, Vol. 3 n° 1, pp. 22–31, 1995. (cited in p. 58)
- [5] Copp D. G., Burnham K. J. and Lockett F. P. “Model comparison for feedforward air/fuel ratio control”. In *IEE Conference Publication*, pp. 670–675, 1998. (cited in p. 58)
- [6] Yao M., Zhang Q., Liu H., Zheng Z. ., Zhang P., Lin Z., Lin T. and Shen J. “Diesel engine combustion control: Medium or heavy EGR?”. *SAE Technical Papers*, 2010. (cited in p. 58)
- [7] Lähde T., Rönkkö T., Virtanen A., Solla A., Kytö M., Söderström C. and Keskinen J. “Dependence between nonvolatile nucleation mode particle and soot number concentrations in an EGR equipped heavy-duty diesel engine exhaust”. *Environmental Science and Technology*, Vol. 44 n° 8, pp. 3175–3180, 2010. (cited in p. 58)
- [8] Nicol A. J., Such C. and Sarnbratt U. “Investigation of fuel injection strategies on a low emission heavy-duty diesel engine with high EGR rates”. In *Institution of Mechanical Engineers: Combustion Engines and Fuels Group - Internal Combustion Engines: Performance, Fuel Economy and Emissions*, pp. 173–183, 2008. (cited in p. 58)
- [9] Lu P., Han J., Lai M., Henein N. A. and Bryzik W. “Combustion visualization of di diesel spray combustion inside a small-bore cylinder under different EGR and swirl ratios”. *SAE Technical Papers*, 2001. (cited in p. 58)
- [10] Asad U. and Zheng M. “Exhaust gas recirculation for advanced diesel combustion cycles”. *Applied Energy*, Vol. 123, pp. 242–252, 2014. (cited in pp. 35, 58, and 60)
- [11] Zheng Ming, Reader Graham T and Hawley J Gary. “Diesel engine exhaust gas recirculation—a review on advanced and novel concepts”. *Energy conversion and management*, Vol. 45 n° 6, pp. 883–900, 2004. (cited in p. 58)
- [12] Zhu H., Bohac S. V., Nakashima K., Hagen L. M., Huang Z. and Assanis D. N. “Effect of fuel oxygen on the trade-offs between soot, NOx and combustion efficiency in premixed low-temperature diesel engine combustion”. *Fuel*, Vol. 112, pp. 459–465, 2013. (cited in p. 58)

- [13] Thangaraja J. and Kannan C. “Effect of exhaust gas recirculation on advanced diesel combustion and alternate fuels - A review”. *Applied Energy*, Vol. 180, pp. 169–184, 2016. (cited in p. 58)
- [14] Karthikeya Sharma T., Amba Prasad Rao G. and Madhu Murthy K. “Control of peak pressures of an HCCI engine under varying swirl and operating parameters”. *Frontiers in Energy*, Vol. 10 n° 3, pp. 337–346, 2016. (cited in p. 58)
- [15] You-cheng S., Min X., Yong G., Yi C., Lei S. and Kang-yao D. “Effects of injection pressure, exhaust gas recirculation and intake pressure on the cycle-to-cycle variations of HCCI combustion”. *Journal of the Energy Institute*, Vol. 89 n° 2, pp. 293–301, 2016. (cited in p. 58)
- [16] Das P., Subbarao P. M. V. and Subrahmanyam J. P. “Control of combustion process in an HCCI-DI combustion engine using dual injection strategy with EGR”. *Fuel*, Vol. 159, pp. 580–589, 2015. (cited in p. 58)
- [17] Asad U and Zheng M. “Tightened intake oxygen control for improving diesel low-temperature combustion”. *Proceedings of the Institution of Mechanical Engineers, Part D: Journal of Automobile Engineering*, Vol. 225 n° 4, pp. 513–530, 2011. (cited in p. 58)
- [18] Wattanapanichaporn O., Jantaradac W., Wannatong K. and T. Aroonsrisopon. “Cylinder-to-Cylinder Variations in Diesel Dual Fuel Combustion under Low-load Conditions”. *Journal of Research and Applications in Mechanical Engineering*, Vol. 1 n° 4, 2012. (cited in p. 58)
- [19] Chen Z., Yao C., Wang Q., Han G., Dou Z., Wei H., Wang B., Liu M. and Wu T. “Study of cylinder-to-cylinder variation in a diesel engine fueled with diesel/methanol dual fuel”. *Fuel*, Vol. 170, pp. 67–76, 2016. (cited in p. 58)
- [20] Yang Z., Winward E. and Stobart R. K. “Improve Cylinder-to-Cylinder Consistency and Reduce Cycle-to-Cycle Variations of a Diesel Engine Using Closed-loop Control of Fuel Path Input Variables”. *IFAC-PapersOnLine*, Vol. 49 n° 11, pp. 239–244, 2016. (cited in p. 58)
- [21] Burkhard J. F. “Individual cylinder fuel control for a turbocharged engine”. *SAE Technical Papers*, Vol. 1, 2014. (cited in p. 58)
- [22] Desantes J. M., Luján J. M., Pla B. and Soler J. A. “On the combination of high-pressure and low-pressure exhaust gas recirculation loops for improved fuel economy and reduced emissions in high-speed direct-injection engines”. *International Journal of Engine Research*, Vol. 14 n° 1, pp. 3–11, 2013. (cited in p. 58)
- [23] Peng Z. and Jia M. “An investigation and evaluation of variable-valve-timing and variable-valve-actuation strategies in a diesel homogeneous charge compression ignition engine using three-dimensional computational fluid dynamics”. *Proceedings of the Institution of Mechanical Engineers, Part D: Journal of Automobile Engineering*, Vol. 222 n° 6, pp. 1047–1064, 2008. (cited in p. 58)
- [24] Jankovic M. and Magner S. W. “Cylinder air-charge estimation for advanced intake valve operation in variable cam timing engines”. *JSAE review*, Vol. 22 n° 4, pp. 445–452, 2001. (cited in p. 58)
- [25] Docquier N. and Candel S. “Combustion control and sensors: A review”. *Progress in Energy and Combustion Science*, Vol. 28 n° 2, pp. 107–150, 2002. (cited in p. 58)
- [26] Jurgen R.K. *Automotive electronics handbook*. New York: McGraw-Hill, 1995. (cited in p. 58)

- [27] Bell J. *Modern Diesel Technology: Electricity and Electronics*. Cengage Learning, 2013. (cited in p. 58)
- [28] Cavina Nicolo, Cerofolini Alberto, Corti Enrico, Ponti Fabrizio, De Cesare Matteo and Stola Federico. “Innovative Techniques for On-Board Exhaust Gas Dynamic Properties Measurement”. *SAE International Journal of Engines*, Vol. 6 n° 2013-01-0305, pp. 217–227, 2013. (cited in p. 58)
- [29] Taghialatela F., Cesario N. and Lavorgna M. “Soft computing mass air flow estimator for a single-cylinder SI engine”. *SAE Technical Papers*, 2006. (cited in p. 59)
- [30] Buehler P. J., Franchek M. A. and Makki I. “Mass air flow sensor diagnostics for adaptive fueling control of internal combustion engines”. In *Proceedings of the American Control Conference*, volume 3, pp. 2064–2069, 2002. (cited in p. 59)
- [31] Brasseur G. “Robust automotive sensors”. In *Conference Record - IEEE Instrumentation and Measurement Technology Conference*, volume 2, pp. 1278–1283, 1997. (cited in p. 59)
- [32] VDO Siemens. “Integrated mass airflow sensor (SIMAF)”. Technical report, Siemens VDO, 2005. (cited in pp. 59 and 69)
- [33] Ziesmer D. A., Chuey M. D. and Hazelton L. “Frequency domain characterization of mass airflow sensors”. *SAE Technical Papers*, 1993. (cited in p. 59)
- [34] Wang X. “Parameter determination of dynamic sensor model with particle swarm optimization technique”. In *2009 International Conference on Measuring Technology and Mechatronics Automation, ICMTMA 2009*, volume 1, pp. 43–46, 2009. (cited in p. 59)
- [35] Xu K., Zhang J., Wang X., Teng Q., Tan J. and Zhang Y. “Improvements of nonlinear dynamic modeling of hot-film MAF sensor”. *Sensors and Actuators, A: Physical*, Vol. 147 n° 1, pp. 34–40, 2008. (cited in p. 59)
- [36] Zhao J. and Wang J. “Engine mass airflow sensor fault detection via an adaptive oxygen fraction observer”. In *2014 American Control Conference*, pp. 1517–1522. IEEE, 2014. (cited in p. 59)
- [37] Betta Giovanni, Capriglione Domenico, Pietrosanto Antonio and Sommella Paolo. “ANN-based sensor fault accommodation techniques”. In *Diagnostics for Electric Machines, Power Electronics & Drives (SDEMPED), 2011 IEEE International Symposium on*, pp. 517–524, 2011. (cited in p. 59)
- [38] Liu Zhiyuan and Wang Changhui. “An LPV adaptive observer for updating a map applied to an MAF sensor in a diesel engine”. *Sensors*, Vol. 15 n° 10, pp. 27142–27159, 2015. (cited in p. 59)
- [39] Asad U. *Advanced diagnostics, control and testing of diesel low temperature combustion*. PhD Thesis, University of Windsor, 2009. (cited in p. 60)
- [40] Benson JD and Stebar Russell Ford. “Effects of charge dilution on nitric oxide emission from a single-cylinder engine”. *SAE Technical Paper*, 1971. (cited in p. 60)
- [41] Yu Robert C and Shahed Syed M. “Effects of injection timing and exhaust gas recirculation on emissions from a DI diesel engine”. *SAE Preprints*, Vol. 811234, 1981. (cited in p. 60)
- [42] Pierpont D. A., Montgomery D. T. and Reitz R. D. “Reducing particulate and nox using multiple injections and egr in a D.I. diesel”. *SAE Technical Papers*, 1995. (cited in p. 60)

- [43] Asad U., Tjong J. and Zheng M. “Exhaust gas recirculation - Zero dimensional modelling and characterization for transient diesel combustion control”. *Energy Conversion and Management*, Vol. 86, pp. 309–324, 2014. (cited in p. 60)
- [44] Bo T., Li G., Palaniyandi J., Hunt R. and Rowe C. “Multiple-cylinder diesel engine CFD simulation using VECTIS”. *SAE Technical Papers*, 2009. (cited in p. 60)
- [45] Dimitriou P., Burke R., Copeland C. and Akehurst S. “Study on the Effects of EGR Supply Configuration on Cylinder-to-Cylinder Dispersion and Engine Performance Using 1D-3D Co-Simulation”. *SAE Technical Papers*, 2015. (cited in p. 60)
- [46] Luján J. M., Climent H., Pla B., Rivas-Perea M. E., François N., Borges-Alejo J. and Soukeur Z. “Exhaust gas recirculation dispersion analysis using in-cylinder pressure measurements in automotive diesel engines”. *Applied Thermal Engineering*, Vol. 89, pp. 459–468, 2015. (cited in p. 60)
- [47] Luján J. M., Galindo J., Serrano J. R. and Pla B. “A methodology to identify the intake charge cylinder-to-cylinder distribution in turbocharged direct injection Diesel engines”. *Measurement Science and Technology*, Vol. 19 n° 6, 2008. (cited in p. 60)
- [48] Payri F., Luján J., Climent H. and Pla B. “Effects of the intake charge distribution in HSDI engines”. *SAE Technical Papers*, 2010. (cited in p. 60)
- [49] Luján J. M., Guardiola C., Pla B. and Cabrera P. “Considerations on the low-pressure exhaust gas recirculation system control in turbocharged diesel engines”. *International Journal of Engine Research*, Vol. 15 n° 2, pp. 250–260, 2014. (cited in pp. 12 and 61)
- [50] Riegel J., Neumann H and Wiedenmann H-M. “Exhaust gas sensors for automotive emission control”. *Solid State Ionics*, Vol. 152-153, pp. 783–800, 2002. (cited in pp. 9, 35, 61, and 62)
- [51] Dueker H., Friese K. and Haecker W. “Ceramic aspects of the bosch lambda-sensor”. *SAE Technical Papers*, 1975. (cited in p. 62)
- [52] Hamann E., Manger H. and Steinke L. “Lambda-sensor with Y2O3-stabilized zro2-ceramic for application in automotive emission control systems”. *SAE Technical Papers*, 1977. (cited in p. 62)
- [53] Zechall R., Baumann G. and Eisele H. “Closed-loop exhaust emission control system with electronic fuel injection”. *SAE Technical Papers*, 1973. (cited in p. 62)
- [54] Engh G. T. and Wallman S. “Development of the volvo lambda-sond system”. *SAE Technical Papers*, 1977. (cited in p. 62)
- [55] Regitz S. and Collings N. “Study of cycle-by-cycle air-to-fuel ratio determined from the exhaust gas composition and a novel fast response device based on a wide band lambda sensor”. *SAE Technical Papers*, 2008. (cited in p. 62)
- [56] Klett S., Piesche M., Heinzelmann S., Weyl H., Wiedenmann H. ., Schneider U., Diehl L. and Neumann H. “Numerical and experimental analysis of the momentum and heat transfer in exhaust gas sensors”. *SAE Technical Papers*, 2005. (cited in p. 62)
- [57] Schilling A. *Model-Based Detection and Isolation of Faults in the Air and Fuel Paths of Common-rail DI Diesel Engines Equipped with a Lambda and a Nitrogen Oxides Sensor*. PhD Thesis, ETH Zurich, 2008. (cited in pp. 62 and 69)
- [58] Germann H., Taglaiferri S. and Geering H. P. “Differences in pre-and post-converter lambda sensor characteristics”. *SAE Technical Papers*, 1996. (cited in p. 63)

- [59] Kato N., Kokune N., Lemire B. and Walde T. “Long term stable NO_x sensor with integrated in-connector control electronics”. *SAE Technical Papers*, 1999.
(cited in p. 63)
- [60] Kato N., Nakagaki K. and Ina N. “Thick film ZrO₂ NO_x sensor”. *SAE Technical Papers*, 1996.
(cited in p. 63)
- [61] Kato N., Hamada Y. and Kurachi H. “Performance of thick film NO_x sensor on diesel and gasoline engines”. *SAE Technical Papers*, 1997.
(cited in p. 63)
- [62] Nakanouchi Y., Kurosawa H., Hasei M., Yan Y. and Kunimoto A. “New type of NO_x sensors for automobiles”. *SAE Technical Papers*, 1996.
(cited in p. 63)
- [63] Smith J.A. “Demonstration of a fast response on-board NO_x sensor for heavy-duty diesel vehicles”. Technical report, California Environmental Protection Agency, 2000.
(cited in p. 63)
- [64] Galindo J., Serrano J. R., Guardiola C., Blanco-Rodriguez D. and Cuadrado I. G. “An on-engine method for dynamic characterisation of NO_x concentration sensors”. *Experimental Thermal and Fluid Science*, Vol. 35 n° 3, pp. 470–476, 2011.
(cited in pp. 63 and 69)
- [65] Manchur T. B. and Checkel M. D. “Time resolution effects on accuracy of real-time NO_x emissions measurements”. *SAE Technical Papers*, 2005.
(cited in pp. 35 and 63)
- [66] Zhuiykov S. and Miura N. “Development of zirconia-based potentiometric NO_x sensors for automotive and energy industries in the early 21st century: What are the prospects for sensors?”. *Sensors and Actuators, B: Chemical*, Vol. 121 n° 2, pp. 639–651, 2007.
(cited in p. 63)
- [67] Moos R. “A brief overview on automotive exhaust gas sensors based on electroceramics”. *International Journal of Applied Ceramic Technology*, Vol. 2 n° 5, pp. 401–413, 2005.
(cited in pp. 9 and 63)
- [68] Hofmann L., Rusch K., Fischer S. and Lemire B. “Onboard emissions monitoring on a HD truck with an SCR system using Nox sensors”. *SAE Technical Papers*, 2004.
(cited in p. 63)
- [69] Nieuwstadt M. and Upadhyay D. “Diagnosis of a urea scr catalytic system”, 2005.
(cited in p. 63)
- [70] Frobert A., Raux S., Creff Y. and Jeudy E. “About cross-sensitivities of NO_x sensors in SCR operation”. *SAE Technical Papers*, Vol. 2, 2013.
(cited in p. 63)
- [71] Heywood J.B. *Internal Combustion engine fundamentals*. McGraw-Hill, New York, 1988.
(cited in p. 64)
- [72] Guzzella L. and Onder C. *Introduction to modeling and control of internal combustion engine systems*. Springer, Berlin Heidelberg, 2010.
(cited in p. 64)
- [73] Wang Z., Zhu Q. and Prucka R. “A Review of Spark-Ignition Engine Air Charge Estimation Methods”. *SAE Technical Papers*, Vol. 2016-April n° April, 2016.
(cited in p. 64)
- [74] Kolewe B., Haghani A., Beckmann R., Noack R. and Jeansch T. “Data-driven estimation of air mass using Gaussian mixture regression”. In *IEEE International Symposium on Industrial Electronics*, pp. 2433–2438, 2014.
(cited in p. 64)

- [75] Malaczynski G. W., Mueller M., Pfeiffer J., Cabush D. and Hoyer K. “Replacing volumetric efficiency calibration look-up tables with Artificial Neural Network-based algorithm for variable valve actuation”. *SAE Technical Papers*, 2010. (cited in p. 64)
- [76] Wu B., Filipi Z., Assanis D., Kramer D. M., Ohl G. L., Prucka M. J. and Divalentin E. “Using artificial neural networks for representing the air flow rate through a 2.4 liter VVT engine”. *SAE Technical Papers*, 2004. (cited in p. 64)
- [77] El Hadeif J., Colin G., Talon V. and Chamailard Y. “Neural model for real-time engine volumetric efficiency estimation”. *SAE Technical Papers*, Vol. 6, 2013. (cited in p. 64)
- [78] Turin R. C., Zhang R. and Chang M. “Volumetric efficiency model for variable cam-phasing and variable valve lift applications”. *SAE Technical Papers*, 2008. (cited in p. 64)
- [79] Kocher L., Koeberlein E., Van Alstine D. G., Stricker K. and Shaver G. “Physically based volumetric efficiency model for diesel engines utilizing variable intake valve actuation”. *International Journal of Engine Research*, Vol. 13 n° 2, pp. 169–184, 2012. (cited in p. 64)
- [80] Chevalier A., Müller M. and Hendricks E. “On the validity of mean value engine models during transient operation”. *SAE Technical Papers*, 2000. (cited in p. 64)
- [81] Smith L. A., Fickenscher T. and Osborne R. P. “Engine breathing - Steady speed volumetric efficiency and its validity under transient engine operation”. *SAE Technical Papers*, 1999. (cited in p. 64)
- [82] Cho H., Song H., Lee J. and Kauh S. “Simulation of a transient torque response for engine performance in a spark ignition engine”. *Proceedings of the Institution of Mechanical Engineers, Part D: Journal of Automobile Engineering*, Vol. 215 n° 1, pp. 127–141, 2001. (cited in p. 65)
- [83] Cary M., Ebrahimi M., Ffrench K. and Sbaschnig R. “Throttle body: Modelling and identification”. *Proceedings of the Institution of Mechanical Engineers, Part D: Journal of Automobile Engineering*, Vol. 215 n° 7, pp. 813–825, 2001. (cited in p. 65)
- [84] Bordjane Mustapha and Chalet David. “Numerical Investigation Of Throttle Valve Flow Characteristics For Internal Combustion Engines”. *Journal of Multidisciplinary Engineering Science and Technology*, Vol. 2 n° 12, pp. 3532–3541, 2015. (cited in p. 65)
- [85] Payri F., Broatch A., Margot X. and Monelletta L. “Sound quality assessment of Diesel combustion noise using in-cylinder pressure components”. *Measurement Science and Technology*, Vol. 20 n° 1, 2009. (cited in pp. 33, 39, 65, 66, and 159)
- [86] Fox J. W., Cheng W. K. and Heywood J. B. “A model for predicting residual gas fraction in spark-ignition engines”. *SAE Technical Papers*, 1993. (cited in pp. 65, 66, and 159)
- [87] Senecal P. K., Xin J. and Reitz R. D. “Predictions of residual gas fraction in IC engines”. *SAE Technical Papers*, 1996. (cited in pp. 65, 66, and 159)
- [88] Zhao J. and Wang J. “Adaptive observer for joint estimation of oxygen fractions and blend level in biodiesel fueled engines”. *IEEE Transactions on Control Systems Technology*, Vol. 23 n° 1, pp. 80–90, 2015. (cited in pp. 65, 70, 71, and 205)

- [89] Kolmanovsky Ilya, Sun Jing, Druzhinina Maria and van Nieuwstadt Michiel. “Charge control for direct injection spark ignition engines with EGR”. In *Proceedings of the American Control Conference*, volume 1, pp. 34–38, 2000. (cited in pp. 65 and 71)
- [90] Kolmanovsky I. and Siverguina I. “Adaptive identification schemes in presence of bounded disturbances: An automotive case study”. In *Proceedings of the IEEE Conference on Decision and Control*, volume 1, pp. 508–513, 2001. (cited in pp. 65 and 71)
- [91] Kolmanovsky I., Sivergina I. and Sun J. “Simultaneous input and parameter estimation with input observers and set-membership parameter bounding: Theory and an automotive application”. *International Journal of Adaptive Control and Signal Processing*, Vol. 20 n° 5, pp. 225–246, 2006. (cited in p. 65)
- [92] Worm J. “An evaluation of several methods for calculating transient trapped air mass with emphasis on the delta P approach”. *SAE Technical Papers*, 2005. (cited in p. 65)
- [93] Desantes JM, Galindo J, Guardiola C and Dolz V. “Air mass flow estimation in turbocharged diesel engines from in-cylinder pressure measurement”. *Experimental Thermal and Fluid Science*, Vol. 34 n° 1, pp. 37–47, 2010. (cited in p. 65)
- [94] Li H., Guo Y., Cheng P., Liu F. and Jiang E. “Study on cycle-to-cycle variations of CAI combustion using NVO strategy”. In *2010 International Conference on Logistics Engineering and Intelligent Transportation Systems, LEITS2010 - Proceedings*, pp. 47–50, 2010. (cited in p. 65)
- [95] Prucka R. G. *An Experimental Characterization of a High Degree of Freedom Spark-Ignition Engine to Achieve Optimized Ignition Timing Control*. PhD Thesis, University of Michigan, 2008. (cited in p. 65)
- [96] Prucka R. G., Filipi Z. S., Assanis D. N., Kramer D. M. and Ohl G. L. “An evaluation of residual gas fraction measurement techniques in a high degree of freedom spark ignition engine”. *SAE International Journal of Engines*, Vol. 1 n° 1, pp. 71–84, 2009. (cited in p. 65)
- [97] Ortiz-Soto E. A., Vavra J. and Babajimopoulos A. “Assessment of residual mass estimation methods for cylinder pressure heat release analysis of HCCI engines with negative valve overlap”. *Journal of Engineering for Gas Turbines and Power*, Vol. 134 n° 8, 2012. (cited in p. 66)
- [98] Yun H. J. and Mirsky W. “Schlieren-streak measurements of instantaneous exhaust gas velocities from a spark-ignition engine”. *SAE Technical Papers*, 1974. (cited in pp. 66 and 193)
- [99] Wang S., Prucka R., Prucka M. and Dourra H. “Control-oriented residual gas mass prediction for spark ignition engines”. *International Journal of Engine Research*, Vol. 16 n° 7, pp. 897–907, 2015. (cited in p. 67)
- [100] Payri F., Luján J. M., Guardiola C. and Rizzoni G. “Injection diagnosis through common-rail pressure measurement”. *Proceedings of the Institution of Mechanical Engineers, Part D: Journal of Automobile Engineering*, Vol. 220 n° 3, pp. 347–357, 2006. (cited in p. 67)
- [101] Macián V., Luján J. M., Guardiola C. and Perles A. “A comparison of different methods for fuel delivery unevenness detection in Diesel engines”. *Mechanical Systems and Signal Processing*, Vol. 20 n° 8, pp. 2219–2231, 2006. (cited in p. 67)

- [102] Catania A. E., Ferrari A., Manno M. and Spessa E. “Experimental investigation of dynamics effects on multiple-injection common rail system performance”. *Journal of Engineering for Gas Turbines and Power*, Vol. 130 n° 3, 2008. (cited in p. 67)
- [103] Catania A. E., Ferrari A. and Spessa E. “Numerical-experimental study and solutions to reduce the dwell-time threshold for fusion-free consecutive injections in a multi-jet solenoid-type CR system”. *Journal of Engineering for Gas Turbines and Power*, Vol. 131 n° 2, 2009. (cited in p. 67)
- [104] Schmid U. and Seidel H. “Study on an injection quantity sensor. I: Evaluation of the integration procedure”. *Journal of Micromechatronics*, Vol. 3 n° 1, pp. 15–32, 2005. (cited in p. 67)
- [105] Schmid U. and Seidel H. “Study on an injection quantity sensor. II: Evaluation of the sensing element”. *Journal of Micromechatronics*, Vol. 3 n° 1, pp. 33–50, 2005. (cited in p. 67)
- [106] Finesso R. and Spessa E. “A control-oriented approach to estimate the injected fuel mass on the basis of the measured in-cylinder pressure in multiple injection diesel engines”. *Energy Conversion and Management*, Vol. 105, pp. 54–70, 2015. (cited in p. 67)
- [107] Gao J. B. and Harris C. J. “Some remarks on Kalman filters for the multisensor fusion”. *Information Fusion*, Vol. 3 n° 3, pp. 191–201, 2002. (cited in p. 68)
- [108] Stiller C., Puente León F. and Kruse M. “Information fusion for automotive applications - An overview”. *Information Fusion*, Vol. 12 n° 4, pp. 244–252, 2011. (cited in p. 68)
- [109] Khaleghi B., Khamis A., Karray F. O. and Razavi S. N. “Multisensor data fusion: A review of the state-of-the-art”. *Information Fusion*, Vol. 14 n° 1, pp. 28–44, 2013. (cited in p. 68)
- [110] Sarnes B. and Schrüfer E. “Determination of the time behaviour of thermocouples for sensor speedup and medium supervision”. *Proceedings of the Estonian Academy of Sciences: Engineering*, Vol. 13 n° 4, pp. 295–309, 2007. (cited in pp. 68, 69, and 210)
- [111] Wang D. Y. “Real-time dynamics of amperometric exhaust oxygen sensors”. *Sensors and Actuators, B: Chemical*, Vol. 126 n° 2, pp. 551–556, 2007. (cited in p. 68)
- [112] Zhuiykov S. *Electrochemistry of Zirconia gas sensors*. Taylor & Francis, 2010. (cited in p. 68)
- [113] Henningsson M. *Data Rich Multivariable Control of Heavy-Duty Engines*. PhD Thesis, University of Lund, 2012. (cited in p. 68)
- [114] Mrosek M., Sequenz H. and Isermann R. “Identification of emission measurement dynamics for Diesel engines”. In *IFAC Proceedings Volumes (IFAC-PapersOnline)*, volume 18, pp. 11839–11844, 2011. (cited in pp. 35 and 68)
- [115] Ogata K. *Modern control engineering*. Prentice Hall, 2001. (cited in p. 68)
- [116] Blanco-Rodríguez D. *Modelling and observation of exhaust gas concentrations for diesel engine control*. PhD Thesis, Universitat Politècnica de València. Departamento de Máquinas y Motores Térmicos, 2013. (cited in pp. 68, 172, and 174)
- [117] Guardiola C., Dolz V., Pla B. and Mora J. “Fast estimation of diesel oxidation catalysts inlet gas temperature”. *Control Engineering Practice*, Vol. 56, pp. 148–156, 2016. (cited in pp. 69, 174, and 216)

- [118] DYTRAN. “Introduction to Piezoelectric Pressure Sensors”. <http://www.dytran.com/>. Accessed: 2016-12-14. (cited in p. 69)
- [119] Kao Minghui and Moskwa John J. “Turbocharged diesel engine modeling for nonlinear engine control and state estimation”. *Journal of Dynamic Systems, Measurement and Control, Transactions of the ASME*, Vol. 117 n° 1, pp. 20–30, 1995. (cited in p. 69)
- [120] Hendricks E., Chevalier A., Jensen M., Sorenson S. C., Trumpy D. and Asik J. “Modelling of the intake manifold filling dynamics”. *SAE Technical Papers*, 1996. (cited in p. 69)
- [121] Fons M., Muller M., Chevalier A., Vigild C., Hendricks E. and Sorenson S. C. “Mean Value Engine Modelling of an SI engine with EGR”. *SAE Technical Papers*, 1999. (cited in p. 69)
- [122] Hendricks Elbert. “Isothermal vs. adiabatic mean value SI engine models”. In *Advances in Automotive Control 2001. Proceedings of the 3rd IFAC Workshop*, 2001. (cited in p. 70)
- [123] Chauvin J., Corde G., Petit N. and Rouchon P. “Motion planning for experimental airpath control of a diesel homogeneous charge-compression ignition engine”. *Control Engineering Practice*, Vol. 16 n° 9, pp. 1081–1091, 2008. (cited in pp. 70, 71, and 205)
- [124] Castillo F., Witrant E., Talon V. and Dugard L. “Simultaneous air fraction and low-pressure EGR mass flow rate estimation for diesel engines”. In *IFAC Proceedings Volumes (IFAC-PapersOnline)*, pp. 731–736, 2013. (cited in pp. 70 and 71)
- [125] Leroy T., Chauvin J., Le Solliec G. and Corde G. “Air path estimation for a turbocharged SI engine with variable valve timing”. In *Proceedings of the American Control Conference*, pp. 5088–5093, 2007. (cited in p. 71)
- [126] Andersson Per. *Intake air dynamics on a turbocharged SI-engine with wastegate*. Department of Electrical Engineering, Linköping University, 2002. (cited in p. 71)
- [127] Hendricks E., Vesterholm T. and Sorenson S. C. “Nonlinear, closed loop, SI engine control observers”. *SAE Technical Papers*, 1992. (cited in p. 71)
- [128] Liu C. “Simultaneous unknown state and input estimation with application to virtual air charge and egr sensors for automotive engines”. In *ASME 2010 Dynamic Systems and Control Conference, DSCC2010*, volume 1, pp. 727–734, 2010. (cited in p. 71)
- [129] Kalman Rudolph Emil. “A new approach to linear filtering and prediction problems”. *Journal of basic Engineering*, Vol. 82 n° 1, pp. 35–45, 1960. (cited in pp. 71 and 177)
- [130] Simon D. *Optimal State Estimation: Kalman, H Infinity, and Nonlinear Approaches*. John Wiley & Sons, 2006. (cited in p. 71)
- [131] Julier Simon J. and Uhlmann Jeffrey K. “New extension of the Kalman filter to nonlinear systems”. In *Proceedings of SPIE - The International Society for Optical Engineering*, volume 3068, pp. 182–193, 1997. (cited in p. 72)
- [132] Wan E. A. and Van Der Merwe R. “The unscented Kalman filter for nonlinear estimation”. In *IEEE 2000 Adaptive Systems for Signal Processing, Communications, and Control Symposium, AS-SPCC 2000*, pp. 153–158, 2000. (cited in p. 72)
- [133] Barbarisi Osvaldo, Alessandro G and Luigi G. “An Extended Kalman Observer for the In-Cylinder Air Mass Flow Estimation”. In *Proceedings of MECA02 International Workshop on Diagnostics in Automotive Engines and Vehicles, Oct., Fisciano SA*, pp. 1–14, 2002. (cited in p. 72)

- [134] Dutka A., Javaherian H. and Grimble M. J. “State-dependent Kalman filters for robust engine control”. In *Proceedings of the American Control Conference*, volume 2006, pp. 1185–1190, 2006. (cited in p. 72)
- [135] Polóni T., Rohál-Ilkiv B. and Arne Johansen T. “Mass flow estimation with model bias correction for a turbocharged Diesel engine”. *Control Engineering Practice*, Vol. 23 n° 1, pp. 22–31, 2014. (cited in p. 72)
- [136] Stotsky A. and Kolmanovsky I. “Simple unknown input estimation techniques for automotive applications”. In *Proceedings of the American Control Conference*, volume 5, pp. 3312–3317, 2001. (cited in p. 73)
- [137] Stotsky A. and Kolmanovsky I. “Application of input estimation techniques to charge estimation and control in automotive engines”. *Control Engineering Practice*, Vol. 10 n° 12, pp. 1371–1383, 2002. (cited in p. 73)
- [138] Dabroom Ahmed and Khalil Hassan K. “Numerical differentiation using high-gain observers”. In *Proceedings of the IEEE Conference on Decision and Control*, volume 5, pp. 4790–4794, 1997. (cited in p. 73)
- [139] Levant A. “Robust Exact Differentiation via Sliding Mode Technique”. *Automatica*, Vol. 34 n° 3, pp. 379–384, 1998. (cited in p. 73)
- [140] Stotsky A., Hedrick J. K. and Yip P. P. “Use of sliding modes to simplify the backstepping control method”. In *Proceedings of the American Control Conference*, volume 3, pp. 1703–1708, 1997. (cited in p. 73)
- [141] Diop S., Grizzle J. W., Moraal P. E. and Stefanopoulou A. “Interpolation and numerical differentiation for observer design”. In *Proceedings of the American Control Conference*, volume 2, pp. 1329–1333, 1994. (cited in p. 73)
- [142] Lee H., Park Y. and Sunwoo M. “Observer design for exhaust gas recirculation rate estimation in a variable-geometry turbocharger diesel engine using a model reference identification scheme”. *Proceedings of the Institution of Mechanical Engineers, Part D: Journal of Automobile Engineering*, Vol. 228 n° 14, pp. 1688–1699, 2014. (cited in p. 73)

Chapter 4

System setup and in-cylinder pressure acquisition

Contents

| | | |
|------------|---------------------------------------|------------|
| 4.1 | Introduction | 85 |
| 4.2 | Experimental set-up | 86 |
| 4.2.1 | Acquisition and control system layout | 86 |
| 4.2.2 | In-cylinder pressure acquisition | 88 |
| 4.2.3 | Engines | 90 |
| 4.3 | Engine tests | 94 |
| 4.3.1 | Steady-state tests | 95 |
| 4.3.2 | Transient tests | 101 |
| 4.4 | Conclusions | 106 |
| 4.A | Time-frequency analysis | 107 |
| | References | 110 |

4.1 Introduction

Since in-cylinder pressure resonance depends on combustion chamber geometry and the combustion itself, several engines, with different size and working with different combustion concepts, will be met in the present work. Various experimental facilities and acquisition systems were used for testing all the engines. The first part of the chapter will be focused on describing each experimental facility. Afterwards, in section 4.3, the main features of the tests

will be summarized for both, steady-state and transient tests. At the end of the section, an appendix explaining the time-frequency tools used has been also included.

4.2 Experimental set-up

In total six experimental facilities were needed to collect all the experimental data. In this section the system layout, the in-cylinder pressure acquisition, and the main features of each engine are described.

4.2.1 Acquisition and control system layout

Generally, two type of system layouts can be distinguished: by-pass and full-pass.

By-pass control. In automotive multi-cylinder engines, the ECU controls all the systems with open-loop 2D tables and low-complexity feed-back controls, e.g. waste-gated or VGT driven turbocharger is controlled by a PID control by setting an intake pressure reference with a 2D table that defines the corresponding threshold as a function of the engine speed and the load.

In order to have control over some actuators but keeping the ECU functionalities active, such as the smoke limit, some ECUs, also named as open-ECUs, incorporate a communication protocol, normally by CAN or Ethernet, which allows the substitution of an ECU command by an external one. This type of engine control, through the ECU, is named by-pass control.

An interface system is connected to the ECU in order to send and receive information to/from the commercial sensors and actuators driven by the ECU. This interface system requires a detailed information of the engine calibration (hex file) and a description of the ECU structure (a2l file).

Full-pass control. In research engines, when no ECU has been yet developed, or when a direct and fast control is desired, ECU can be suppressed by directly sending the desired input to the actuators. Specific hardware is required to control each actuator, such as injectors, turbocharger, VVT, or

EGR valve, with the adequate protocol and power stages.

Figure 4.1 shows a scheme of these two controls. On one hand, by-pass is a safer way of engine control by only manipulating the desired value, but on the other hand, the communication loop becomes longer, and thus the time required to interact with the engine increases while the engine protections can preclude some extreme control actions.

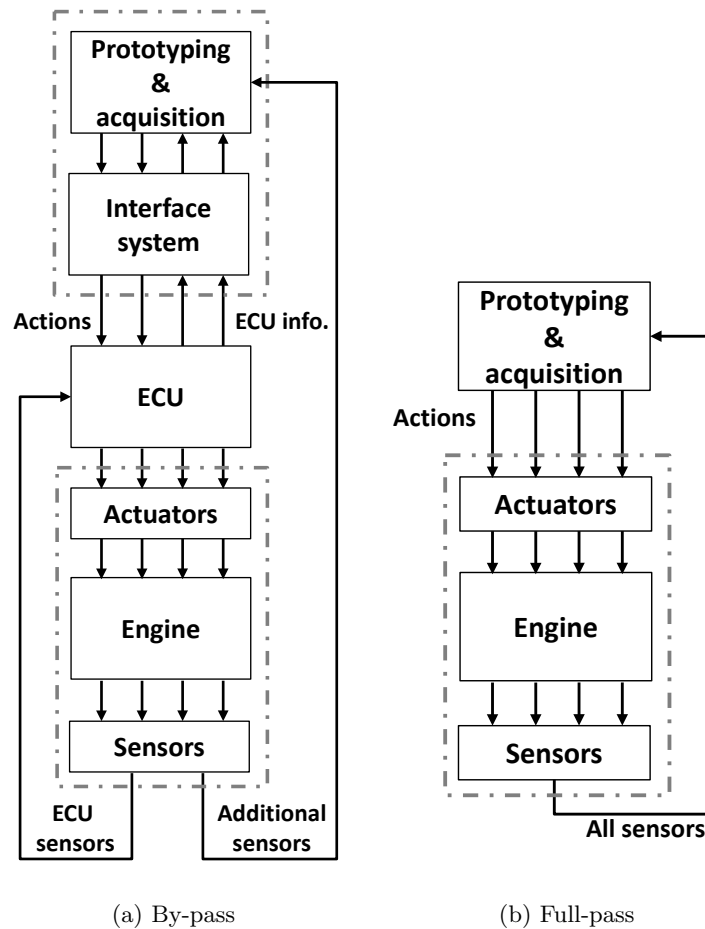


Figure 4.1. System layout for sensor acquisition and engine control.

Regarding the hardware and software employed, many systems have been used in the six installations. All of them allowed a fast sampling rate for analog converters in the in-cylinder pressure sensors (above 100 kHz), isolated

acquisition modules for thermocouples, a real-time acquisition and storage of sensor data, an interface module for connecting with the ECU, and a prototyping system with sufficient capabilities. In the case of single-cylinder engines, specific modules for each actuator were independently controlled.

Some of the hardware and software used are: real-time PXI (programmed with Labview) for acquisition and prototyping, dSpace (programmed with simulink and controlled with ControlDesk) for acquisition, prototyping, and interfacing, ETAS ES910 (programmed with Intercario and manipulated with INCA) as an interface system, and AVL Indicom system for acquisition purposes.

4.2.2 In-cylinder pressure acquisition

Although new piezo-resistor pressure sensors are being introduced in the market for low-cost in-cylinder pressure sensing [1,2], piezoelectric sensors are extensively used in research applications. These sensors are characterized by its fast response, ruggedness, high stiffness, extended ranges, and the ability to also measure quasi-static pressures [3].

However, piezo-electric pressure sensors must be properly processed to allow a valid signal. Commonly a four-steps procedure is recommended before the combustion analysis [4,5]:

1. Acquisition: The analog signal received by in-cylinder pressure sensors must be converted in digital by an analog converter module. The precision, i.e. number of bits per measurement, and the sampling frequency, i.e. number of values converted per second, are the two main important parameters of this conversion.
2. Pegging: The raw pressure signal given by piezo-electric sensors needs from a reference value offset, such as explained in section 2. The two most common methodologies are referencing by an additional intake pressure measurement or by fitting the offset at compression.
3. Signal averaging: When a steady analysis is desired, it is usual to average most of the signals, e.g. air mass flow, injected fuel mass, or engine speed, thus, several authors consider also necessary to average in-cylinder pressure cycles to analyse only a representative thermodynamic cycle [6,7].

4. Signal filtering: Finally, in order to eliminate non-desired components of the pressure signal, such as high frequency noise, a low-pass filter is commonly applied in combustion analysis.

Signal processing is always a balance between rejecting noise and discarding relevant information. The data included in this dissertation was not averaged using multiple cycles in order to conserve cycle-to-cycle information. The conversion from analog to digital was performed with 16 bits in all 6 engines and the acquisition frequency was driven by an angular encoder. Two digital filters have been considered, a low-pass filter to retain the basic information from combustion and a band-pass filter to capture the content of the frequencies where the first radial mode of the pressure resonance is located. The two limits of these filters, f_{LP}^c and f_{HP}^c , can be computed from the engine chamber geometry and the maximum and minimum speed of sound, a_{min} and a_{max} , such as:

$$f_{LP}^c = \frac{a_{min}B_{1,0}}{\pi D} \quad (4.1)$$

$$f_{HP}^c = \frac{a_{max}B_{1,0}}{\pi D} \quad (4.2)$$

A summary of the in-cylinder pressure acquisition characteristics is given in Table 4.1.

Table 4.1. Characteristics of in-cylinder pressure acquisition.

| Engine | Make | Model | Pegging | Frequency [Samp./CAD] | f_{LP}^c [kHz] | f_{HP}^c [kHz] |
|--------|---------|-------|------------------|--------------------------|---------------------|---------------------|
| A | Kistler | 6041A | with pV^κ | 5 | 3.5 | 10 |
| B | AVL | GH13P | with p_{int} | 5 | 4 | 12 |
| C | AVL | | with p_{int} | 5 | 4 | 12 |
| D | Kistler | 6125C | with p_{int} | 5 | 2.5 | 7 |
| E | Kistler | 6125A | with p_{int} | 10 | 3.5 | 10 |
| F | Kistler | 6061B | with p_{int} | 4 | 3.5 | 10 |

Time-based vs. crank-based acquisition. Most of in-cylinder pressure acquisition systems use an external digital signal provided by an angular encoder to acquire the samples at constant angular sampling, such as:

$$p_k = p(\alpha_k) = p_0 + p(k\Delta\alpha) \quad (4.3)$$

In this manner, each sample is properly located in the piston stroke and consequently, the volume, computed from the crank angle evolution, can be

phased with the in-cylinder pressure signal if the location of the TDC is known. Having a good phasing between the pressure signal and the volume evolution is crucial in combustion analysis, as most of the calculations depend on both measurements.

However, when analysing the signal in the frequency domain, e.g. the Fourier transform, constant frequency harmonics are computed, and a constant time elapse between samples is preferred, such as:

$$p_k = p(t_k) = p_0 + p(k\Delta t) \quad (4.4)$$

Some authors use crank-based acquisition and assume constant engine speed during the cycle to calculate the frequency spectrum. Nevertheless, for a consistent time-frequency analysis and an adequate phasing, the instantaneous engine speed should be known, either by measuring the time between samples or by using a dynamic cam model, as follows:

$$\Delta t(\alpha) = \frac{\Delta \alpha}{6n(\alpha)} \quad (4.5)$$

Although some cycles were recorded time-based at 1 MHz to detect high-frequency noises, all the in-cylinder pressure data presented in this dissertation was recorded crank-based and the instantaneous engine speed was measured by encoders or modelled by crankshaft dynamic models.

The time between crank-based samples was measured in Engines A, C, and D, and in parallel, a crankshaft dynamic model, such as the one commented in Appendix 2.A developed from [8], was validated and applied to the rest of the engines. The model uses the in-cylinder pressure and the engine properties to calculate the instantaneous engine speed, when no encoder signal is available.

4.2.3 Engines

In this dissertation, six engines: two conventional CI engines, one SI engine, and three on-research engines working with new combustion concepts, i.e. RCCI, PPCI, CAI and SACI, will be used. Each engine was labelled with a letter ranging from A to F, which will be used for identifying the engine in future sections. With the exception of engine F, where no detailed information of the engine parameters was given for confidentiality reasons, the main

characteristics of the engines have been collected in Table 4.2.

Table 4.2. Main characteristics of engines.

| | | A | B | C | D | E | F |
|-----------------|------|--------|-------|--------|--------------------|-------------------|-----------|
| Combustion mode | | SI | CI | CI | CI RCCI PPCI | SI CAI SACI | SI CAI |
| Cylinders | [-] | 3 | 4 | 4 | 1 | 4 | 1 |
| V_{dis} | [cc] | 499.6 | 374.6 | 492.1 | 1800.6 | 499.6 | 299.8 |
| Strokes | [-] | 4 | 4 | 4 | 4 | 4 | 2 |
| Bore length | [mm] | 82 | 73.5 | 81 | 123.6 | 86 | X |
| Stroke length | [mm] | 94.6 | 88.3 | 95.5 | 152 | 86 | X |
| Rod length | [mm] | 146 | 136.8 | 152 | 225 | 145.5 | X |
| K_c | [-] | 1:10.1 | 1:17 | 1:16.2 | 1:15 | 1:11.2 | X |

Engine A: A four-stroke light-duty engine was used to analyse various knocking conditions in SI combustion. The engine was equipped with a single-stage turbocharger, VVT system, and direct gasoline injection. Gasoline injection timing was set at 270 CAD before TDC, while the valves timing was kept constant at 387 and 180 CAD before TDC for the IVO and IVC respectively, and at 146 and 357 CAD after TDC for the EVO and EVC.

Intake pressure was measured by a piezo-resistive pressure sensor at the intake, the air-to-fuel ratio was estimated from a lambda sensor at the exhaust, and a fuel balance was employed for fuel mass flow metering, which allowed an accurate measurement in steady-state conditions.

Engines B and C: Engines B and C are two four-stroke CI engines with 1.5 and 2 litres of total displacement, respectively. Both engines disposed from common-rail injection system, a high-pressure EGR loop and a single-stage turbocharger. The former, engine B, was equipped with extra sensors in order to have more precise information about the intake and exhaust temperature and composition of the gases. A scheme of the system layout of these two multi-cylinder CI engines is shown in Figure 4.2: ECU sensors are marked in black while the additional sensors equipped in engine B are marked in grey.

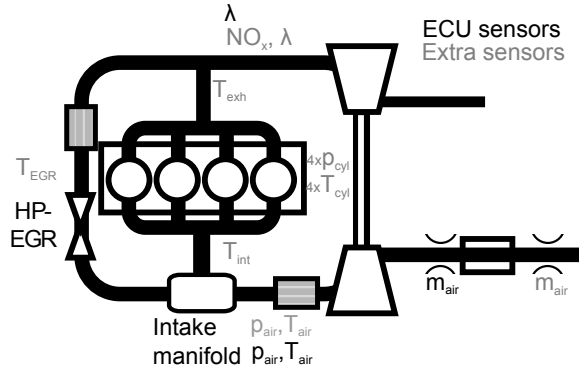


Figure 4.2. Experimental set-up scheme of CI engines: ECU sensors are marked in black while the additional sensors equipped in engine B are marked in grey.

A piezo-resistive intake pressure sensor was used for pegging and an additional hot film anemometer was used to compare with the default one used by the ECU. In engine B, thermocouples were placed at each runner, at the turbine inlet, and at the end of the intake manifold. Thermocouples had 1.5 mm of diameter as a trade-off between durability and time response.

Engine D: Engine D was developed from a heavy-duty truck engine for studying the autoignition of a mixture composed from two different fuels (RCCI) [9–14]. The detailed geometry of the bowl is shown in Figure 4.3.

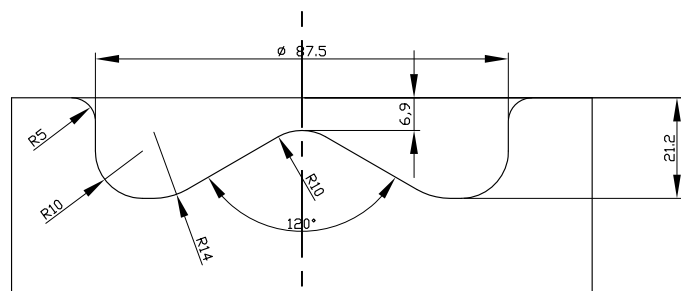


Figure 4.3. Detailed bowl geometry of engine D (dimensions are in mm).

The engine was equipped with port fuel gasoline and direct diesel injection systems, having both injection systems a specific hardware for controlling them. This injection hardware enables to vary the in-cylinder fuel blending

ratio and the fuel mixture properties according with the engine operating conditions. An hydraulic VVT system was controlled by a specific electronic control unit, a screw compressor supplied the required boost pressure, and a low-pressure EGR was included to control the fraction of burnt gases at the intake manifold.

Engine E: A conventional light-duty spark-ignited engine was modified to enable multi-mode combustion, namely SI, CAI, and SACI. A custom piston modified by head machining allowed to increase the compression ratio from 9.2 to 11.25. A high pressure cooled EGR system was connected downstream of a 58 mm throttle body. These two elements, the throttle and the EGR, were moved further upstream to ensure a proper mixing. A turbocharger, controlled with a waste-gate valve, was also included in the system layout to provide sufficient intake boost.

The original engine already dispose a double overhead camshaft (DOHC) with a phasing authority of 50 degrees of crank angle degrees in the VVT system of each valve, which was used to perform NVO strategies required to control the HCCI and SACI combustion concepts.

Engine F: Engine F is a novel design for an ultra low cost-gasoline engine (ULC-GE), which is currently in research. It will be a 2S uniflow-scavenged twin-cylinder engine with VVT and DI [15]. The uniflow scavenging process consists on using intake ports and exhaust valves, such as depicted in Figure 4.4. In this manner, a high number of ports can be incorporated at the intake and more space is available at the cylinder head for the exhaust valves [16]. A mechanical blower, driven by the crankshaft pumps the fresh air into the cylinder.

To obtain a DoF to control the scavenging but also paying attention to its cost, a VVT system in the exhaust valves was considered. This VVT system can change the angular position of the EVO and EVC, but not the valve lift profile. Furthermore, an air-assisted fuel injection system was also included. This system is composed from two injectors: the first introduces gasoline inside a pressurized chamber and the second injects that mixture in the cylinder. This system improves the fuel atomization without the need of high injection

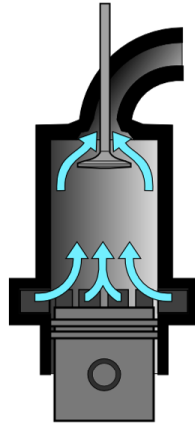


Figure 4.4. Scavenging process in a uniflow 2S engine.

pressures.

This engine offers the possibility of studying the in-cylinder trapped mass in a 2S engine with a complex scavenging process. As consequence of the uniflow 2S scavenging, significant cycle-to-cycle variations are expected, while the trapped mass is hard to measure due to the relevance of the short-circuit and residual gases.

4.3 Engine tests

In this section all the tests conducted in the aforementioned experimental facilities will be described. Several test campaigns were performed to analyse various modes of combustion and also the response of the methodology under varying operating conditions. This section is divided in two parts: First, the steady test campaigns developed at each engine will be presented, by highlighting the analysis performed. Later, in the second part of this section, the engines where transient tests have been conducted will be pointed out and the transient tests will be described.

4.3.1 Steady-state tests

Each engine was used for analysing the in-cylinder pressure resonance and the method capabilities at different combustion and engine characteristics. Here, the steady-state test campaigns, which will be later used for the dissertation, are explained:

Engine A: A knock study in a SI engine. Regarding the overall steady-state conditions, the engine speed, the air mass flow, and the intake temperature were modified to have more variability on the in-cylinder chamber conditions that can benefit the phenomenon of knock. A set of eight operating conditions, which are shown in Table 4.3, have been performed.

Table 4.3. Operating conditions tested in Engine A.

| OP | m_{air} [g/s] | n [rpm] | T_{cool} [°C] |
|----|--------------------|--------------|--------------------|
| A | 25 | 1500 | 85 |
| B | 22 | 1500 | 85 |
| C | 25 | 1500 | 90 |
| D | 22 | 1500 | 90 |
| E | 19 | 1250 | 85 |
| F | 16 | 1250 | 85 |
| G | 16 | 1250 | 90 |
| H | 19 | 1250 | 90 |

At each steady-state test, various SA settings, ranging from 0 to 13 CAD before TDC, were applied by performing steps. These steps have been maintained till the number of cycles recorded was sufficient for the knock percentage estimation, i.e. in advanced SA, many cycles were recorded for coping with low-knocking conditions, while in retarded SA, only few cycles were required. Figure 4.5 shows the SA steps performed at point A.

To consider steady-state conditions, blocks of 49 cycles were recorded, leaving an interval of few seconds between each acquisition block. As an example, in Figure 4.5, where only the acquired cycles have been represented, 188 blocks of 49 cycles have been collected: the first 11 steps were furnished with 16 blocks of 49 cycles, while the 3 latest steps were furnished with only

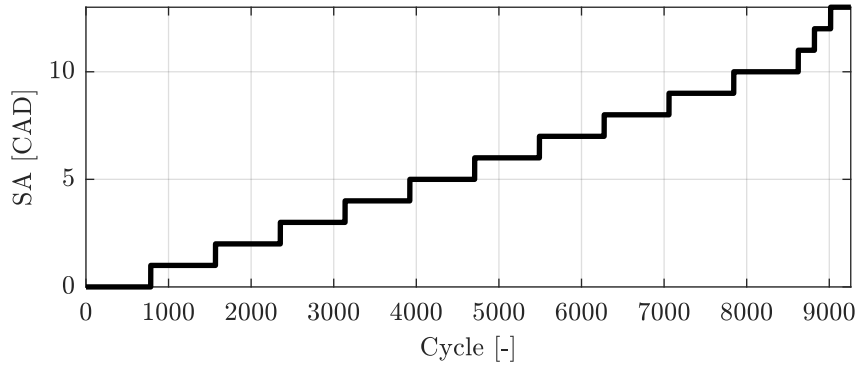


Figure 4.5. SA evolution in SA step tests in engine A at steady-state conditions I.

4 blocks. In the aggregate of all OP, 1820 blocks of 49 cycles were recorded.

Engine B: Full range CI engine with perturbations. A starting dataset of points (with 39 OP), which covers all the operating range, was extended by performing variations over the SOI of the main injection, over the SOI of both injections, namely pilot and main, over the EGR, over the intake pressure, and over the rail pressure. Finally, a total of 342 points were collected. At each test, data from 100 cycles was recorded by starting the measurement when operating conditions were stabilized.

Figure 4.6 plots the 342 points together, starting map and variations, and points out the clusters where the variations have been performed. For more detailed information, a quantification of the variations is given in table 4.4, where the maximum and minimum values are collected for each cluster.

Engine C: Full range CI engine with EGR variations. The test campaign in engine C was devoted to cover all the operating range in a CI engine and vary as much as possible the EGR. Variations in the EGR were performed, ranging from 0 to 30% at high loads and up to 60% at low loads, in 33 selected operating conditions. Finally a big dataset furnished with 808 tests was analysed, which has been shown in Figure 4.7. At each test, 100 cycles were

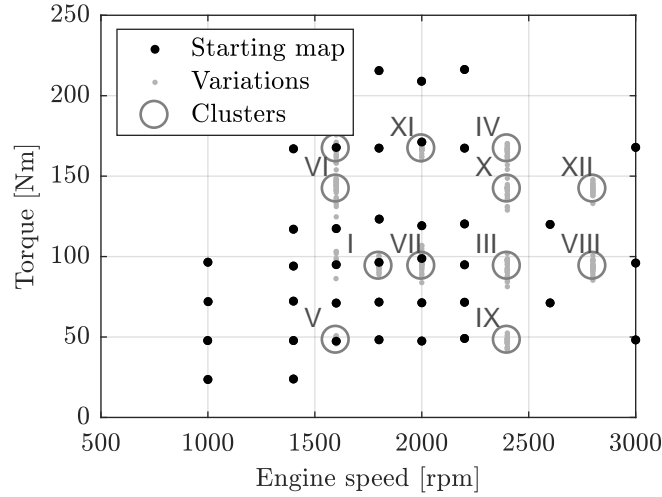


Figure 4.6. Steady tests performed in Engine B: Basic operating map is shown as black dots, variations over SOI, EGR, intake pressure, and rail pressure are shown as small grey dots, and clusters are marked and enumerated by big grey circles.

| Cl | n [rpm] | BMEP [bar] | SOI [CAD] | | EGR [%] | | Pintake [bar] | | Prail [bar] | |
|------|---------|------------|-----------|-----|---------|------|---------------|------|-------------|-------|
| | Avr | Avr | min | max | min | max | min | max | min | max |
| I | 1800 | 9.13 | -5.0 | 10 | | | 1.04 | 1.17 | | |
| II | 1600 | 15.23 | -5.0 | 10 | none | 16.8 | 1.16 | 1.91 | 744.2 | 1043 |
| III | 2400 | 9.23 | -5.0 | 10 | none | 42.8 | 1.14 | 2.03 | 947.2 | 1247 |
| IV | 2400 | 15.60 | -2.5 | 10 | none | 17.5 | 1.37 | 2.40 | 1095 | 1395 |
| V | 1600 | 4.89 | -5.0 | 10 | none | 45.9 | 1.02 | 1.11 | 398.4 | 646.8 |
| VI | 1600 | 13.18 | -5.0 | 10 | none | 23.0 | 1.15 | 1.90 | 695.6 | 994.7 |
| VII | 2000 | 9.44 | -2.5 | 10 | none | 32.6 | 1.09 | 1.67 | 698.8 | 998.8 |
| VIII | 2800 | 9.68 | -2.5 | 10 | none | 16.9 | 1.24 | 2.11 | 1097 | 1397 |
| IX | 2400 | 5.12 | -2.5 | 10 | none | 47.6 | 1.05 | 1.70 | 647.8 | 947.2 |
| X | 2400 | 13.36 | -2.5 | 7.5 | none | 25.4 | 1.46 | 2.45 | 1047 | 1346 |
| XI | 2000 | 15.69 | -2.5 | 7.5 | none | 20.0 | 1.48 | 2.10 | 893.1 | 1193 |
| XII | 2800 | 13.99 | 0.0 | 10 | none | 18.7 | 1.75 | 2.42 | | |

Table 4.4. Settings variations over 12 clusters at different operating conditions.

recorded to detect regulation anomalies and cycle-to-cycle dispersion.

Engine D: RCCI and CI concepts in a heavy-duty engine. Engine D, with a unitary displacement of 1800 cc, is representative of a heavy-duty truck engine. This single-cylinder engine, devoted to research applications, was equipped with port fuel gasoline injection to perform RCCI combustion. Two steady-state datasets are used in this dissertation. The main dataset consisted in 54 OP, the engine speed was maintained at 1200 rpm while tests were run at 25%, 50%, 75%, and 100% load, in RCCI and in conventional

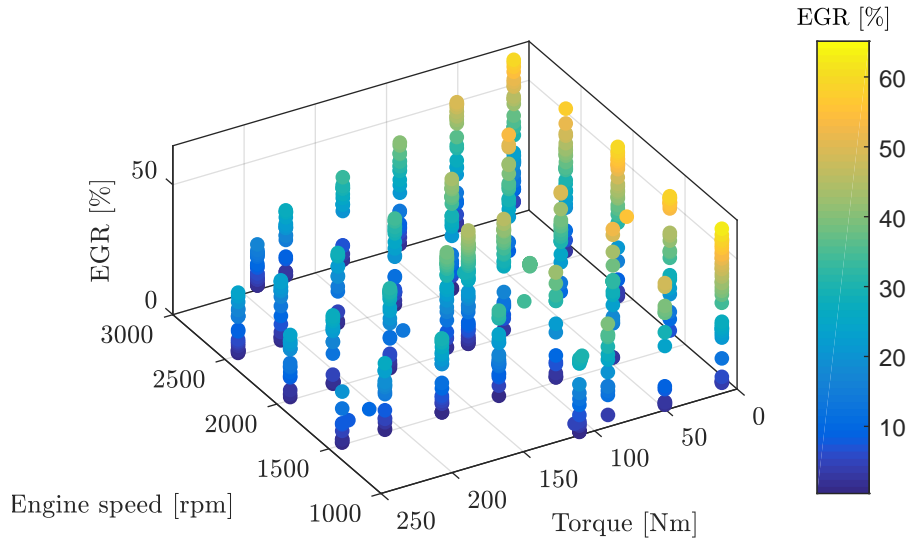


Figure 4.7. Full dataset recorded in Engine C: 808 tests, which are divided in 33 OP with EGR variations.

CI combustion modes. Each OP contains in-cylinder pressure information of 100 cycles. Figure 4.8 shows the trapped mass and the air mass of the 54 OP recorded, emphasizing conventional CI combustion OP with black circles.

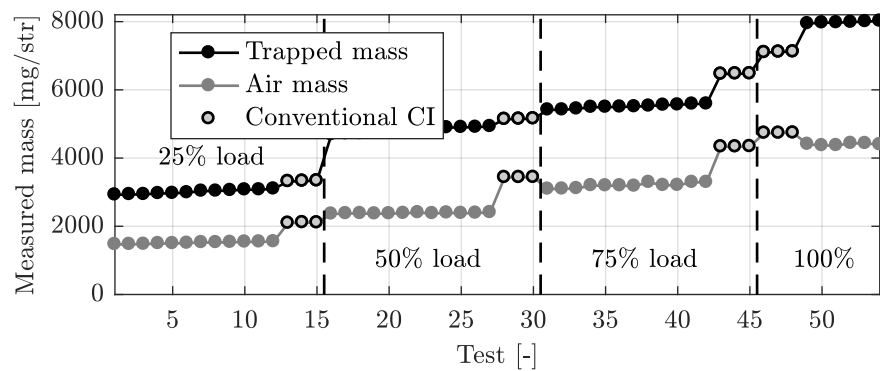


Figure 4.8. Tests conducted in Engine D: 42 tests in RCCI and 12 in CI at 25%, 50%, 75%, and 100% load.

The second database was conducted to characterize the resonance evolution in that engine. Five operating conditions were analysed by keeping the engine speed at 1200 rpm and the EGR around 40%. Two tests were run at 25% load by setting the air mass flow at 55 kg/h and the total injected mass fuel at 70 mg/str, and the other three at 75% by setting the air mass flow at 113 kg/h and the injected fuel mass at 175 mg/str. In these two blocks the start of combustion was moved by varying the gasoline fraction. The characteristics of the five tests are shown in Table 4.5. The particularities of these five tests are the time-based acquisition of the in-cylinder pressure signal (at 1 MHz) and the instantaneous engine speed measurement by using an encoder sensor.

Table 4.5. Operating conditions tested in Engine D by acquiring the in-cylinder pressure at 1 MHz of sampling frequency.

| test | n [rpm] | Load [%] | CA10 [CAD] | CA90 [CAD] | p_{max} [bar] | T_{max} [°C] |
|------|------------|-------------|---------------|---------------|--------------------|-------------------|
| 1 | 1200 | 25 | 1.6 | 25.0 | 88.1 | 1341 |
| 2 | 1200 | 25 | -2.2 | 16.9 | 92.3 | 1365 |
| 3 | 1200 | 75 | 7.0 | 32.7 | 145.7 | 1349 |
| 4 | 1200 | 75 | 15.9 | 39.2 | 109.6 | 1236 |
| 5 | 1200 | 75 | 0.6 | 28.2 | 200.7 | 1450 |

Engine E: SI, CAI and SACI with NVO strategies. The tests conducted in engine E can be divided in two parts: a first test campaign, where the residual mass was controlled by NVO strategies to perform CAI and SACI combustion concepts, and a second one, where conventional SI combustion was used in eight different configurations settings. In all the tests, information from 300 cycles was recorded and the engine speed was maintained at 2000 rpm.

Figure 4.9 shows the measured mass for the air flow, the EGR, and the estimated IGR, while Table 4.6 gives specific information of each control input for the aforementioned tests.

Engine F: λ variations in CAI combustion. In this engine, 45 tests were recorded by performing 6 loads (from low to maximum load) at 4000 rpm and changing the intake air mass flow by means of the boost pressure. Figure 4.10 illustrates the test campaign. At each test, in-cylinder pressure information

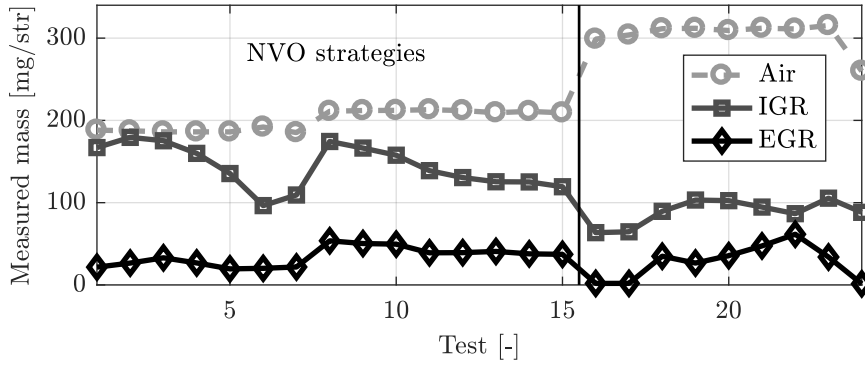


Figure 4.9. Mass flows in the tests performed in Engine E: the first 15 test correspond to CAI and SACI modes controlled by NVO strategies while the rest are SI controlled combustion.

Table 4.6. Control inputs and combustion modes for the tests performed in Engine E.

| Test | Mode | P ₂ [bar] | SA [CAD] | IVO [CAD] | IVC [CAD] | EVO [CAD] | EVC [CAD] | m_{fuel} [mg] |
|------|------|----------------------|----------|-----------|-----------|-----------|-----------|-----------------|
| 1 | CAI | 1.19 | -20.8 | 435 | 589 | 144 | 302 | 13.4 |
| 2 | CAI | 1.24 | -19.5 | 435 | 589 | 140 | 298 | 13.4 |
| 3 | CAI | 1.24 | -39.8 | 435 | 589 | 142 | 300 | 13.4 |
| 4 | CAI | 1.16 | -40.5 | 435 | 589 | 148 | 306 | 13.4 |
| 5 | SACI | 1.05 | -40.5 | 435 | 589 | 156 | 314 | 13.3 |
| 6 | SACI | 0.87 | -51.5 | 435 | 589 | 166 | 324 | 13.2 |
| 7 | SACI | 0.93 | -52.6 | 435 | 589 | 159 | 317 | 13.3 |
| 8 | CAI | 1.40 | -22.3 | 430 | 584 | 156 | 314 | 15.6 |
| 9 | CAI | 1.34 | -38.0 | 430 | 584 | 156 | 314 | 15.5 |
| 10 | SACI | 1.31 | -41.1 | 430 | 584 | 158 | 316 | 15.4 |
| 11 | SACI | 1.21 | -42.1 | 430 | 584 | 160 | 318 | 15.3 |
| 12 | SACI | 1.16 | -50.9 | 430 | 584 | 161 | 319 | 15.4 |
| 13 | SACI | 1.14 | -53.1 | 430 | 584 | 161 | 319 | 15.4 |
| 14 | SACI | 1.13 | -53.4 | 430 | 584 | 160 | 318 | 15.4 |
| 15 | SACI | 1.09 | -54.4 | 430 | 584 | 162 | 320 | 15.5 |
| 16 | SI | 0.84 | 29.4 | 284 | 574 | 106 | 391 | 21.8 |
| 17 | SI | 0.86 | 29.1 | 284 | 574 | 106 | 391 | 22.1 |
| 18 | SI | 1.03 | 46.3 | 282 | 572 | 131 | 416 | 22.3 |
| 19 | SI | 1.08 | 45.3 | 280 | 570 | 137 | 422 | 22.4 |
| 20 | SI | 1.08 | 49.2 | 280 | 570 | 137 | 422 | 22.5 |
| 21 | SI | 1.08 | 54.3 | 280 | 570 | 130 | 415 | 22.4 |
| 22 | SI | 1.08 | 65.2 | 280 | 570 | 119 | 404 | 22.5 |
| 23 | SI | 1.10 | 49.6 | 282 | 572 | 130 | 415 | 22.5 |
| 24 | SI | 0.89 | 43.0 | 275 | 565 | 130 | 415 | 22.5 |

of 250 cycles was recorded while the rest of the parameters was averaged in this period.

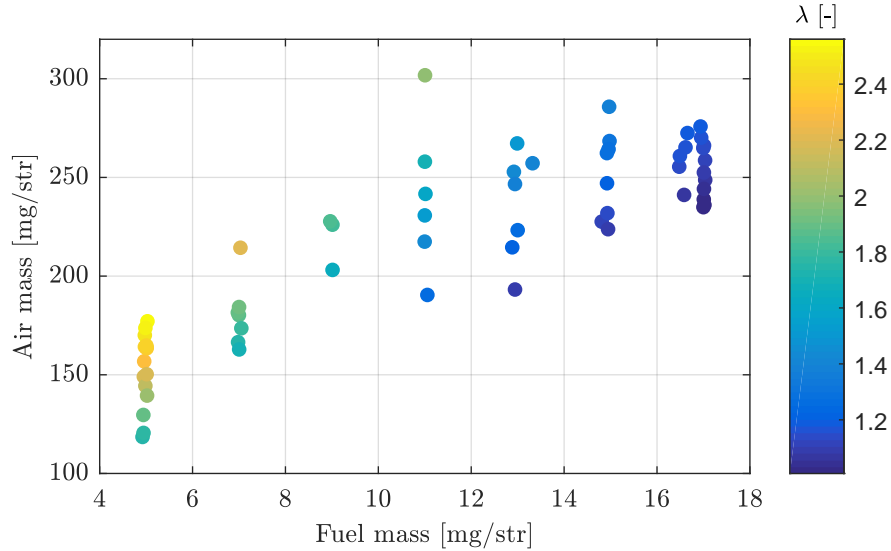


Figure 4.10. Tests performed in engine F.

4.3.2 Transient tests

To analyse the trapped mass estimation methodology in complete driving cycles and to design an adequate filter taking into account the dynamics of the systems, some transient tests have been designed.

4.3.2.1 Closed-loop knock control

When analysing in-cylinder pressure resonance in SI engines, knock, understood as the uncontrolled autoignition of the end gas, is a current research topic for detection and control algorithms. To validate a novel knock detection methodology, which will be later described in next section, the conventional controller strategy, which was explained in Section 2, was programmed and successfully validated.

Six tests were performed by varying the constants of the controller, namely K_{ret} and K_{adv} , and by using both knock detection algorithms, the current approach and a novel methodology. The constants of the controller must be

chosen to follow:

$$k_{ret} = \frac{1 - p_{KE}}{p_{KE}} k_{adv} \quad (4.6)$$

where p_{KE} is the desired probability of knock event. Table 4.7 summarizes the characteristics of the controller at the six tests, while an example of the SA response in Engine A can be reviewed above in Figure 2.7. The knock probability is given with both, the conventional MAPO methodology and the new detection approach, while k_{ret} is computed using the MAPO threshold on the first three tests and using the new methodology on the last three.

Table 4.7. Tests performed with conventional knock control.

| | | Current approach | | | Novel approach | | |
|-----------------|-------|------------------|--------|--------|----------------|--------|--------|
| | | Test 1 | Test 2 | Test 3 | Test 1 | Test 2 | Test 3 |
| k_{adv} | [CAD] | 0.015 | 0.015 | 0.015 | 0.015 | 0.015 | 0.015 |
| p_{KE} (MAPO) | [%] | 0.29 | 0.68 | 1.48 | 0.16 | 0.59 | 1.37 |
| p_{KE} (ND) | [%] | 2.32 | 3.75 | 9.54 | 1.53 | 5.03 | 9.92 |
| k_{ret} | [CAD] | 4.98 | 2.13 | 0.98 | 0.98 | 0.28 | 0.13 |
| time | [sec] | 3000 | 500 | 500 | 3000 | 500 | 500 |

4.3.2.2 Steps

To analyse the dynamics of the engine, rapid changes at various control inputs were performed in some engines. They can be divided in three type of steps:

Instantaneous mass change: VVT steps. VVT systems allow a cycle-to-cycle variation in trapped mass. Among the engines selected, Engine D allowed fully flexible variable valve timing and IVC steps were performed by maintaining IVO, EVO, and EVC constants. Engine E, with a most common cam-phasing system, only allowed variations of EVO and IVO, but the valve lift profile could not be changed. Figure 4.11 shows a step of 10 CAD in the EVC and EVO in Engine E, where the measured air mass has been also represented in the right y-axis.

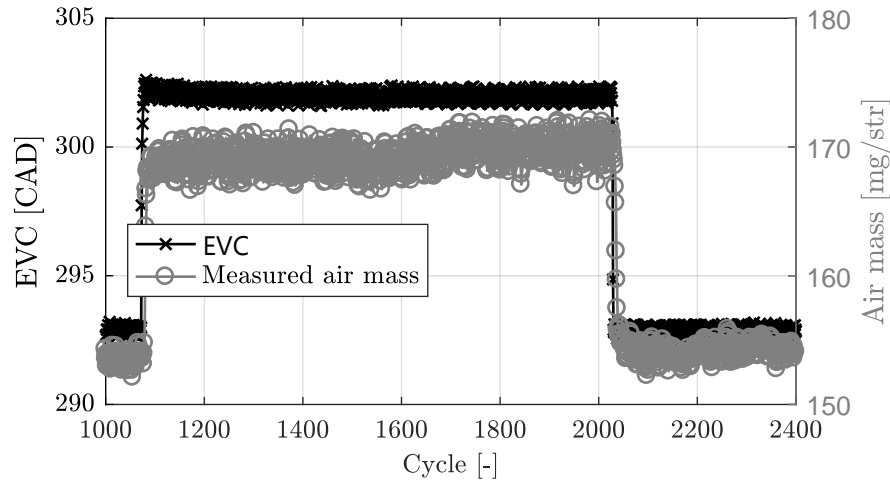


Figure 4.11. Air mass and EVC timing in a VVT step in Engine E.

Variations in the air path: boost pressure and EGR steps. The air-path loop response is affected by the intake manifold dynamics. Consequently, the effect of the variations on the control inputs, such as the EGR valve or the VGT, are driven by the transport equation at the intake, commented above in Section 3.

In Engine B, with more manageable test bench facilities, EGR and VGT steps were performed in 4 operating conditions, namely 1600 rpm and 8 bar, 1600 rpm and 14 bar, 2400 rpm and 8 bar and 2400 rpm and 14 bar, of engine speed and BMEP respectively.

Injection settings modifications: SOI and fuel mass steps. Although, the injection does not directly influence the trapped mass, it substantially alters the combustion, affecting the raw emission of the engine. The same four operating conditions tested in the EGR and VGT steps were used for performing cycle-to-cycle SOI steps in Engine B. These steps will be used for the validation of a NO_x model based on the trapped mass measurement, which will be explained afterwards in Section 8.

4.3.2.3 Cycles

Finally, complete cycles have been evaluated, comprising several minutes of continuous test where all in-cylinder pressure cycles and many other variables were recorded. Some of these tests, such as the low excited dynamic test (LEDT) and the high excited dynamic test (HEDT), have been designed to excite the dynamics of the engine, while others, such as the NEDC and WLTP, are automotive homologation cycles which were used for validation purposes.

LEDT and HEDT: The HEDT and LEDT were two tests designed to excite the temperature engine dynamics by performing engine speed and load steps. They consist on 28 steps going through all the operating map during 56 minutes. At the end of each step, steady-state information of the engine can be harnessed, while during the step the response of each subsystem can be analysed. The LEDT was designed to progressively increase the overall temperature of the engine, performing always small steps where the temperature steady-state was reached. Conversely, the HEDT is based on sharp variations where the temperature dynamics are heavily excited.

These tests are part of a test campaign in Engine B, and both were evaluated with the commercial ECU calibration and by closing the EGR valve. Figures 4.12 and 4.13 show the engine speed and load requirements for the both cycles. Each figure is divided in two parts: the left part represents the time spent at each operating condition (darker colors means unusual points and lighter colors more frequent values) and the right part shows the evolution of the engine speed and load during the 3350 s of the test.

NEDC: The NEDC consists in two parts: the urban and the extra-urban. The former is characterized by block with 200 seconds of period, which is repeated four times. This block aims to simulate an urban environment, with low-medium loads and idling zones. The latter, located at the end of the test, has a duration of 400 seconds and demands higher loads and smoother variations.

Figure 4.14 illustrate the characteristics of the NEDC test. It must be noticed that only four points at low load and idling are representative of these test.

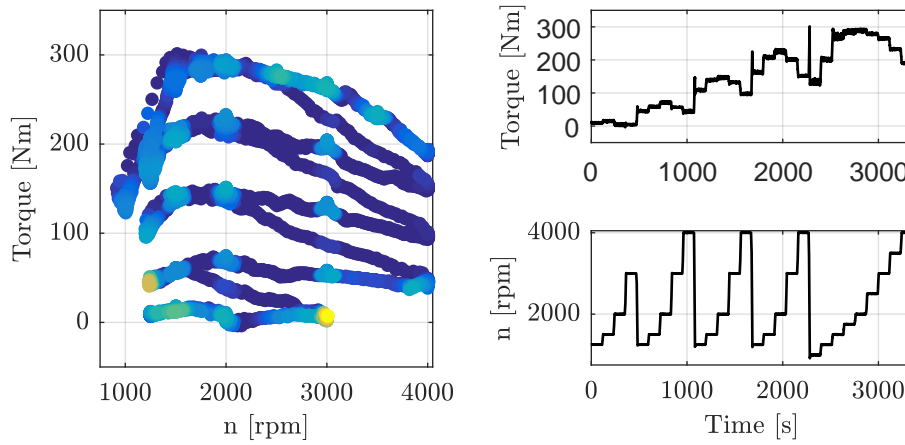


Figure 4.12. Engine speed and load during the LEDT cycle: left plot represents the time spent at each operating condition and right plot the evolution of the operating conditions.

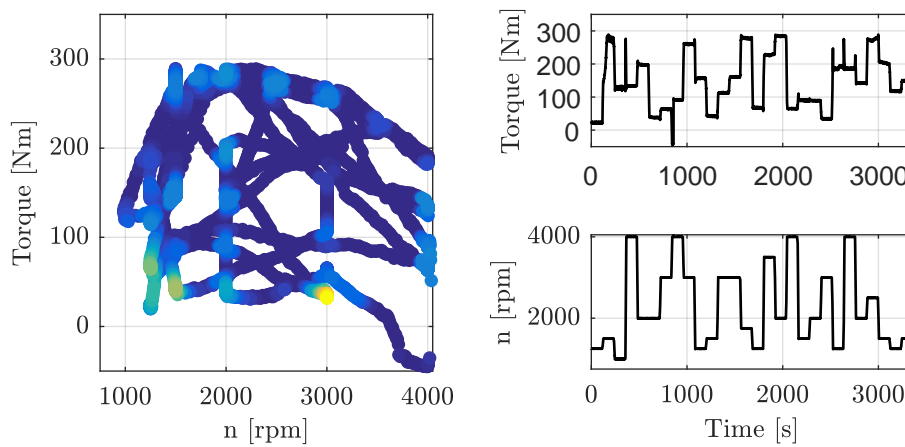


Figure 4.13. Engine speed and load during the HEDT cycle: left plot represents the time spent at each operating condition and right plot the evolution of the operating conditions.

WLTP: As stated in the first section, the WLTP aims to perform a more realistic driving cycle and will replace the European NEDC for the legislation of light duty-engines. The WLTP has an entire duration of 30 minutes, it is representative of the vehicles driven in Europe and Japan, and the idling

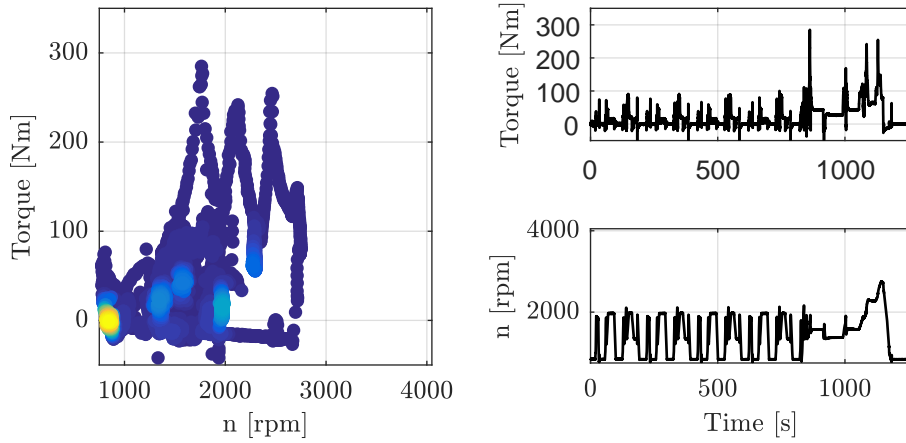


Figure 4.14. Engine speed and load during the NEDC cycle: left plot represents the time spent at each operating condition and right plot the evolution of the operating conditions.

represents a 13.4% of the cycle.

Figure 4.15 shows the frequency and the evolution of each operating condition. Clearly, when NEDC and WLTP are compared, i.e. Figure 4.14 and 4.15, the second one is closer to real-life driving: the dynamics are more reasonable and the frequencies of the operating conditions are better distributed over the overall map.

4.4 Conclusions

A huge amount of data has been collected to analyse the in-cylinder pressure resonance in different conditions. Six engine facilities, covering SI, CI, RCCI, SACI, and CAI combustion concepts, have been used for the design and validation of a novel methodology of trapped mass estimation based on the in-cylinder pressure resonance, which is developed in this thesis.

Despite the heterogeneity of experimental facilities, all the experimental set-ups allowed high flexibility in the control of the engine and an acquisition system capable of recording many consecutive in-cylinder pressure cycles. Several test campaigns, comprising steady-state and transient tests, have been

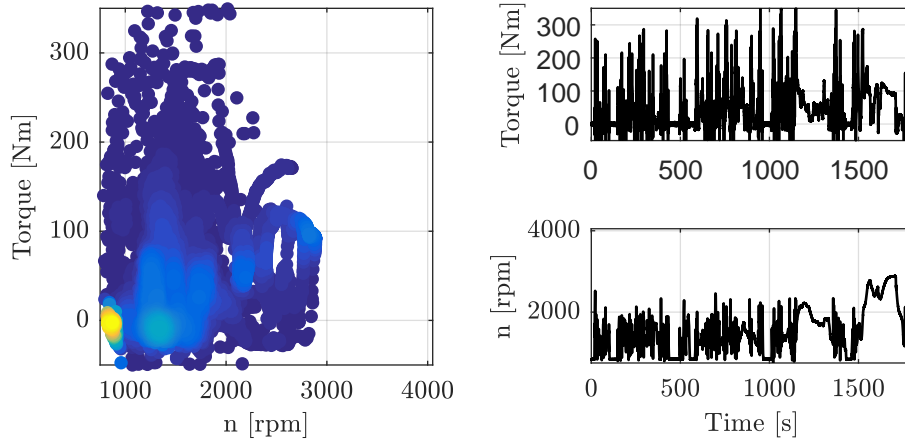


Figure 4.15. Engine speed and load during the WLTP cycle: left plot represents the time spent at each operating condition and right plot the evolution of the operating conditions.

designed to illustrate the response of the method and its applications, namely NO_x , knock, IGR, and exhaust temperature modelling, in various operating conditions.

4.A Time-frequency analysis

The Fourier transform is a well-known tool for the analysis of a signal in the frequency domain. It decomposes a given signal in the time domain $s(t)$ in constant frequency harmonics $S(f)$, such as:

$$S(f) = \int_{-\infty}^{\infty} s(t)e^{-j2\pi ft} dt \quad (4.7)$$

which can be discretized in the crank angle domain as:

$$S(f) \approx \sum_{\alpha=-\infty}^{\alpha=\infty} s(\alpha)e^{-j2\pi ft(\alpha)} \Delta t(\alpha) \quad (4.8)$$

where $\Delta t(\alpha)$ was defined in Equation (4.5) and $t(\alpha)$ can be obtained through:

$$t(\alpha) = \sum_{\Phi=\Phi_0}^{\Phi=\alpha} \Delta t(\Phi) = \sum_{\Phi=\Phi_0}^{\Phi=\alpha} \frac{\Delta \alpha}{6n(\Phi)} \quad (4.9)$$

However, the Fourier transform does not give information on the frequency content of a signal in a given time, but it gives the frequency content of all the signal. Time-frequency analysis is related with the mathematical tools and hypothesis needed to obtain the frequency components of a signal as a function of the time. In this dissertation two spectrum operations have been used: the STFT and the WD.

Short time Fourier transform (STFT). The STFT consists on breaking up the signal and separately analyses each piece of the signal. The selection of a finite-time interval makes that from the continuum of possible frequencies, only those which coincide with the orthogonal trigonometric basis will project onto a single basis vector; all other frequencies will exhibit non zero projections on the entire basis set. This is known as spectral leakage and is the result of processing finite-duration data (continuous or sampled). Although the amount of spectral leakage is influenced by the sampling frequency, sampling is not the cause of leakage [17].

Windows, i.e. weighting functions which aim to reduce the order of discontinuity at the boundary of the finite observation interval, are applied to data in order to reduce the effect the spectral leakage when dividing the signal ($s_t(\Phi) = s(\Phi)w(\Phi - \alpha)$). The STFT consists on applying a window function at various locations and performing a Fourier transform to analyse its frequency content, such as:

$$P_{STFT}(\alpha, f) = |S_t(f)|^2 = \left| \sum_{\Phi=-\infty}^{\Phi=\infty} s(\Phi)w(\Phi - \alpha)e^{-j2\pi ft(\Phi)}\Delta t(\Phi) \right|^2 \quad (4.10)$$

The window functions (*Blackman-Harris*, *Hamming*...) have been designed to reduce the spectral leakage. The length of the window is always a trade-off between frequency and time resolution. On one hand, a small window avoids the inclusion of frequency content of the surrounding instants on the instant frequency. But on the other hand, narrowing the window implies losing frequency resolution. The intervals in Equation (4.10) are chosen to determine the frequency resolution of the STFT, when the intervals are bigger than the window size, it is named as zero-padding, as all the terms around the window are multiplied by zero.

In this work a fourth order *Blackman-Harris* window of 17.8 ms, i.e. 25.6 CAD at 1200 rpm, was used, and the number of elements computed in the

STFT was adjusted in order to obtain a frequency resolution around 10 Hz, e.g. $2^{12} = 4096$ at 1200 rpm and 0.2 CAD/sample, which gives a resolution of 8.79 Hz.

Wigner distribution (WD). Another mathematical tool is the Wigner distribution. The WD is based on identifying the harmonics that exist at both sides of the given instant by multiplying the signal at a past time by the signal at the future. It can be understood as a folding of the signal over the studied time and is described by:

$$P_{WD}(\alpha, f) = \sum_{\Phi=-\infty}^{\Phi=\infty} s^*\left(\alpha - \frac{1}{2}\Phi\right)s\left(\alpha + \frac{1}{2}\Phi\right)e^{-j2\pi f\Phi}\Delta t(\Phi) \quad (4.11)$$

The main problem of the Wigner Distribution is existence of the cross terms, also named as ghost terms. They are virtual frequency components caused by the folding of the signal, e.g. an harmonic which appears at $t - \tau$ and at $t + \tau$, even if it does not exist at t , will also appear at the WD in t . Practically, the cross terms entail filtering the resonance, because the high amplitude low frequency components disturb the rest of the harmonics. When the WD is compared with the STFT, the computational burden discards the WD in most of real-time applications.

Figure 4.16 shows an in-cylinder pressure signal that has been band-pass filtered between 2.5 kHz and 7 kHz, together with two spectral distributions: the STFT and the WD. The intensity of each harmonic is represented by the colormap in logarithmic scale (dB). Clearly, the STFT dilutes the frequency spectrum much more than the WD, but on the other hand, the STFT does not suffer from virtual frequency components, such as the ones appearing in the WD.

Other distributions based on the Kernel Method [18], such as Choi Williams distribution [19] or Zhao-Atlas-Marks distribution [20], maintain the desired properties of the WD and reduce the ghost terms but at the expense of a significant increment in complexity.

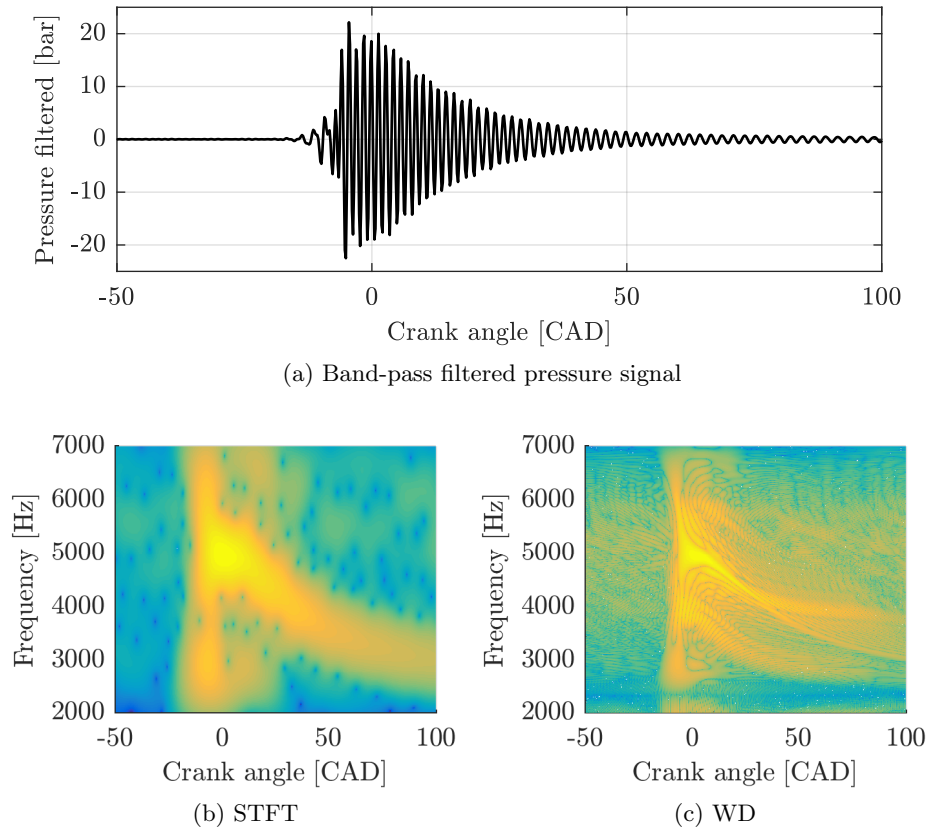


Figure 4.16. Time frequency analysis of the first resonant mode of the in-cylinder pressure signal.

References

- [1] Von Berg J., Ziermann R., Reichert W., Obermeier E., Eickhoff M., Krötz G., Thoma U., Boltshauser Th, Cavalloni C. and Nendza J. P. “High temperature piezoresistive B-SiC-on-SOI pressure sensor for combustion engines”. *Materials Science Forum*, Vol. 264-268 n° PART 2, pp. 1101–1104, 1998. (cited in pp. 13 and 88)
- [2] Chen L. and Mehregany M. “A silicon carbide capacitive pressure sensor for in-cylinder pressure measurement”. *Sensors and Actuators, A: Physical*, Vol. 145-146 n° 1-2, pp. 2–8, 2008. (cited in pp. 13 and 88)
- [3] PCB Piezotronics. “Introduction to Dynamic Pressure Sensors”. <http://www.pcb.com/>. Accessed: 2016-12-14. (cited in p. 88)
- [4] Wang J., Zhang Y., Xiong Q. and Ding X. “Data acquisition of cylinder combustion pressure oriented to diesel engine control”. In *2009 IEEE Circuits and Systems International Conference on Testing and Diagnosis, ICTD09*, 2009. (cited in p. 88)

-
- [5] Corti E. and Solieri L. “Rapid control prototyping system for combustion control”. *SAE Technical Papers*, 2005. (cited in p. 88)
- [6] Kumar Maurya R., Pal D. D. and Kumar Agarwal A. “Digital signal processing of cylinder pressure data for combustion diagnostics of HCCI engine”. *Mechanical Systems and Signal Processing*, Vol. 36 n° 1, pp. 95–109, 2013. (cited in p. 88)
- [7] Maurya R. K. “Estimation of optimum number of cycles for combustion analysis using measured in-cylinder pressure signal in conventional CI engine”. *Measurement: Journal of the International Measurement Confederation*, Vol. 94, pp. 19–25, 2016. (cited in p. 88)
- [8] Li H. and Stone B. J. “Time domain modelling of a reciprocating engine”. *Mechanical Systems and Signal Processing*, Vol. 13 n° 1, pp. 169–178, 1999. (cited in pp. 43 and 90)
- [9] Benajes J., Molina S., García A., Belarte E. and Vanvolsem M. “An investigation on RCCI combustion in a heavy duty diesel engine using in-cylinder blending of diesel and gasoline fuels”. *Applied Thermal Engineering*, Vol. 63 n° 1, pp. 66–76, 2014. (cited in p. 92)
- [10] Molina S., García A., Pastor J. M., Belarte E. and Balloul I. “Operating range extension of RCCI combustion concept from low to full load in a heavy-duty engine”. *Applied Energy*, Vol. 143, pp. 211–227, 2015. (cited in p. 92)
- [11] Benajes J., Pastor J. V., García A. and Monsalve-Serrano J. “The potential of RCCI concept to meet EURO VI NOx limitation and ultra-low soot emissions in a heavy-duty engine over the whole engine map”. *Fuel*, Vol. 159, pp. 952–961, 2015. (cited in pp. 42 and 92)
- [12] Benajes J., Pastor J. V., García A. and Monsalve-Serrano J. “An experimental investigation on the influence of piston bowl geometry on RCCI performance and emissions in a heavy-duty engine”. *Energy Conversion and Management*, Vol. 103, pp. 1019–1030, 2015. (cited in p. 92)
- [13] Benajes J., Molina S., García A. and Monsalve-Serrano J. “Effects of direct injection timing and blending ratio on RCCI combustion with different low reactivity fuels”. *Energy Conversion and Management*, Vol. 99, pp. 193–209, 2015. (cited in p. 92)
- [14] Benajes J., Pastor J. V., García A. and Boronat V. “A RCCI operational limits assessment in a medium duty compression ignition engine using an adapted compression ratio”. *Energy Conversion and Management*, Vol. 126, pp. 497–508, 2016. (cited in pp. 42 and 92)
- [15] Lopez J. J., Novella R., Valero-Marco J., Coma G. and Justet F. “Evaluation of the Potential Benefits of an Automotive, Gasoline, 2-Stroke Engine”. *SAE Technical Papers*, 2015. (cited in p. 93)
- [16] Vashishtha A., Rathinam B., Delahaye L., Ravet F. and Justet F. “Study of intake ports design for Ultra Low Cost (ULC) Gasoline Engine using STAR-CD”. *SAE Technical Papers*, 2012. (cited in p. 93)
- [17] Harris F. J. “On the Use of Windows for Harmonic Analysis with the Discrete Fourier Transform”. *Proceedings of the IEEE*, Vol. 66 n° 1, pp. 51–83, 1978. (cited in p. 108)
- [18] Cohen L. *Time-Frequency Analysis*. Prentice-Hall, New York, 1995. (cited in p. 109)
- [19] Choi H. and Williams W. J. “Improved time-frequency representation of multicomponent signals using exponential kernels”. *IEEE Transactions on Acoustics, Speech, and Signal Processing*, Vol. 37 n° 6, pp. 862–871, 1989. (cited in p. 109)

- [20] Zhao Y., Atlas L. E. and Marks R. J. "Use of cone-shaped kernels for generalized time-frequency representations of nonstationary signals". *IEEE Transactions on Acoustics, Speech, and Signal Processing*, Vol. 38 n^o 7, pp. 1084–1091, 1990. (cited in p. 109)

Chapter 5

In-cylinder pressure resonance characterisation

Contents

| | | |
|------------|---|------------|
| 5.1 | Introduction | 113 |
| 5.2 | Resonance theory: the cylindrical assumption | 114 |
| 5.3 | Exceptions to the cylindrical theory | 118 |
| 5.3.1 | Effect of bowl-in-piston geometries | 121 |
| 5.3.2 | Effect of in-cylinder inhomogeneities | 124 |
| 5.4 | Resonance excitation | 127 |
| 5.4.1 | Knock event definition in SI engines | 131 |
| 5.5 | Conclusions | 135 |
| | References | 136 |

5.1 Introduction

The resonant modes of the combustion chamber were characterized in 1938 when Draper solved the wave equation with cylindrical contour conditions. Since then, many works have used Draper's approximation in order to quantify the oscillation or to take it aside for an easier combustion analysis.

This chapter is devoted to characterize the in-cylinder pressure resonant modes of IC engines. The first section is focused on the frequency evolution during the expansion stroke. Draper's equation was validated in pent-roof

combustion chambers and a novel analysis of bowl-in-piston chambers is presented by using results from experimental data and simulations with the finite element method (FEM). Then, an analysis of the excitation of various types of combustion is presented, i.e. flame propagation in SI engines, diffusive flame evolution in CI engines, and autoignition in HCCI engines, and a new knock event definition is suggested, allowing the detection of weak knocking conditions without the need of an adaptive threshold.

5.2 Resonance theory: the cylindrical assumption

The in-cylinder pressure resonance phenomenon in automotive engines can be modelled by the wave equation for a continuous fluid medium in cylindrical coordinates, such as:

$$\frac{d^2\phi}{dr^2} + \frac{1}{r} \frac{d\phi}{dr} + \frac{1}{r^2} \frac{d^2\phi}{d\theta^2} + \frac{d^2\phi}{dz^2} = \frac{1}{a^2} \frac{d^2\phi}{dt^2} \quad (5.1)$$

where ϕ is the velocity potential, namely:

$$u = -\frac{d\phi}{dx}, v = -\frac{d\phi}{dy}, w = -\frac{d\phi}{dz} \quad (5.2)$$

being u, v, w the velocity components in the rectangular coordinates x, y, z .

Draper in a research for the NACA (current NASA) solved the wave equation by using Bessel functions and cylindrical contour conditions [1]. The analytical solution is composed by series of harmonics with varying frequency, such as:

$$p_{res} = \sum A_{i,j,g}(t) e^{i\Phi_{i,j,g}(t)} \quad (5.3)$$

where $A_{i,j,g}$ is the amplitude, which decreases because of the damping, and $\Phi_{i,j,g}$ is the phase of the harmonics, which for a non-constant frequency harmonic is defined as:

$$\Phi_{i,j,g}(t) = 2\pi \int_{\tau=-\infty}^{\tau=t} f_{i,j,g}(\tau) d\tau + \Phi_{i,j,g,0} \quad (5.4)$$

where $\Phi_{i,j,g,0}$ is the initial phase and $f_{i,j,g}$ is the frequency evolution of the resonant modes.

To illustrate the resonant frequency evolution in cylindrical combustion chambers, two cycles of engines with pent-roof combustion chambers, namely engines A and E, have been selected: a knocking cycle in Engine A at 1500 rpm and high load conditions, and a fast homogeneous combustion in Engine E at 2000 rpm and low load conditions. Figure 5.1 shows the pressure trace of these two cycles in the left axis and the mass fraction burnt evolution in the right axis.

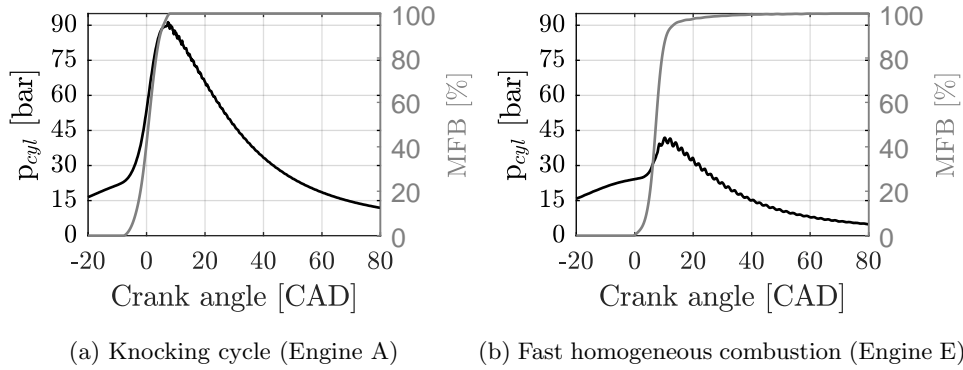


Figure 5.1. In-cylinder pressure trace and MFB evolution in SI like engines.

Draper stated that the frequency evolution of each mode is a function of the chamber geometry and proportional to the speed of sound, as follows:

$$f_{i,j,g}(t) = a(t) \sqrt{\frac{B_{i,j}^2}{(\pi D)^2} + \frac{g_k^2}{(2h)^2}} \quad (5.5)$$

where $B_{i,j}$ and g_k are constants characterizing each mode, which have been collected in Table 2.2, h and D are the height and the bore length of the cylinder, and a is the speed of sound.

As in IC engines, combustion is located near the TDC for achieving high fuel efficiencies [2, 3], the height of the combustion chamber is relatively small when the combustion starts ($h \approx 0$). As a consequence the axial modes ($g_k \neq 0$)

have high associated frequencies and taking into account that high frequencies are damped faster, Equation (5.5) can be simplified by neglecting the axial modes, which yields:

$$f_{i,j}(t) = \frac{a(t)B_{i,j}}{\pi D} \quad (5.6)$$

and if this equation is combined with the speed of sound definition, the evolution of the resonant frequency is defined by the in-cylinder chamber conditions, such as:

$$f_{i,j}(t) = \frac{B_{i,j}\sqrt{\gamma(t)RT(t)}}{\pi D} \quad (5.7)$$

In fact, the first radial mode ($B_{1,0}=1.842$) is normally the most significant [4] and it is slowly damped due to the lower frequency range. Therefore, in order to simplify the resonance analysis, the work presented in this dissertation will be focused on this mode.

Figure 5.2 shows the pressure trace after applying a band-pass filter between 4 and 10 kHz. Note that the resonance in the knocking cycle (left plot) is excited in two instants: a small excitation when the flame is initiated by the spark (around 5 CAD before the TDC) and a much bigger excitation after the EOC, when the autoignition of the end gas occurs (around 10 CAD after TDC).

The properties of the gas, i.e. $c_p(t)$, $c_v(t)$, $\gamma(t)$ and R , can be approximated by dividing the gas mixture in three species, namely air, fuel, and burnt products, such as suggested in [5]. Lapuerta et al. considered the overall properties of the gas as a combination of each specie, as follows:

$$R = R_a Y_a + R_f Y_f + R_b Y_b \quad (5.8)$$

$$c_v = c_{v,a} Y_a + c_{v,f} Y_f + c_{v,b} Y_b \quad (5.9)$$

$$c_p = R + c_v \quad (5.10)$$

$$\gamma = \frac{c_p}{c_v} \quad (5.11)$$

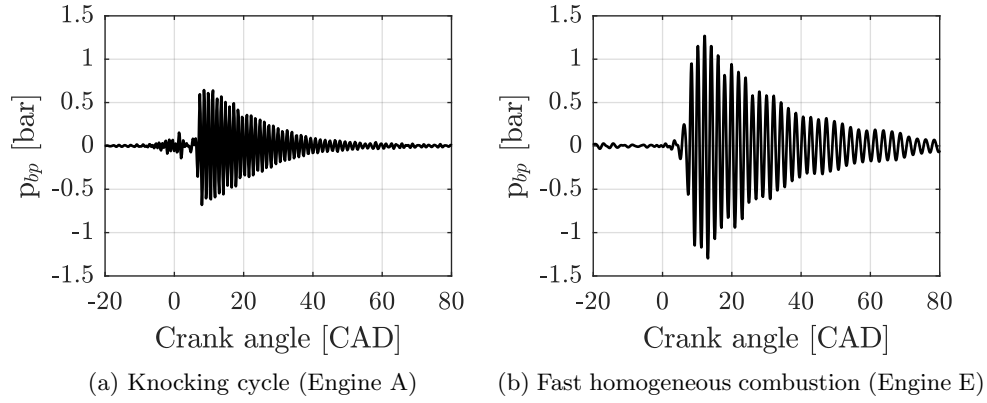


Figure 5.2. In-cylinder pressure signal pass-band filtered between 4 and 10 kHz for the example cycles of Figure 5.1.

where the variations of the gas constants R due to the in-cylinder conditions, e.g. temperature, can be neglected, as follows:

$$R_a = 55.95 \text{ J/kg K} \quad (5.12)$$

$$R_f = 287 \text{ J/kg K} \quad (5.13)$$

$$R_b = 285.4 \text{ J/kg K} \quad (5.14)$$

and the evolution of the specific heat at constant volume can be modelled by polynomial expressions for the in-cylinder temperature, such as:

$$c_{v,a} = k_{11}T^{0.5} + k_{12} + k_{13}T^{-0.5} + k_{14}T^{-1} + k_{15}T^{-1.5} \quad (5.15)$$

$$c_{v,f} = k_{21} + k_{22}T + k_{23}T^2 + k_{24}T^3 + k_{25}T^{-2} \quad (5.16)$$

$$c_{v,b} = k_{31} + k_{32}T + k_{33}T^2 + k_{34}T^3 \quad (5.17)$$

where the constants k_{ij} founded in [5] are collected in Table 5.2.

Figure 5.3 shows two type of spectra (WD and STFT) over the signals shown in Figure 5.2. Here, the theoretical resonant frequency evolution of the first mode, defined by Equation (5.7) has been represented by a black line, which clearly fits the most excited frequency in the pressure signal.

Table 5.1. Polynomial characterization of the polynomial expressions of c_v for paraffinic hydrocarbons such as $C_{12}H_{26}$ and C_8H_{18} .

| | k_{i1} | k_{i2} | k_{i3} | k_{i4} | k_{i5} |
|----------|---------------------|-----------------------|------------------------|-----------------------|--------------------|
| k_{1j} | -1.04×10^1 | 2.52×10^3 | -6.72×10^4 | 9.17×10^5 | 4.17×10^6 |
| k_{2j} | 2.00×10^0 | 6.95×10^1 | -4.05×10^{-3} | 9.10×10^{-7} | 1.46×10^6 |
| k_{3j} | 6.41×10^2 | 4.30×10^{-1} | 1.13×10^{-4} | 8.98×10^{-9} | |

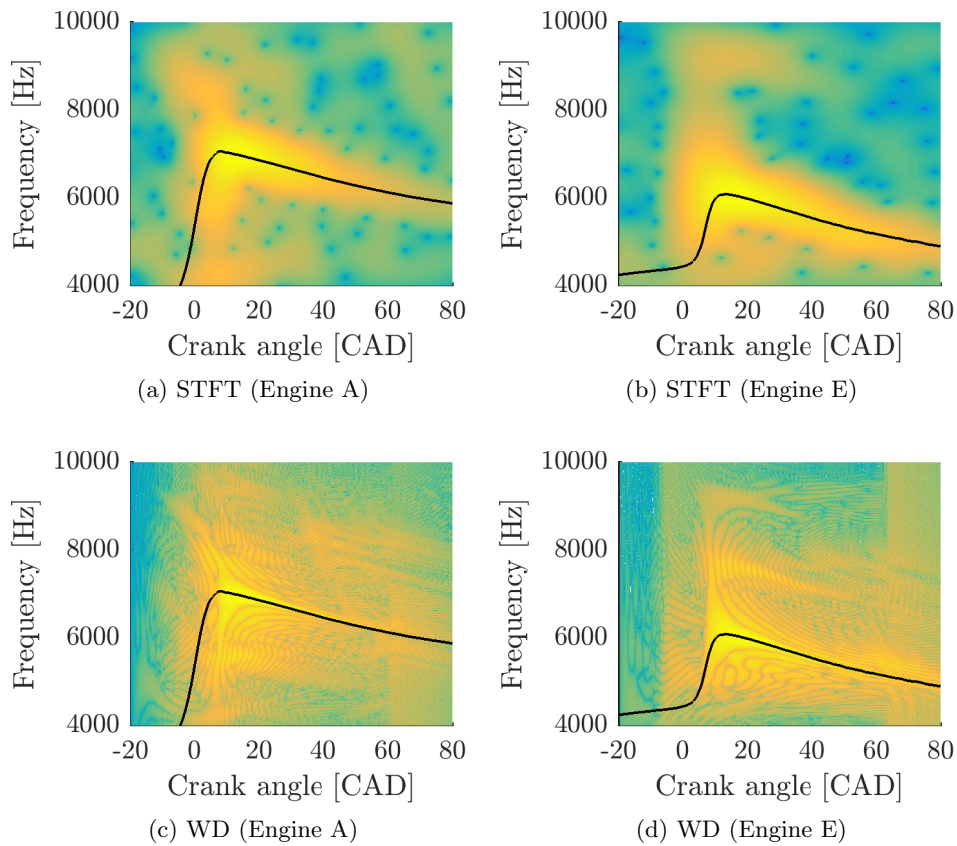


Figure 5.3. Time-frequency spectrum of the in-cylinder pressure signal in engines with pent-roof combustion chamber shown in Figure 5.2: the black line represents the Draper's approximation based on a cylindrical combustion chamber assumption.

5.3 Exceptions to the cylindrical theory

The acoustical response of the combustion chamber may differ from the cylindrical theory for two reasons: bowl-in-piston geometries and the combus-

tion inhomogeneities. The former contradicts the contour conditions used by Draper to solve the wave equation. Some authors already noticed different resonance evolution in this type of combustion chamber such as reported in [6,7]. The later is inconsistent with the assumption of homogeneous temperature distribution, which results in constant sound speed along the chamber. Although in-cylinder inhomogeneities can be negligible in HCCI combustion, they may be much more relevant in a diffusive flame of a conventional CI combustion, where high temperature gradients are expected.

An analysis of these two effects has been performed in Engine D by recording some specific tests, where special attention has been paid to the in-cylinder pressure acquisition, and by modelling the in-cylinder pressure oscillations by FEM with a detailed mesh grid of the chamber combustion geometry.

Specific test campaign. In the five tests of this test campaign, whose characteristics are shown in Table 4.5, in-cylinder pressure was acquired at 1 MHz and the instantaneous engine speed was measured to phase the pressure with the volume signal. The instantaneous engine speed was estimated by measuring the time between digital edges of an optical encoder signal with a resolution of 0.2 CAD, such as depicted in Figure 5.4.

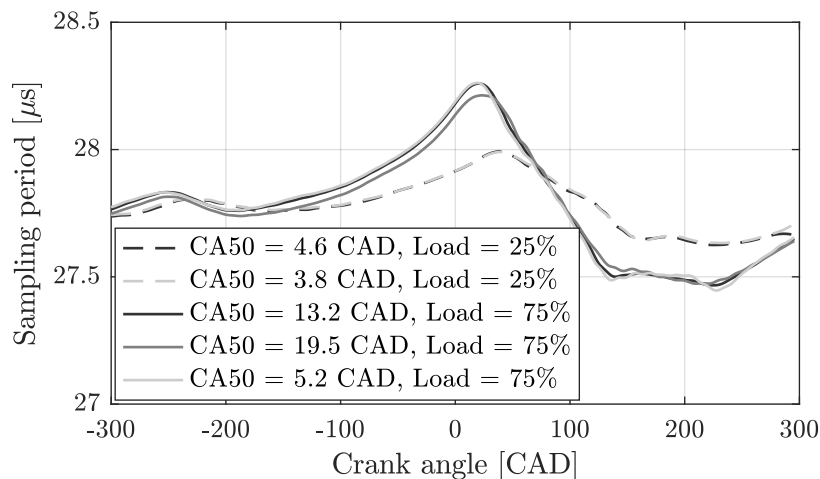


Figure 5.4. Time between digital edges in an optical encoder set at 0.2 CAD in Engine D.

FEM model. For a specific bowl geometry, the natural frequencies and the associated pressure modes can be computed through a FE-based eigenvalue problem [8]. Similar work was presented in [9] for validating the Draper's equation in a pent-roof combustion chamber. Here, the aim is analysing the differences in a bowl-in-piston geometry with diverse zones. Figure 5.5 depicts a particular finite element discretization used in the computations for a crank angle $\alpha = 10$ CAD. The first mode (1,0) is also represented by showing the pressure distribution in the figure for illustration purposes. In this particular case, an asymmetric behavior can be observed, with a diametrical nodal line (green) separating pressure regions in phase opposition.

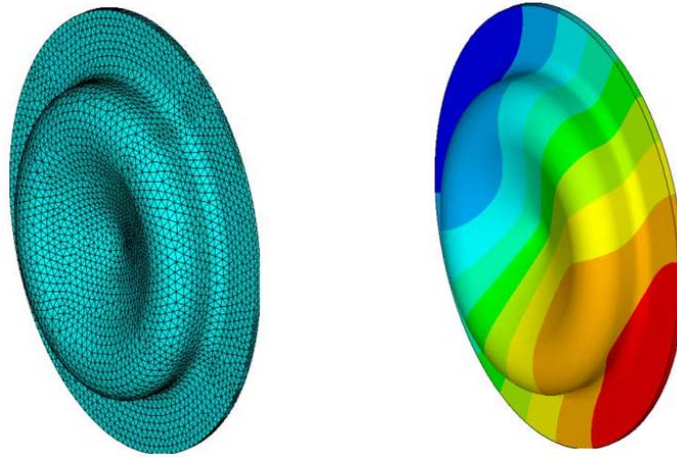


Figure 5.5. Finite element discretization of Engine D near the TDC and FEM results of the in-cylinder pressure oscillations of the first resonant mode.

The numerical calculations have been carried out with a refined FE mesh consisting of three-dimensional 10-node quadratic tetrahedral elements. To guarantee an accurate prediction, the final bowl discretization contains 115659 nodes and 78284 elements, whose approximate size is 0.0025 m. This provides more than 65 quadratic elements per wavelength for the frequency associated with mode (1,0). An approximate variation of 0.008% is found in the natural frequency $f_{1,0}$ between two consecutive meshes with a refinement ratio of 2, from an element size of 0.005 m to 0.0025 m [10]. Thus, it can be assumed that the FE solution has reached the asymptotic range of convergence and the estimated frequency is sufficiently accurate for the current calibration procedure.

5.3.1 Effect of bowl-in-piston geometries

Figure 5.6 shows the results of the STFT and the WD for a cycle extracted from test 1 (1200 rpm and 25% load) in Engine D, together with the Draper's approximation, which was calculated by Equation (5.7). The temperature of the cylinder was computed from the ideal gas law by measuring the mass with a MAF sensor and the EGR by CO₂ intake balance. Note that in comparison with Figure 5.3, where pent-roof combustion chamber was considered, the frequency content of the pressure signal only follows the cylindrical theory at the end of the stroke ($\alpha > 80$ CAD), where the effect of the bowl can be neglected.

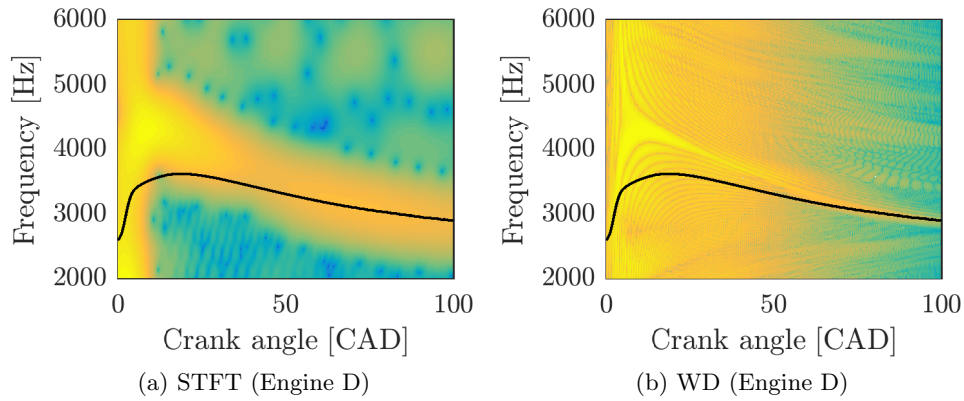


Figure 5.6. Time-frequency spectrum of the in-cylinder pressure in a bowl-in-piston engine (Engine D): the black line represents the Draper's approximation based on a cylindrical combustion chamber assumption.

Equation (5.7) can be rewritten to calculate the Bessel constant $B_{1,0}^c$ from the measured data, as follows:

$$B_{1,0}^c(t) = \frac{f_{res}(t)\pi D}{\sqrt{\gamma(t)RT(t)}} \quad (5.18)$$

The STFT and the WD were calculated for all the cycles at each test and the resonant evolution of the first mode was computed by finding the most excited frequency at each crank angle position. In parallel, twenty mesh grids, from 0 to 100 CAD in 5 CAD steps, were created to simulate the in-cylinder pressure waves by FEM. Figure 5.7 shows the evolution of the Bessel constant estimated using Equation (5.18) from the resonant frequency founded at each test, by averaging the 100 cycles, in conjunction with the FEM results.

The experimental Bessel constant evolution was represented by a dashed line when combustion is still taking place ($\alpha < CA90$) in order to distinguish the effect of the bowl and the consequences of the combustion.

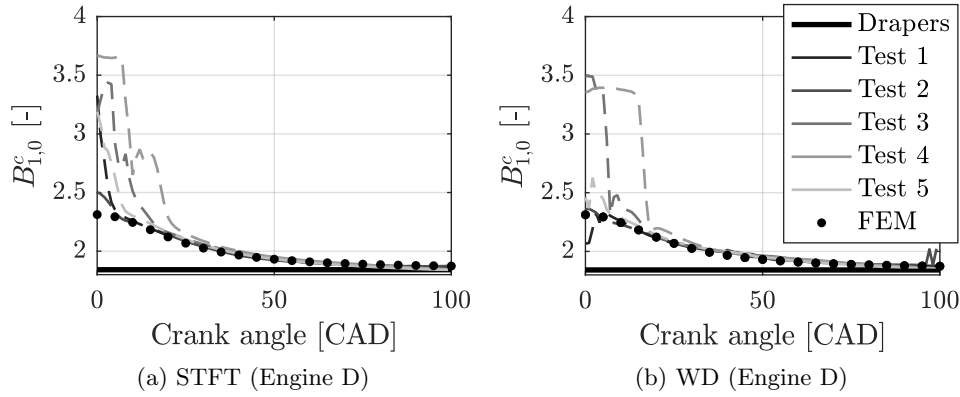


Figure 5.7. Experimental and FEM results of the proportionality between the speed of sound and the resonant frequencies ($B_{1,0}^c(\alpha) = \pi D \frac{f_{res}(\alpha)}{a(\alpha)}$) at various CAD.

Note that FEM results agree with experimental data if combustion is not taking place ($\alpha > CA90$). Indeed, all the experimental results, with various operating conditions, coincide in the same proportion between the speed of sound and the resonant frequency.

More detailed information of the metrics is included in Table 5.2 for tests 1 and 3, at 25 and 75% load, respectively. Here, the average and the standard deviation of $B_{1,0}^c(\alpha)$ for the 100 cycles was calculated in three locations, namely 25, 45 and 65 CAD after the TDC. Two conclusions can be drawn:

- The Bessel factor $B_{1,0}^c(\alpha)$ tends to Draper's value ($B_{1,0} = 1.842$) at the end of the expansion stroke
- Once combustion is complete, the effective Bessel constant, computed according to Equation (5.18), varies only as a function of the chamber geometry since the ratio of the resonant frequency to the speed of sound is independent of the operating conditions.

This last hypothesis, i.e. there is always a direct proportionality between the speed of sound and the resonant frequency for a given geometry, was

Table 5.2. Experimental results of $f\pi D/a$ over different tests.

| test | CA [α] | a [m/s] | Increment | STFT | | WD | |
|------|-----------------|---------|-----------|-----------|-------------|-----------|-------------|
| | | | | \bar{B} | $\sigma(B)$ | \bar{B} | $\sigma(B)$ |
| 1 | 25 | 740.41 | - | 2.085 | 0.006 | 2.075 | 0.008 |
| 3 | | 774.73 | +4.6% | 2.090 | 0.01 | 2.076 | 0.015 |
| 1 | 45 | 683.87 | - | 1.941 | 0.009 | 1.957 | 0.007 |
| 3 | | 726.98 | +6.3% | 1.944 | 0.009 | 1.975 | 0.024 |
| 1 | 65 | 637.10 | - | 1.891 | 0.009 | 1.908 | 0.007 |
| 3 | | 681.27 | +6.93% | 1.882 | 0.01 | 1.898 | 0.01 |

proved by simulating by FEM significant differences in the in-cylinder chamber conditions and checking the resulting proportionality. Table 5.3 collects the results of the FEM simulation when increments and decrements of 10% on the speed of sound have been performed near the TDC, where the resonance differs more from the cylindrical theory. It must be noticed that insignificant variations are found and the hypothesis is consistent with the results.

Table 5.3. FEM results over different chamber conditions.

| α [CAD] | a [m/s] | Increment | $f_{1,0}$ [Hz] | $f\pi D/a$ [-] |
|----------------|---------|-----------|----------------|----------------|
| 5 | 852.1 | - | 5057.8 | 2.29362 |
| | 766.9 | -10% | 4552.0 | 2.29365 |
| | 937.3 | +10% | 5563.6 | 2.29364 |
| 30 | 786.8 | - | 4125.2 | 2.02599 |
| | 708.1 | -10% | 3712.7 | 2.02601 |
| | 865.5 | +10% | 4537.7 | 2.02598 |

Consequently, in non-cylindrical combustion chambers, the Bessel parameter $B_{1,0}^c(\alpha)$ must be calibrated during the piston stroke to precisely predict the resonant frequency evolution. Three methods are suggested:

1. Empirical calibration: the easiest solution for predicting the resonant frequency evolution in a given combustion chamber with bowl consists on using sensor data at some training points and identifying the Bessel parameter through:

$$B_{1,0}^c(\alpha) = \frac{\sqrt{m}f_{res}(\alpha)\pi D}{\gamma(\alpha)p(\alpha)V(\alpha)} \quad (5.19)$$

The main handicap of this methodology is that measurements of the trapped mass are required, and errors on the sensors can be propagated to the final calibration. A precise residuals estimation stands a major challenge.

2. FEM procedure: as it has been presented above, the geometry of the combustion chamber can be modelled with mesh grids and the pressure oscillations can be predicted by FEM. Despite the complexity, this procedure allows a resonance calibration free from measurement errors.
3. Cylindrical assumption far from the TDC: in engines where there are no FEM simulations and neither reliable trapped mass information available, the Bessel parameter evolution could be modelled by assuming a cylindrical response far from the TDC. This procedure consists on first estimating the trapped mass far from the TDC, i.e. between 80 and 120 CAD ATDC, through:

$$m_{cyl} = \frac{B_{1,0}^2 \gamma(\alpha) p(\alpha) V(\alpha)}{(\pi D)^2} = \frac{3.393 \gamma(\alpha) p(\alpha) V(\alpha)}{(\pi D f_{res})^2} \quad \text{if } \alpha > 80 \text{ CAD} \quad (5.20)$$

Once the trapped mass is known, the rest of the Bessel evolution can be predicted by propagating the Bessel constant to the TDC with in-cylinder pressure data and the instantaneous volume estimation.

$$B_{1,0}^c(\alpha) = \frac{\sqrt{m_{cyl}} f_{res}(\alpha) \pi D}{\gamma(\alpha) p(\alpha) V(\alpha)} \quad \text{if } \alpha < 80 \text{ CAD} \quad (5.21)$$

The main drawback of this calibration methodology is requiring resonance excitation at the end of the expansion stroke, as it can only be applied in engines with low resonance damping or in cycles where the resonance is heavily excited.

5.3.2 Effect of in-cylinder inhomogeneities

To characterize the effect of the chamber inhomogeneities during combustion, a two zone FEM, with burnt and un-burnt products, was programmed. The model assumes a combustion with constant volume in order to separate the aforementioned bowl influence from the inhomogeneities effect. Figure 5.8 shows a scheme of the FEM model.

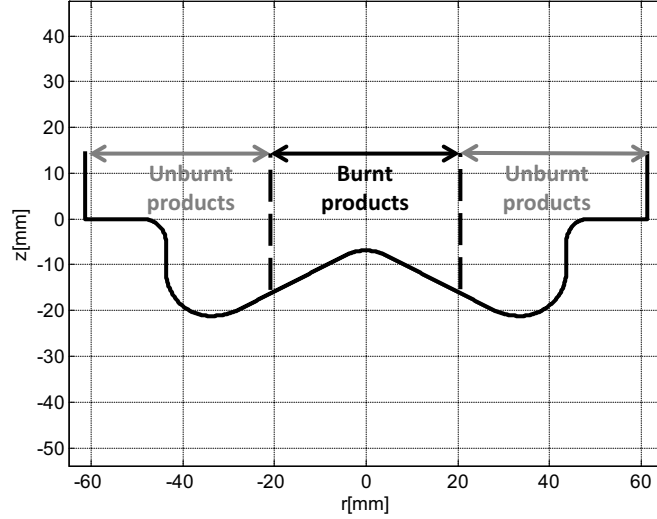


Figure 5.8. Scheme of the two zones simulation.

The simulated combustion was designed from experimental data of the engine, working at 25% load and 1200 rpm. The simulated bulk temperature of the gases T_s was obtained from the heat release rate, by assuming constant volume ($dV = 0$), as follows:

$$dQ = mc_v dT + pdV = mc_v dT_s \quad (5.22)$$

The quantity of each specie, namely burnt and unburnt gases, was obtained by assuming the same MFB evolution, and each gas temperature was inferred by assuming the same in-cylinder pressure in all the combustion chamber. Once the combustion with constant volume was modelled, five simulations, at various MFB ratios, were processed by FEM. The MFB and temperature evolution are plotted in Figure 5.9, where the simulated locations are also marked with crosses. The same simulations were repeated by assuming a single zone with constant temperature.

Table 5.4 collects the results of the single zone and the multi-zone simulation, $f_{1,0}^{1z}$ and $f_{1,0}^{2z}$ respectively. Clearly, important discrepancies, above 10%, appear when combustion is taking place. However, it must be remarked that the model is assuming an infinite temperature gradient by simulating two separated zones. Although, it could not be neglected, the actual effect of the

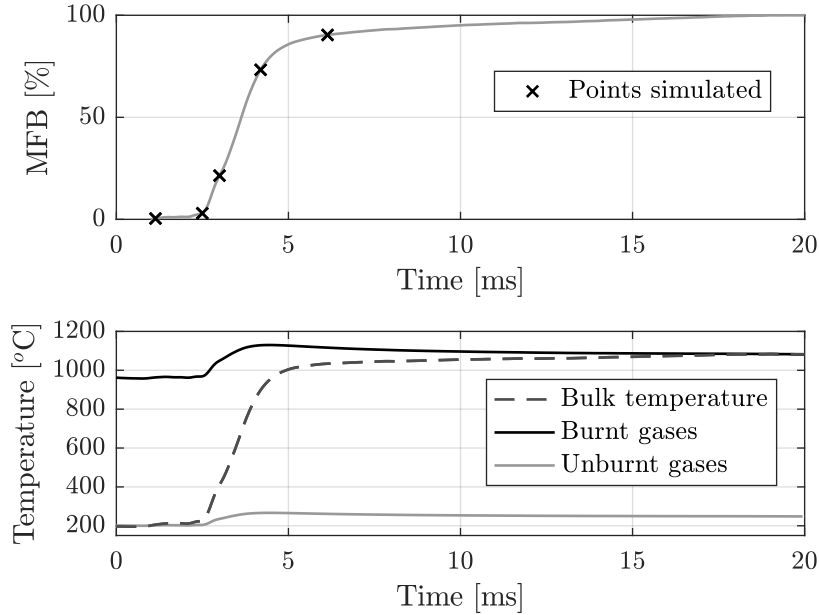


Figure 5.9. MFB and temperature evolution in the combustion simulation at constant volume.

temperature inhomogeneities could be lower in a real combustion.

Table 5.4. FEM results over temperature chamber variations.

| Time [ms] | MFB [%] | $f_{1,0}^{1z}$ [Hz] | $f_{1,0}^{2z}$ | Difference [%] |
|-----------|---------|---------------------|----------------|----------------|
| 1.1 | 1 | 2295.9 | 2306.8 | 0.47 |
| 2.5 | 2.4 | 2346.6 | 2462.1 | 4.69 |
| 3.0 | 20.3 | 2729.0 | 3081.6 | 11.44 |
| 4.2 | 73.4 | 3585.8 | 3857.4 | 7.04 |
| 6.1 | 91.4 | 3802.0 | 3899.2 | 2.49 |

In conclusion, a Bessel parameter evolution can be used to predict the resonant frequency only if the temperature is homogeneous and the gases are properly mixed, i.e. after combustion. When combustion takes place, the acoustical response of the chamber can not be computed from the mean speed of sound.

5.4 Resonance excitation

In IC engines, the resonance excitation is caused by combustion, and hence it mainly depends on the type of combustion. Figures 5.10, 5.11, 5.12, and 5.13, are devoted to represent each combustion mode and its characteristic resonance response. Each figure, contains five plots, labelled from a) to e). The first three plots show 100 consecutive cycles in grey lines, where a single cycle, highlighted in black, was chosen to illustrate the resonance evolution. Plots d) and e) are time-frequency analysis representations, namely STFT and WD, of this selected cycle. Plot a) shows the evolution of the pressure signal in bar, plot b) shows the heat release rate in J/CAD, computed by the apparent heat release law ($\kappa = 1.3$):

$$HRR = \frac{\kappa}{\kappa - 1}pdV + \frac{1}{\kappa - 1}dpV \quad (5.23)$$

plot c) represents the evolution of the amplitude of the first resonant mode, computed by using a STFT with a smaller Blackman-Harris window of 1 ms, i.e. 7.2 CAD at 1200 rpm, and later finding out the maximum within the expected frequency range, namely from 2 to 6 kHz in Engine D and from 4 to 10 kHz in Engine E.

The first two figures, namely Figures 5.10 and 5.11, are based on data from two steady-state points in Engine D. The first one is a CI conventional combustion at full load. Only diesel direct injection was used (228 mg/str) and the SOI of the main injection was located at 12 CAD before the TDC. The second test is an HCCI combustion at 50% load, where 89% of the fuel was gasoline (105 mg/str) port fuel injected at 335 CAD before the TDC, and only 11% of the fuel was diesel (7mg/str), directly injected in the cylinder in two similar injections at 60 and 40 CAD before the TDC, in order to ensure a proper mixture before combustion starts.

The resonance in a CI conventional combustion is excited by the first pre-mixed combustion of the injected fuel, but it is not affected by the diffusive flame combustion, where most of the fuel is burnt at high loads. This can be noticed in Figure 5.10: although the combustion last till 20 CAD after TDC, the resonance gets its highest value just after the combustion starts, around 5 CAD before TDC, and it gets damped during the diffusive flame combustion.

In Figure 5.11 the effect of an homogeneous combustion in the resonance excitation is shown. The combustion only lasts few CAD and, after that, sig-

nificant pressure oscillations vibrate during the rest of the piston stroke. Notice that, although the load was half of that in the presented CI combustion, the resonance is much higher, and it is clearly visible even at the end of the stroke.

Figures 5.12 and 5.13 show two test at low load in Engine E (tests 20 and 5 respectively, according to Table 4.6). In test 20 (Figure 5.12) conventional SI combustion is performed, while in test 5 a SACI combustion is achieved by controlling the amount of residual gases with NVO strategies.

In low load SI combustion, such as in the cycles represented in Figure 5.12, the combustion is dominated by the flame propagation speed which is initiated by the spark. In most of the cycles, the combustion is smooth and the resonance is not excited at all. It must be noticed that some cycles exhibit some resonance excitation around 20 CAD after TDC, this resonance excitation is caused by the autoignition of a small part of the end gas, which is possible due to the unburned gas temperature increment.

In a SACI combustion, the spark is used to create a flame which is propagated through the chamber and elevates the in-cylinder pressure and temperature till the rest of the mixture is auto-ignited. The majority of the mixture is burnt in an HCCI combustion while the SI flame is only used to trigger the auto-ignition. The effect in the resonance is clear: the in-cylinder pressure waves are mostly excited after the autoignition is produced. The difference between SI combustion with knock and SACI is that in a SACI mode the autoignition of the end gas is controlled by varying the spark and controlling the recirculated gases (EGR or IGR), while knock is a random phenomenon in high load conditions induced by temperature hot spots.

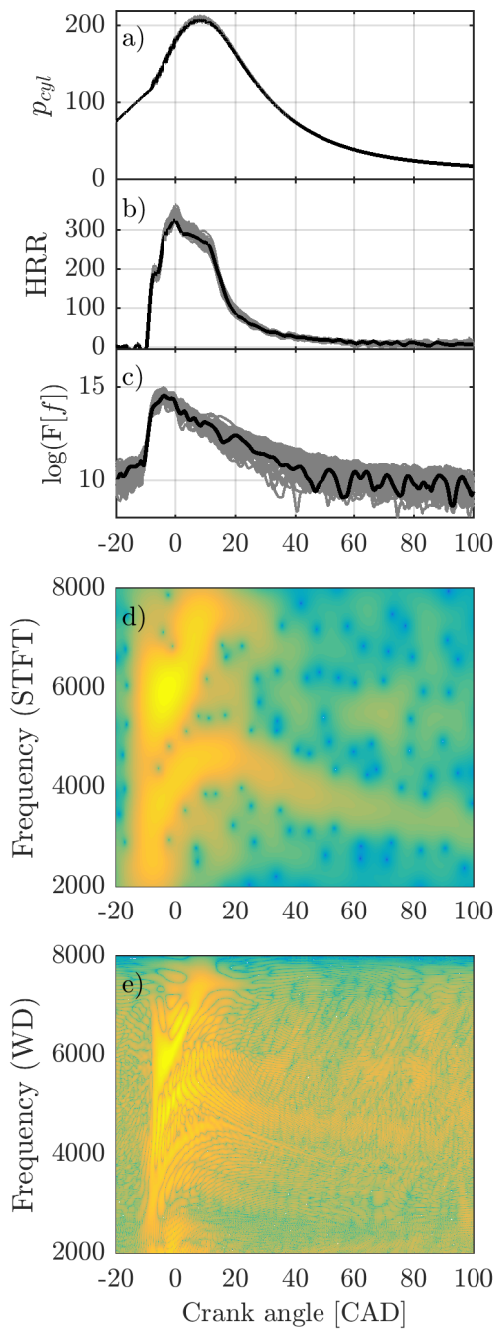


Figure 5.10. CI (Engine D).

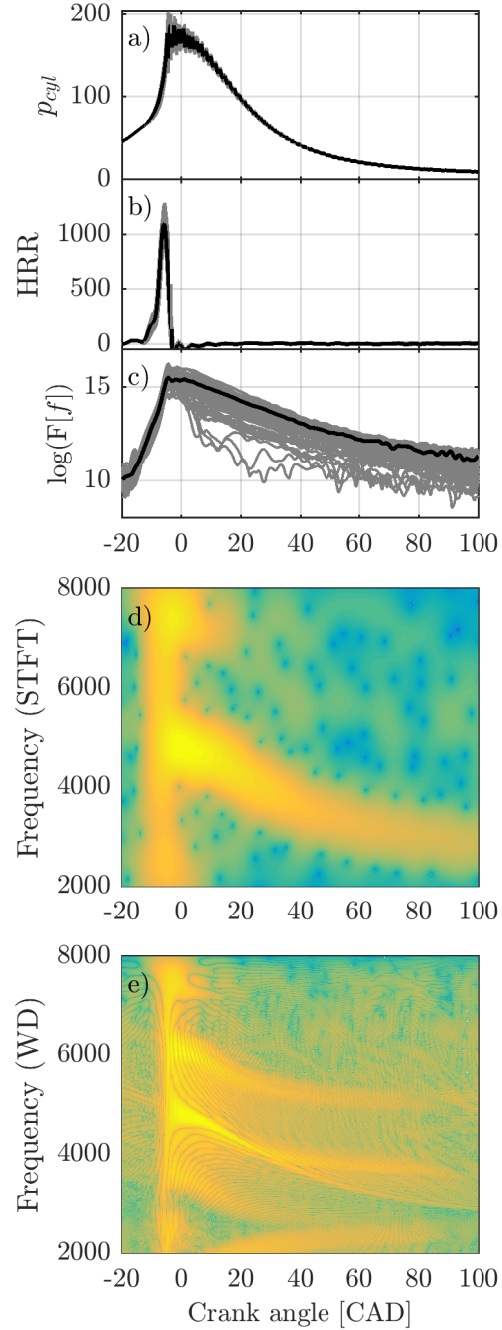


Figure 5.11. HCCI (Engine D).

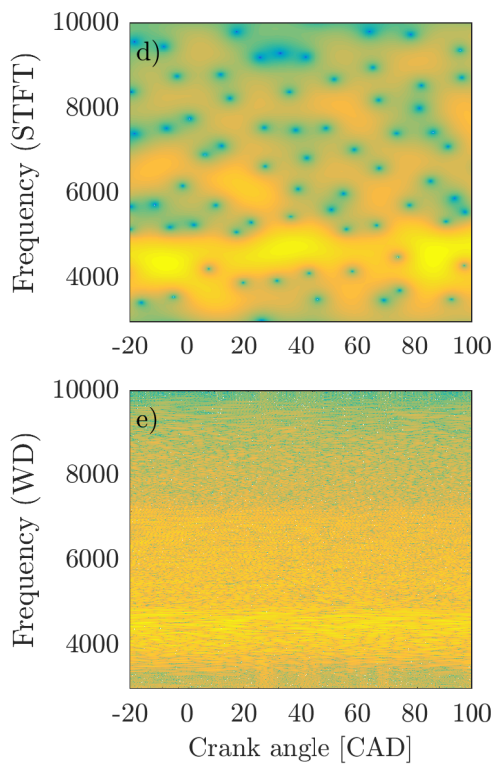
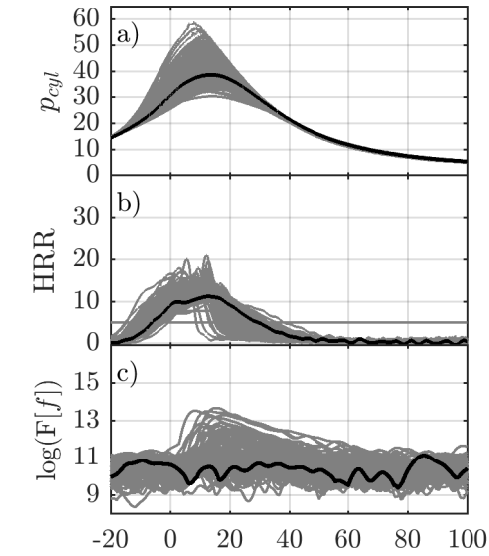


Figure 5.12. SI (Engine E).

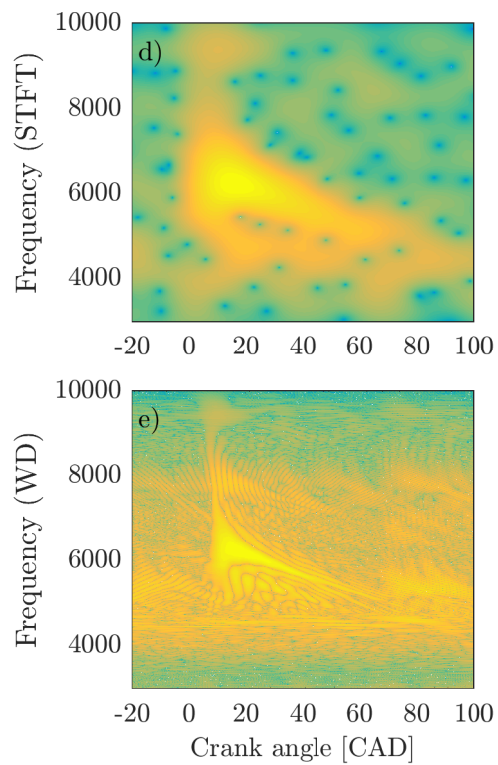
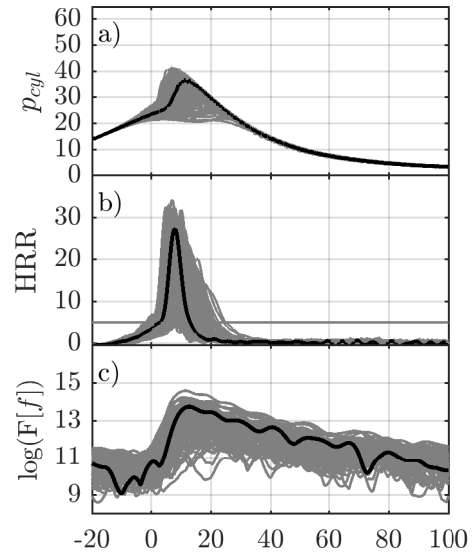


Figure 5.13. SACI (Engine E).

5.4.1 Knock event definition in SI engines

Knock is defined in SI engines as an abnormal phenomenon caused by the autoignition of the end gas during the flame propagation. The autoignition of the end gas occurs when the in-cylinder chamber conditions reach the auto-ignition point before all the fuel is burnt by the SI conventional flame propagation. The auto-ignition point (or knock onset, KO) was described by Livengood and Wu [11] by:

$$\int_{IVC}^{KO} \frac{1}{\tau} = 1 \quad (5.24)$$

where τ represents the autoignition delay, which is computed from the in-cylinder chamber conditions, such as:

$$\tau = C_1 p^{C_2} e^{C_3/T_{ub}} \quad (5.25)$$

Where C_1 , C_2 , and C_3 are constants which describe the autoignition properties of the fuel, and the unburned gas temperature can be computed by assuming a polytropic evolution in the end-gas expansion when combustion starts, as follows:

$$T_{ub} = \begin{cases} \frac{pV}{mR} & \text{if } \alpha < SOC \\ T_{ub}^{SOC} \left(\frac{p}{p^{SOC}} \right)^{\frac{\kappa-1}{\kappa}} & \text{otherwise} \end{cases} \quad (5.26)$$

However, current knock detection algorithms are focused on quantifying the in-cylinder pressure oscillation but they not distinguish the source of the excitation. The most extended indicator is the maximum amplitude pressure oscillation (MAPO) which detects the maximum of the pressure signal after a band pass filter between the frequency range has been applied:

$$MAPO = \max p_{bp} \quad (5.27)$$

However, for identifying if there is knock or there is not, a MAPO threshold must be provided. Normally, in SI engines, knock is maintained at a desired level in a given operating condition, by using the spark advance. In high loads, where knock appears, the SA is advanced as much as possible to achieve high fuel efficiency, till knock is detected. A low MAPO threshold would confuse normal SI combustion with knock, leading to lower engine efficiencies, while a high MAPO threshold would not detect some low knocking cycles leading to dangerous knocking operating conditions or sharp control actions.

Figure 5.14 shows three cycles in Engine A working at OP I with the SA set at 13 CAD before TDC. The pressure signal filtered with a pass-band filter is shown in conjunction with a normal MAPO threshold (0.4 bar), the heat release rate evolution, the unburned gas temperature, and the non-filtered pressure signal.

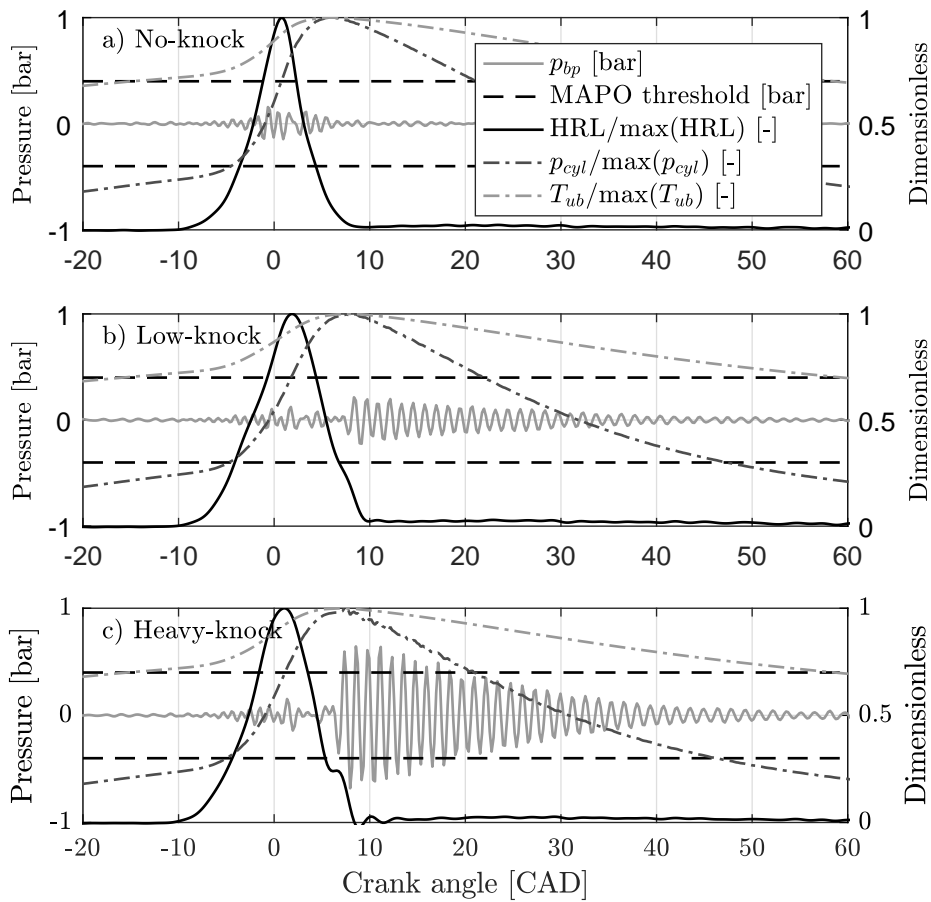


Figure 5.14. Three cycles in Engine A working at OP I with the SA at 13 CAD before TDC: a) non-knock, b) low-knock, and c) heavy-knock..

The auto-ignition of the end-gas, when it occurs, it tends to appear in the final phase of the combustion, next to the maximum pressure and temperature

of the unburned gas, which corresponds to the maximum contribution to the autoignition point, as derived from Equations (5.24) and (5.25). Note that in Figure 5.14 the maximum pressure oscillation of cycle a) and cycle b) is almost the same, while clearly exist autoignition in cycles b) and c).

To determine if there is autoignition or not, a quantification of the resonance energy is proposed in two zones. Two windows of 2.7 ms, i.e. 24 CAD at 1500 rpm, one at the combustion w_C and a second one after the EOC w_A , are proposed. The two indexes are defined by integrating the frequency content in the resonance range, such as:

$$I_A = \int_{f_{min}}^{f_{max}} F [w_A(\alpha)p(\alpha)] df \quad (5.28)$$

$$I_C = \int_{f_{min}}^{f_{max}} F [w_C(\alpha)p(\alpha)] df \quad (5.29)$$

where F indicates a Fourier transform.

Figure 5.15 shows the two window locations in the heavy-knock cycle shown in Figure 5.14.

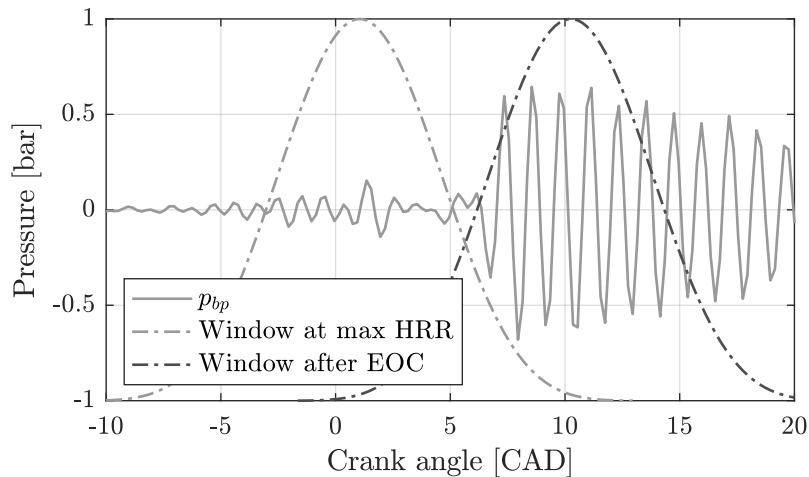


Figure 5.15. A cycle with heavy-knock and the two windows proposed: one at the maximum HRR and other after the EOC.

The final determination of knock is made by comparing the resonance in these two locations, as it is illustrated in Figure 5.16.

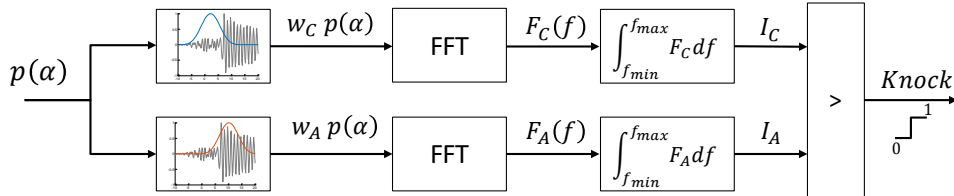


Figure 5.16. Scheme of the new knock event definition algorithm.

Figure 5.17 plots the autoignition Index I_A versus the combustion Index I_C of all the cycles recorded at OP I in Engine A, by using various SA settings. The dashed line represents the new knock event criteria based on detecting more resonance energy at the final phase of the combustion than at the maximum HRR ($I_A > I_C$). In the left plot, the knocking cycles identified with a MAPO threshold of 0.4 have been marked by black dots, while in the right plot, a MAPO threshold of 0.2 was used.

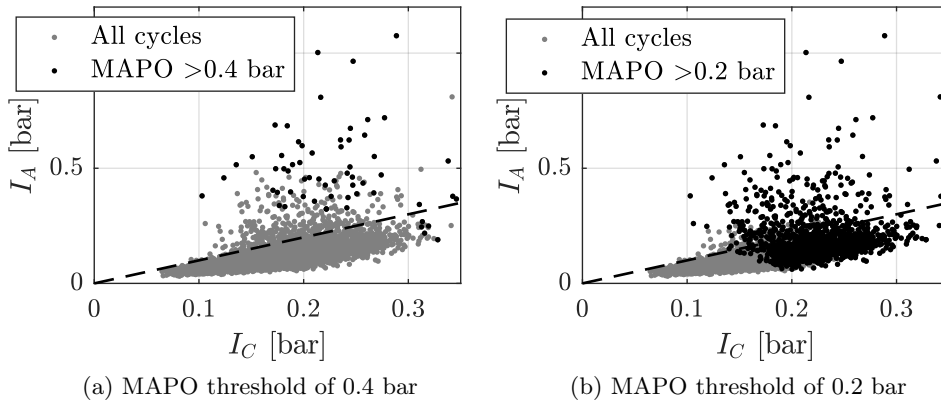


Figure 5.17. Autoignition Index (I_A) versus combustion Index (I_C) at various SA settings at OP I in Engine A. The knocking cycles detected by the MAPO criteria have been highlighted by black dots.

Clearly, by using a MAPO threshold of 0.2 bar many cycles have been identified as knocking when the pressure wave energy at the EOC is lower than at the combustion, while a MAPO threshold of 0.4 bar may not detect

some cycles with evident knock. To illustrate these two errors, two cycles, have been plotted in Figure 5.18. The left plot represents the type 1 error, i.e. detecting a knock when there is not, which is committed with low thresholds. The right plot illustrates the type 2 error, i.e. accepting a knocking cycle, which is characteristic of high thresholds. The main problem of MAPO is that there is no calibration able to differentiate between the excitation of the normal combustion and the one made by the autoignition of the end gas. These two errors may be solved if the new knock event definition is applied ($I_A > I_C$) in commercial applications.

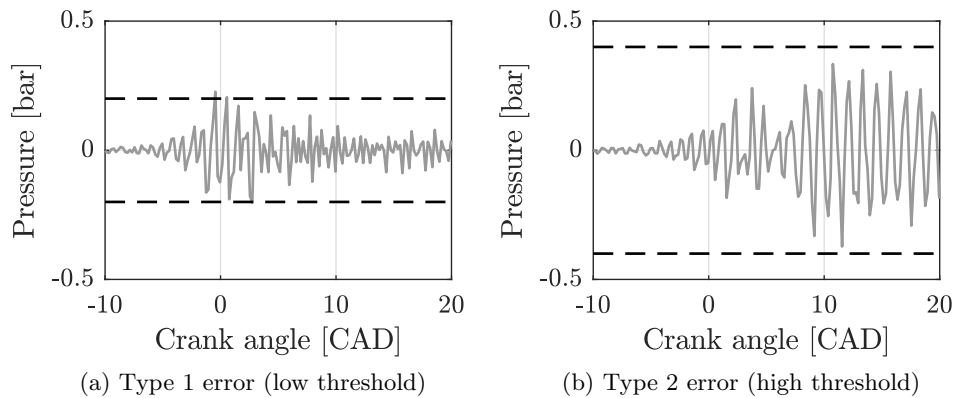


Figure 5.18. Typical errors when using the MAPO index to detect knock.

5.5 Conclusions

In this chapter the basics on the resonance phenomenon have been analysed. The first part of the chapter was devoted to analyse the frequency evolution of the resonant modes: firstly, the Draper's correlation was validated in cylindrical chambers, i.e. in SI engines. Secondly, an analysis of the frequency evolution in bowl-in-piston geometries was presented by using FEM and experimental data. The frequency evolution in engines with bowl can be characterized by a curve in the crank angle domain, and three calibration procedures have been proposed. Finally, the effect of temperature gradients in the chamber was simulated by a two-zones model in FEM. Errors above 10% were identified when comparing with a single-zone model, which point out the convenience of analysing the resonance after combustion has ended.

The second part of the chapter has been focused on analysing the excitation of the resonance. In-cylinder pressure data from various engines has been used to illustrate the effect of the combustion type, namely autoignition, diffusive flame, or flame propagation, in the resonance excitation. Finally, an analysis of the knock phenomenon in SI engine was included and a new knock detection algorithm based on an analysis of the pressure wave energy at the combustion and at after the end of the combustion has been proposed.

References

- [1] Draper C. S. “The physical effects of detonation in a closed cylindrical chamber”. Technical report, National Advisory Committee for Aeronautics, 1938.
(cited in pp. 37, 38, and 114)
- [2] Hubbard M., Dobson P. D. and Powell J. D. “Closed loop control of spark advance using a cylinder pressure sensor”. *Journal of Dynamic Systems, Measurement and Control, Transactions of the ASME*, Vol. 98 Ser G n° 4, pp. 414–420, 1976. (cited in p. 115)
- [3] Pipitone E. “A comparison between combustion phase indicators for optimal spark timing”. *Journal of Engineering for Gas Turbines and Power*, Vol. 130 n° 5, 2008.
(cited in p. 115)
- [4] Eng J. A. “Characterization of pressure waves in HCCI combustion”. *SAE Technical Papers*, 2002.
(cited in pp. 42 and 116)
- [5] Lapuerta M., Armas O. and Hernández J. J. “Diagnosis of DI Diesel combustion from in-cylinder pressure signal by estimation of mean thermodynamic properties of the gas”. *Applied Thermal Engineering*, Vol. 19 n° 5, pp. 513–529, 1999.
(cited in pp. 32, 116, 117, 147, 149, and 209)
- [6] Broatch A., Margot X., Gil A. and Donayre C. “Computational study of the sensitivity to ignition characteristics of the resonance in di diesel engine combustion chambers”. *Engineering Computations (Swansea, Wales)*, Vol. 24 n° 1, pp. 77–96, 2007.
(cited in pp. 39 and 119)
- [7] Torregrosa A. J., Broatch A., Margot X., Marant V. and Beauge Y. “Combustion chamber resonances in direct injection automotive diesel engines: A numerical approach”. *International Journal of Engine Research*, Vol. 5 n° 1, pp. 83–91, 2004.
(cited in pp. 39 and 119)
- [8] Zienkiewicz O. C., Taylor R. L. and Zhu J. Z. *The Finite Element Method: its basis and fundamentals*. Oxford: Elsevier Butterworth-Heinemann, 2005. (cited in p. 120)
- [9] Scholl D., Davis C., Russ S. and Barash T. “The volume acoustic modes of spark-ignited internal combustion chambers”. *SAE Technical Papers*, 1998.
(cited in pp. 38 and 120)
- [10] Fuenmayor F. J., Denia F. D., Albelda J. and Giner E. “H-adaptive refinement strategy for acoustic problems with a set of natural frequencies”. *Journal of Sound and Vibration*, Vol. 255 n° 3, pp. 457–479, 2002.
(cited in p. 120)
- [11] Livengood J. C. and Wu P. C. “Correlation of autoignition phenomena in internal combustion engines and rapid compression machines”. *Symposium (International) on Combustion*, Vol. 5 n° 1, pp. 347–356, 1955. (cited in pp. 34, 131, and 199)

Chapter 6

Trapped mass estimation by using the resonance

Contents

| | | |
|------------|---|------------|
| 6.1 | Introduction | 137 |
| 6.2 | A trapped mass estimation from resonance | 138 |
| 6.3 | A resonance oriented transform | 142 |
| 6.4 | Analysis of the accuracy | 146 |
| 6.4.1 | Method simplifications | 148 |
| 6.4.2 | Quantification in a real operation | 154 |
| 6.5 | Validation in steady-state conditions | 155 |
| 6.5.1 | SI combustion (Engine A) | 157 |
| 6.5.2 | CI combustion (Engine C) | 157 |
| 6.5.3 | Heavy-duty engine with RCCI combustion (Engine D) | 159 |
| 6.5.4 | Two strokes engine with CAI combustion (Engine F) | 160 |
| 6.5.5 | Summary of results | 162 |
| 6.6 | Conclusions | 163 |
| | References | 164 |

6.1 Introduction

The previous chapter was devoted to determine the frequency evolution of the in-cylinder pressure resonant modes. In this chapter, an application of the resonance to estimate the trapped mass is presented. It harnesses the

relation between the speed of sound and the resonant frequency to develop robust procedures to infer the trapped mass.

The first part of the chapter makes use of the STFT to determine the resonant frequency evolution and later obtains the trapped mass by assuming that the mix behaves as an ideal gas. The second part of the chapter describes a new transformation which converts the signal in time domain to harmonics with variable frequency, characterized by virtual masses. The new transformation avoids some disadvantages of the time-frequency analysis and reduces the computational burden. A third part of the chapter is devoted to analyse the main sources of errors while the last part shows some results in various engines.

6.2 A trapped mass estimation from resonance

Equation (5.7) can be rearranged to express the trapped mass as a function of the resonant frequency, the engine parameters, i.e. the Bessel parameter and the bore length, and the in-cylinder conditions, i.e. the pressure, the volume, and γ , as follows:

$$m(\alpha) = \frac{\gamma(\alpha) p(\alpha) V(\alpha) B_{1,0}(\alpha)^2}{(\pi D f_{res}(\alpha))^2} \quad (6.1)$$

where $f_{res}(\alpha)$ must be obtained by analysing the pressure signal in the time-frequency domain and by identifying the frequency with the maximum amplitude in the resonance range at each crank angle location.

In this work the STFT was chosen to compute f_{res} . Although the STFT dilutes the spectrum at each crank angle location by including frequency components of the surroundings, it is a robust methodology which can be implemented online due to the low computational time of the FFT, i.e. the decimation in time algorithm, as it was shown above, in Appendix 4.A.

Equation (6.1) gives an evolution of the trapped mass which accomplishes the wave equation and the ideal gas assumption. Consequently, not only a trapped mass value, but also the evolution during the piston stroke is obtained. Figure 6.1 shows the trapped mass evolution obtained at three consecutive cycles and the averaged value of 100 cycles in Engine D working at 1200 rpm

and 50% load.

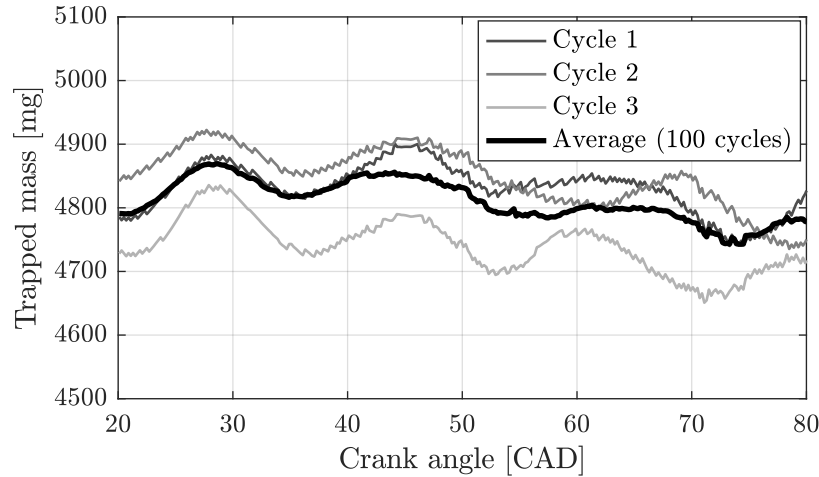


Figure 6.1. Intra-cycle trapped mass evolution measured in test 1 of Engine D.

Although trapped mass should be constant, the oscillations observed in Figure 6.1 are caused by some errors, which are attributed to limitations at the instantaneous frequency determination through the STFT, such as spectral leakage. However, the trapped mass remains almost constant, with variations below 2%, which is consistent with the mass conservation principle if the blow-by is negligible.

Quality metrics. The trapped mass is obtained by averaging the mass evolution during certain period, while the variation of the trapped mass gives an insight on the measurement quality. Figure 6.2 shows the cycle-by-cycle trapped mass measured during 100 consecutive cycles in Engine D working at 1200 rpm and 50% load. Here, the dots represent the trapped mass value computed by averaging the trapped mass evolution from 40 to 70 CAD after TDC, while the bars illustrate the intra-cycle variance in this period. The intra-cycle variations (in bars) must be understood as an index of the measurement quality and not an actual measurement of the trapped mass variation during the piston stroke

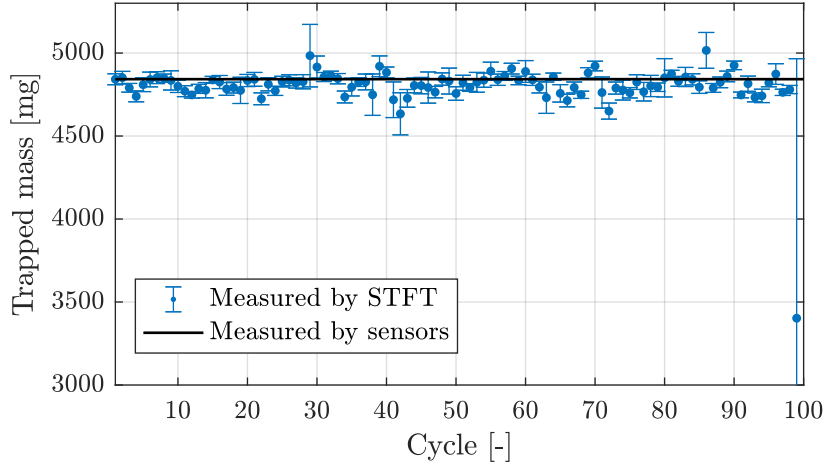


Figure 6.2. Cycle-to-cycle trapped mass evolution measured in test 1 of Engine D.

It must be noticed that the trapped mass measured at the 99% of the cycles has low intra-cycle variability and it is consistent with the trapped mass value measured by sensors, represented with a black line. The cycle-to-cycle differences in trapped mass do not exceed 50 mg which represents a 1% of the absolute value (5000 mg), and is consistent with the commonly cycle-to-cycle variability found in CI engines. The only cycle which is inconsistent with the sensors (the 99th cycle), can be also identified by the high intra-cycle variations, which points out possible errors at the resonant frequency identification.

Region of analysis (Combustion effect). The period analysed to be considered is a compromise between combustion proximity and resonance damping, i.e. when analysing the frequency content during combustion other frequencies can be confused with the resonant modes, but if the analysis is done at the end of the expansion stroke, the resonance could be already damped. Figure 6.3 shows the spectra of the 99th cycle, pointed out in Figure 6.2.

The left plot of Figure 6.3 shows the spectrogram of the cycle where 3 crank angle locations have been selected, while the right plot shows the frequency components between 2 and 8 kHz at each location with a continuous line and the modelled resonant frequency of the first mode with a dashed line.

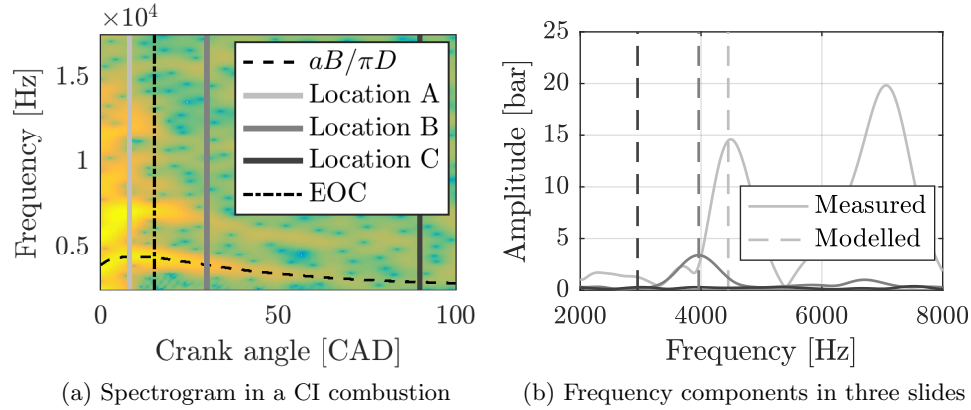


Figure 6.3. Time-frequency analysis of the 99th cycle recorded at 1200 rpm and 50% load in Engine D.

On the one hand, a window located near combustion, such as location A, has to differentiate the desired resonant frequency between the rest of the frequency content excited during combustion, the acoustics of the chamber may be affected by in-cylinder inhomogeneities, as shown in Section 5.3.2, and the sensitivity to manufacturing discrepancies and phasing errors is higher near the TDC, as will be demonstrated later. As the analysis is moved back, the first radial mode becomes more distinguishable, because other resonant modes with higher frequencies are damped faster, as it happens in location B. On the other hand, an analysis of the resonance far from combustion may encounter low excitation in the resonant modes, as it happens in location C.

Cycle-to-cycle resolution. Resonance is characterized by the excitation of the combustion, and consequently, the methodology has one cycle resolution, as the pressure waves of one cycle are independent from others.

To illustrate the potential of the method, nine examples of regulation problems in Engine C, where the VGT and EGR controls did not completely stabilize the intake charge, have been processed by the resonance methodology. Table 6.1 shows the operating conditions of these tests, namely engine speed, load, intake pressure, and EGR, Figure 6.4 shows the intake pressure at each of the 100 cycles analysed, obtained by averaging the instantaneous pressure from 180 to 170 CAD-BTDC, and Figure 6.5 plots the output of the methodology at each of the 100 cycles recorded. Clearly, the method is capable to detect the

transient evolution of the trapped mass while other methodologies, e.g. EGR measurement, may suffer from transport delays and insufficient time response.

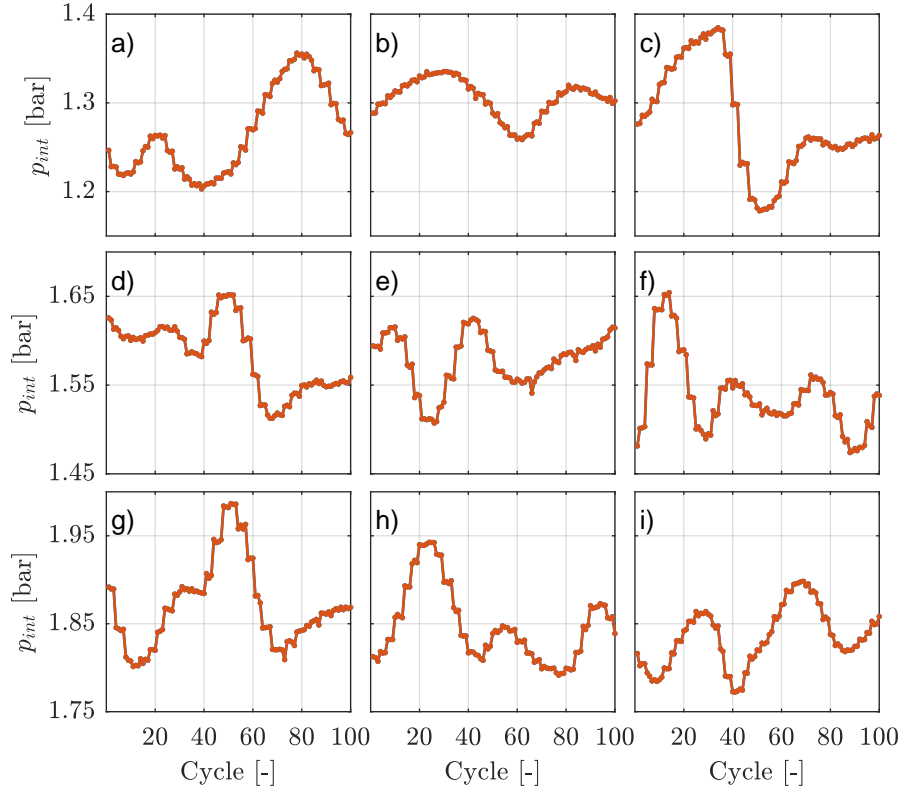


Figure 6.4. Cycle-to-cycle intake pressure measured in nine operating conditions with regulation problems in Engine C.

6.3 A resonance oriented transform

In Figure 6.6 a scheme of the estimation of the trapped mass when using the STFT is shown. It can be summarized in four steps: computing the spectrum of the pressure signal $F(\alpha, f)$, finding the most excited frequency at each crank angle location $f_{res}(\alpha)$, computing the evolution of the trapped

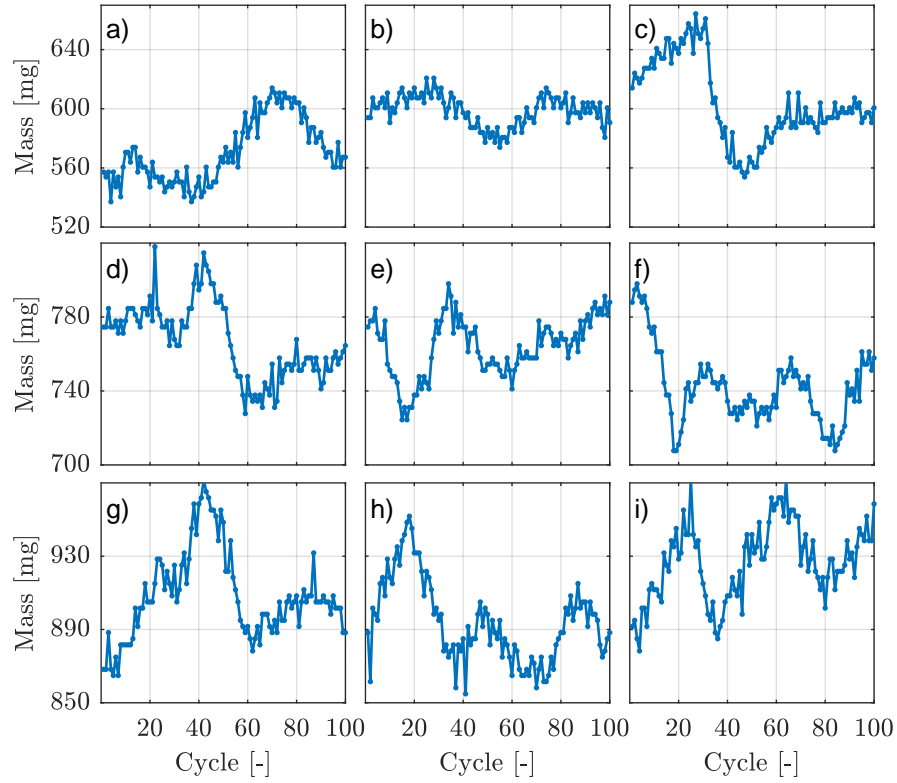


Figure 6.5. Cycle-to-cycle measurements of the trapped mass in nine operating conditions with regulation problems in Engine C.

Table 6.1. Characteristics of six operating conditions with regulation problems in Engine C.

| Example | a | b | c | d | e | f | g | h | i |
|-----------------|------|------|------|------|------|------|------|------|------|
| n [rpm] | 2000 | 2000 | 2000 | 2000 | 2000 | 2000 | 2000 | 2000 | 1500 |
| Load [Nm] | 10 | 10 | 10 | 115 | 115 | 115 | 170 | 115 | 170 |
| p_{int} [bar] | 1.66 | 1.75 | 1.84 | 1.93 | 1.91 | 1.80 | 2.27 | 2.49 | 2.24 |
| EGR [%] | 53 | 1 | 57 | 38 | 4 | 29 | 28 | 29 | 3 |

mass during the piston stroke $m(\alpha)$, and identify the trapped mass and the

quality metrics in certain period, m_{cic} and Q_{cic} respectively.

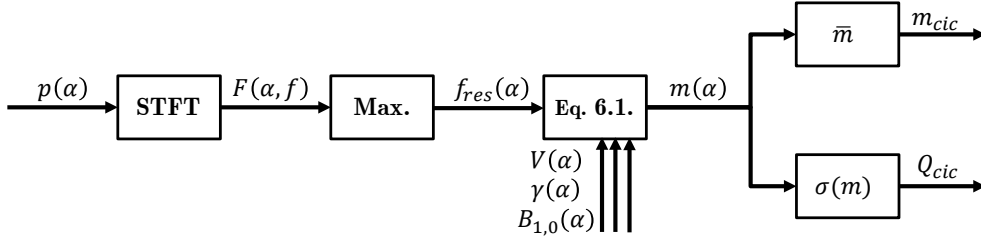


Figure 6.6. Scheme of the trapped mass estimation based on the STFT.

The main problematic of the methodology relies on the first two steps related with the resonant frequency identification f_{res} . A wrong identification at any crank angle location may lead to significant errors in the trapped mass estimation and high intra-cycle variations. Although, various algorithms could be designed to detect the most likely trapped mass estimation by discarding faulty identifications, the problem partially relies on using an analysis for identifying constant harmonics in various crank angle locations, when the aim is finding an harmonic with varying frequency during the expansion stroke.

To avoid time-frequency analysis made for constant harmonics, such as the STFT or the WD, a variation of the Fourier transform, by taking into account variable frequencies is proposed. The Fourier transform is made from a convolution of a given signal, in our case $p(t)$, with an harmonic of constant frequency ($f(t) = f$), as follows:

$$F(f) = \int_{-\infty}^{\infty} p(t) e^{-j2\pi \int_{-\infty}^t f(\tau) d\tau} dt = \int_{-\infty}^{\infty} p(t) e^{-j2\pi ft} dt \quad (6.2)$$

The novel transformation differs from the classical Fourier approach in decomposing the signal by using varying harmonics characterized by virtual masses, defined as:

$$f(t, m) = \frac{\sqrt{\gamma(t)p(t)V(t)}B_{1,0}(\alpha)}{\sqrt{m}\pi D} \quad (6.3)$$

Leading to the following expression for the new transformation:

$$S(m) = \int_{-\infty}^{\infty} p(t) e^{-j2\pi \int_{-\infty}^t f(\tau) d\tau} dt = \int_{-\infty}^{\infty} p(t) e^{-j2\pi \int_{-\infty}^t \frac{B_{1,0}(\alpha) \sqrt{\gamma(\tau) p(\tau) V(\tau)}}{\pi D \sqrt{m}}} d\tau dt \quad (6.4)$$

Which can be rewritten in a discrete form as follows:

$$S(m) = \sum T_s(\alpha) p(\alpha) e^{-j2\pi \sum T_s(\phi) \frac{B_{1,0}(\alpha) \sqrt{\gamma(\phi) p(\phi) V(\phi)}}{\pi D \sqrt{m}}} \quad (6.5)$$

where $T_s(\alpha)$ is the sampling period, which is constant in a time-based acquisition or in a crank-based acquisition where the intra-cycle engine speed fluctuations can be neglected. The limits of the discrete integration can be restricted to α_1 and α_2 in order to analyse only the effect of the resonance in a part of the signal. However, the length of the piece analysed must be always sufficient to detect the pressure wave oscillation. Note that $B_{1,0}(\alpha)$ is constant in engines with pent-roof chamber.

Such methodology allows a direct analysis of the resonance by reducing one dimension of complexity. However, the interference of the low-frequency content of the pressure signal in the transformation must be avoided by performing a high-pass (or a band-pass) filter.

Figure 6.7 shows the result of the direct transform (DT) applied to the cycle shown in Figure 6.3. The highest peak represents the most excited resonant mode, and its mass value is correlated with the Bessel parameter used.

If Equation (6.5) is used with $B_{1,0}$, and the first radial mode is the most significant, as it normally is, the maximum peak of the transformation directly gives the actual trapped mass. Other resonant modes, which also evolve following Equation (6.3) but with a different Bessel parameter, could be represented by other virtual masses, such as:

$$m_{i,j} = m_{cic} \left(\frac{B_{i,j}}{B_{1,0}} \right)^2 \quad (6.6)$$

In Figure 6.7 the two first modes are represented by virtual masses of 4758 mg and 1868 mg, for the first and the second mode respectively, which are consistent with the ratio of the Bessel parameters ($B_{1,1}/B_{1,0} \approx 1.63$). It must be highlighted that even in cycles where the second resonant mode is the

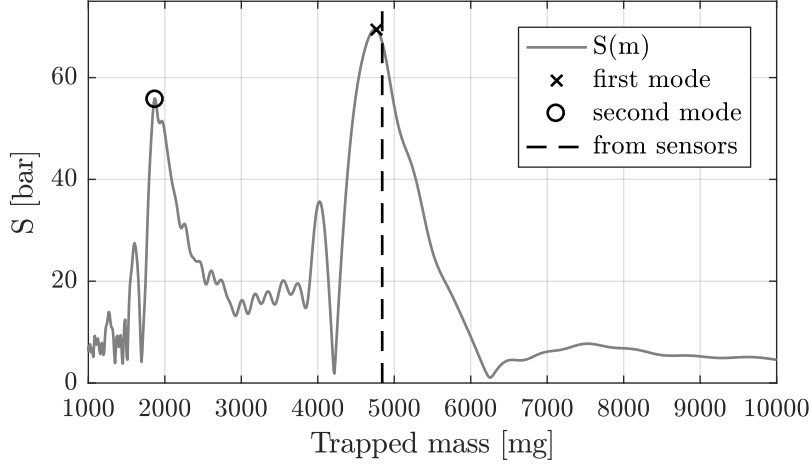


Figure 6.7. Resonance transform of a pressure cycle in test 1 of Engine D.

most significant, the distance of the virtual masses would be 2.65 times the actual trapped mass, which ensures a proper estimation if another methodology with low precision, such as the volumetric efficiency, is used as reference.

The amplitude of the identified peak gives an insight of how excited was the mode. The quality of the measurement can be computed by comparing the amplitude of the peak with the average amplitude, as follows:

$$Q_{cic} = \frac{S(m_{cic})}{\bar{S}} = S(m_{cic}) \frac{\int_{m_{min}}^{m_{max}} dm}{\int_{m_{min}}^{m_{max}} S(m) dm} \quad (6.7)$$

Figure 6.8 shows a scheme of the final implementation of the method.

6.4 Analysis of the accuracy

One of the advantages of the new methodology, based on the in-cylinder pressure signal, is avoiding conventional sensors, such as MAF or λ , which may suffer from some bias due to ageing or malfunctions. The new method can replace, or be combined with traditional sensors, to improve the accuracy and the time response of the final estimation.

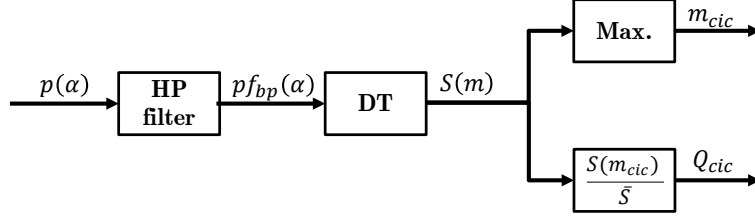


Figure 6.8. Scheme of the trapped mass estimation based on the direct transform (DT).

However, there are other sources of errors affecting the new trapped mass methodology. These errors can be derived by applying linear error propagation [1] to Equation (6.1), following:

$$\begin{aligned}
 \varepsilon(m) &= \left| \varepsilon(p) \frac{\delta m}{\delta p} \right| + \left| \varepsilon(V) \frac{\delta m}{\delta V} \right| + \left| \varepsilon(\gamma) \frac{\delta m}{\delta \gamma} \right| + \left| \varepsilon(f_{res}) \frac{\delta m}{\delta f_{res}} \right| + \left| \varepsilon(B_{1,0}) \frac{\delta m}{\delta B_{1,0}} \right| \\
 \frac{\varepsilon(m)}{m} &= \left| \frac{\varepsilon(p)}{p} \right| + \left| \frac{\varepsilon(V)}{V} \right| + \left| \frac{\varepsilon(\gamma)}{\gamma} \right| + 2 \left| \frac{\varepsilon(f_{res})}{f_{res}} \right| + 2 \left| \frac{\varepsilon(B_{1,0})}{B_{1,0}} \right| \quad (6.8)
 \end{aligned}$$

Equation (6.8) indicates that a 5% error in the pressure, the Volume or γ , is propagated through Equation (6.1) to a 5% error in the trapped mass, however, a 5% error in the resonance identification (or in the Bessel calibration), would cause a 10% error in the trapped mass.

Errors at the Bessel constant calibration $B_{1,0}$ can be reduced selecting an appropriate training dataset, while the precision of the resonance frequency identification f_{res} depends on the frequency response of the pressure sensor, which is not affected by ageing, and the method employed to determine the frequency components in the in-cylinder pressure signal, e.g. STFT. It must be highlighted that the resonance frequency errors $\varepsilon(f_{res})$ do not depend on its intensity but on its value, consequently, if there is sufficient energy on the first resonant modes, errors are negligible. The resolution of the in-cylinder pressure sensor, and the bits employed to acquire the signal, may be the limiting factor for the method applicability when low resonance excitation exist, i.e. if the acquired signal does not guarantee sufficient resolution to discern the pressure waves, the final estimation of the trapped mass may be erratic.

The gas properties, such as γ , depend on the gas composition and the in-cylinder temperature [2], but its value in nominal condition at the expansion

stroke do not change more than 4%, which implies a maximum 2% error if a constant value is set.

The accuracy in the low-frequency content of the in-cylinder pressure is directly propagated to the trapped mass, as can be derived from Equation (6.1). However, pegging uncertainties, i.e. pressure offset, are propagated by the in-cylinder pressure level, being negligible when high pressure conditions exist.

Regarding errors in the volume determination, manufacturing discrepancies cause a constant volume bias, which would be critical near the TDC but negligible far from it, while phasing errors, such as inaccurate TDC location, torsion of the crankshaft, and errors at the instantaneous speed measurement, can lead to crank angle errors, and hence volume errors, which depend on the volume derivative.

Figure 6.9 analyses the effect of 100 mbar deviation in the pegging procedure (error 1) and 0.2 CAD error at location of the TDC (error 2) in a real CI combustion cycle in Engine B. The part of the cycle which may be used for the resonance identification has been highlighted by a continuous line.

As it can be derived from figure 6.9, the selected location for using the new method may amplify conventional errors in the pressure signal, e.g. an analysis between 20 and 50 CAD would add 0.6% error for each 0.2 CAD deviation but only 0.25% for each 100 mbar error, but an analysis between 50 and 80 CAD would be affected by 0.45% error for each 0.2 CAD deviation and a 0.5% error per each 100 mbar error caused by pegging.

6.4.1 Method simplifications

In addition to the in-cylinder pressure signal, the method also makes use of a Bessel parameter calibration (when bowl-in-piston geometries are considered) and estimations of γ and the instantaneous engine speed. Although a precise estimation of all can be afforded by using models or measurements, as suggested in Chapters 2 and 5, they can be replaced by a constant value for control oriented applications.

To analyse the effect of the simplifications, a virtual resonance with 1 bar of amplitude, which perfectly follows Draper's equation and is not attenuated

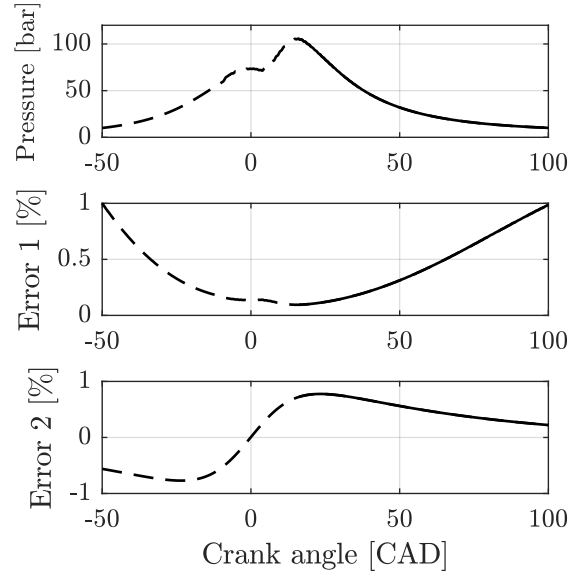


Figure 6.9. Errors derived from pegging and phasing in a real CI combustion cycle at 1200 rpm and 75% load in Engine B: error 1 represents the uncertainty caused in the trapped mass estimation by a deviation of 100 mbar in the pegging procedure, and error 2 shows the effect of 0.2 CAD error in the phasing of the pressure signal.

over the time, was added to the low-pass filtered pressure signal of the cycle shown in Figure 6.9, by using the measured trapped mass, which was 627.8 mg. Figure 6.10 shows the virtual pressure wave used, and the output of the resonance methodology with no simplifications in the transformation. Obviously, the peak of the transform coincide with the trapped mass measured.

Assuming constant γ The specific heat ratio γ can be calculated by using an estimation of the air and burnt gases at the expansion stroke, such as suggested in [2]. The effect of the composition and the temperature is shown in figure 6.11, where the gamma evolution is plotted for three mixture compositions: all air ($\lambda = \infty$), all burnt products ($\lambda = 1$), and 50% of air.

A constant γ may be assumed for simplifying the methodology and reducing the computational burden. Figure 6.12 shows the effect of using two values of γ , when using the new method for the trapped mass estimation between 30

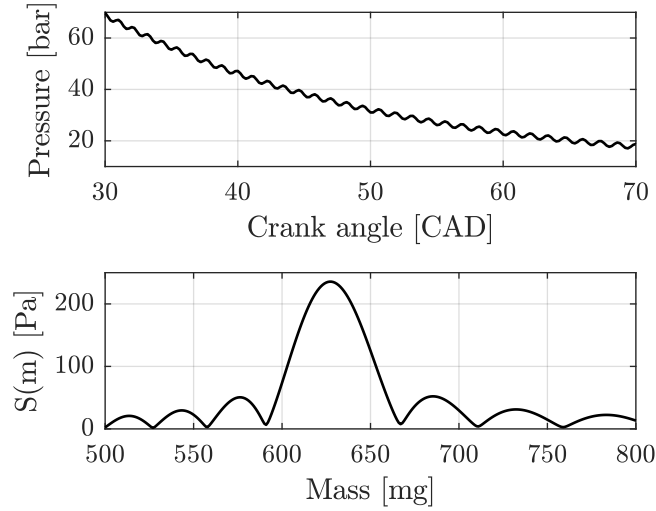


Figure 6.10. Virtual pressure wave used to analyse the effect of some simplifications.

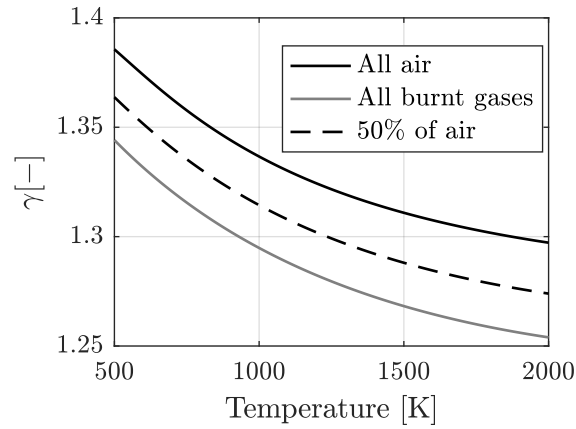


Figure 6.11. Effect of the composition and the temperature in γ .

and 70 CAD in the aforementioned virtual pressure signal.

During the expansion stroke examined (from 30 to 70 CAD) the variations of γ are negligible (below 1%) and only matters the average level. Two solutions are proposed for control applications: either the average value is modelled for any given operating condition or a constant value is used for all the points.

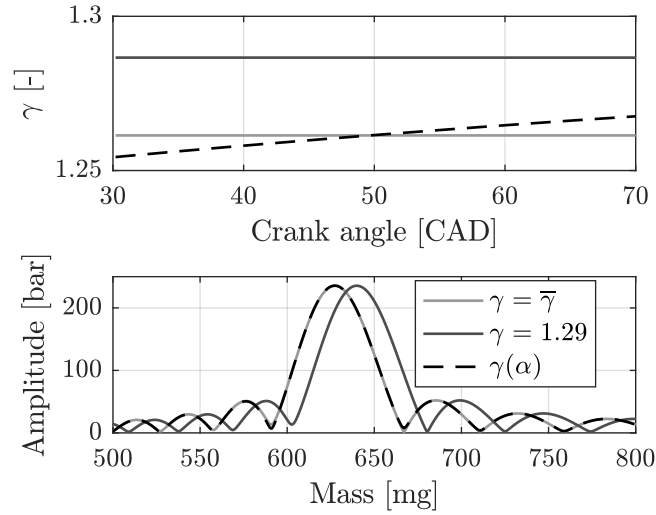


Figure 6.12. Effect of assuming a constant gamma at the trapped mass estimation.

An estimation of the error committed by the later will be presented afterwards.

Effect of the engine speed fluctuations Commonly, the acquisition of the in-cylinder pressure signal is made with constant crank angle period (crank-based) in order to have the pressure signal properly phased with the geometry evolution, and hence with the instantaneous volume.

Figure 6.13 shows the instantaneous engine speed measured by an encoder with 0.2 CAD resolution in Engine B working at 1600 rpm at 6 loads.

From figure 6.13 is derived that the sampling period P :

$$P = \frac{60\Delta\alpha}{360n} \quad (6.9)$$

is not constant, and its evolution is strongly correlated with the load and the engine speed.

The effect of the engine speed fluctuations in the trapped mass estimation is intrinsically related with the region analysed, i.e. if the resonance was

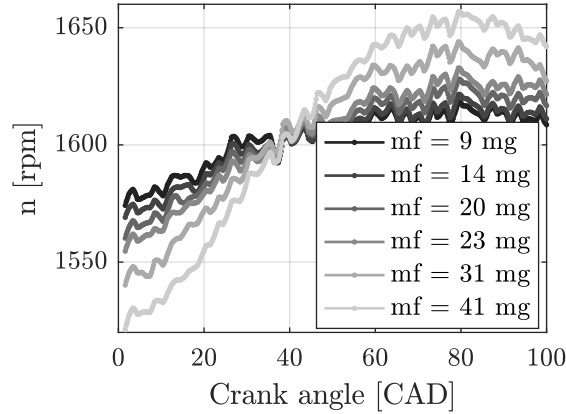


Figure 6.13. Instantaneous engine speed measured in Engine B at 6 different loads.

identified where the maximum engine speed variations are located, the average period would be different at each load, but if the resonance was identified around 40 CAD the mean engine speed of the cycle could be used.

Figure 6.14 shows the effect of assuming a constant engine speed during all the cycle by analysing the resonance in two regions: from 20 to 60 CAD and from 60 to 100 CAD. It must be noticed that if the node where the engine speed fluctuates was known, assuming a constant engine speed would not affect the final trapped mass measurement.

Effect of the Bessel parameter evolution In Chapter 5 the evolution of the Bessel parameter was derived, by FEM and experimental data, for bowl-in-piston geometries. Although the Bessel parameter tends to the cylindrical value at the end of the expansion stroke, the proportion between the speed of sound and the resonant frequency is significantly different near the TDC.

Figure 6.15 shows the effect of neglecting the Bessel parameter variations. Clearly, using the cylindrical theory in these cases, i.e. $B_{1,0} = 1.842$, may have significant deviations from the real trapped mass. However, if the range analysed is kept constant, a representative value could be used for all the piston stroke, at the expense of having some noise, i.e. a lower peak, in the resonance transformation.

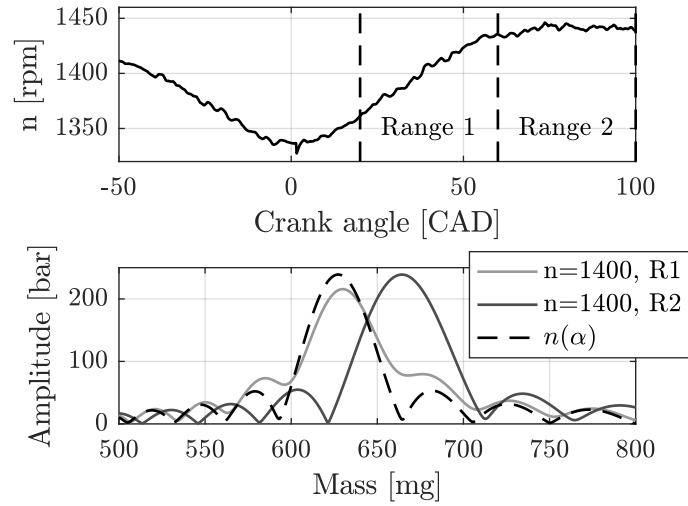


Figure 6.14. Effect of neglecting engine speed fluctuations at the trapped mass estimation by analysing the resonance in two different locations.

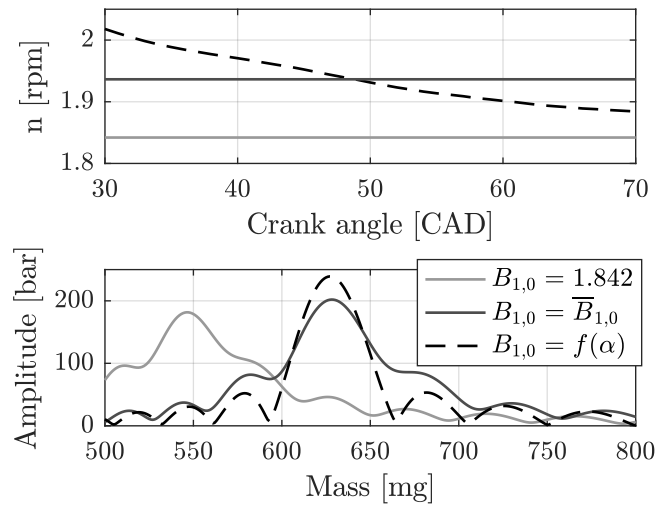


Figure 6.15. Effect of neglecting the Bessel parameter evolution at the trapped mass estimation in bowl-in-piston geometries.

6.4.2 Quantification in a real operation

The trapped mass error depends on the in-cylinder pressure evolution, and thus, it varies with the operating conditions. In order to quantify the effect of each error source when using the same window at the resonance identification, an analysis of the aforementioned errors has been performed in 39 operating conditions in a conventional CI Engine by analysing the pressure trace between 30 and 80 CAD. Figure 6.16 shows the trapped mass and the λ measured as a function of the engine speed and the injected fuel over the 39 tests recorded in Engine B.

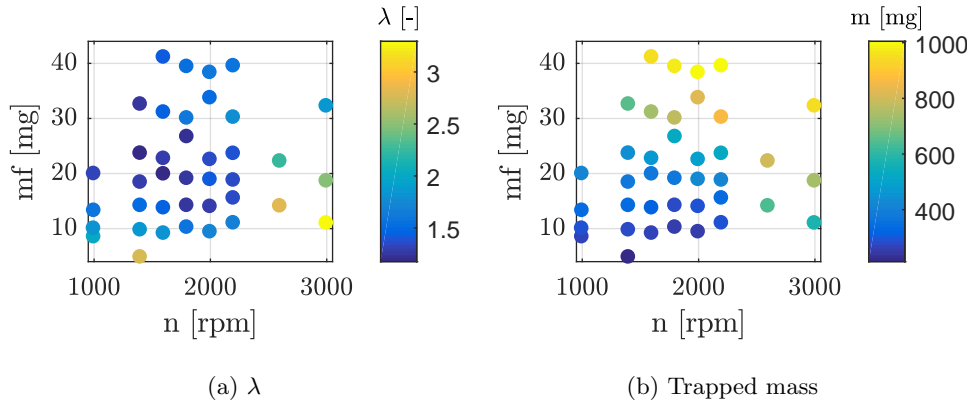


Figure 6.16. Operating conditions of the tests used to analyse the effect of various errors in the method.

To separate the effect of the combustion from the other error sources, a virtual pressure wave was designed. This virtual resonance consisted in a damped harmonic oscillation following the Draper's equation, defined by:

$$p_v = A_{max} e^{-k_d t} e^{2\pi i f_{res}(t)} \quad (6.10)$$

where A_{max} is the maximum amplitude of the oscillation and k_d is the damping constant, both were identified at a single operating condition as 1 and 700, respectively.

Finally, four errors were added to the signal analysed in order to see the effect in the trapped mass estimation. These errors consisted in 100 mbar of pressure offset, 1 CAD error at the phasing, neglecting the engine speed fluctuations and using a $\gamma = 1.29$ for all the operating conditions. These errors

represent extreme values to limit the uncertainty of the trapped mass estimation in a real engine. Figure 6.17 shows the error founded for each uncertainty.

Note that the consequences of the method simplifications, both neglecting engine speed fluctuations and assuming constant γ , can be bounded to a 2% error. The former is critical at low engine speed conditions, but its effect can be neglected at high engine speed conditions. The later is a consequence of not taking into account the effect of λ and the exhaust temperature at the gas properties, which may be easily improved by using the speed-density method for an auxiliary estimation of the trapped mass.

The effect of a pressure offset caused by a bad pegging procedure is only noticeable at low loads, where the pressure at the expansion stroke may be low. However, even at the lowest load operating conditions, the pressure level at the expansion uses to be 10 times bigger than at the reference point, which ensures a small effect on the final trapped mass estimation.

As it is derived from Figure 6.16 b), the consequences of an error at TDC location slightly change with the operating conditions. Therefore, a re-calibration procedure would substantially reduce the error, which may be bounded to less than 0.5 %.

6.5 Validation in steady-state conditions

The methodology was validated in steady-state conditions in four engines with different characteristics, namely engines A, C, D, and F. The main characteristics of the engines have been shown in Chapter 4, the employed parameters to run the method, i.e. the frequency range (f_{min} and f_{max}), the stroke range analysed (α_1 and α_2), and the mass values used (m_{min} and m_{max}), are collected in Table 6.2, while the specific methodologies employed to estimate the trapped mass will be reviewed below.

Regarding the Bessel parameter evolution $B_{1,0}(\alpha)$, in engine A a constant value of 1.842 was setted, as the combustion chamber could be considered cylindrical, in engine D the evolution of the Bessel parameter was obtained at 20 points, from 0 to 100 CAD-AFTC in 5 CAD steps by FEM simulations, while in engines B and F a training data set of some tests at high load (where

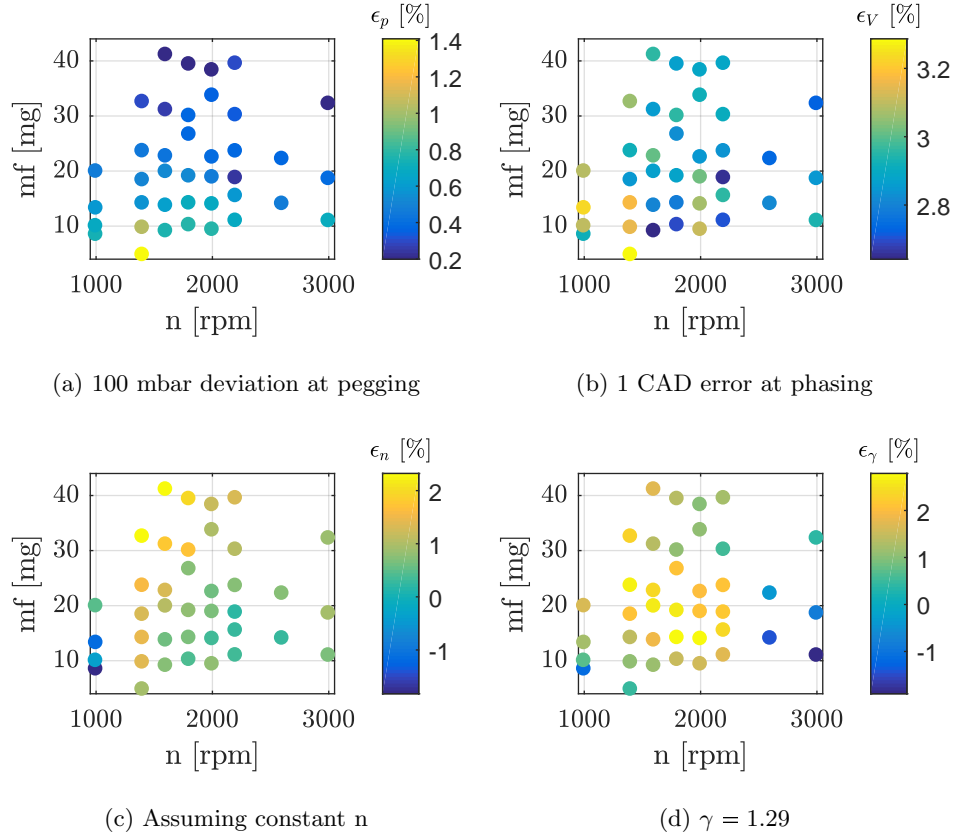


Figure 6.17. Errors identified when applying different uncertainties to the pressure signals of the 39 operating conditions.

the resonance use to be more excited) were chosen to empirically calibrate its evolution.

Table 6.2. Implementation parameter for the resonance method.

| Engine | f_{min} [kHz] | f_{max} [kHz] | α_1 [CAD] | α_2 [CAD] | m_{min} [mg] | m_{max} [mg] |
|--------|--------------------|--------------------|---------------------|---------------------|-------------------|-------------------|
| A | 4 | 10 | 30 | 100 | 300 | 850 |
| C | 3 | 8 | 30 | 70 | 400 | 1400 |
| D | 2 | 6 | 30 | 80 | 2000 | 10000 |
| F | 4 | 10 | 30 | 80 | 150 | 600 |

6.5.1 SI combustion (Engine A)

As mentioned before, Engine A was run at eight operating conditions, varying the SA at each test. Although the resonance excitation was much higher in cycles with knock, a measurement of the mass was achievable in almost all the cycles (95-100%).

To check out the measurement given from resonance, two type of sensors were used: a MAF sensor and a λ sensor, and a fuel balance fuel mass flow metering, which implies accurate measurements in steady-state conditions. This measurement, used in conjunction with a lambda sensor provides an air mass flow estimation, by using:

$$m_{air} = \lambda F_{st} m_{fuel} \quad (6.11)$$

where F_{st} is the stoichiometric ratio (14.7 for gasoline).

Figure 6.18 shows a comparison of the methodologies over the eight operating conditions. It must be noticed that the measurement obtained from resonance is closer to the one obtained from the fuel balance, while the measurement from the MAF sensor seems to have some bias when the operating conditions change. In the Chapter 8, these measurements will be used to feed a knock model and an analysis of the errors will be added.

6.5.2 CI combustion (Engine C)

As commented in Chapter 4, the test campaign in Engine C consisted in 808 tests covering all the operating range in a conventional four stroke CI engine, by varying the EGR settings in 33 operating conditions (n , N_e). The trapped mass was estimated by using a combination of sensors, i.e. a temperature sensor after the EGR mixing for applying the density method, two MAF sensors (one from the engine and another from the test cell), a λ sensor, and a gas analyser to estimate the EGR by CO₂ balance.

At each test, 100 cycles were recorded. In total 80800 cycles with in-cylinder pressure information were used, from them, only 74278 cycles, a 92%, were considered acceptable attending to their quality Q_{cic} . Figure 6.19 shows the measurement obtained from the resonance in front of the measurements

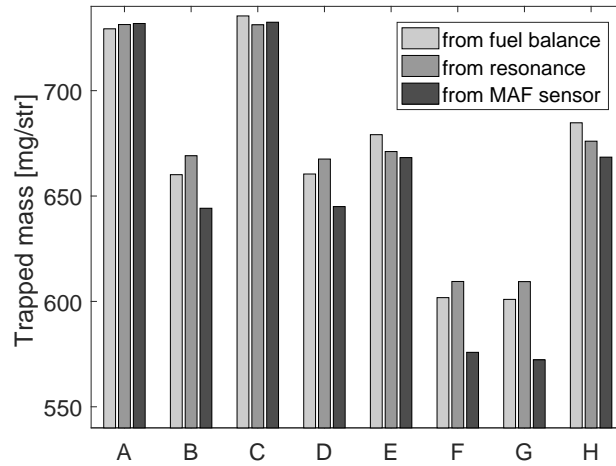


Figure 6.18. Results of the trapped mass estimation in Engine A.

obtained from sensors. As there were too many cycles, a density plot was used: the color of the plots represent the frequency of the cycles, being the lighter colors the most frequent values. The continuous black line represents the expected value consistent with the sensors, while the dashed red lines mark a 10% error, which is considered a limit for the employed methods. The left plot shows all the cycles together, while the right plot only shows the accepted points with sufficient resonance excitation.

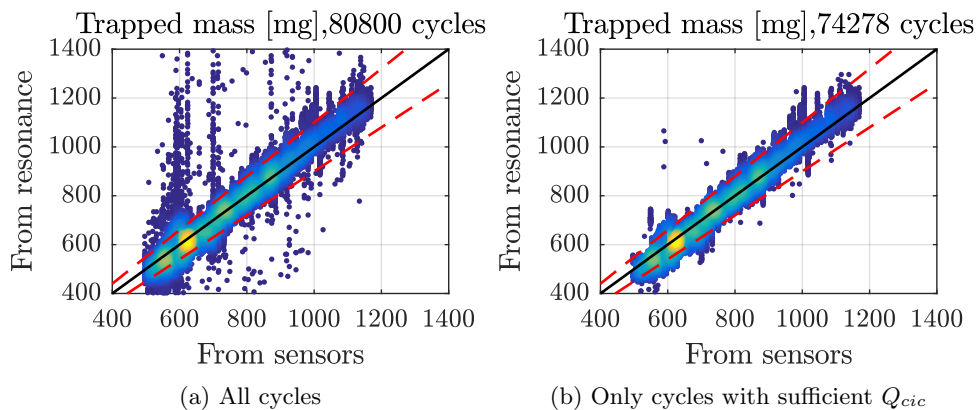


Figure 6.19. Results of the trapped mass estimation in Engine C: all cycles.

It must be highlighted that the measurement provided by sensors consists in a single value for all the 100 cycles while the resonance method gives a measurement for each cycle. As consequence, virtual errors are created as the reference measurement do not take into account cycle-to-cycle variations, which become significant when regulation problems appear, such as the ones shown in Figure 6.5.

6.5.3 Heavy-duty engine with RCCI combustion (Engine D)

Engine D, representative of a truck engine, was used to validate the methodology in a reseach facility, by measuring the air mass by a test cell anemometer, the EGR by an exhaust gas analyser, and the injected fuel by a mass flow meter. The residual gasses have been modelled by modelling the valves with an emptying and filling model, such as described in [3–5].

Figure 6.20 shows the comparison of the values obtained from resonance and the values estimated by sensors. The resonance was sufficiently excited in all the cycles and the values have a good fit with the measurements obtained by the test cell sensors, finding only small discrepancies below 2.5%.

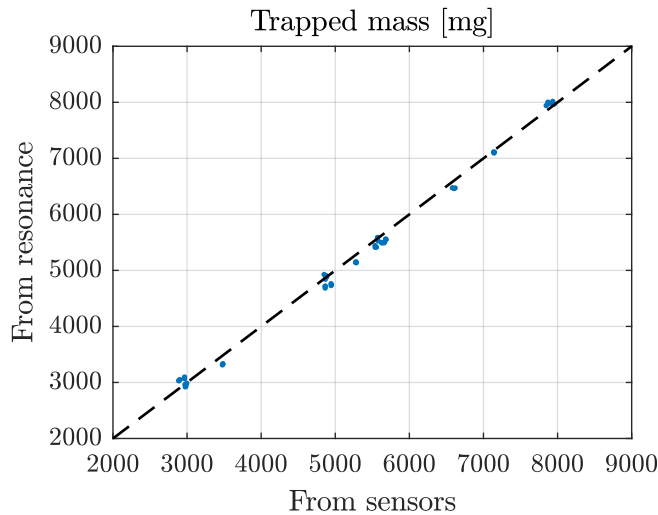


Figure 6.20. Results of the trapped mass estimation in Engine D.

6.5.4 Two strokes engine with CAI combustion (Engine F)

Finally, the method was applied to a two stroke engine with a complex scavenging process, which was described in Chapter 4. Because residual gasses may vary cycle-to-cycle, each cycle may have a different resonance excitation.

Figure 6.21 shows the pressure trace of 250 cycles of a test run at 4000 rpm with a 9 mg injection and with a λ of 1.58. Here, the wide variance in combustions is pointed out. Note that some cycles are auto-ignited near the TDC, heavily exciting the resonant modes, while others do not ignite (misfires).

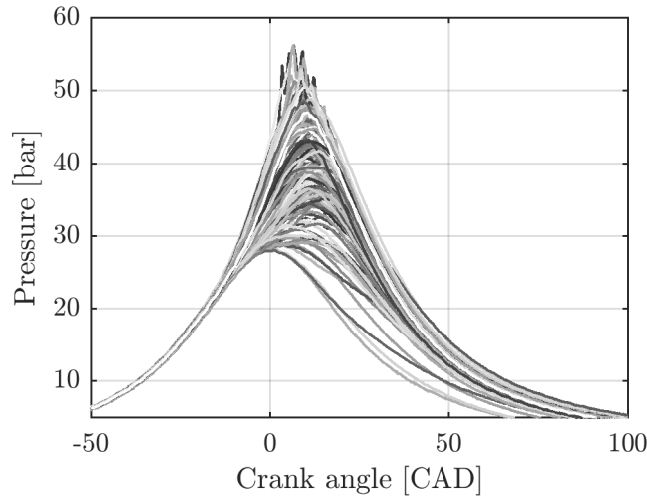


Figure 6.21. Pressure trace of 250 cycles recorded at 4000 rpm and medium load.

The combustion variance depended on the conditions: in some tests, e.g. medium load and low λ , the percentage of accepted cycles was below 10%, while in others, e.g. low load and low λ , the percentage of accepted cycles exceeded 80%.

Figure 6.22 shows two tests to illustrate the performance of the method: in the left plot, a test where the combustion is more stabilized, obtained by injecting 5 mg/str of fuel and inserting 120 mg/str of air, while in the right plot a test with a higher combustion variance, which corresponds with the one shown in Figure 6.21, and was obtained by injecting 9 mg/str of fuel and

inserting 210 mg/str of air. The color scale corresponds to the quality of the each measurement. Although there are many cycles with the same trapped mass value, some others are clearly erratic with a low quality index.

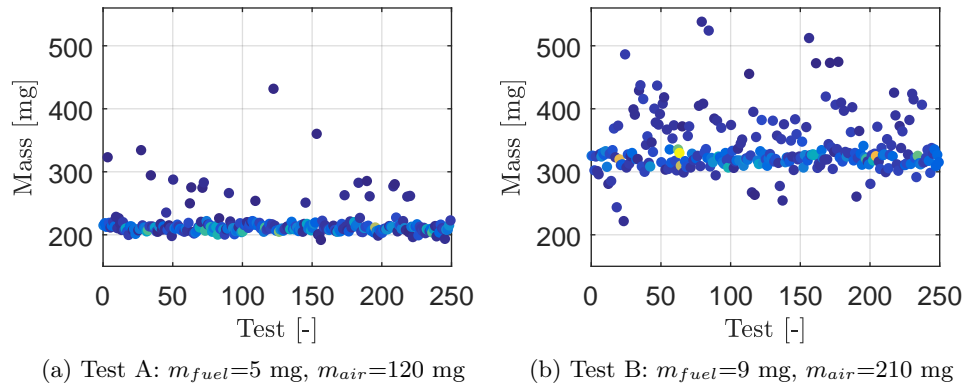


Figure 6.22. Cycle-to-cycle trapped mass evolution at two tests with different settings in Engine F.

Figure 6.23 shows the value of trapped mass versus the quality Index at the 250 cycles of tests A and B. In this Figure the quality index limitation is represented by an horizontal continuous line and the final measurement of the test is shown by a vertical dashed line.

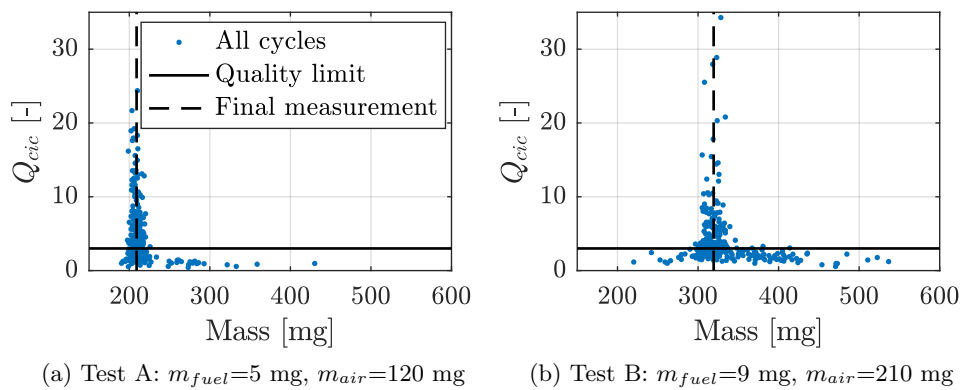


Figure 6.23. Trapped mass value vs. Quality Index at two tests with different settings in Engine F.

The same procedure for avoiding outliers, illustrated in Figure 6.23, was applied to the 45 tests and, in parallel, the trapped mass was computed in three steps: Firstly, the measurements coming from sensors, such as MAF or λ , were collected. Secondly, the short-circuit is quantified by injecting methane in the intake manifold (as a gas tracer), as described in [6]. And thirdly, the residual gasses are estimated by an enthalpy balance at the first part of the compression, as described in [6].

Figure 6.24 collects the values obtained from resonance, the final result provided by the aforementioned procedure, and the measured value of air mass flow.

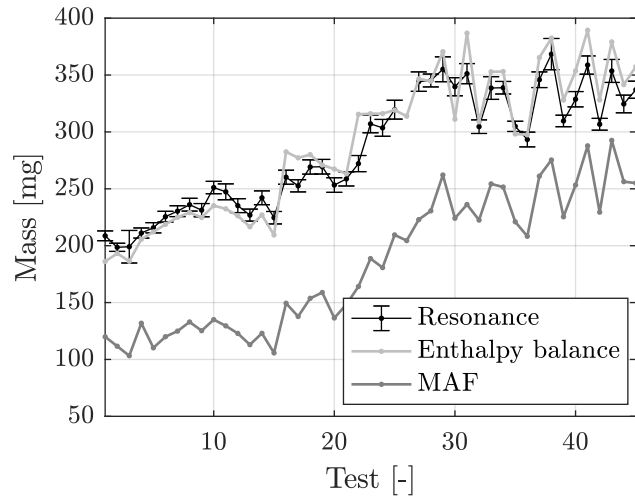


Figure 6.24. Results of the trapped mass estimation in Engine F.

Errors in the enthalpy balance procedure can be attributed to the measurement of the temperatures, which may have 3D effects and be affected by wall heat losses. Figure 6.24 demonstrates the potential of the method in two-strokes engines, where significant short-circuit and residual gasses exist, which are difficult to calculate with conventional sensors.

6.5.5 Summary of results

Table 6.3 collects the differences found in the four engines, as well as the assumptions employed. Only the combustion chamber of Engine A, a

conventional SI engine, had a pent-roof combustion chamber, in the rest of them, Engine D by FEM and engines C and F by experimental data from a training dataset, an evolution of the Bessel parameter during the piston stroke was considered. The engine speed fluctuations are neglected in Engines D and F. In engine A an encoder was installed to measure the instantaneous engine speed each 0.2 CAD, but in engine C a camshaft model was required. The ratio between specific heat capacities (γ) was modelled by semi-empirical equations in all the engines, except in Engine F, because the speed-density approach was not feasible due to the short-circuit. As it can be noticed, the differences founded are consistent with the expected accuracy of the auxiliary methods:

- In engine A, where no EGR exists and the total mass was precisely measured by a fuel balance and a lambda sensor at the exhaust, the differences founded are minimal, below 1%, which may be related to the λ sensor or to the residual gases.
- In engine C and D, where some errors may be caused due to the EGR measurement (by intake CO₂ balance), the differences are maintained between 2 and 3 %.
- And finally, in engine F, where significant short-circuit and residual gases exist, which may complicate the measurement of the trapped mass, the differences are higher, but still consistent with the measured trapped mass, with differences below 5%.

Table 6.3. Summary of the differences founded between the measured mass and the resonance methodology.

| Engine | γ | $n(\alpha)$ | $B_{1,0}(\alpha)$ | Differences [%] |
|--------|------------------|-------------|-------------------|-----------------|
| A | $\gamma(\alpha)$ | measured | $B_{1,0} = 1.842$ | 0.71 |
| C | $\gamma(\alpha)$ | modelled | Calibration | 2.64 |
| D | $\gamma(\alpha)$ | constant | FEM | 2.17 |
| F | $\gamma = 1.29$ | constant | Calibration | 4.36 |

6.6 Conclusions

A novel methodology for estimating the trapped mass was presented. The new method proposes an analysis of the in-cylinder pressure waves excited by

combustion to determine the in-cylinder trapped mass.

Two method implementations have been suggested, either by using the STFT or by performing a direct transformation. The later allows a fast estimation of the trapped mass and avoids errors related with the time-frequency analysis.

The possible errors, such as bad pegging or wrong TDC location, have been analysed and quantified. Even in the worst scenarios, the effect of all the errors can be bounded to 5%, which may be substantially improved by adding a dynamic model for the instantaneous engine speed estimation and an auxiliary estimation of the trapped mass by the speed-density method to approximate the properties of the burnt gases.

Finally, four engines were selected to represent conventional SI and CI engines, and engines working with new combustion concepts which are still in research, such as RCCI and CAI. The method was successfully implemented in all the engines and shown consistent results with auxiliary methods, e.g. in Engines A and D, where a higher precision of the sensors was expected, the discrepancies between the measurements from resonance and the test-cell were below 3%.

References

- [1] JCGM. "Evaluation of Measurement Data - Guide to the Expression of Uncertainty in Measurement". Technical report, Joint Committee for Guides in Metrology (JCGM), 2008. (cited in p. 147)
- [2] Lapuerta M., Armas O. and Hernández J. J. "Diagnosis of DI Diesel combustion from in-cylinder pressure signal by estimation of mean thermodynamic properties of the gas". *Applied Thermal Engineering*, Vol. 19 n° 5, pp. 513–529, 1999. (cited in pp. 32, 116, 117, 147, 149, and 209)
- [3] Payri F., Broatch A., Margot X. and Monelletta L. "Sound quality assessment of Diesel combustion noise using in-cylinder pressure components". *Measurement Science and Technology*, Vol. 20 n° 1, 2009. (cited in pp. 33, 39, 65, 66, and 159)
- [4] Fox J. W., Cheng W. K. and Heywood J. B. "A model for predicting residual gas fraction in spark-ignition engines". *SAE Technical Papers*, 1993. (cited in pp. 65, 66, and 159)
- [5] Senecal P. K., Xin J. and Reitz R. D. "Predictions of residual gas fraction in IC engines". *SAE Technical Papers*, 1996. (cited in pp. 65, 66, and 159)

-
- [6] Benajes J., Novella R., De Lima D., Tribotté P., Quechon N., Obernesser P. and Dugue V. “Analysis of the combustion process, pollutant emissions and efficiency of an innovative 2-stroke HSDI engine designed for automotive applications”. *Applied Thermal Engineering*, Vol. 58 n° 1-2, pp. 181–193, 2013. (cited in p. 162)

Chapter 7

Sensor data fusion

Contents

| | | |
|------------|-------------------------------------|------------|
| 7.1 | Introduction | 167 |
| 7.2 | Model description | 168 |
| 7.2.1 | Sensor and model dynamics | 172 |
| 7.3 | Observer design | 175 |
| 7.3.1 | Identification of outliers | 179 |
| 7.4 | Results | 181 |
| 7.4.1 | Dynamic measurement of trapped mass | 181 |
| 7.4.2 | Suppression of sensors | 182 |
| 7.5 | Conclusions | 184 |
| 7.A | Parameters of the EKF | 184 |
| | References | 186 |

7.1 Introduction

The resonance method offers a direct trapped mass estimation, which may substitute current sensors included in commercial engines. However, the resonance method requires from sufficient combustion excitation, and in some operating conditions a trustful measurement is only achieved at some cycles.

This chapter is devoted to present the mathematical tools required to implement the method in transient conditions: to reject the outliers and erratic measurements, and to combine properly the available measurements. Here,

an observer is proposed by using a variable noise in a Kalman filter.

Firstly, the system dynamics is analysed and the relevant equations are collected together. Secondly, the design of the observer, a Kalman filter, is presented with special attention to discontinuous measurements, such as the trapped mass given by the resonance method or the absence of EGR when the EGR valve is closed, and finally, some experimental results will be shown, covering control input steps and a WLTP cycle.

7.2 Model description

The observer was designed for a four-stroke light-duty CI engine, with EGR and turbocharger. Figure 7.1 illustrates a conventional configuration with some of the sensors that may be useful for a trapped mass observer design. The sensors labelled in black (intake pressure, intake air temperature, lambda, and air mass flow sensors) are sensors commonly available in commercial ECUs, while the in-cylinder pressure sensor, can be only found at some specific engines and in test bench facilities.

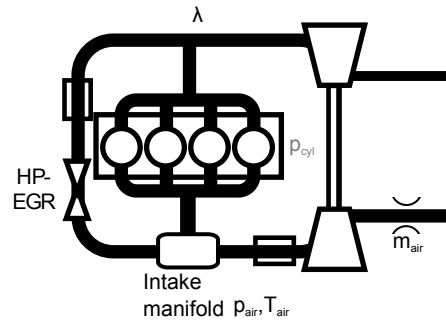


Figure 7.1. Engine scheme and locations of the sensors used for the trapped mass identification.

The exhaust oxygen concentration measurement can be extracted from an UEGO or a smart NO_x sensor, as future engines with SCR will probably dispose from this sensor. The intake pressure sensor can be replaced by the in-cylinder pressure sensor if the pegging procedure is made by assuming an isentropic compression [1–3]. The EGR valve position was also used in the

observer to identify no EGR conditions.

For modelling the system a general state-space representation in a discrete form is suggested, such as:

$$x^{k+1} = Fx^k + f(u) + w \quad (7.1)$$

$$y^k = Hx^k + g(u) + v \quad (7.2)$$

where y are the considered measurements, x the internal states of the system, u the inputs, and w and v the associated noise at each equation.

A discrete implementation with a period of one cycle is proposed in order to facilitate the implementation in current cycle-by-cycle control loops. In the discretization process, the derivatives are obtained from the forward discrete derivative:

$$\dot{x} = \frac{dx}{dt} = \frac{x^{k+1} - x^k}{\Delta t_{cic}} \quad (7.3)$$

where Δt_{cic} is the time in s of one cycle:

$$\Delta t_{cic} = \frac{120}{n} \quad (7.4)$$

And the mass flow terms, represented by \dot{m} in Chapter 3, will be replaced by m when the mass flow units are kg/str, following:

$$m[\text{kg/str}] = \Delta t_{cic}[\text{s/str}] \dot{m}[\text{kg/s}] \quad (7.5)$$

Mass flow models The total trapped mass m_{cyl} is composed from the intake mass flow m_{int} , the injected fuel mass m_f , and the residual gases m_{res} , as follows:

$$m_{cyl}^k = m_{int}^k + m_{res}^k + m_f^k = (1 + RGF^k)m_{int}^k + m_f^k \quad (7.6)$$

The residual gas fraction RGF can be estimated through:

$$RGF = \frac{[pV^\gamma]_{EVO}}{[pV^\gamma]_{EVC}} \quad (7.7)$$

where an isentropic expansion is assumed between the EVO and the EVC.

The intake mass m_{int} is computed through the speed density method. As follows:

$$m_{int}^k = \eta_v^k \frac{p_{int}^k V_{dis}}{RT_{int}^k} \quad (7.8)$$

where η_v is the volumetric efficiency, and V_{dis} the displaced volume.

And the injected fuel mass is derived from an open-loop 2D look-up-table, which takes into account the rail pressure and the energizing time.

Intake manifold dynamics As stated in Chapter 3, the intake manifold pressure dynamics are derived from the thermodynamic laws and the mass conservation principle. If the variations of temperature at the intake manifold are considered, the discrete form is given by:

$$p_{int}^{k+1} = p_{int}^k + \frac{\gamma R}{V_m} \left(m_{air}^k T_{air}^k + m_{EGR}^k T_{EGR}^k - \eta_v^k \frac{p_{int}^k V_{dis}}{R} \right) \quad (7.9)$$

where the speed density method described in Equation (7.8) is used.

If the isothermal model is taken, Equation (7.9) is reduced to:

$$p_{int}^{k+1} = p_{int}^k + \frac{T_{int}^k R}{V_m} \left(m_{air}^k + m_{EGR}^k - \eta_v^k \frac{p_{int}^k V_{dis}}{RT_{int}^k} \right) \quad (7.10)$$

The work presented in this chapter was performed in Engine B, where there was an inter-cooler at the EGR and no measurement of T_{EGR} was available. Consequently, for simplicity and taking into account that the error committed by the T_{EGR} estimation could be higher than the assumption of constant temperature at the intake manifold, the isothermal model was preferred.

The intake manifold volume V_m has been inferred by performing VGT steps with the EGR valve closed in 4 operating conditions, namely 1600 rpm and 8 bar, 1600 rpm and 14 bar, 2400 rpm and 8 bar and 2400 rpm and 14 bar, of engine speed and BMEP respectively. Figure 7.2 shows the VGT step performed at 1250 rpm and 60% load, where the intake pressure was varied from

1.16 to 1.45 and back to 1.16 bar. The isothermal model represented by a black line was feed with the fitted value of intake manifold volume, which was 1.89 l.

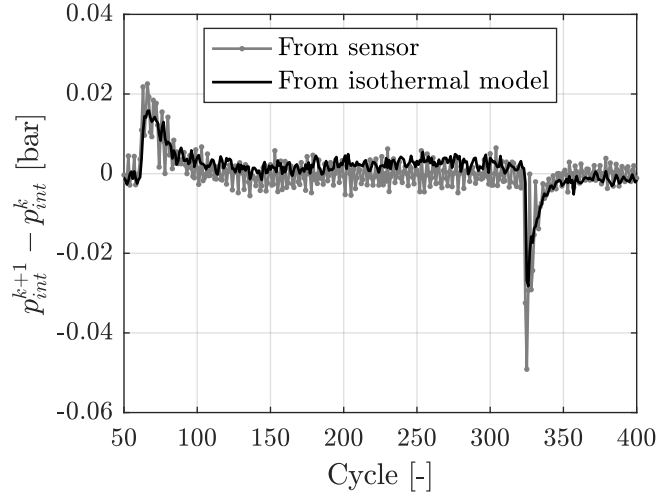


Figure 7.2. Intake pressure variations in a VGT step (from 1.16 to 1.45 and back to 1.16 bar) in Engine B working at 1250 rpm and 60% load.

Exhaust oxygen concentration The exhaust oxygen concentration can be related to the injected fuel mass and the air mass flow, through:

$$F_{exh}^k = \left[1 - \frac{m_f^k F_{st}}{m_{air}^k} \right] F_{air} \quad (7.11)$$

where F_{air} is the atmospheric oxygen concentration ($F_{air} = 21\%$), F_{st} is the stoichiometric air to fuel ratio, i.e. 14.6 with diesel, and complete combustion was assumed.

The λ signal can be related to the oxygen concentration by:

$$\lambda^k = \frac{1 + \frac{F_{exh}^k}{F_{st} F_{air}}}{1 - \frac{F_{exh}^k}{F_{air}}} = \frac{m_{air}^k}{m_f^k F_{st}} \quad (7.12)$$

7.2.1 Sensor and model dynamics

Adding additional states is a common tool for filtering the signals and modelling the response of some sensors. Some of the applications are the following:

Filtering noise. Some values given by the ECU are directly measured. Nevertheless, they are affected by various sources of noise, which may be propagated through the system if they are not filtered. A common solution to filter the measurement given by sensors is adding a state, such as:

$$x^{k+1} = x^k + w \quad (7.13)$$

$$y^k = x^k + v \quad (7.14)$$

The ratio of the noise associated to each equation, w and v , will determine the intensity of the filter. Doing so, a variable filter is included, which can be updated as a function of the operating conditions.

Additional states were added for filtering the air mass flow measurement and the EGR estimation, as follows:

$$m_{air}^{k+1} = m_{air}^k + w_{m_{air}}^k \quad (7.15)$$

$$m_{EGR}^{k+1} = m_{EGR}^k + w_{m_{EGR}}^k \quad (7.16)$$

Models and bias Many other variables used by the ECUs are obtained through models, commonly given by 2D tables as a function of the operating conditions. These models use to be affected by ageing or manufacturing dispersion, which cause certain model bias. In these cases, adding a state with a virtual bias is preferred, as it will keep the time response of the model and will let the actualization to the bias, which will be filtered taking into account the rest of the equations [4].

As an example, the injected fuel mass is normally modelled with a 2D table with the rail pressure and the energizing time as inputs. If the state was the injected fuel mass, when the operating conditions are rapidly changed, the fuel flow would be filtered from the last value to the new one, but if the state

is a virtual bias, the signal would be rapidly actualized.

The injected fuel mass is normally modelled with a 2D table with the rail pressure and the energizing time as inputs, while the volumetric efficiency is tabbed with the operating conditions. Here, a bias of the fuel injection model, and a bias of the volumetric efficiency were included with states to correct the measurements. As follows:

$$m_f^k = m_{f,OL}(p_{rail}^k, TOI^k) + \theta_f^k \quad (7.17)$$

$$\eta_v^k = \eta_{v,OL}(n^k, N^k) + \theta_\eta^k \quad (7.18)$$

$$\theta_f^{k+1} = \theta_f^k + w_{\theta_f}^k \quad (7.19)$$

$$\theta_\eta^{k+1} = \theta_\eta^k + w_{\theta_\eta}^k \quad (7.20)$$

Time response of sensors The response of the sensor can be modelled by a first order system, as it was reviewed above, in Chapter 3. Figure 7.3 shows the oxygen concentration measured from the NO_x sensor (in grey) and from the λ sensor (in black) in a load step, from 60 to 15% load, at 1600 rpm in Engine B.

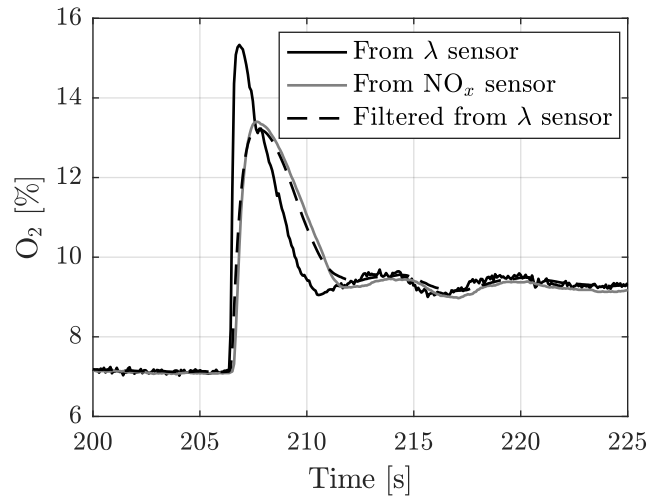


Figure 7.3. Oxygen fraction measured from λ and NO_x sensor.

On the one hand, the λ sensor does commonly exhibit a time response of 100 ms, i.e. less than 1 cycle when the engine speed is below 1200 rpm, as

consequence, the measurement was considered instantaneous. On the other hand, the NO_x sensor does actually show an appreciable time response. The dashed line represents the signal measured by the λ sensor, after applying a first order system, in order to represent the same effect than the observed in the NO_x sensor.

To include the sensor measurement in the system, a state x_m must be added to take into account the sensor dynamics, as follows:

$$x_m^{k+1} = a_S x_m^k + (a_S - 1)x^k + w \quad (7.21)$$

$$y^k = x_m^k + v \quad (7.22)$$

where a_S defines the time response of the sensor.

The intake temperature was measured by a thermocouple located at the intake. A state was added to the system in order to filter the 3D effects caused by incomplete mixing and the sensor noise, such as:

$$T_{int}^{k+1} = T_{int}^k + w_{T_{int}} \quad (7.23)$$

For a commercial application, if a NTC sensor is considered, a first order system, such as proposed in [5], should be included to take into account the slow response of that sensors.

Time delay of sensors The delay of a sensor, caused by the acquisition system or the sensing phenomenon itself, may be significant for some sensors and could vary as a function of the operating conditions [4]. This delay can be included by additional states.

As an example, the following equations:

$$x_{a1}^{k+1} = x^k \quad (7.24)$$

$$x_{a2}^{k+1} = x_{a1}^k \quad (7.25)$$

$$x_{a3}^{k+1} = x_{a2}^k \quad (7.26)$$

$$x_{a4}^{k+1} = x_{a3}^k \quad (7.27)$$

$$y^k = k_0 x^k + k_1 x_{a1}^k + k_2 x_{a2}^k + k_3 x_{a3}^k + k_4 x_{a4}^k + v \quad (7.28)$$

allow to correct a given measurement y of a state x , adding a variable delay, up to 4 cycles, with additional states x_{ai} . The parameters k_0, k_1, k_2, k_3 and k_4 , define the current delay, e.g. for a delay of 4 cycles k_0, k_1, k_2 , and k_3 are 0 and k_4 is 1. In a general form, the number of additional states must be higher than the expected maximum delay.

The present work was validated off-line in experimental data, which was automatically phased by the acquisition platform, and no time delays were required.

7.3 Observer design

The final set of measurements y is composed from the trapped mass given by the resonance m_{cyl} , the EGR actuation u_{EGR} , the intake pressure p_{int} , the lambda measurement λ , the oxygen concentration given by the smart NO_x sensor F_{SS} , the intake temperature measured by the thermocouple T_{int} , and the air mass flow detected by the hot film anemometer m_{air} . Being the states and the measurements of the state space representation, as follows:

$$x = \begin{pmatrix} \theta_\eta \\ \theta_{fuel} \\ m_{EGR} \\ m_{air} \\ T_{int} \\ p_{int} \\ F_{SS} \end{pmatrix}, y = \begin{pmatrix} m_{cyl} \\ m_{EGR} \\ m_{air} \\ T_{int} \\ p_{int} \\ 1/\lambda \\ F_{SS} \end{pmatrix} \quad (7.29)$$

The rest of the variables, such as the injected fuel mass, the residual gas fraction or the volumetric efficiency values given by the models, $m_{f,OL}$, RGF and η_{OL} respectively, are inputs for the system (u).

Collecting the equations of the states presented above, the evolution of the states is defined by:

$$\theta_\eta^{k+1} = \theta_\eta^k \quad (7.30)$$

$$\theta_f^{k+1} = \theta_f^k \quad (7.31)$$

$$m_{EGR}^{k+1} = m_{EGR}^k \quad (7.32)$$

$$m_{air}^{k+1} = m_{air}^k \quad (7.33)$$

$$T_{int}^{k+1} = T_{int}^k \quad (7.34)$$

$$p_{int}^{k+1} = p_{int}^k + \frac{T_{int}^k R}{V_m} \left[m_{air}^k + m_{EGR}^k - \left(\eta_{v,OL}^k + \theta_\eta^k \right) \frac{p_{int}^k V_{dis}}{RT_{int}^k} \right] \quad (7.35)$$

$$F_{SS}^{k+1} = a_{SS} F_{SS}^k + (a_{SS} - 1) \left[1 - \frac{\left(m_{f,OL}^k + \theta_f^k \right) F_{st}}{m_{air}^k} \right] F_{air} \quad (7.36)$$

and the observations are described by:

$$m_{cyl}^k = (1 + RGF^k) \left(\eta_{v,OL}^k + \theta_\eta^k \right) \frac{p_{int}^k V_{dis}^k}{RT_{int}^k} + \left(m_{f,OL}^k + \theta_f^k \right) \quad (7.37)$$

$$m_{EGR}^k = u_{EGR}^k \quad (7.38)$$

$$m_{air}^k = m_{air}^k \quad (7.39)$$

$$T_{int}^k = T_{int}^k \quad (7.40)$$

$$p_{int}^k = p_{int}^k \quad (7.41)$$

$$1/\lambda = \frac{\left(m_{f,OL}^k + \theta_f^k \right) F_{st}}{m_{air}^k} \quad (7.42)$$

$$F_{SS}^k = F_{SS}^k \quad (7.43)$$

It must be noticed that, for clarity purposes, the associated noises, w and v , were not represented in this final set of equations and neither from Equation (7.6) to Equation (7.12).

The selected noise for the evolution of the states w takes into account cycle-to-cycle variations, while the noise related with the observations v is related to the sensor capabilities. Commonly, w and v are modelled as constant Gaussian noise, but in the studied case two exceptions were made:

- EGR measurement: As it was commented in Chapter 3, the EGR is hard to measure and is commonly estimated on-line through the speed density method, by subtracting the measured air mass flow. Nevertheless,

when the EGR valve is closed, there is one degree of freedom less, and the system is substantially simplified.

In order to restrict the EGR flow to zero when the EGR valve is closed but leaving it unobserved when it is opened, a boolean noise is suggested. The noise associated to the EGR measurement is 0 when the intake valve is closed ($m_{EGR} = 0$) and infinite, or substantially high, when the valve is opened.

A better estimation of the EGR could be afforded by using the flow orifice principle, such as suggested in Section 3.3.2.

- Trapped mass from resonance: Regarding the measurement of the trapped mass obtained from the resonance method, described in the previous section, a similar approach is proposed. In the previous chapter, It was demonstrated that faulty measurements in the resonance methodology are partially caused by low resonance excitation. Here, a specific method for erratic measurements identification is proposed below. The method does take into account the resonance excitation and the trapped mass variation in order to determine the validity of the measurement.

In this work, an Extended Kalman filter is used. The Kalman filter allows a fast correction of the states for a linear state-space system [6], generally described by:

$$x^{k+1} = F^k x^k + f(u^k) + Q^k \quad (7.44)$$

$$y^k = H^k x^k + g(u^k) + R^k \quad (7.45)$$

$$(7.46)$$

by solving an iterative Ricatti matrix equation and updating a Kalman gain, such as determined from Equations (3.31) to (3.33).

The matrices F^k and H^k are obtained by linearising the non-linear equations, from Equation (7.30) to Equation (7.43). All the terms of these equations are collected in the Appendix, at the end of the chapter.

The matrices Q^k and R^k represent the associated noise at each equation and they are chosen to be diagonal, i.e. no cross-terms are considered. The values used for the noise associated to the evolution of the states Q^k is consistent with the expected cycle-to-cycle variations and are collected in table

7.1. For simplicity all of them are assumed to be constant but a more complex design with variable noise as a function of the operating conditions could be developed. They have been calibrated in the WLTP cycle for ensuring a fast response of the filter with sufficient robustness. Note that the values of the Q^k and R^k are not actual physical values, but calibratable parameters that characterize the performance of the Kalman filter.

Table 7.1. Noise suggested for the state equation.

| State | Parameter | Equation | Value | Unit |
|-----------------|-----------|----------|-------|----------|
| θ_η | Q_{11} | (7.30) | 0.01 | [-] |
| θ_{fuel} | Q_{22} | (7.31) | 1 | [mg/str] |
| m_{EGR} | Q_{33} | (7.32) | 20 | [mg/str] |
| m_{air} | Q_{44} | (7.33) | 10 | [mg/str] |
| T_{int} | Q_{55} | (7.34) | 10 | [K] |
| p_{int} | Q_{66} | (7.35) | 100 | [mbar] |
| F_{SS} | Q_{77} | (7.36) | 1 | [%] |

In the case of the observations, the suggested noise values R^k are collected in table 7.2.

Table 7.2. Noise suggested for the observation equation.

| State | Parameter | Equation | Value | Unit |
|-----------------|-----------|----------|----------------|----------|
| \hat{m}_{cyl} | R_{11} | (7.37) | 10 or ∞ | [mg/str] |
| \hat{m}_{EGR} | R_{22} | (7.38) | 0 or ∞ | [mg/str] |
| \hat{m}_{air} | R_{33} | (7.39) | 5 | [mg/str] |
| \hat{T}_{int} | R_{44} | (7.40) | 1 | [K] |
| \hat{p}_{int} | R_{55} | (7.41) | 10 | [mbar] |
| $\hat{\lambda}$ | R_{66} | (7.42) | 0.1 | [-] |
| \hat{F}_{SS} | R_{77} | (7.43) | 1 | [%] |

Note that R_{11} and R_{22} are characterised by a constant value if the measurement is considered valid, otherwise the measurement will not be taken into account.

7.3.1 Identification of outliers

In the proposed Kalman filter, when the resonance quality I_q does not reach a pre-defined limit, the associated noise is substantially increased in order to neglect that measurement.

Figure 7.4 shows the effect of removing the cycles with low resonance content in a WLTP cycle in Engine B with the EGR valve closed. The quality Index was defined between 0 and 1, being 0 the most excited cycle, and 1 the worst one. A limit I_q^{lim} of 0.55 was selected for this case. On the one hand, only 10.519 cycles were accepted (over 22.600), but on the other hand, almost all the cycles were close to the air mass flow measurement.

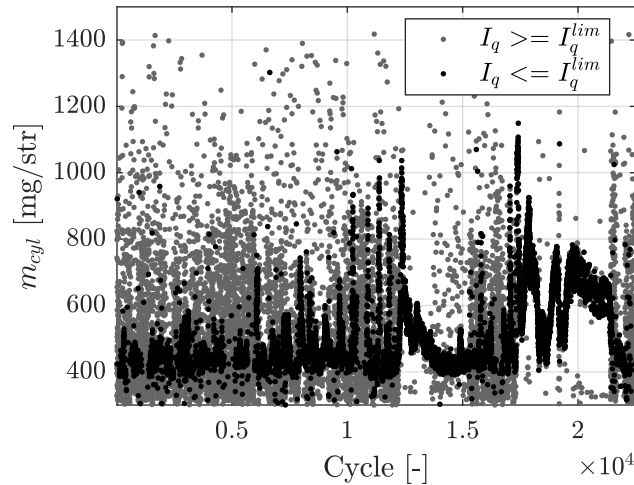


Figure 7.4. Low resonance cycles detection procedure in a WLTP cycle.

The method can give erratic measurements at some cycles, e.g. when another resonance mode does interfere. For detecting these cycles an adaptive methodology for outliers identification is suggested. The method consists on a raw estimation of the trapped mass variations for considering intake pressure changes and an update of the cycle-to-cycle trapped mass variance.

From the speed density method, Equation (7.6), it is derived that the trapped mass changes are proportional to the intake pressure variations if the intake temperature and the volumetric efficiency are considered constant. As

follows:

$$m_{int}^k \approx m_{int}^{k-1} \frac{p_{int}^k}{p_{int}^{k-1}} \quad (7.47)$$

Consequently, the trapped mass measurement m_{cyl}^k is accepted if:

$$\hat{m}_{cyl}^k \in \left[m_{cyl}^{k-1} \frac{p_{int}^k}{p_{int}^{k-1}} - k_\sigma \sigma_m^k, m_{cyl}^{k-1} \frac{p_{int}^k}{p_{int}^{k-1}} + k_\sigma \sigma_m^k \right] \quad (7.48)$$

where $k_\sigma \sigma_m^k$ is the margin related to the cycle-to-cycle trapped mass variations.

The estimation of the cycle-to-cycle trapped mass variations σ_m^k is obtained by an IIR filter characterized by k_f , as follows:

$$\sigma_m^k = k_f \sigma_m^{k-1} + (1 - k_f) |m_{cyl}^k - m_{filt}^k| \quad (7.49)$$

where m_{filt} is obtained by using another IIR filter over the trapped mass estimation m_{cyl} .

Figure 7.5 illustrates the outliers identification procedure over a VGT step in Engine B, working at 1250 rpm and 60% load, when using $k_\sigma = 5$ and $k_f = 0.9$. Note that the adaptation of σ_m is required to contemplate sudden changes in the trapped mass and to deal with various operating conditions, which may be characterized by different cycle-to-cycle dispersion.

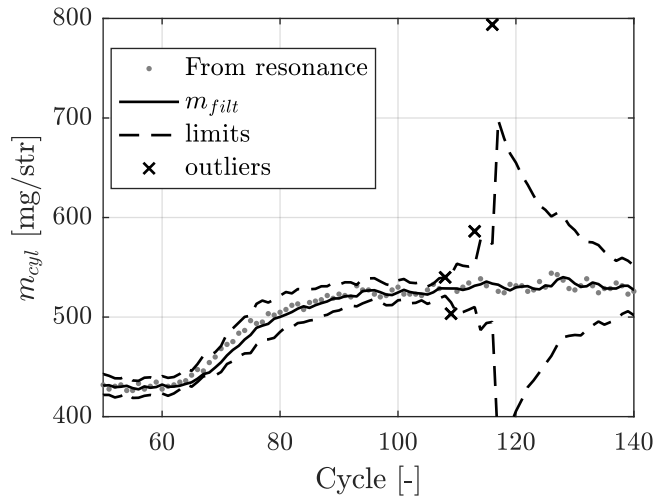


Figure 7.5. Outliers identification procedure illustrated in a VGT step.

7.4 Results

Following, results from the Kalman filter will be shown in transient tests in Engine B. First, a complete WLTP cycle is analysed. The EGR valve was closed in order to compare the final measurement with the air mass flow meter, as there was not any reliable measurement of EGR available in transient conditions. Later, EGR and VGT steps were performed in various operating conditions to analyse the capabilities of the sensor data fusion algorithm. Four set of sensors are proposed and results of the four systems are shown in the steps performed at 60% load and 1250 rpm.

7.4.1 Dynamic measurement of trapped mass

Figure 7.6 shows the result of the Kalman filter in 1050 cycles of the WLTP cycle. The full cycle is shown below, in Figure 7.7, where the lambda and the bias encountered at the injected fuel and the volumetric efficiency tables have been also plotted. The measurement of the air mass flow and the estimated injected fuel is plotted with a green line, while the in-cylinder flow value, i.e. removing the residual gases, is plotted with a black line for the model output and with dots for the resonance estimation.

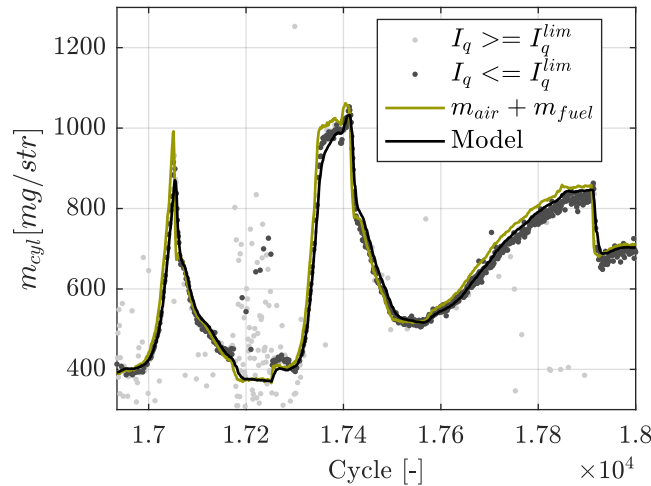


Figure 7.6. Trapped mass estimation in 1050 cycles of the WLTP cycle in Engine B.

The implementation in the WLTP cycle shows the capabilities of the Kalman filter to take into account the dynamics of the intake manifold, while maintaining sufficient robustness when the resonance is not sufficiently excited.

The air mass flow meter measures the effect of turbocharger variations, while the output of the resonance model gives an estimation of the in-cylinder trapped mass, which takes into account the accumulation effect of the intake manifold. The difference of that dynamics can be noticed in Figure 7.6, at the peak located between the cycle 17.000 and the cycle 17.100, where the black line, which represents the output of the Kalman filter, is consistent with both, the air mass flow measurement and the resonance estimation, by using Equation (7.10).

The areas where the resonance is poorly excited, e.g. idle, the kalman filter assumes a high noise at the measurement given by the resonance method, and the model output is obtained through the intake pressure variations. This is shown in Figure 7.6, around the cycle 17.200, where the resonance method did not give any appropriate measurement.

7.4.2 Suppression of sensors

The proposed Kalman filter is based on a dynamic intake manifold model to estimate the intake charge. Later it uses the λ or the NO_x sensor in combination with the previously obtained intake charge value to estimate the injected fuel mass.

The trapped mass value obtained from the in-cylinder pressure resonance allows a precise estimation of the intake charge, and hence, a direct estimation of the EGR which implies an online adaptation of the volumetric efficiency. Nevertheless, some sensors could be removed in order to alleviate the costs.

Four set of sensors are proposed, which are collected in table 7.3. The Kalman filter at the WLTP cycle, shown in Figure 7.7, was runned with the first set of sensors, namely the air mass flow meter, the trapped mass measurement from resonance and the λ sensor. The second set of sensors aims to eliminate the air mass flow meter by using the measurement given by the resonance and the λ sensor. Finally, the last set of sensors, which is the most common in commercial vehicles, shows the consequences of not having a direct

measurement of the trapped mass.

Table 7.3. *Suggested set of sensors.*

| Number | Resonance | MAF | λ | NO_x |
|--------|-----------|-----|-----------|---------------|
| 1 | Yes | Yes | Yes | No |
| 2 | Yes | No | Yes | No |
| 3 | No | Yes | Yes | No |

Regarding the rest of the sensors suggested in Equation (7.29), note that the intake pressure sensor can be replaced by a pegging methodology by using the in-cylinder pressure evolution and assuming an adiabatic compression, such as suggested in [1–3], the intake temperature could be replaced by the intake air temperature with minimum effects, and a feedback measurement of the exhaust oxygen concentration can be used indistinctly from the λ or the NO_x sensor, i.e. the results of the Kalman filter were almost identical.

Figures 7.8 and 7.9 show a VGT and an EGR step at 60% load and 1250 rpm. The result of the Kalman filter, when using the first set of sensors, is shown with a black line. The final trapped mass value, given by the model, follows the measurements given by the in-cylinder pressure resonance (third plot) by modifying the volumetric efficiency (first plot) in order to capture its variations. The lambda measurement (fourth plot) is achieved by modifying the injected fuel mass given by the ECU model (second plot).

Figures 7.10 and 7.11 plot the results of the same steps shown in Figures 7.8 and 7.9, but adding the output of the other set of sensors.

Note that when the EGR valve is closed, all the set of sensors exhibit an acceptable precision, as shown in the VGT step (Figure 7.10). However, if the air mass flow is not available, the injected fuel mass can not be corrected.

Regarding the EGR estimation, a measurement of the trapped mass is required for determining the EGR quantity with sufficient precision. If the set 2 is selected, a small error of few mg at the injected fuel model becomes in significant errors at the air mass flow estimation and hence, in the final EGR distribution. If a constant volumetric efficiency is used (set 3) the value of the EGR can not be precisely estimated.

7.5 Conclusions

A Kalman filter has been designed in order to combine various sensors to estimate the trapped mass in reciprocating engines. The final algorithm is aimed to include the novel methodology, which uses the in-cylinder pressure waves to estimate the trapped mass at the cycles where combustion sufficiently excites resonance.

The proposed Kalman filter is able to produce a trapped mass output consistent with the measured air mass flow, following the transport equations of the intake manifold, and to give an estimation of the trapped mass when no measurement is available by using the speed density method.

The algorithm was successfully implemented in a WLTP cycle and in transient EGR and VGT steps. Various set of sensors were proven to show the adaptability of the method to various configurations.

7.A Parameters of the EKF

The final shapes of matrices F and H are:

$$F = \begin{pmatrix} 1 & 0 & 0 & 0 & 0 & 0 & 0 \\ 0 & 1 & 0 & 0 & 0 & 0 & 0 \\ 0 & 0 & 1 & 0 & 0 & 0 & 0 \\ 0 & 0 & 0 & 1 & 0 & 0 & 0 \\ 0 & 0 & 0 & 0 & 1 & 0 & 0 \\ F_{61} & 0 & F_{63} & F_{64} & F_{65} & F_{66} & 0 \\ 0 & F_{72} & 0 & F_{74} & 0 & 0 & 0 \end{pmatrix} \quad (7.50)$$

and

$$H = \begin{pmatrix} H_{11} & 1 & 0 & 0 & H_{15} & H_{16} & 0 \\ 0 & 0 & 1 & 0 & 0 & 0 & 0 \\ 0 & 0 & 0 & 1 & 0 & 0 & 0 \\ 0 & 0 & 0 & 0 & 1 & 0 & 0 \\ 0 & 0 & 0 & 0 & 0 & 1 & 0 \\ 0 & H_{62} & 0 & H_{64} & 0 & 0 & 0 \\ 0 & 0 & 0 & 0 & 0 & 0 & 1 \end{pmatrix} \quad (7.51)$$

The terms represented by indices are the following:

From Equation (7.35):

$$F_{61} = -\frac{V_{dis}}{V_m} p_{int}^k \quad (7.52)$$

$$F_{63} = \frac{R}{V_m} T_{int}^k \quad (7.53)$$

$$F_{64} = \frac{R}{V_m} T_{int}^k \quad (7.54)$$

$$F_{65} = \frac{R}{V_m} (m_{air}^k + m_{EGR}^k) \quad (7.55)$$

$$F_{66} = 1 - \frac{V_{dis}}{V_m} (\eta_{OL}^k + \theta_\eta^k) \quad (7.56)$$

From Equation (7.36):

$$F_{72} = -(1 - a_{SS}^k) \frac{V_{dis} F_{st}}{V_m m_{air}^k} \quad (7.57)$$

$$F_{74} = (1 - a_{SS}^k) \frac{V_{dis} F_{st} (m_{f,OL}^k + \theta_f^k)}{V_m (m_{air}^k)^2} \quad (7.58)$$

$$F_{77} = a_{ss}^k \quad (7.59)$$

$$(7.60)$$

From Equation (7.37):

$$H_{11} = \frac{V_{dis} p_{int}^k}{RT_{int}^k} (1 + RGF) \quad (7.61)$$

$$H_{15} = -\frac{(\eta_{OL}^k + \theta_\eta^k) V_{dis} p_{int}^k}{RT_{int}^k{}^2} (1 + RGF) \quad (7.62)$$

$$H_{16} = \frac{(\eta_{OL}^k + \theta_\eta^k) V_{dis}}{RT_{int}^k} (1 + RGF) \quad (7.63)$$

$$(7.64)$$

And finally, from Equation (7.42):

$$H_{62} = \frac{F_{st}}{m_{air}^k} \quad (7.65)$$

$$H_{64} = -\frac{(m_{f,OL}^k + \theta_f^k) F_{st}}{(m_{air}^k)^2} \quad (7.66)$$

$$(7.67)$$

References

- [1] Brunt M. F. J. and Pond C. R. “Evaluation of techniques for absolute cylinder pressure correction”. *SAE Technical Papers*, 1997. (cited in pp. 30, 168, and 183)
- [2] Lee K., Yoon M. and Sunwoo M. “A study on pegging methods for noisy cylinder pressure signal”. *Control Engineering Practice*, Vol. 16 n° 8, pp. 922–929, 2008. (cited in pp. 30, 168, and 183)
- [3] Fanelli I., Camporeale S. M. and Fortunato B. “Efficient On-Board Pegging Calculation from Piezo-Electric Sensor Signal for Real Time In-Cylinder Pressure Offset Compensation”. *SAE International Journal of Engines*, Vol. 5 n° 2, pp. 672–682, 2012. (cited in pp. 30, 168, and 183)
- [4] Blanco-Rodríguez D. *Modelling and observation of exhaust gas concentrations for diesel engine control*. PhD Thesis, Universitat Politècnica de València. Departamento de Máquinas y Motores Térmicos, 2013. (cited in pp. 68, 172, and 174)
- [5] Guardiola C., Dolz V., Pla B. and Mora J. “Fast estimation of diesel oxidation catalysts inlet gas temperature”. *Control Engineering Practice*, Vol. 56, pp. 148–156, 2016. (cited in pp. 69, 174, and 216)
- [6] Kalman Rudolph Emil. “A new approach to linear filtering and prediction problems”. *Journal of basic Engineering*, Vol. 82 n° 1, pp. 35–45, 1960. (cited in pp. 71 and 177)

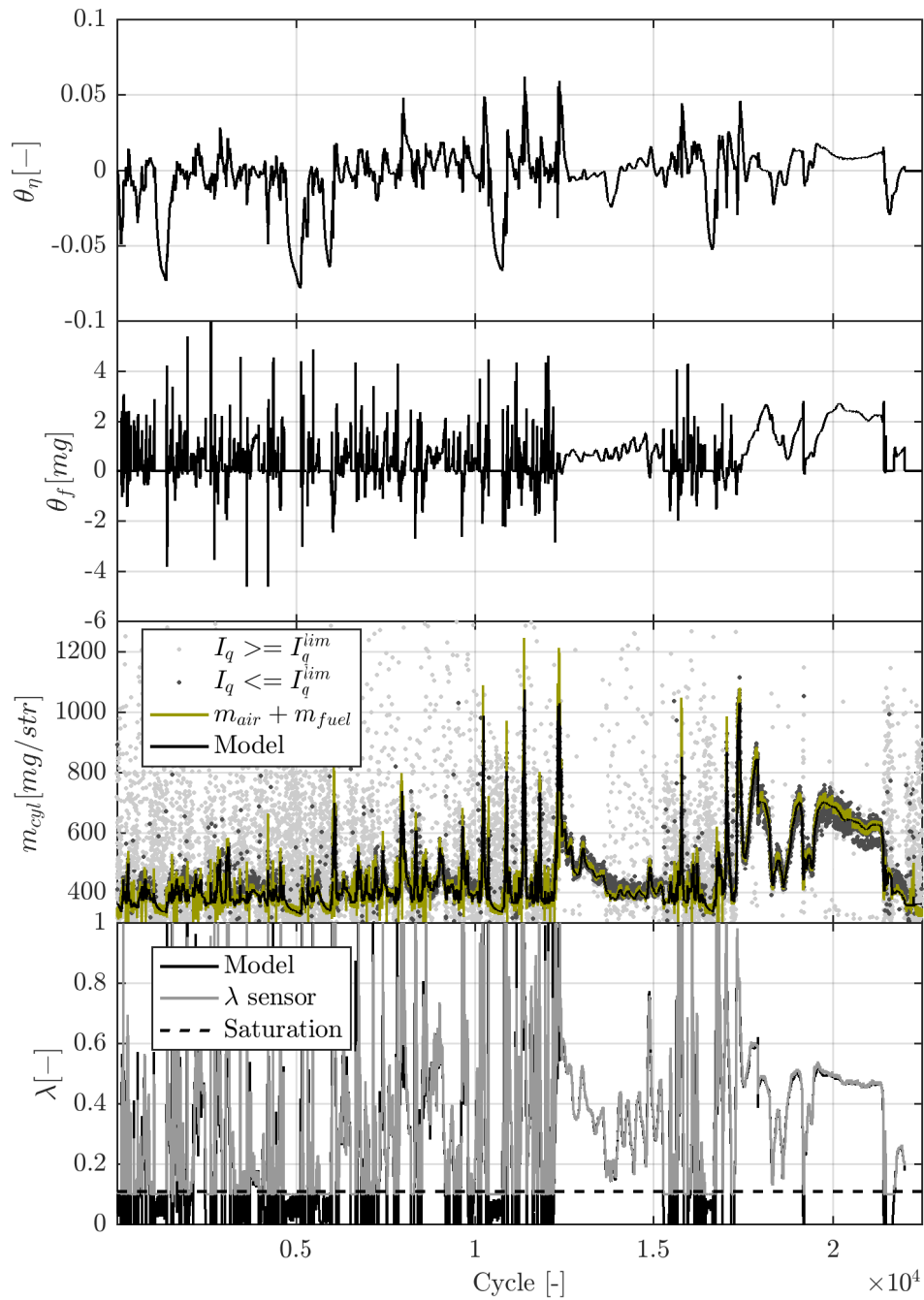


Figure 7.7. Kalman filter output in a WLTP cycle in Engine B with the EGR valve closed.

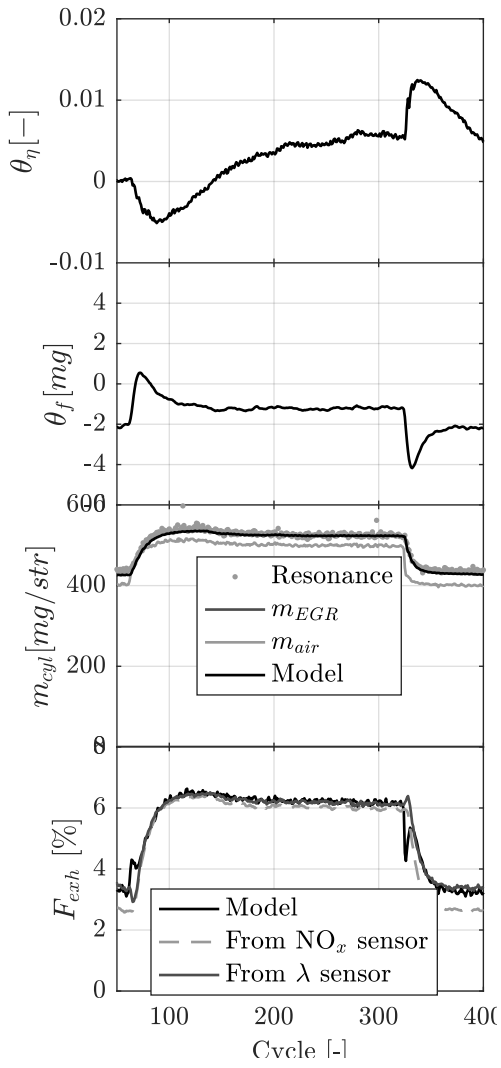


Figure 7.8. VGT step at 60% load and 1250 rpm in Engine B when using the set 1 of sensors.

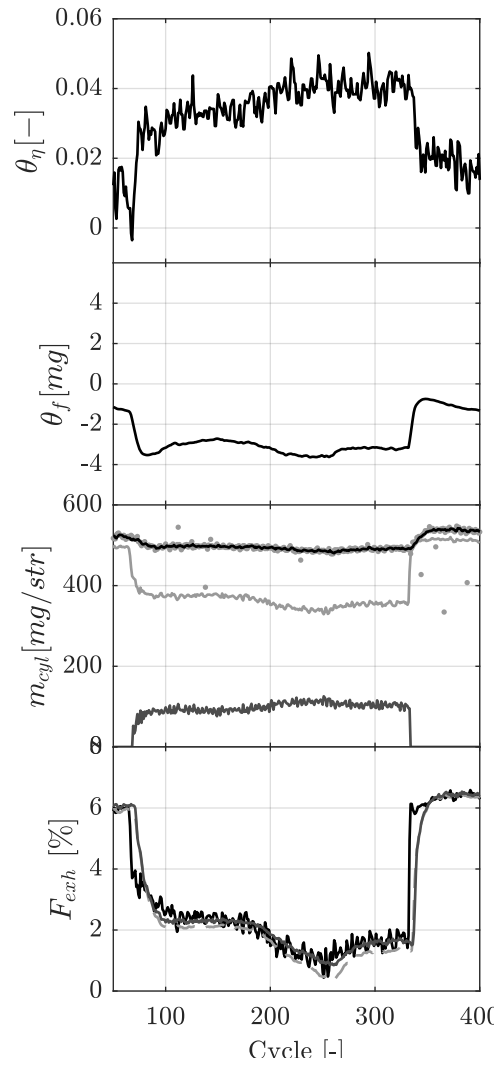


Figure 7.9. EGR step at 60% load and 1250 rpm in Engine B when using the set 1 of sensors.

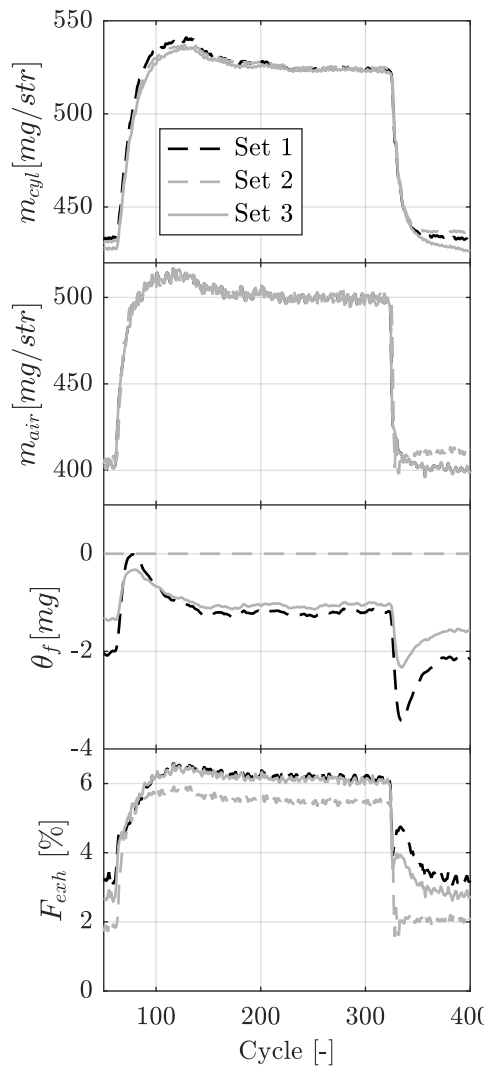


Figure 7.10. VGT step at 60% load and 1250 rpm in Engine B when using all sets fo sensors.

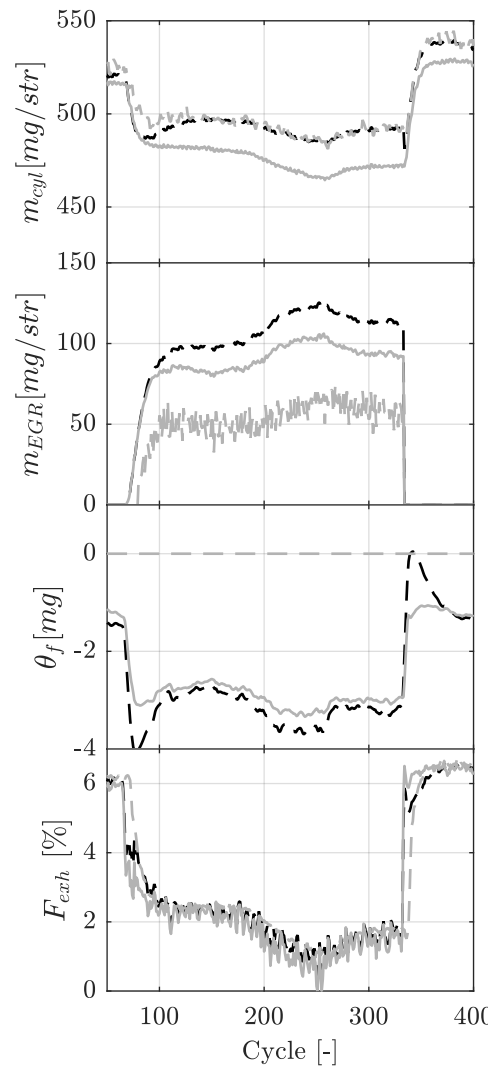


Figure 7.11. EGR step at 60% load and 1250 rpm in Engine B when using all sets fo sensors.

Chapter 8

Applications of the resonance method for onboard engine control and diagnosis

Contents

| | | |
|------------|--|------------|
| 8.1 | Introduction | 192 |
| 8.2 | Residual gases estimation with NVO strategies | 192 |
| 8.2.1 | Model description | 193 |
| 8.2.2 | Results and discussion | 193 |
| 8.3 | Knock model for SI engines | 197 |
| 8.3.1 | Model description | 199 |
| 8.3.2 | Results and discussion | 203 |
| 8.4 | Exhaust temperature estimation | 205 |
| 8.4.1 | Model description | 206 |
| 8.4.2 | Results and discussion | 210 |
| 8.5 | NO_x model for CI engines | 216 |
| 8.5.1 | Model description | 217 |
| 8.5.2 | Results and discussion | 220 |
| 8.6 | Conclusions | 225 |
| | References | 227 |

8.1 Introduction

Chapter 6 has presented the new methodology for the trapped mass estimation, which makes use of the in-cylinder pressure resonance. Chapter 7 proposed an observer for combining that measurement with sensors that are currently installed in commercial engines, in order to obtain a robust and accurate measurement of the trapped mass in transient conditions. This chapter is devoted to point out the potential of such measurement by using the trapped mass obtained from resonance to estimate various engine parameters, which may be used for engine diagnosis or control optimization.

The proposed applications are the following:

1. An estimation of the residual mass for engines with NVO strategies.
2. A knock model based on an estimation of the autoignition time delay.
3. A model of the exhaust gases temperature by assuming an adiabatic expansion through the valves and heat losses to the manifold.
4. An application to estimate the thermal NO_x production in a diffusive flame combustion.

All the applications are feed with the trapped mass estimation obtained from resonance and can be used on-board if the engine is equipped with in-cylinder pressure sensor. Those applications are just some examples which demonstrate significant improvements when comparing with conventional mass flow sensors.

8.2 Residual gases estimation with NVO strategies

Negative valve overlap (NVO) strategies are one of the techniques to phase the combustion in engines with new combustion concepts, such as HCCI, CAI or SACI, since they provide a precise control of the residual mass which influences the combustion timing [1, 2]. In a NVO strategy the exhaust valve closes well before the TDC of the exhaust stroke thereby trapping high levels of residuals.

One of the main concerns when performing NVO strategies is the errors at the residual mass estimation, since current methodologies, previously mentioned in Chapter 3, need from information from unobservable in-cylinder

parameters, such as the exhaust temperature, e.g. Fitzgerald method [3], or the EGR, e.g. Yun and Mirsky [4].

8.2.1 Model description

The proposed methodology consists on profiting of the trapped mass estimation from resonance for deriving the cylinder conditions at the EVO, such as:

$$T_{EVO} = \frac{p_{EVO} V_{EVO}}{m_{cyl} R} \quad (8.1)$$

and the exhaust process is modelled through an isentropic process, as in Yun and Mirsky [4]. Hence, the residual mass, i.e. the mass at the EVC, can be calculated as:

$$m_{res} = m_{cyl} \frac{V_{EVC}}{V_{EVO}} \left(\frac{p_{EVC}}{p_{EVO}} \right)^{\frac{1}{\gamma}} \quad (8.2)$$

Finally, intake and exhaust flow during intake and exhaust strokes may be determined by analyzing the succession m_{cyl} and m_{res} :

$$\begin{aligned} m_{exh}(k) &= m_{cyl}(k) - m_{res}(k) \\ m_{int}(k) &= m_{cyl}(k) - m_{res}(k-1) \end{aligned} \quad (8.3)$$

Figure 8.1 summarizes in a block diagram the main operations and signal manipulations. Note that, the first mode of the resonance is in the range of 3 to 7 kHz, but in-cylinder pressure frequency contents must be preserved (i.e. non filtered) up to 15 kHz in order to discern from other resonant modes. This corresponds to a minimum angular resolution of 0.5 CAD/sample at 1250 rpm as an indicative value. In addition, if the engine speed is not sufficiently constant during the cycle, measuring or modelling the instantaneous sampling rate is advised.

8.2.2 Results and discussion

Engine E was used to perform 15 different NVO settings under SACI and HCCI combustion modes, whose characteristics are collected in Table 4.6. Some tests with the engine working in conventional SI combustion were also

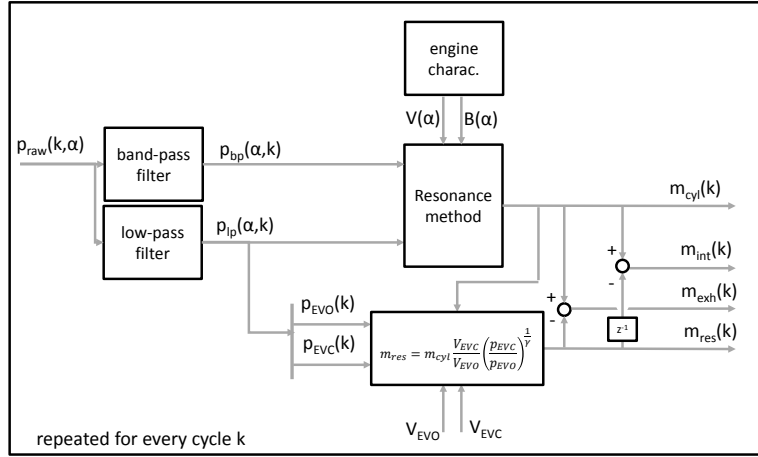


Figure 8.1. Method block diagram.

recorded.

The trapped mass m_{cyl} was computed during the expansion stroke, between 35 CAD after the TDC, when combustion has finished, to 50 CAD after the TDC, when the resonance is still not damped. The method assumed a constant γ of 1.3. In its present formulation, the method did not consider the effect of gas mix composition or in-cylinder heat transfer during the exhaust stroke. Both of them could be considered, but at the cost of increasing the complexity of the method and the calibration process.

The calibration was done considering that the cylinder behaves as an infinite cylinder when the piston is sufficiently far from the top dead center, such as explained in Chapter 6. Thus, only in-cylinder pressure information was used. Since the excitation in HCCI combustion is higher than in the rest of operating conditions, 3000 consecutive cycles of a single operation point with such combustion mode were used. Considering that at the end of the expansion $B = 1.841$, the value of the complete function $B(\alpha)$ may be determined, as shown in Figure 8.2. The detection window has been also indicated with dashed lines.

In order to validate the novel methodology, the cylinder flow was determined by measuring the air mass flow and the EGR in steady conditions, and the residual gases were obtained by using Yun and Mirsky method, as follows:

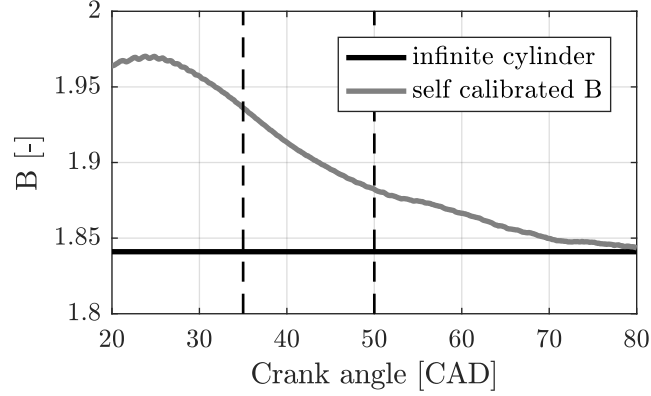


Figure 8.2. Calibration of the Bessel coefficient in Engine E.

$$m_{res} = \frac{(m_a + m_f + m_{egr}) \frac{V_{EVC}}{V_{EVO}} \left(\frac{p_{EVC}}{p_{EVO}} \right)^{\frac{1}{\gamma}}}{1 - \frac{V_{EVC}}{V_{EVO}} \left(\frac{p_{EVC}}{p_{EVO}} \right)^{\frac{1}{\gamma}}} \quad (8.4)$$

As a characteristic example, Figure 8.3 shows the results obtained for the first operating point, operated in CAI combustion mode. Here, cycle to cycle results for residuals (bottom) and exhaust mass (top) are provided; median for the method (solid line) and for the reference (dashed) is also represented. In the Figures the median is preferable to the mean in order to reject the effect of possible outliers. Although 300 cycles were examined, left plots only show 30 to illustrate the cycle-to-cycle evolution. Method results (green) are compared with Yun and Mirsky method (gray) in the case of m_{res} , and test cell sensors for $m_{air} + m_{EGR} + m_{fuel}$ (gray) for the exhaust flow. Right plots show the histograms of the method for both residuals and exhaust mass, and also histogram for Yun and Mirsky method. Histogram for the measured exhaust flow is not provided since the sensors where not fast enough.

As it may be appreciated, the proposed method median result match very well the reference method in both, residuals and exhaust mass, and most of the cycles exhibit sufficient resonance excitation (84% of the cycles were accepted). Indeed, the new method provides a lower cyclic variability in the residual mass when compared to Yun and Mirsky method. This could be a consequence of the assumption of constant cycle to cycle exhaust mass used

in Yun and Mirsky method, which is not strictly true.

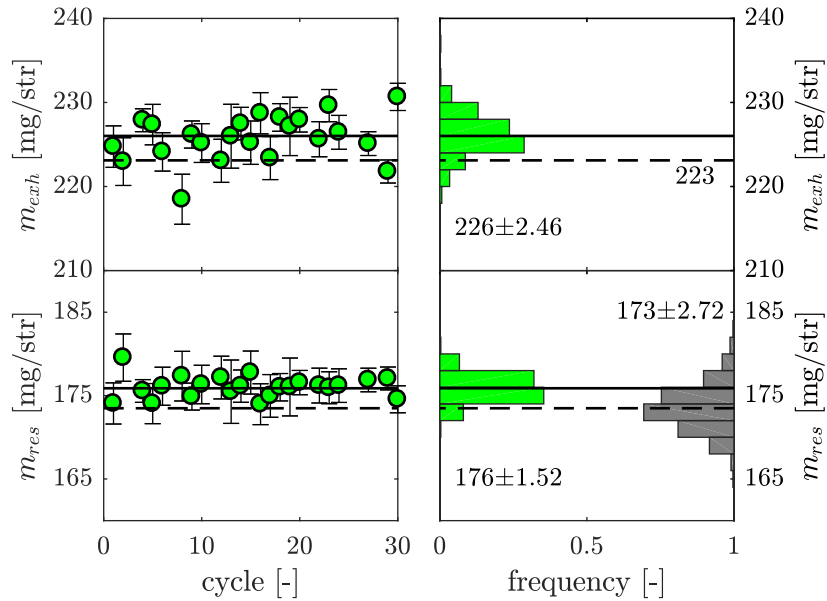


Figure 8.3. Results of the residual mass estimation in Engine E .

Figure 8.4 shows the results of the novel methodology over the 15 tested NVO settings. As it may be appreciated, the method exhibits an excellent linearity, being $r^2 = 0.997$ and the mean average error MAE = 2.8 mg/str.

One of the characteristics of the method is that provides one cycle resolution, as the resonance response is independent from previous cycles. Figure 8.5 shows two VVT steps to illustrate the capabilities of the method in transient conditions.

The right part of Figure 8.5 shows an intake valve step, where both, IVO and IVC, were varied at cycle 1000, and and back to the original position at cycle 2000, while the left part of Figure 8.5 shows an exhaust valve step, where a similar step was performed at the exhaust valves. The output of the method exhibits an instantaneous variation at the intake and residual mass. At the intake valves step, both magnitudes have been reduced, while the exhaust valves variation had an opposite effect on these magnitudes, as the residual

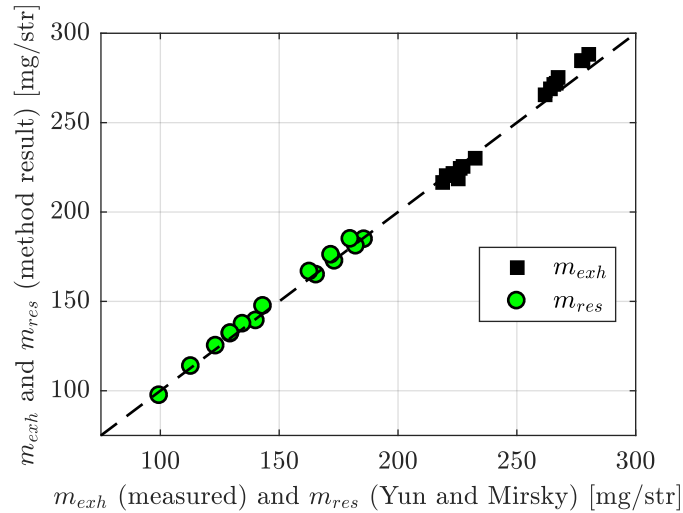


Figure 8.4. Steady results under various NVO strategies in Engine E.

gas fraction was substantially modified.

8.3 Knock model for SI engines

As mentioned in Chapter 3, current knock control strategies are based on a stochastic SA control to maintain the knock probability under a desired threshold. Stochastic methods are constantly advancing the SA till a knock event is detected, and then, the SA is retarded to avoid other knocking events [5]. The main drawback of stochastic methods is the need of knocking cycles information to control the engine, which may lead to engine damage if the knock threshold is too high or lower efficiency if the knock threshold is too restricted.

Model-based methodologies use the spark advance for keeping in-cylinder conditions, e.g. un-burned gas temperature, within a desired range. However, deterministic models can not predict knock with sufficient accuracy, as knock has a stochastic nature due to the existence of temperature hot-spots and other unmeasurable effects [6, 7].

Following, an estimation of the knock probability is suggested by harnessing in-cylinder pressure resonance to determine the un-burned gas tem-

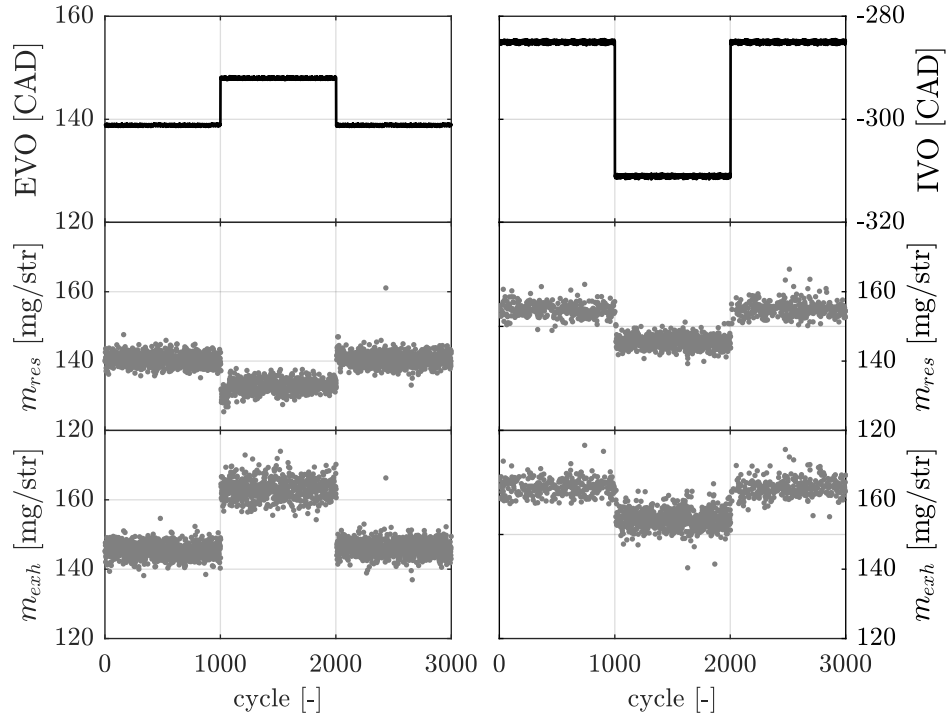


Figure 8.5. Transient results under intake and exhaust valves steps in Engine E.

perature and by adding an exogenous noise over the in-cylinder temperature model. This noise represents uncertainties such as temperature hot spots, in-cylinder pressure pegging, wall heat transfer, residual mass variations, and sensor errors. Hence, the model is developed with the assumption that the random nature of knock is due only to in-cylinder temperature uncertainties. It is beyond the scope of this work to prove this assumption; however, the experimental results show that it improves the prediction capabilities of a control-oriented knock model. The model can be summarized by the following steps:

1. The content of the in-cylinder pressure on the frequency band of resonance (between 4 kHz and 10 kHz) is used for characterizing the acoustical waves and estimating the in-cylinder trapped mass.

2. The low-frequency band of the pressure signal is used to analyse the combustion, compute the temperature of the unburned gases, and estimate the autoignition index AI through an Arrhenius-like function.
3. An exogenous noise is added to the unburned gas temperature φ_T and it is propagated along the model. This yields to a probability distribution of the autoignition index φ_{AI} (not a single value).
4. The knock probability is obtained by integrating the autoignition delay probability distribution which predicts an autoignition of the end-gas before the combustion ends.

Figure 8.6 shows a scheme of the complete model. Note that the in-cylinder pressure signal is the only input required for computing the knock probability.

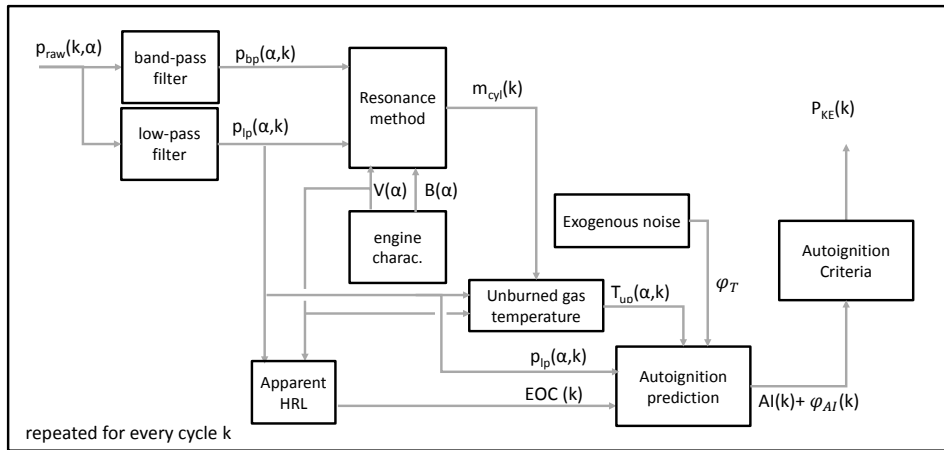


Figure 8.6. Model scheme for knock probability estimation.

8.3.1 Model description

Arrhenius-based knock model Knock, a phenomenon caused by the autoignition of the end-gas, is characterized by the in-cylinder chamber conditions and it can be modelled by an Arrhenius-like function, such as in Livenood and Wu [8–10]

$$\tau = C_1 e^{\frac{C_3}{T_{ub}}} p^{C_2} \quad (8.5)$$

where τ is the ignition delay and T_{ub} are the pressure and temperature of the unburned gasses, respectively, and C_1 , C_2 and C_3 are constants defining the autoignition process.

Autoignition is produced when

$$AI = \int_{IVC}^{EOC} \frac{1}{\tau} d\alpha > 1 \quad (8.6)$$

and the unburned temperature can be calculated by assuming a polytropic process after the spark is produced.

$$T_{ub} = \begin{cases} \frac{pV}{m_{cyl}R} & \text{if } \alpha < SA \\ T_{ub}^{SA} \left(\frac{p}{p^{SA}} \right)^{\frac{\kappa-1}{\kappa}} & \text{otherwise} \end{cases} \quad (8.7)$$

where κ is the polytropic exponent.

Note that the trapped mass m_{cyl} is used in an exponential function (Eq. 8.5), such that, if there was an error in the trapped mass input, it would become in a high deviation at the autoignition delay output.

The resonance methodology is specially suitable for the knock modelling of SI engines for three reasons:

- SI engines normally do not have a bowl. Theory based on a cylindrical combustion chamber thus fits the physics better.
- Knocking conditions are produced at high loads, where combustion heavily excites the resonant frequencies, even in the absence of knock.
- Conventional SI combustion is performed in stoichiometric conditions and the resulting end-gas properties can be more easily identified.

Figure 8.7 shows the probability functions of the AI index defined in Equation (8.6) for four values of SA steps at the same operation point. The AI index increases as the spark is advanced because combustion causes higher in-cylinder pressure values, and hence, higher temperatures of the unburned gas. The variability of the AI for a given SA setting is due to the cycle-to-cycle variability of the flame propagation in SI combustion.

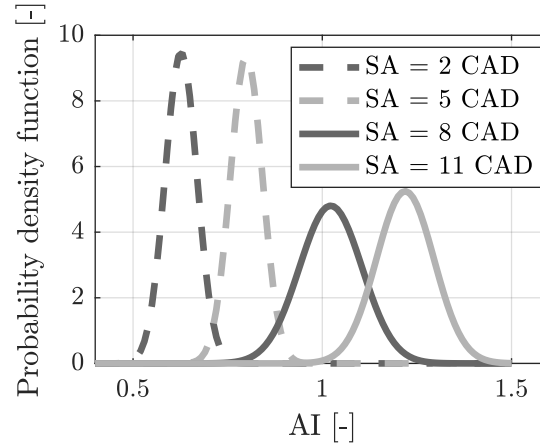


Figure 8.7. AI probability functions of various SA steps in the same operation point.

Figure 8.8 shows the knock probability found when varying the SA in 14 steps from 0 to 13 CAD before the TDC. The knock probability was calculated by dividing the data in groups of similar AI values, with a resolution of 0.025. Clearly, the knock events are more frequent when the AI index increases, nevertheless, the autoignition hypothesis stated at Equation (8.6) is not strictly fulfilled, as some cycles with AI values below 1 present knock and others above do not.

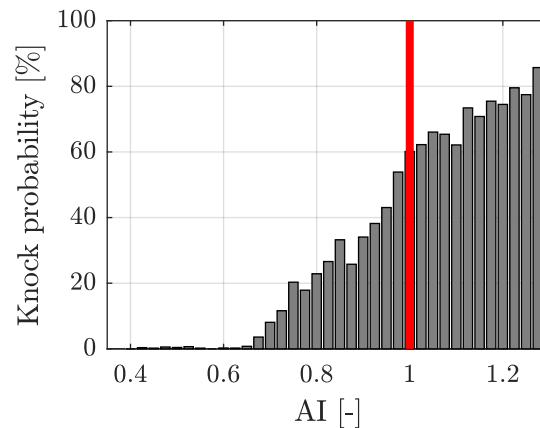


Figure 8.8. Knock probability measured as a function of the AI index in the same operation point when varying the SA from 0 to 13 CAD before TDC.

Exogenous noise and knock probability estimation Errors at the temperature estimation of the unburned gas preclude a deterministic prediction of knock. These errors can be caused by unobservable effects, e.g. temperature hot spots or residual mass variations, but also by measurement and modelling errors, such as pegging errors or errors at the occurring estimations of the trapped mass.

The proposed methodology makes use of an error probability distribution φ_T , which is added in the computed unburned gas temperature and takes into account all the uncertainties in the measurement. This probability distribution is used to calculate, at each cycle, a probability distribution for the autoignition parameter defined in Equation (8.6), as follows:

$$\varphi_{AI} = AI(T_{ub} + \varphi_T) \quad (8.8)$$

The computation of φ_{AI} through Equations (8.5) and (8.6) can have an inadmissible computational cost. In order to reduce the number of operations, a constant gradient of AI around T_{ub} can be assumed, simplifying the computation of AI around the T_{ub} as follows:

$$AI(T_{ub} + \Delta T) = AI(T_{ub}) + \frac{dAI}{dT}(T_{ub})\Delta T \quad (8.9)$$

where $\frac{dAI}{dT}(T_{ub})$ is obtained through:

$$\frac{dAI}{dT} = \int_{IVC}^{EOC} \left(\frac{C_3}{T_{ub}^2} \right) \frac{1}{C_1} e^{\frac{-C_3}{T_{ub}}} p^{-C_2} d\alpha \quad (8.10)$$

The knocking probability is computed by integrating the probability function above the knocking criteria. As follows:

$$p_{KE} = \int_{AI>1} \varphi_{AI} \quad (8.11)$$

where φ_{AI} is the probability distribution of AI, by using an exogenous noise on the temperature of the unburned gases and propagating that noise through Equation (8.9).

Following these steps, if the exogenous noise was set to 0, the function of the knock probability would be a digital function. If the noise was a bias in any measurement, this would result in an offset of the final probability function. And if the error was a random function, it would smooth the probability

function by having the 50% probability at $AI = 1$. Figure 8.9 exemplifies the effect of various exogenous noises at the knock probability function by using a constant temperature sensitivity dAI/dT of 0.04.

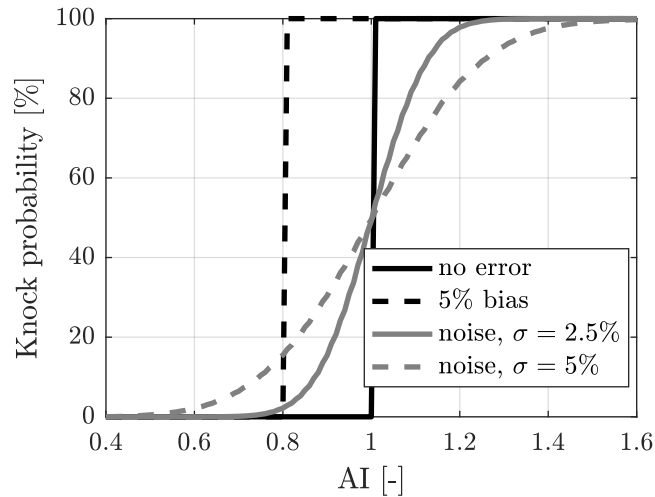


Figure 8.9. Effect of various types of errors to the knock probability function.

8.3.2 Results and discussion

The resonance method was implemented between 30 and 80 CAD after TDC. As the engine is closed-loop controlled by a lambda sensor to have stoichiometric conditions, all the gases after combustion are burned products and the value of γ can be computed by a single polynomial equation. The instantaneous sampling period $T(\alpha)$ is proportional to the engine speed, which was measured by a counter input, each 0.1 CAD.

The knock model was calibrated with experimental data of point H, by using the least squares method, while the rest of the operating conditions, collected in Table 4.3, were used for validation purposes.

The exogenous noise was chosen to be a normal distribution with 0 mean and standard deviation of 5.29%, a value for a proper fitting of a training dataset of point H, as shown in Figure 8.10. Following, each cycle was independently analysed and an exogenous noise with $\sigma = 5.29\%$ is used for running

the knock prediction model.

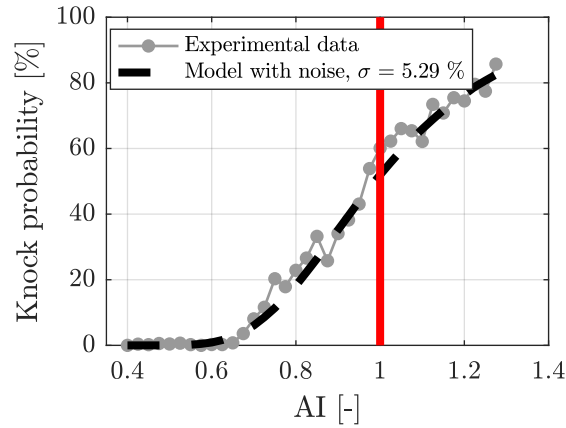


Figure 8.10. Experimental data and model fitted at OP H.

Regarding the constants of the Arrhenius autoignition model, the values suggested by Douaud and Eyzat [10] were used in the present work, namely $C_2 = -1.7$ and $C_3 = 3800$. The model is easily adaptable for a model-based knock control scheme and the only parameter that needs calibration is C_1 , which indeed represent an offset on the sensor.

Figure 8.11 shows the results of the knock model at the validation data set when using both, the trapped mass estimation obtained from the air mass flow meter (left plot) and from the resonance methodology (right plot). Although the uncertainties in the unburned gases temperature may depend on the operating conditions, note that the variations are negligible and a single model with constant noise can be used for all.

The left plot of Figure 8.11 shows the results of the knock model when T_{ub} is computed by using the air mass flow sensor for all the operating conditions. The model shows an offset when the operating conditions are varied, but the curve has a similar shape. This offset is caused by air mass flow sensor errors and not because of the noise calibration. If traditional sensors were employed, each operating condition would need a different value of C_1 for dealing with the sensor bias, and the model would require a constant adaptation when transients were performed.

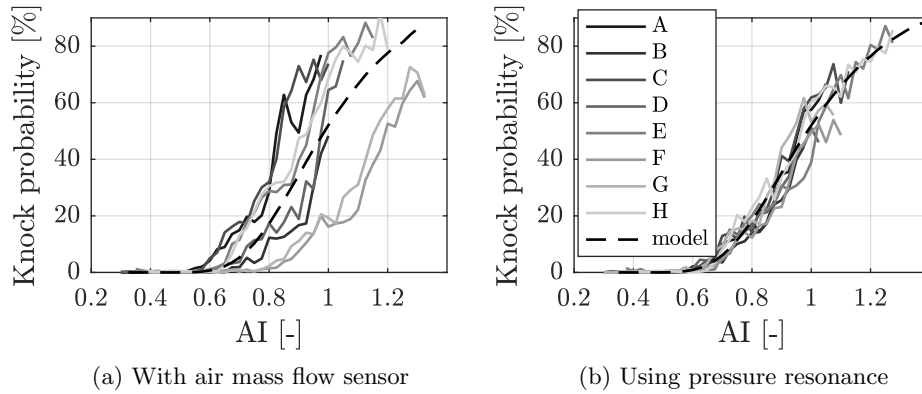


Figure 8.11. Knock probability calculation.

The right plot of Figure 8.11 shows the results obtained when the unburned temperature is detected by using the resonant frequency. Note that all the experimental lines collapse around the predicted value and only a single value of C_1 , calibrated at the training dataset of point H, was required for running the model. This model could be used for knock control by maintaining the AI index at a desired level, e.g. if the AI index was maintained at 0.8, the percentage of knocking cycles would remain below 20%.

8.4 Exhaust temperature estimation

Exhaust temperature is an important parameter for engine control: an accurate and fast estimation of the exhaust gases temperature permits maintaining non-damaging exhaust conditions [11]; turbocharger and after-treatment systems control and optimization require an exhaust temperature measurement or estimation [12–14], since turbine available power and catalyst light-off strongly depends on temperature; and finally, EGR rate observers and models rely on exhaust gases temperature to estimate its value [15, 16].

Current ECUs usually incorporate pre-calibrated look-up tables providing an estimation of the exhaust gas temperature for an open loop control of the engine. Although this is a cost-effective solution, ageing, manufacturing discrepancies and sensor bias can result into significant errors in the exhaust

temperature estimation.

Following, a new model for inlet turbine temperature estimation, which is based on the trapped mass estimation from resonance, is presented. The model only uses the in-cylinder pressure signal, the engine speed and lambda measurements through a three step process:

1. Firstly, the resonance method is combined with the gas state law for the estimation of the in-cylinder gas temperature during the expansion stroke.
2. Secondly, the expansion of the exhaust gases at the exhaust valves is modelled by a polytropic expansion, with the polytropic coefficient experimentally determined from the pressure trace at the end of the expansion stroke.
3. And, finally, the temperature drop from the cylinder to the turbine inlet is modelled with a nodal model with two temperature nodes: a first node in contact with the engine coolant representing the heat transfer to the liquid-cooled runner, and a second node considering the heat transfer to the surroundings to model the rest of the exhaust manifold. Herein, only convection is considered, by neglecting conduction and radiation.

Figure 8.12 illustrates the scheme of the complete model for the exhaust temperature estimation.

8.4.1 Model description

Exhaust gas expansion at the valves was modelled by a polytropic expansion:

$$T_{exp} = k_1 p^{\frac{k_2-1}{k_2}} \quad (8.12)$$

where the temperature-to-pressure ratio k_1 and the polytropic coefficient k_2 are parameters to be identified. In particular, they may be easily fitted just considering that $T_{exp} = T_{cyl}$ during the end section of the expansion stroke, while the valves are still closed and the combustion is finished. In the present work the polytropic exponent was identified between 100 and 150 CAD after

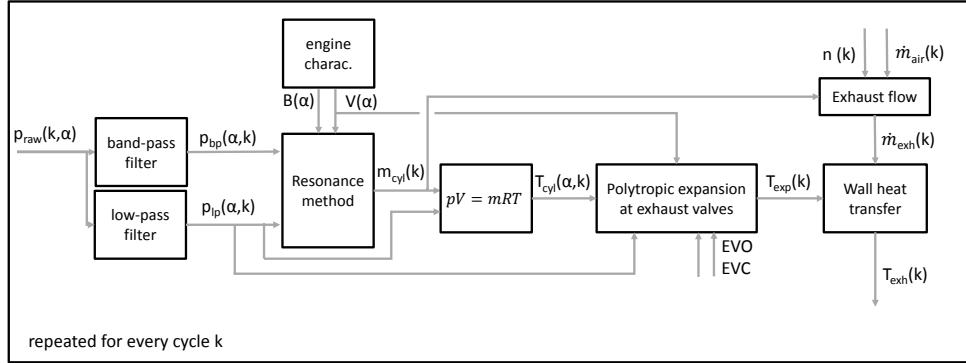


Figure 8.12. Model scheme for exhaust temperature estimation.

TDC, just before Exhaust Valve Opening (EVO).

After EVO, ideal gas law ($pV = mRT$) cannot be used because of the existence of mass flow through the exhaust valve and the mass inside the cylinder is unknown. However, if the polytropic coefficient k_2 is assumed to be reasonably constant, Equation (8.12) may be still used for inferring the in-cylinder gas temperature. The final engine-out temperature is calculated between 250 and 300 CAD after TDC, where expansion is finished and exhaust valve is not yet closed. Doing so, the effect of the gas composition (γ) and the thermal losses are modelled during the exhaust through k_1 and k_2 . Although the valve flow process may have higher wall heat losses, and thus different k_1 and k_2 , this wall heat transfer is calibrated together with the temperature drop caused by the coolant at the exhaust manifold.

The temperature drop along the exhaust has been modelled by a simplified lumped model with two metal nodes [17]: one representing the section of the runner in the cylinder head, which is refrigerated by the engine coolant, and other in contact with the surroundings. Figure 8.13 aims to represent the heat transfer phenomenon in the exhaust manifold by a resistor analogy scheme.

Herein, some simplifications have been included to reduce the model complexity:

- The heat transfer coefficient to the coolant is much higher than that to the exhaust gases ($h_{cool} \gg h_{gas1}$), which implies that, when operating

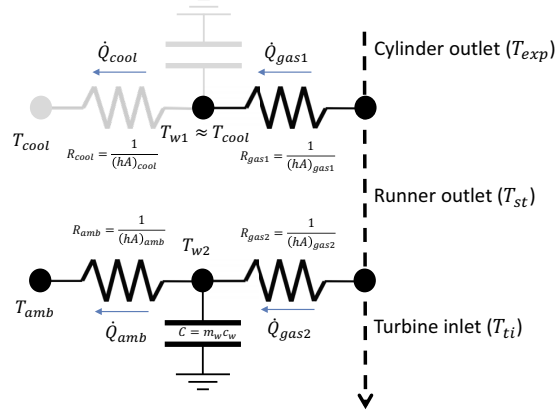


Figure 8.13. Resistor analogy of the heat transfer nodes in the exhaust manifold.

in steady state, the temperature of the first node is near to the coolant temperature ($T_{w1} \approx T_{cool}$). In addition, if the heat transfer to the coolant is assumed to be sufficiently high with regards to the heat capacity of the manifold, dynamics may be neglected and $T_{w1}(t) \approx T_{cool}(t)$.

- For the case of \dot{Q}_{gas1} and \dot{Q}_{gas2} , only convection is assumed to be relevant. Solving the partial differential equation of the gas temperature drop [18] yields to:

$$T_o = T_w + (T_i - T_w)e^{\frac{hA}{\dot{m}c_p}} \quad (8.13)$$

where T_w is T_{cool} for the first section and T_{w2} for the second one, T_o is the outlet temperature (T_{st} or T_{ti} respectively), T_i is the inlet temperature (T_{exp} or T_{st}), h the convective coefficient, A is the effective area of the pipe wall, \dot{m} is the exhaust mass flow, and c_p the constant pressure heat capacity of the gas.

- The exhaust gas convective coefficient only depends on the Reynolds number, as Serrano et al. proposed in [19]:

$$h \approx k_{h1} Re^{0.8} = k_{h1} \left(\frac{4\dot{m}}{\pi\mu D_d} \right)^{0.8} = k_{h2} \dot{m}^{0.8} \quad (8.14)$$

where Re is the Reynolds number, μ is the dynamic viscosity of the fluid, D_d is the diameter at the duct, and k_{h1} and k_{h2} are proportional constants.

- The constant pressure heat capacity of the gas is approximated by semi-empirical models, by dividing the mixture in fresh air and burnt products. The correlations proposed by Lapuerta et al. [20] were employed in this work.
- In the test bench, the heat transfer between the exhaust manifold and the surroundings has a constant convective coefficient, as a consequence, the heat transfer can be modelled as:

$$\dot{Q}_{amb} = (hA)_{amb} (T_{w2} - T_{amb}) \quad (8.15)$$

So the second node is defined by the following differential equation:

$$\frac{dT_{w2}}{dt} m_w c_w = (hA)_{gas} (T_{gas} - T_{w2}) + (hA)_{amb} (T_{amb} - T_{w2}) \quad (8.16)$$

where the wall mass m_w and the wall heat capacity c_w are constant. Thus Equation (8.16) can be rewritten as:

$$\frac{dT_{w2}}{dt} = \dot{m}^{0.8} k_{wg} (T_{gas} - T_{w2}) + k_{amb} (T_{amb} - T_{w2}) \quad (8.17)$$

Including all these simplifications, the final thermal model is defined by the following equations:

$$T_{st} = T_{cool} + (T_{exp} - T_{cool}) e^{\frac{k_{w1} \dot{m}^{-0.2}}{c_p(T_{exp}, \lambda)}} \quad (8.18)$$

$$\frac{dT_{w2}}{dt} = \dot{m}^{0.8} k_{wg} (T_{gas} - T_{w2}) + k_{amb} (T_{amb} - T_{w2}) \quad (8.19)$$

$$T_{ti} = T_{w2} + (T_{st} - T_{w2}) e^{\frac{k_{w2} \dot{m}^{-0.2}}{c_p(T_{st}, \lambda)}} \quad (8.20)$$

where k_{w1} , k_{w2} , k_{wg} and k_{amb} are constants that characterize the thermal properties of the exhaust manifold.

Main weakness of the presented thermal model derives from its simplicity. Despite Equation (8.14) models the effect of the variation of the operating conditions on the convective coefficient of the exhaust gases, such coefficient and the equivalent areas attached to the heat transfer at each one of the nodes may vary as a consequence of the flow conditions; this is specially relevant at Equation (8.18) due to the significant pressure and temperature pulsation and three-dimensional effects. In order to overcome this, a correction coefficient k_{corr} depending on engine speed n and load N was added to k_{w1} :

$$k'_{w1} = k_{w1} k_{corr}(n, N) \quad (8.21)$$

where k'_{w1} is the coefficient to be used in Equation (8.18) replacing k_{w1} .

8.4.2 Results and discussion

Engine B was equipped with thermocouples at each runner and at the turbine inlet, and a pressure sensor at the exhaust manifold. The engine-out temperature measurements of all the cylinders were averaged, while the thermocouple located at the turbine inlet was used for calibration and validation purposes.

Thermocouples had 1.5 mm of diameter as a trade-off between durability and time response. However, as the time response of the employed sensors is expected to be of few seconds, fast temperature variations, i.e. cycle-to-cycle, cannot be sensed [21]. For providing a comparison value for the validation of the method, thermocouple dynamics were modelled by a first order system, such as:

$$\frac{T_{mod}(s)}{T_{ti}(s)} = \frac{K}{1 + \tau s} \quad (8.22)$$

where s is the Laplace variable, K is the steady state gain and τ is the time constant. T_{mod} is then a filtered value of T_{ti} for considering sensor dynamics.

Taking into account the entire process, three dynamic scales can be distinguished:

- The evolution of the temperatures associated to the in-cylinder processes, gas expansion through exhaust valve and heat transfer to the cylinder head (corresponding to T_{cyl} , T_{exp} and T_{st}): they have an instantaneous response and may vary cycle-to-cycle, so they do not require any dynamic compensation.
- The manifold wall temperature evolution (T_{w2} , and affecting T_{ti}): they are described by Equation (8.16), which has a time bandwidth ranging from few seconds to few minutes.
- The temperature sensor response (T_{mod}): with a typical time response between 100 ms and 5 sec.

In order to validate the method and characterize all the required parameters for the model dynamics, three kind of tests, described in Chapter 4 were used.

1. Steady tests: Variations over the EGR, VGT, and the injection settings at various operating conditions were used to compare the presented

model with current methods based on look-up tables, and also for determining the steady state thermal behaviour of the exhaust. Table 4.4 collects detailed information of these tests.

2. Engine speed and load steps: sharp variations in load and engine speed were performed and they were kept constant for two minutes to identify the dynamics of Equation (8.17). The steps levels were defined to reach all the operating conditions at the entire working map. Figures 4.12 and 4.13, in Chapter 4, show the engine speed and the BMEP for the performed transient test. Two repetitions were made: one with the EGR valve closed and other with the default EGR valve controls.
3. WLTP cycle: finally, a cycle was used to validate the method under realistic operating conditions. Figure 4.15 shown BMEP and engine speed during the WLTP cycle. Sensor dynamics were identified from this test and found to be consistent with the thermocouple characteristics.

Model calibration: In a first approximation to the model calibration, the heat transfer to the surroundings by convection is neglected in front of the heat exchange in the runner:

$$\dot{Q}_{amb} \ll \dot{Q}_{gas1} \quad (8.23)$$

Consequently, while operating in steady conditions, the only temperature drop is caused by the liquid cooled section of the exhaust ($T_{ti} = T_{st}$) and the steady state formulation is reduced to Equation (8.18).

The correction parameter, $k_{corr}(n, N)$, is then computed for the steady points in order to model the effective area of the equivalent heat exchanger as a function of the operating conditions. A set of 39 tests, ranging from 1000 to 3000 rpm and from 2.5 to 21 bar of BMEP, was used. Figure 8.14 shows the final calibration results when neglecting the ambient heat exchange. As expected, as load is increased the efficiency of the cooling process at the runners diminishes, thus resulting in a lower value of $k_{w1}k_{corr}$. The effect of the engine speed is empirically calibrated and deals with discrepancies at the convective coefficient calculation.

Once $k_{corr}(n, N)$ is obtained by the aforementioned assumptions, the complete model reported at Equations (8.18) to (8.20) can be fitted by using the specific dynamic test shown in Figure 4.13. The final identified constants were 1.2163×10^{-4} , 1.316×10^3 and 0.0048 for k_{wg} , k_{amb} and k_{w2} respectively. It

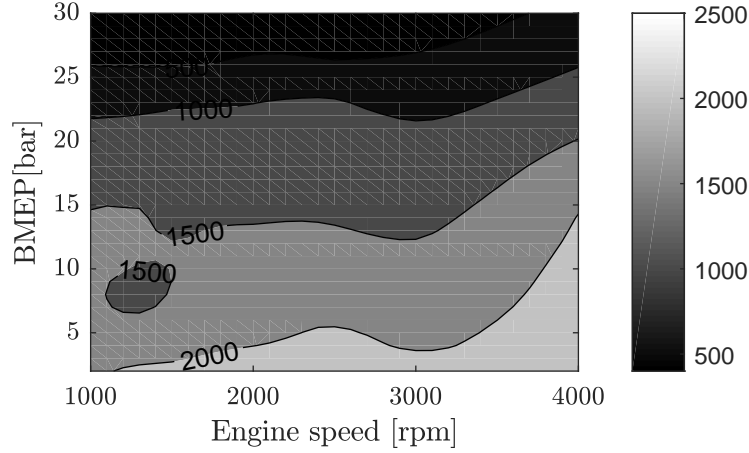


Figure 8.14. $k_{w1}k_{corr}(n, N)$ table for the pressure based model.

must be noticed that only the set of 39 operating points with the nominal settings and the dynamic test shown in Figure 4.13 (with the EGR valve closed) were used for calibration purposes.

In parallel, a look-up table was also fitted; this kind of modelling method is extensively used in current ECUs and will be used for comparison. The table $\Delta T(n, N)$ maps the difference between the exhaust and the intake manifold temperature as a function of the engine speed and load. A thermocouple was used for measuring intake temperature T_{int} and the temperature at the turbine inlet T_{ti} was modelled through:

$$T_{ti} = T_{int} + \Delta T(n, N) \quad (8.24)$$

Figure 8.15 shows the final look-up table for this engine. The calibration relative error at the training dataset was 0.1% for the in-cylinder pressure based model and 0.4% for the conventional look-up table model.

Results in steady conditions As reported before, 342 steady operation tests were available, including tests with nominal settings and varying the injection settings, the EGR rate, the intake pressure and the rail pressure at different operating conditions. The conventional procedure for exhaust temperature estimation, based on look-up tables, was compared with the new in-cylinder pressure based methodology. Note that only 39 tests of the data

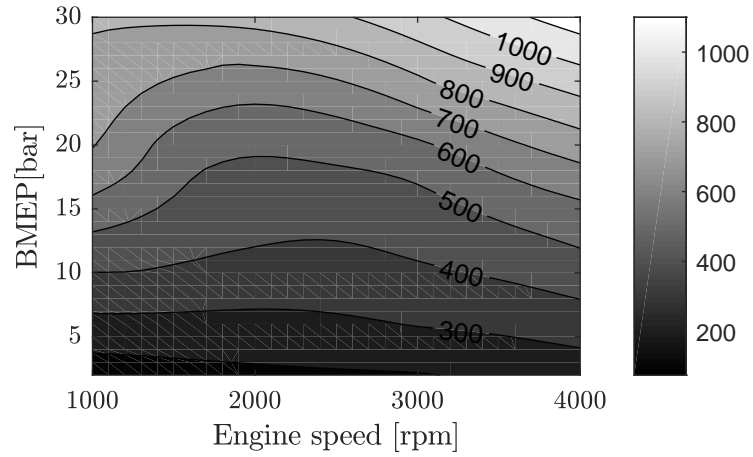


Figure 8.15. $\Delta T(n, N)$ look-up table for conventional model.

set were used for the calibration of both models, and the validation dataset includes a wide variation of injection timing, EGR rate, boost pressure and rail pressure.

Figure 8.16 shows the histogram of the relative errors for both models while table 8.1 splits the dataset according to the varied control setting.

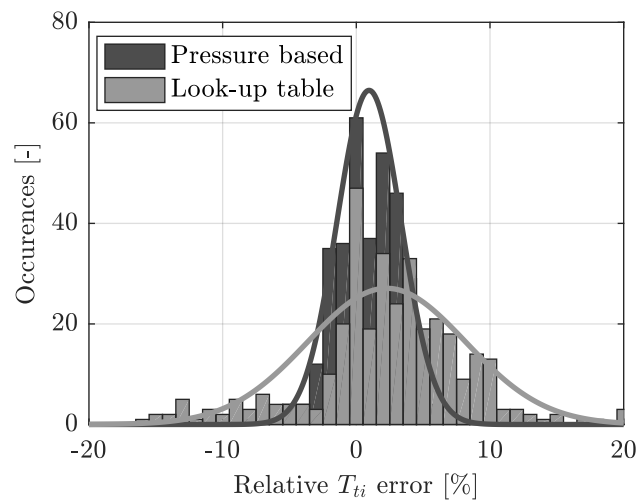


Figure 8.16. Relative errors at the inlet temperature estimation for both models.

Table 8.1. Summary of mean relative errors in the temperature estimation for both models in the validation dataset.

| Variations | SOI | EGR | p_{int} | p_{rail} | All |
|----------------|------|------|-----------|------------|------|
| Pressure based | 2.08 | 2.71 | 2.45 | 2.4 | 2.08 |
| Look-up table | 4.84 | 4.91 | 7.28 | 3.17 | 4.76 |

It can be noticed that the pressure based model behaves adequately when combustion settings are changed: the errors at the turbine inlet temperature estimation are lower than 20 K, and the maximum relative error is 7.4%. On the other hand, relying on a simple look-up table model does not ensure a good estimation when varying control settings: the average temperature error is 35.65 K and the maximum relative error reaches 22.42%. Mean average error for the look-up table approach in the complete dataset is 4.76%, while the same metric for the proposed model is 2.08%. Despite look-up table model could be improved by adding correction factors accounting for the cross-effect of the different disturbances, this would imply additional training tests and a significant calibration work.

Results in transient tests Figure 8.17 shows the measured temperature T_{meas} and the main outputs of the temperature model: the wall temperature estimation T_{w2} , the engine outlet temperature T_{exp} , and the turbine inlet temperature T_{ti} in the dynamic test described in Figure 4.13 in Chapter 4. Here, both tests, with and without EGR, are shown.

Note that the dynamics of the model adequately fit the thermocouple measurement, and that even for the tests with EGR the bias is kept to a low value. The mean relative error in the turbine inlet temperature estimation for both tests was below 2%. In addition, the model is able to represent the slow response of the wall temperature, which is the responsible of the turbine inlet variation during the sections with constant load.

The model results for the complete WLTP cycle are shown in Figure 8.18, where engine-out gases temperature, wall temperature, final temperature corrected by the sensor dynamics and the measured temperature evolutions are plotted.

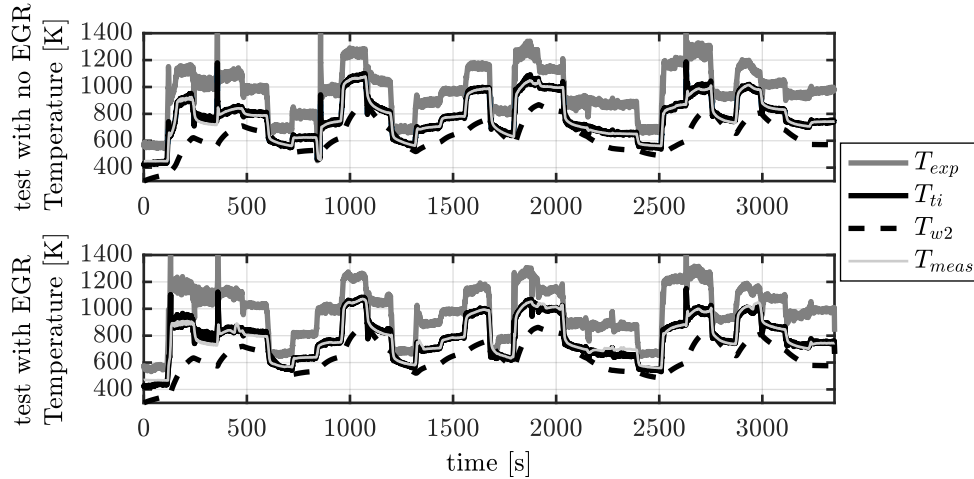


Figure 8.17. Exhaust temperature outputs of the model and measured value during the transient test without EGR (top) and with EGR (bottom).

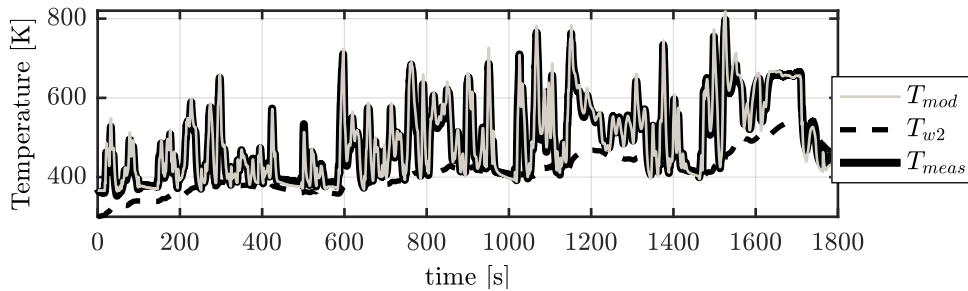


Figure 8.18. Exhaust temperature estimation during the complete WLTP cycle.

In this test, engine dynamics were heavily excited and the temperature sensor response was not sufficient for determine the fast changes in gas temperature. In order to verify the estimation provided by the pressure-based temperature method, the method output must be filtered with the sensor model in Equation (8.22).

For that, sensor time response was modelled as a first order system with a time response of 3.1 s, which is consistent with the sensor characteristics provided by the manufacturer. Figure 8.19 shows, for a sector of the WLTP

cycle, the model output with (T_{mod}) and without (T_{ti}) including sensor dynamics during the same part of the transient cycle. It may be appreciated that the filtered response is coherent with the sensor measurement, and for all the transients in the plot the model behaves in accordance with the sensor.

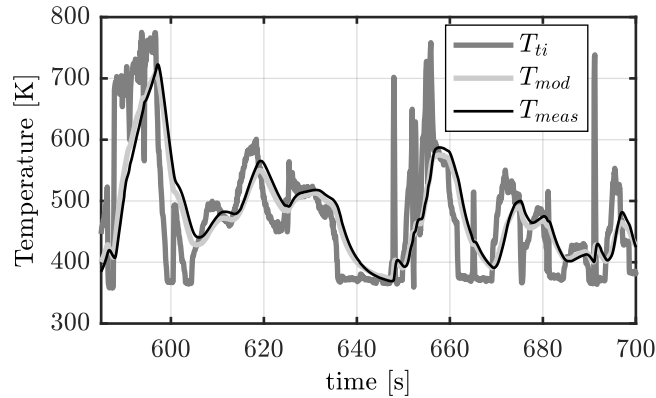


Figure 8.19. Measured temperature (T_{meas}) and model output with (T_{mod}) and without (T_{ti}) considering sensor dynamics during a section of the WLTP cycle.

Once again, the filtered model temperature T_{mod} agrees with the measurement T_{meas} ; average temperature error was 9.62 K, which represent a 1.88 % of mean relative error. In addition, the model was able to represent the progressive heating up of the engine, and its effect in the turbine inlet temperature. Note that a look-up table model is not able to predict this effect unless a thermal model is added.

In addition, the bandwidth of the model is higher than that of the sensor, as it is able to represent cycle-to-cycle variations in the engine-out temperature. In fact, this is an important feature of the model: since it permits a fast estimation of the exhaust gases temperature, it may be used for correcting the thermocouple time response, as in [22, 23].

8.5 NO_x model for CI engines

New stringent antipollution Diesel legislation is forcing Diesel engines to reduce NO_x production. Many Car manufacturers are introducing post-treatment systems, such as Lean NO_x Trap (LNT) or Selective Catalytic Reduction (SCR) [24], which require NO_x feedback for an efficient operation [25, 26]. In

engines with no after-treatment devices, closed loop NO_x control seems to be realizable if a fast and reliable NO_x measurement is available. Improving transient operation of both, CI combustion and after-treatment operation, requires from fast and accurate on-board NO_x measurements, and although NO_x sensors are currently being installed on commercial engines, they do not have an optimal time response for transient operation (around 750 ms). NO_x models present an opportunity to improve transient sensor response, or even to replace physical sensors and lowering then the costs.

Following, a study of NO_x formation mechanism is presented in order to improve current models precision by using the resonance method for mass estimation. It proposes a method capable of determining NO_x emissions with one cycle resolution, by relying only on the pressure signal, the air mass flow and lambda. The method is derived from a previous work [27], where the thermal NO_x formation mechanism is obtained from the adiabatic flame temperature and the heat release rate, and the final NO_x are corrected for taking into account the reduction mechanism.

The new NO_x model presents two important contributions: Firstly, a different parametrization is proposed. Doing so, thermal mechanism can be separated from other NO_x formation mechanisms. And secondly, errors at trapped mass estimation when using traditional methods are evidenced, as the method obtains better results when is fed with the trapped mass obtained from resonance.

Figure 8.20 shows a schema of the full method for NO_x estimation. It must be noticed that the full system only requires from in-cylinder pressure, lambda and air mass sensors.

8.5.1 Model description

The thermal NO_x formation was reviewed in Chapter 2; it can be modelled by an Arrhenius function to account for the reaction rate and another term which should take into account the instantaneous amount of reactants.

Here, the temperature governing the chemical kinetics is assumed to be close to the adiabatic flame temperature but differing a ΔT , which depends

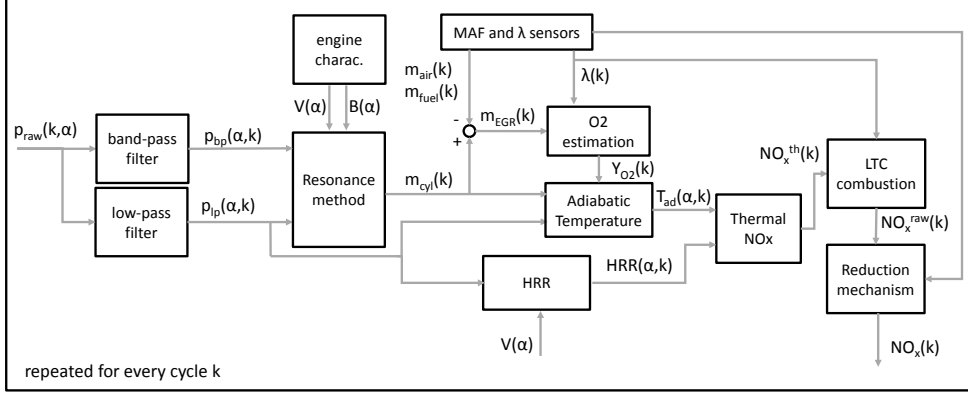


Figure 8.20. Complete Scheme of the method proposed for NO_x estimation.

on the combustion flame and thus the operating point considered:

$$T_{reac}(\alpha) = T_{ad}(\alpha) + \Delta T(n, N) \quad (8.25)$$

The reactant concentration is mainly function of the mass flow through the flame and therefore can be considered proportional to the mass fuel burnt and hence the heat release rate (HRR). Leading to a simplified thermal NOx model such as:

$$dNO_x^{th}(\alpha) = k_f HRR(\alpha) e^{-k_{act}/T_{reac}(\alpha)} \quad (8.26)$$

where k_f represents the proportionality between $HRR(\alpha)$ and the amount of reactants passing through the flame.

Finally, integrating over combustion, it yields:

$$NO_x^{th} [kg/str] = \int_{SOC}^{EOC} k_f HRR e^{-\frac{k_{act}}{T_{ad} + \Delta T(n, N)}} d\alpha \quad (8.27)$$

where $HRR(\alpha)$ and $T_{ad}(\alpha)$ can be obtained from pressure signal.

The current method uses the trapped mass obtained from resonance to calculate the unburned gas temperature, as in Equation (8.7). The adiabatic temperature of the flame is obtained by adding to the unburned gas temperature the shift in temperature due to the heat released during combustion

ΔT_{nd} and a correction that accounts for the energy absorbed by the partial dissociation of the combustion products ΔT_{diss} . As follows:

$$T_{ad} = T_{ub} + \Delta T_{nd} - \Delta T_{diss} \quad (8.28)$$

where the temperature increase due to heat released is only function of the oxygen available Y_{O_2} which may be described by:

$$\Delta T_{nd} = 37630.5 \left(\frac{Y_{O_2}}{3.48} \right) \quad (8.29)$$

and the dissociation effects can be described by:

$$\Delta T_{diss} = A (T_{ub} + \Delta T_{nd})^B \quad (8.30)$$

These expressions were obtained by fitting a large amount of data with a code that calculates the combustion reaction in equilibrium conditions [27,28]. In this work two zones have been differentiated for being more precise: below 2600 K where $A = 1.55 \times 10^{-7}$ and $B = 2.677$, and above 2600 K, where $A = 7.136 \times 10^{-10}$ and $B = 3.36$.

A parameter has been included to account for other NO_x formation mechanism, such as N_2O or prompt. This parameter modifies the total amount of NO_x by a correction factor based on the maximum adiabatic flame temperature, as the adiabatic flame temperature drives the thermal NO_x formation. This correction factor ranges from 1 at high flame temperatures, where nearly all NO_x are due to thermal mechanism, to almost 0 at low oxygen concentration, where thermal NO_x formation is negligible. As follows:

$$K(T_{ad}^{max}) = \frac{NO_x^{th}}{NO_x^{total}} = (m(T_{ad}^{max} - T_0))^n \quad (8.31)$$

where m , T_0 , and n , are three parameters to fit the curve.

Finally, the reduction mechanism can be incorporated, such as suggested in [27], by assuming an amount of NO_x reduced from the EGR and from the reentrained NO_x into the flame. As follows:

$$Y_{NO_x,exh} = \frac{NO_x^{th}(1 - F_r K_{re} \epsilon)}{m_{air} + m_{fuel} + m_{EGR} F_r \epsilon} \quad (8.32)$$

where F_r is the relative stoichiometric ratio and K_{re} represents the amount of NO_x reentrained into the flame.

8.5.2 Results and discussion

The method was tested in Engine B by performing variations in the EGR valve, the boost pressure, and the injection settings in 12 operating conditions. All the operating points were described in Chapter 4: Figure 4.6 plotted the 342 points tested, while a quantification of the variations was given in Table 4.4.

The same methodology was applied using two models:

- Model A: By assuming all NO_x are produced by thermal mechanism and using conventional methods for calculating the trapped mass. This model is similar to the ones currently proposed by other authors [27]. The trapped mass was estimated by modelling the volumetric efficiency with a look up table $\eta_v(n, N)$, such as:

$$m = \frac{\eta_v(n, N)V_{dis}p_{int}}{RT_{int}} \quad (8.33)$$

- Model B: By using the resonance method for trapped mass estimation and including a correction for other NO_x formation mechanism based on the oxygen availability.

Calibration The 39 OP from the basic map plus a hundred of test randomly selected were used to train the model while the rest of the tests (203 OP) based on variations of SOI, EGR, rail pressure and intake pressure, guaranteed a fair validation of the data. Note that the operating conditions of the clusters of variations do not necessarily coincide with the basic operating map.

The calibration was divided in three steps: Firstly, tests with no EGR were used to calibrate the volumetric efficiency map, $\eta_v(n, N)$, and the Bessel factor, $B(\alpha)$, with an air mass flow sensor. Secondly, tests with high adiabatic flame temperature were selected for characterize the thermal NO_x formation mechanism, $\Delta T(n, N)$, by using the smart NO_x sensor measurement. And Finally, tests with low flame temperature were employed to fit the correction over the

thermal NO_x , $K(T_{ad}^{max})$. Figure 8.21 illustrates the calibration methodology. Of interest, only variations in maximum adiabatic temperature are mandatory in order to distinguish thermal NO_x formation from other mechanism. The easiest way of varying the maximum adiabatic temperature is by varying the intake oxygen availability by modifying the EGR.

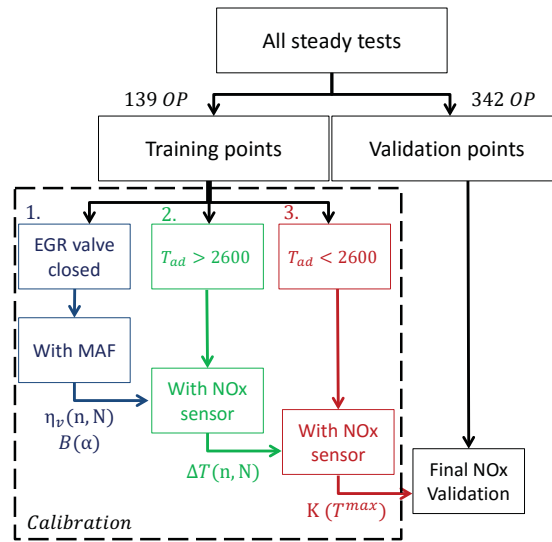


Figure 8.21. Calibration of the NO_x methodology.

The Bessel coefficient calibrated for the resonance methodology was found to be 2.1 at 20 CAD and 1.9 at 50 CAD after the TDC, which are consistent values with the first cylindrical radial mode (1.842). The volumetric efficiency values obtained ranged from 0.8 to 0.9 in the studied operating conditions. The whole volumetric efficiency table is shown in Figure 8.22.

Figure 8.23 shows the final map for the temperature correction when using in-cylinder resonant modes for inferring the trapped mass. The correction factor varies from -60 K to -220K, which is approximately an 8% of the flame temperature. The boundary NO_x production layer length, and hence the temperature reaction reduction seems to increase as load is reduced and engine speed is increased. This coefficient is aimed to capture the diffusive flame characteristics by a temperature reaction correction. Diffusive flame combus-

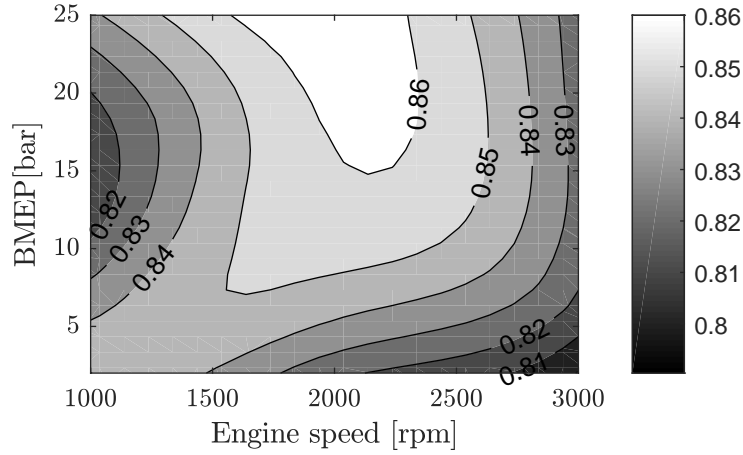


Figure 8.22. Volumetric efficiency look-up table.

tion was ensured by selecting tests with high adiabatic flame temperatures.

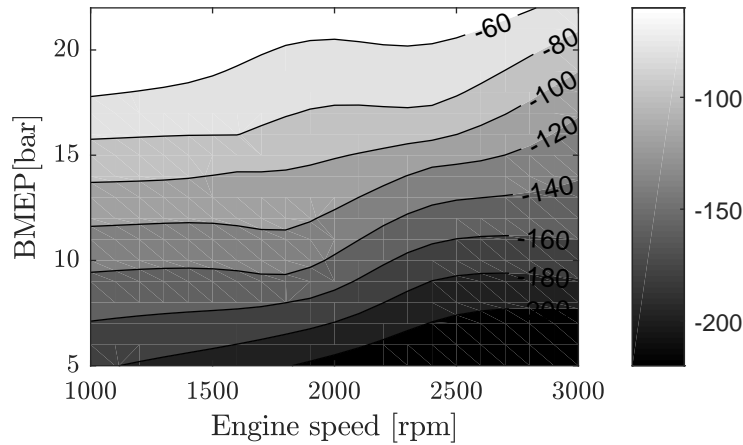


Figure 8.23. Temperature reaction coorection map obtained from OP of the training dataset with $T_{ad}^{max} > 2600K$.

Figure 8.24 shows the ratio NOx_{th}/NOx_{tot} measured as a function of the maximum adiabatic flame temperature. The identified parameters of Equation (8.31) are 2000, 0.0015 and 2.67 for T_0 , m and n respectively.

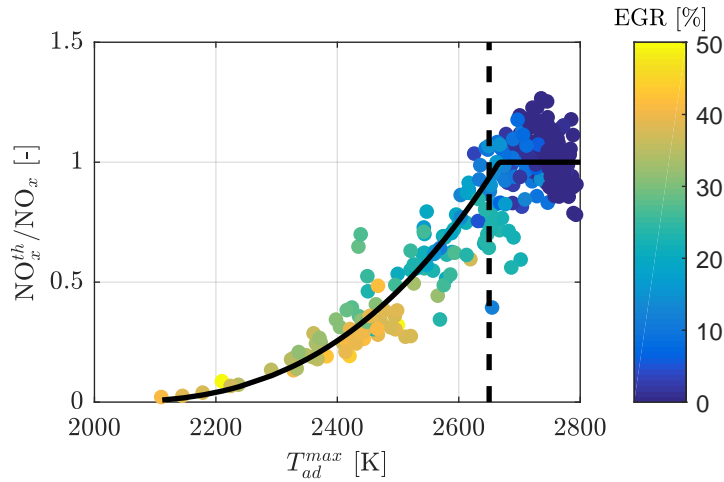


Figure 8.24. thermal NO_x and NO_x measured ratio as a function of the maximum adiabatic flame temperature and EGR.

It must be noticed that the coefficient strongly depends on the adiabatic flame temperature, the main responsible of LTC combustion. At conventional CI combustion, with no EGR, all NO_x are produced from thermal formation. However, at LTC zone ($EGR > 30\%$) thermal formation explains less than 50% of the total NO_x .

Validation Figure 8.25 compares the output of the method (model B) with the NO_x sensor measurements. It must be noticed that the model is able to predict the NO_x produced, even when high variations of the control inputs are made.

Figure 8.26, shows the mean absolute error (MAE) and the mean relative error (MRE) of both models, A and B, in groups of tests with similar NO_x production.

The average error of model B is 0.041 mg/str, while model A has 0.057 mg/str error. This 30% error reduction is mainly due to the estimation of the trapped mass from resonance, as the effect of the thermal NO_x correction is negligible at high NO_x concentration. The N_2O and Prompt correction improves the precision of the model at low NO_x concentrations: model A has almost 25% error while model B around 15%.

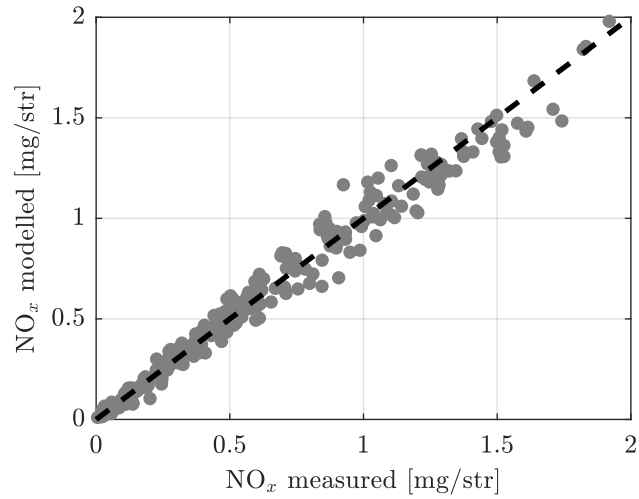


Figure 8.25. MAE and MRE for model A and model B as a function of NO_x.

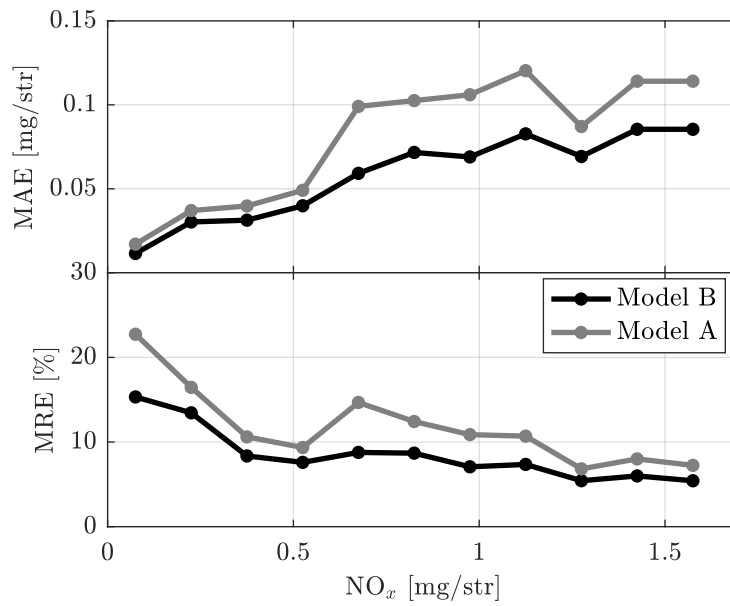


Figure 8.26. MAE and MRE for model A and model B as a function of NO_x.

Figure 8.27 splits the model errors in the four inputs variations, namely EGR, SOI, VGT, and rail pressure.

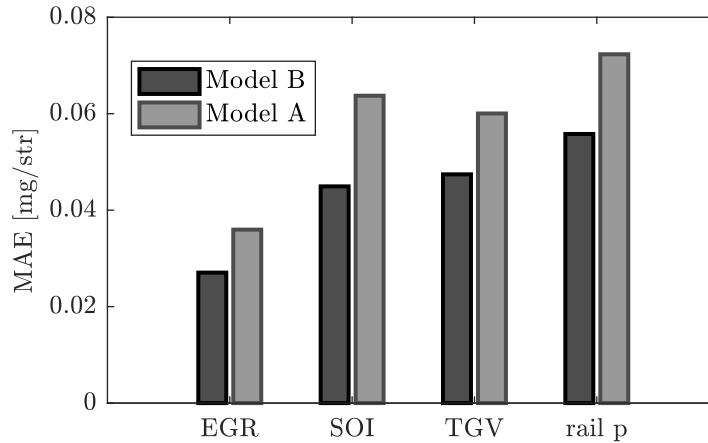


Figure 8.27. MAE of model A and model B at the different control input variations.

Rail pressure sensitivity is explained by diffusive flame characteristics, as rail pressure variations do modify the flame length and turbulence. Model errors caused by SOI are mainly due to premixed combustion increase or partial misfires when SOI was set far before from TDC or far after, respectively. It must be noticed that all variations were made at standard engine configuration, so EGR measurement errors may also exist in VGT, rail pressure and SOI variations.

Regardless of the variations contemplated, the inclusion of the resonance methodology permits a significant reduction of the average error.

8.6 Conclusions

This Chapter has presented four applications of the resonance method, namely residual gases estimation in engines with NVO, knock prediction in SI engines, exhaust temperature estimation, and NO_x modelling.

The estimation of the trapped mass given by the resonance methodology provides the aforementioned applications with a direct measurement with one cycle resolution. The inclusion of the resonance methodology significantly re-

duces the modelling errors and improves the transient response of the models:

- The method provides a cycle-to-cycle estimation of the residual gases in engines with NVO strategies, which may be harnessed to phase the combustion in engines working with new combustion concepts, such as HCCI or SACI. In contrast with other methodologies, which hesitate from unobservable parameters, such as EGR or exhaust temperature, the method only requires from the in-cylinder pressure signal. The method shown consistency with current methodologies in steady conditions and cycle-to-cycle transient response when VVT steps are performed.
- Knocking conditions in conventional SI engines proved to be a good environment to evaluate the in-cylinder pressure waves and obtain a trapped measurement estimation. This estimation can be harnessed to avoid MAF sensor bias and solve one of the error sources when predicting knock by autoignition models. A knock model was developed by modelling unpredictable errors, such as hot spots, with an exogenous noise. The model reproduced the engine knock probability with sufficient accuracy at various operating conditions when resonance was processed for obtaining the trapped mass, but it shown significant errors when MAF sensor was used.
- The estimation of the trapped mass allowed the computation of the engine-out gases temperature, which was used to estimate the exhaust gases temperature at each cycle by assuming a polytropic expansion at the exhaust valves and a lumped model with one state to reproduce the wall heat transfer. Thermocouples located at the exhaust manifold were used to compare the novel methodology with current methods, which are based on look-up tables. Current methods had a 4.76% average error when variations at the EGR, VGT, SOI, and rail pressure are performed over the nominal point, while the output of the new methodology only differ from the sensor measurement in a 2.08%.
- Finally, emissions models based on the adiabatic flame temperature were modified in order to compute the total NO_x from an in-cylinder pressure signal, a lambda, and a MAF sensor. The model used the in-cylinder pressure resonance to estimate cycle-by-cycle the unburned gas temperature, which was used to model the reaction rate of the NO_x formation. Resonance was proven to be crucial for the NO_x estimation, as the model had a 30% error reduction when the trapped mass was estimated from the in-cylinder pressure waves, and not from speed-density methods.

References

- [1] Cairns Alasdair and Blaxill Hugh. “The effects of combined internal and external exhaust gas recirculation on gasoline controlled auto-ignition”. Technical report, SAE Technical Paper, 2005. (cited in p. 192)
- [2] Wheeler Jennifer, Polovina Dusan, Frasinél Vasile, Miersch-Wiemers Oliver, Mond Alan, Sterniak Jeff and Yilmaz Hakan. “Design of a 4-cylinder GTDI engine with part-load HCCI capability”. *SAE International Journal of Engines*, Vol. 6 n° 2013-01-0287, pp. 184–196, 2013. (cited in p. 192)
- [3] Fitzgerald R. P., Steeper R., Snyder J., Hanson R. and Hessel R. “Determination of cycle temperatures and residual gas fraction for HCCI negative valve overlap operation”. *SAE International Journal of Engines*, Vol. 3 n° 1, pp. 124–141, 2010. (cited in p. 193)
- [4] Yun H. J. and Mirsky W. “Schlieren-streak measurements of instantaneous exhaust gas velocities from a spark-ignition engine”. *SAE Technical Papers*, 1974. (cited in pp. 66 and 193)
- [5] Peyton Jones J. C., Frey J. and Shayestehmanesh S. “Stochastic Simulation and Performance Analysis of Classical Knock Control Algorithms”. *IEEE Transactions on Control Systems Technology*, Vol. PP n° 99, 2016. (cited in pp. 40 and 197)
- [6] Spelina J. M., Peyton Jones J. C. and Frey J. “Characterization of knock intensity distributions: Part 1: Statistical independence and scalar measures”. *Proceedings of the Institution of Mechanical Engineers, Part D: Journal of Automobile Engineering*, Vol. 228 n° 2, pp. 117–128, 2014. (cited in pp. 40 and 197)
- [7] Kawahara N., Tomita E. and Sakata Y. “Auto-ignited kernels during knocking combustion in a spark-ignition engine”. *Proceedings of the Combustion Institute*, Vol. 31 II, pp. 2999–3006, 2007. (cited in pp. 40 and 197)
- [8] Livengood J. C. and Wu P. C. “Correlation of autoignition phenomena in internal combustion engines and rapid compression machines”. *Symposium (International) on Combustion*, Vol. 5 n° 1, pp. 347–356, 1955. (cited in pp. 34, 131, and 199)
- [9] Chen L., Li T., Yin T. and Zheng B. “A predictive model for knock onset in spark-ignition engines with cooled EGR”. *Energy Conversion and Management*, Vol. 87, pp. 946–955, 2014. (cited in pp. 34 and 199)
- [10] Douaud A. M. and Eyzat P. “Four-octane-number method for predicting the anti-knock behavior of fuels and engines”. *SAE Technical Papers*, 1978. (cited in pp. 34, 199, and 204)
- [11] Goudarzi K., Moosaei A. and Gharaati M. “Applying artificial neural networks (ANN) to the estimation of thermal contact conductance in the exhaust valve of internal combustion engine”. *Applied Thermal Engineering*, Vol. 87, pp. 688–697, 2015. (cited in p. 205)
- [12] Macek J. and Vitek O. “Determination and Representation of Turbocharger Thermodynamic Efficiencies”. *SAE Technical Papers*, 2016. (cited in p. 205)
- [13] Chen P. and Wang J. “Control-oriented model for integrated diesel engine and aftertreatment systems thermal management”. *Control Engineering Practice*, Vol. 22 n° 1, pp. 81–93, 2014. (cited in p. 205)
- [14] Schmitt J. and Parmentier M. “Exhaust temperature predictor : an alternative approach to predictive control applied to diesel aftertreatment”. In *IFAC Proceedings Volumes*, volume 7, pp. 730–731, 2013. (cited in p. 205)

- [15] Chauvin J., Corde G., Petit N. and Rouchon P. “Motion planning for experimental airpath control of a diesel homogeneous charge-compression ignition engine”. *Control Engineering Practice*, Vol. 16 n° 9, pp. 1081–1091, 2008.
(cited in pp. 70, 71, and 205)
- [16] Zhao J. and Wang J. “Adaptive observer for joint estimation of oxygen fractions and blend level in biodiesel fueled engines”. *IEEE Transactions on Control Systems Technology*, Vol. 23 n° 1, pp. 80–90, 2015.
(cited in pp. 65, 70, 71, and 205)
- [17] Olmeda P., Dolz V., Arnau F. J. and Reyes-Belmonte M. A. “Determination of heat flows inside turbochargers by means of a one dimensional lumped model”. *Mathematical and Computer Modelling*, Vol. 57 n° 7-8, pp. 1847–1852, 2013.
(cited in p. 207)
- [18] Eriksson L. “Mean value models for exhaust system temperatures”. *SAE Technical Papers*, 2002.
(cited in pp. 31 and 208)
- [19] Serrano J. R., Olmeda P., Arnau F. J., Reyes-Belmonte M. A. and Tartoussi H. “A study on the internal convection in small turbochargers. Proposal of heat transfer convective coefficients”. *Applied Thermal Engineering*, Vol. 89, pp. 587–599, 2015.
(cited in p. 208)
- [20] Lapuerta M., Armas O. and Hernández J. J. “Diagnosis of DI Diesel combustion from in-cylinder pressure signal by estimation of mean thermodynamic properties of the gas”. *Applied Thermal Engineering*, Vol. 19 n° 5, pp. 513–529, 1999.
(cited in pp. 32, 116, 117, 147, 149, and 209)
- [21] Sarnes B. and Schrüfer E. “Determination of the time behaviour of thermocouples for sensor speedup and medium supervision”. *Proceedings of the Estonian Academy of Sciences: Engineering*, Vol. 13 n° 4, pp. 295–309, 2007.
(cited in pp. 68, 69, and 210)
- [22] Guardiola C., Dolz V., Pla B. and Mora J. “Fast estimation of diesel oxidation catalysts inlet gas temperature”. *Control Engineering Practice*, Vol. 56, pp. 148–156, 2016.
(cited in pp. 69, 174, and 216)
- [23] Fulton B., Van Nieuwstadt M., Petrovic S. and Roettger D. “Exhaust manifold temperature observer model”. *SAE Technical Papers*, Vol. 1, 2014.
(cited in p. 216)
- [24] Brijesh P. and Sreedhara S. “Exhaust emissions and its control methods in compression ignition engines: A review”. *International Journal of Automotive Technology*, Vol. 14 n° 2, pp. 195–206, 2013.
(cited in pp. 9 and 216)
- [25] Chi J and DaCosta H. “Modeling and Control of a Urea-SCR Aftertreatment System”. *SAE paper 2005-01-0966*, 2005.
(cited in pp. 9 and 216)
- [26] Devarakonda M, Parker G, Johnson J and Strots V et al. “Model-Based Estimation and Control System Development in a Urea-SCR Aftertreatment System”. *SAE Int. J. Fuels Lubr.*, Vol. 1 n° 1, pp. 646–661, 2009.
(cited in pp. 9 and 216)
- [27] Guardiola C., López J. J., Martín J. and García-Sarmiento D. “Semiempirical in-cylinder pressure based model for NOX prediction oriented to control applications”. *Applied Thermal Engineering*, Vol. 31 n° 16, pp. 3275–3286, 2011.
(cited in pp. 36, 217, 219, and 220)
- [28] Arrègle J., Javier López J., Guardiola C. and Monin C. “Sensitivity study of a NOX estimation model for on-board applications”. *SAE Technical Papers*, 2008.
(cited in p. 219)

Chapter 9

Conclusions and future work

Contents

| | | |
|------------|---|------------|
| 9.1 | Main contributions and conclusions | 229 |
| 9.1.1 | Resonance characterization | 230 |
| 9.1.2 | Trapped mass estimation | 232 |
| 9.1.3 | Sensor data fusion | 234 |
| 9.1.4 | Applications for control and diagnosis | 235 |
| 9.2 | Future work | 237 |

9.1 Main contributions and conclusions

This dissertation presented a novel methodology for trapped mass estimation by analysing the in-cylinder pressure resonance. For that purpose, the following topics have been covered along the text:

- Resonance has been analysed in various engines, ranging from small SI engines with pent-roof combustion chambers to heavy-duty diesel-like engines. The evolution of the contents of the in-cylinder pressure in the resonant modes has been analysed both, with FEM simulations and processing combustion pressure cycles. The resonance excitation of the in-cylinder pressure resonance has been studied in various combustion modes, conventional ones, such as CI and SI, and new combustion concepts, such as RCCI, SACI, or CAI.

- A method for determining the trapped mass from the frequency evolution of the first resonant mode has been developed. In a first approximation, the methodology makes use of the STFT for the resonant evolution identification, while later on, a specific transformation specifically developed for identifying the first resonant mode is presented.
- A Kalman filter, which combines various sensors at different locations, has been proposed to provide sufficient accuracy and robustness at the estimation of the trapped mass and its components, namely fresh air, EGR and injected fuel mass. Dynamics of the intake manifold and transient response of the sensors have been modelled in order to guarantee a good estimation in engine transients.
- Four applications for the new trapped mass estimation methodology are developed, namely residual gases estimation, knock prediction, exhaust temperature estimation, and NO_x modelling. These four applications show the potential of such measurement for combustion control and diagnosis. The new applications are compared with current methodologies and the contributions of the new estimations have been pointed out.

Next, a short overview of these points is given and the main conclusion derived are highlighted.

9.1.1 Resonance characterization

Resonance frequency evolution. The analytical solution of the radial modes of a cylindrical combustion chamber, which states a proportional relation between the speed of sound and the resonant frequency, such as:

$$f_{res} = \frac{aB}{\pi D} \quad (9.1)$$

has been proven in two conventional SI engines (engines A and E), both with pent-roof combustion chambers.

In-cylinder pressure signals were processed by STFT and WD, and the instantaneous engine speed was measured or modelled by crankshaft dynamics models. The speed of sound was computed by measuring the trapped mass from an air mass flow anemometer, a lambda sensor, and an EGR estimation from CO₂ balance in the case of Engine E.

Non-cylindrical combustion chambers. The rest of the tested engines, with various in-piston geometries, shown higher resonant frequencies near the TDC, while the resonant frequency evolution coincided with the cylindrical theory at the end of the expansion stroke.

FEM simulations and specific tests at various engine operating conditions shown that the proportionality between the speed of sound and the resonant frequencies only depends on the geometry, i.e. the crank angle evolution, and hence, the resonant frequency evolution can be calibrated during the piston stroke.

Three methodologies for the calibration of the Bessel constant $B(\alpha)$ in engines with bowl have been proposed: an independent FEM simulation, an empirical calibration with experimental data obtained from auxiliary sensors, and a direct calibration with in-cylinder pressure data, by assuming that the combustion chamber behaves as a perfect cylinder of the nominal bore at the end of the expansion stroke.

Temperature in-homogeneities. In order to simulate the temperature field of a stratified combustion, such as in a CI diffusive flame, FEM simulations with two zones at different temperature were designed. The simulations with stratified combustion (2 zones) were compare with simulations that assume an homogeneous field (single zone).

Results shown discrepancies around 10% when combustion is taking place. Although an infinite gradient was studied during the simulations and the actual effect should be smaller, the resonance in a stratified combustion must be carefully analysed, taking into account that combustion inhomogeneities may lead to additional errors.

Resonance excitation. A qualitative analysis was made with various engines to analyse the effect of the type of combustion on the resonance pressure waves. With the following conclusions:

- Fast combustions, such as in HCCI modes, heavily excite resonance, however, slow combustions, such as in low-load SI combustion, do not.

- Resonance in conventional CI combustion is characterized by the nearly homogeneous autoignition of the first injected fuel, but the later diffusive flame combustion, where most of the fuel is burnt at high loads, does not significantly influence resonance.
- In SI engines, where combustion is produced by flame propagation, little resonance excitation was found. Nevertheless, the fast auto-ignition of the end-gas heavily excites the resonant modes. When the autoignition of the end-gas is uncontrolled and non-desired, it is known as knock, while some new combustion strategies, i.e. SACI, try to use the flame propagation to ignite an homogeneous mixture of fuel, fresh air, and burnt products, in a controlled scheme.

A new procedure to detect knock is proposed. It is based on comparing the resonance content in the pressure signal caused by regular SI combustion, i.e. near the maximum heat release rate, and the content of the signal where autoignition occurs, i.e. near the EOC. The new knock event definition permits low-knocking cycle detection and does not require a predefined threshold.

9.1.2 Trapped mass estimation

This dissertation presented a novel methodology to estimate the trapped mass from the in-cylinder pressure resonance.

In a first approximation, the trapped mass estimation is made by computing the resonant frequency evolution by analysing the pressure signal in the time frequency domain, with the STFT, and later deriving the trapped mass by relying in the ideal gas law and in the proportionality between the speed of sound and the frequency evolution of the first resonant mode. Doing so, an output of the trapped mass evolution is obtained, which facilitates detecting erratic measurements with significant trapped mass variations along a given cycle.

In order to avoid a time-frequency analysis, which is based on constant frequency harmonics, a new transformation is suggested. The new transformation divides the signal in frequency varying harmonics. The frequency evolution of those harmonics is characterized by virtual trapped masses, and its evolutions follows the resonance theory (Draper's equation). The virtual trapped mass which makes maximum the new transformation must be the actual trapped mass if sufficient resonance excitation exist, while its amplitude

gives an insight of how resonance has been excited.

Some of the contributions of the methodology are:

- The method offers a cycle-to-cycle measurement of the trapped mass. The resonance at each combustion event can be considered independent from the previous cycle.
- Resonance is directly sensed at the combustion chamber. The output of the new method is not affected by intake or exhaust manifold dynamics, such as in mass flow sensors.
- The method can be together with traditional sensors in order to correct their calibration as the engine ages.
- The computation of the trapped mass is made during the expansion stroke, consequently, pegging errors have negligible effect on the final measurement.

The possible errors at the resonance method have been bounded by including virtual errors at real pressure data in various operating conditions, covering the full operating map of a light-duty CI engine. The effect of the gas properties, i.e. the composition is not estimated, is limited to a 2%. If the instantaneous engine speed is not measured and the method is applied between 30 to 80 CAD after the TDC the influence of the engine speed oscillations is limited to a 2%. The effect of an error at pegging or at the TDC phasing strongly depends on the region analysed: pegging errors are negligible at high pressure values (near the TDC), but the sensitivity of phasing errors is maximum at the minimum volume location (at the TDC). Nevertheless, for a normal region of analysis (from 30 to 80 CAD after TDC) an error of 100 mbar at pegging produces trapped mass errors below 1% and 1 CAD error at phasing may cause a 3% error, but may be solved by a re-calibration of the system.

The new methodology was applied in four engines with different combustion modes: a conventional SI engine (Engine A), a conventional light-duty CI engine (engine B), a heavy-duty engine with RCCI combustion (Engine D), and a two-strokes engine with CAI combustion (Engine F). The trapped mass

was measured with test-cell sensors and the differences obtained are consistent with the expected accuracy of the sensors, i.e. below sensors uncertainty:

- In engine A, with no EGR and a precise estimation of the air by a fuel flow meter and a lambda sensor, the average error was 0.71 %.
- In engine B, where the estimation of the trapped mass was performed by the speed-density method the average error was 2.64 %.
- In engine D, where the air mass flow was measured by a hot-film anemometer and the EGR by CO₂ balance at the intake, the error was 2.17 %.
- In engine F, where the short-circuit and residual gasses represent a significant percentage of the trapped mass and they are inferred through artificial CH₄ insertion and enthalpy balance, the error was 4.37 %. But here there is reasonable concerns on the reference measurement accuracy.

9.1.3 Sensor data fusion

A Kalman filter has been designed to combine the resonance method, which requires from an in-cylinder pressure sensor, with some of the sensors that are currently installed in a commercial engine, concretely, a lambda sensor (or a NO_x sensor with oxygen concentration measurement), the EGR valve position, an air mass flow meter, a piezo-resistive pressure sensor at the intake and a temperature sensor at the intake. It must be noticed that the piezo-resistive pressure sensor can be replaced by the in-cylinder pressure sensor if pegging is performed by assuming an isentropic compression.

The intake manifold dynamics were included with an isothermal model, because EGR was cooled at the inter-cooler and temperature differences could be neglected. If significant differences of temperature exist, the adiabatic model and an estimation of the EGR temperature, through an additional sensor or an exhaust thermal model, must be used. Additional states are proposed to take into account the time delay at the onboard sensor acquisition, and a first order system was used for modelling the NO_x sensor dynamics. Although dynamics of the lambda and air mass flow sensors are neglected, they can also be included with additional first order systems.

A methodology for outliers identification at the resonance method has been presented. The method uses an adaptive cycle-to-cycle trapped mass variation and the resonance excitation metrics to detect failures at the resonance

method implementation. In the cycle where an outlier was detected, high measurement noises were associated to the trapped mass measurement. Similarly, zero noise at the EGR measurement was setted when the EGR valve was closed, but a high noise was used when it was opened and not reliable EGR measurement was available.

The Kalman filter was implemented in a commercial light-duty CI engine. The transient performance of the Kalman filter was illustrated in a WLTP cycle, while VGT and EGR steps were conducted at eight operating conditions to try different sensor sets.

An observer, such as the one designed in this dissertation, allows a transient estimation of the trapped mass which takes into account the intake manifold dynamics and uses a direct measurement of the trapped mass, i.e. by using the resonance method. The observer corrects the injected fuel mass ECU estimation with the lambda sensor and uses this estimation, information from the hot-film anemometer, and the speed-density method to improve the resonance method estimation, and obtains a robust trapped mass estimation.

Several set of sensors can be used. If the EGR valve is closed (or in engines with no EGR), the resonance method can substitute the air mass flow sensor, with the additional improvements of a direct measurement at the cylinder and one cycle resolution. If EGR is used, the resonance method gives a useful estimation of total mass, and hence, an additional information of the real EGR if a hot-film anemometer and an injected fuel mass estimation are available. The exhaust oxygen concentration (provided by a lambda or a NO_x sensor) was used to improve the injected fuel mass estimation, but it is not mandatory if the ECU model is reliable enough.

9.1.4 Applications for control and diagnosis

Four applications of the resonance method have been developed to illustrate the potential of such measurement in engine control and diagnosis, namely residual mass estimation, knock prediction for SI engines, exhaust gas temperature estimation, and NO_x modelling for CI engines. These are four examples of onboard models that make use of a trapped mass estimation to calculate engine parameters, but many others can be proposed.

Residual gas estimation in engines with NVO. The resonance method was used to determine the in-cylinder conditions before the EVO and the residual mass was obtained by modelling the exhaust process through an isentropic process. The method was validated in a modified SI engine which was operated in SACI and CAI modes. The transient performance of the model was illustrated by intake and exhaust valves step and the steady accuracy was determined by comparing the method with Yun and Mirsky method, which requires from an EGR measurement. The EGR was measured by CO₂ balance at the intake and both methods shown an excellent linearity, being $r^2=0.997$ and the MAE=2.8 mg/str.

Knock prediction for SI engines. A knock model was developed by using an estimation of the autoignition time through an Arrhenius function and adding an exogenous noise at the in-cylinder gas temperature estimation, which accounts for uncertainties during its estimation, such as temperature hot spots or gas properties. The model was validated in a conventional SI engine at medium-high load operation. The knock prediction shown a good correlation with experimental data when the resonance method is used, but the prediction made through the air mass flow meter did not properly predict knock when the operating conditions change, which points out the advantages of the resonance method for correcting MAF sensor bias.

Exhaust gas temperature estimation. The resonance method is used to estimate the engine-out temperature of the gases by assuming an isentropic expansion through the valves. The temperature drop along the exhaust manifold is modelled with a lumped model with two temperature nodes: a first node in contact with the engine coolant (at constant temperature), and a second that represents the rest of the exhaust manifold with a variable temperature in contact with the surroundings. The method was implemented in a light-duty CI engine in 12 operating conditions with variations at the injection settings, EGR, VGT, and rail pressure controls and it was compared with an open loop 2D table, such as used in current ECUs. The new method exhibits a 2.08 % difference with thermocouples located at the exhaust while current methods a 4.76 %, which represents a 129 % error reduction. The new method was also implemented in a WLTP cycle, showing potential to estimate the temperature of the exhaust gases with a better time response than temperature sensors.

NO_x model for CI engines. A NO_x model is developed by modifying a previously published work, which proposed an Arrhenius function with the adiabatic flame temperature for the reaction rate estimation and the heat release rate for modelling the reactants concentration. In the new model, a new parametrization is proposed, and the content at the resonance band (4-10 kHz) of the in-cylinder pressure signal is used to estimate the trapped mass through the resonance method, while its output and the low frequency content of the pressure signal are used to calculate the adiabatic flame temperature and the heat release rate. The method was programmed with the resonance method and with the output of the speed-density method, and both models were validated under the same experimental data used for the exhaust temperature model. The model using the resonance method exhibits a 30% error reduction in comparison with the one using the speed-density method, which highlights the benefits of the resonance method.

9.2 Future work

Test cell implementation. In the author's opinion, the resonance method is a mature technique for determining the trapped mass in test bench facilities. The method was successfully implemented with experimental data from six engines, with different combustion modes and engine sizes. Furthermore, the resonance method has been successfully implemented in real-time operation in a state-of-the-art prototyping system, concretely a PXIe8133, which consist in a Quad-Core processor with 1,73 GHz.

However, in order to provide an adaptable implementation, which may be included in a commercial acquisition and processing software, some parts of the method must be improved.

The minimum requirements for a resonance identification must be studied. One of the main drawbacks of the method is the need of sufficient resonance energy at the studied pressure trace. The availability of such energy depends on the combustion excitation, but also on the in-cylinder pressure sensor used. On the one hand, slow combustions at low-load conditions may not sufficiently excite the resonance, specially in conventional SI and CI modes. On the other hand, several new pressure sensors are being introduced in the market, lowering the price of traditional piezo-electric sensors. However, the response of those sensors at the frequency band of resonance may be not adequate and

some noises could disturb the trapped mass estimation obtained from the resonance method.

Firstly, for an adequate implementation of the method, more knowledge on the resonance to predict its excitation and damping would be advisable. Moreover, concrete strategies, e.g. some cycles without pilot injection at CI engines, could be designed to obtain a trapped mass measurement at steady conditions.

Secondly, in order to widespread the method in commercial applications a deep analysis on the sensor characteristics at the resonance band seems mandatory.

And finally, the calibration procedure and the resonance method implementation should be systematized to provide the most appropriate options to the user, taking into account the range of possible engines, the calibration methodologies and the available sensors.

On-board implementation. The implementation of the resonance method in current commercial ECUs faces two challenges. On the one hand, the acquisition of the pressure trace must be performed above 20 kHz in order to capture the resonance band. On the other hand, the computational burden of the calculations may exceed the ECU capabilities. These two issues should be carefully studied to determine the feasibility of such implementation.

Although new ECUs are being developed, with a significant increase in the computational capabilities, the method could be optimized to reduce the number of operations. The resonance method could be improved by developing an iterative methodology to find the maximum virtual trapped mass, instead of the current raw approximation which consists on using a set of virtual trapped mass candidates.

Transient estimation of the trapped mass. The observer suggested in Chapter 7 can be improved by better studying the transient behaviour of the engine. The exhaust manifold dynamics are neglected, and the lambda sensor is restricted to improve the injected fuel model. If exhaust and EGR dynamics are included, the measurement of the exhaust concentration could be also

combined to identify the EGR mass evolution, and hence, improve the final trapped mass estimation. Indeed, there is no direct EGR estimation used (only when the EGR valve is closed). An EGR model, such as provided by the orifice principle, would improve the final observer output, specially in fast transient conditions with poor resonance excitation. Furthermore, a deeper analysis of the error metrics and the time response of the sensors would also improve the transient capabilities of the observer.

CL control systems Some systems in the engine are open-loop controlled, such as the EGR, and the engine operation is not optimal as the engine ages. The resonance method could be used to provide some feedback to adapt existing models or directly CL control these systems.

Furthermore, many authors have highlighted the relevance of transient operation at the overall engine performance and the resonance method offers new models and methods with 1 cycle resolution which may improve current controls and make them faster.

Although the method and some applications were implemented onboard, the output was not used for feedback in a control scheme. A control oriented work with the resonance method could correct bias and errors caused by ageing and manufacturing discrepancy and improve the transient operation of the engines.

References

Alphabetic Index of Authors

- ACEA.** *ACEA position paper on electrically chargeable vehicles.* European Automobile Manufacturers' Association, 2012. (cited in p. 5)
- Adams M and Lükewille A.** *The European Environment State and Outlook 2010: Air pollution.* European Environment Agency. Publications Office of the European Union, 2010. (cited in p. 3)
- Adomeit P., Sehr A., Weinowski R., Stapf K. G., Seebach D., Pischinger S., Hoffmann K., Abel D., Fricke F., Kleeberg H. and Tomazic D.** "Operation strategies for controlled auto ignition gasoline engines". *SAE International Journal of Engines*, Vol. 2 n° 1, pp. 164–172, 2009. (cited in p. 11)
- Akimoto K., Komatsu H. and Kurauchi A.** "Development of pattern recognition knock detection system using short-time fourier transform". In *IFAC Proceedings Volumes (IFAC-PapersOnline)*, volume 7, pp. 366–371, 2013. (cited in pp. 38 and 41)
- Al-Durra A., Fiorentini L., Canova M. and Yurkovich S.** "A model-based estimator of engine cylinder pressure imbalance for combustion feedback control applications". In *Proceedings of the American Control Conference*, pp. 991–996, 2011. (cited in p. 43)
- Al-Himyari B.A., Yasin A. and Gitano H.** "Review of Air-Fuel Ratio Prediction and Control Methods". *Asian Journal of Applied Sciences*, 2014. (cited in p. 58)
- Alberts T. E., Liu S. and Lally R. W.** "Investigation of an inexpensive piezoelectric pressure sensor for internal combustion engine spark timing control". *SAE Technical Papers*, 2006. (cited in p. 31)
- Ali S. A. and Saraswati S.** "Cycle-by-cycle estimation of IMEP and peak pressure using crankshaft speed measurements". *Journal of Intelligent and Fuzzy Systems*, Vol. 28 n° 6, pp. 2761–2770, 2015. (cited in p. 43)
- Alsabaan M., Naik K., Khalifa T. and Nayak A.** "Optimization of fuel cost and emissions with vehicular networks at traffic intersections". *IEEE Conference on Intelligent Transportation Systems, Proceedings, ITSC*, pp. 613–619, 2012. (cited in p. 13)
- Aly S.E.** "Diesel engine waste-heat power cycle". *Applied Energy*, Vol. 29, pp. 179–189, 1988. (cited in p. 9)
- Andersson Per.** *Intake air dynamics on a turbocharged SI-engine with wastegate.* Department of Electrical Engineering, Linköping University, 2002. (cited in p. 71)

- Anderton D.** “Relation between combustion system and engine noise”. *SAE Technical Papers*, 1979. (cited in p. 33)
- Aquino C. F.** “Transient A/F control characteristics of the 5 liter central fuel injection engine”. *SAE Technical Papers*, 1981. (cited in p. 10)
- Armas O.** *Diagnostico experimental del proceso de combustión en motores Diesel de inyección directa*. PhD Thesis, Universitat Politècnica de València. Departamento de Máquinas y Motores Térmicos - Departament de Màquines i Motors Tèrmics, 1998. (cited in p. 31)
- Armas O., Rodríguez J., Payri F., Martín J. and Agudelo J. R.** “Effect of the trapped mass and its composition on the heat transfer in the compression cycle of a reciprocating engine”. *Applied Thermal Engineering*, Vol. 25 n° 17-18, pp. 2842–2853, 2005. (cited in p. 12)
- Arrègle J., Javier López J., Guardiola C. and Monin C.** “Sensitivity study of a NOx estimation model for on-board applications”. *SAE Technical Papers*, 2008. (cited in p. 219)
- Asad U.** *Advanced diagnostics, control and testing of diesel low temperature combustion*. PhD Thesis, University of Windsor, 2009. (cited in p. 60)
- Asad U, Divekar P, Chen X and Zheng M et al.** “Mode Switching Control for Diesel Low Temperature Combustion with Fast Feedback Algorithms”. *SAE Int. J. Engines*, Vol. 5 n° 3, pp. 850–863, 2012. (cited in p. 12)
- Asad U., Tjong J. and Zheng M.** “Exhaust gas recirculation - Zero dimensional modelling and characterization for transient diesel combustion control”. *Energy Conversion and Management*, Vol. 86, pp. 309–324, 2014. (cited in p. 60)
- Asad U and Zheng M.** “Tightened intake oxygen control for improving diesel low-temperature combustion”. *Proceedings of the Institution of Mechanical Engineers, Part D: Journal of Automobile Engineering*, Vol. 225 n° 4, pp. 513–530, 2011. (cited in p. 58)
- Asad U. and Zheng M.** “Exhaust gas recirculation for advanced diesel combustion cycles”. *Applied Energy*, Vol. 123, pp. 242–252, 2014. (cited in pp. 35, 58, and 60)
- Asprion J., Chinellato O. and Guzzella L.** “A fast and accurate physics-based model for the NOx emissions of Diesel engines”. *Applied Energy*, Vol. 103, pp. 221–233, 2013. (cited in p. 36)
- Austen A. E. W. and Priede T.** “Origins of diesel engine noise”. *SAE Technical Papers*, 1959. (cited in p. 33)
- Baert RSG, Beckman DE and Veen A.** “Efficient EGR Technology for Future HD Diesel Engine Emission Targets”. *SAE paper 1999-01-0837*, 1999. (cited in p. 12)
- Bailey M.M.** “Comparative Evaluation of Three Alternative Power Cycles for Waste Heat Recovery Form the Exhaust of Adiabatic Diesel Engines”. Technical report, National Aeronautics and Space Administration, 1985. (cited in p. 9)
- Baratta M. and Misul D.** “Development and assessment of a new methodology for end of combustion detection and its application to cycle resolved heat release analysis in IC engines”. *Applied Energy*, Vol. 98, pp. 174–189, 2012. (cited in p. 28)
- Barbarisi Osvaldo, Alessandro G and Luigi G.** “An Extended Kalman Observer for the In-Cylinder Air Mass Flow Estimation”. In *Proceedings of MECA02 International Workshop on Diagnostics in Automotive Engines and Vehicles, Oct., Fisciano SA*, pp. 1–14, 2002. (cited in p. 72)

- Bass J.C., Kushch A.S. and Elsner N.B.** “Thermoelectric Generator (TEG) on Heavy Diesel Trucks”. Technical report, Hi-Z Technology Inc., 2001. (cited in p. 9)
- Beasley M., Cornwell R., Fussey P., King R., Noble A., Salamon T., Truscott A. and Landsmann G.** “Reducing diesel emissions dispersion by coordinated combustion feedback control”. *SAE Technical Papers*, 2006. (cited in p. 28)
- Bell J.** *Modern Diesel Technology: Electricity and Electronics*. Cengage Learning, 2013. (cited in p. 58)
- Benajes J., Molina S., García A., Belarte E. and Vanvolsem M.** “An investigation on RCCI combustion in a heavy duty diesel engine using in-cylinder blending of diesel and gasoline fuels”. *Applied Thermal Engineering*, Vol. 63 n^o 1, pp. 66–76, 2014. (cited in p. 92)
- Benajes J., Molina S., García A. and Monsalve-Serrano J.** “Effects of direct injection timing and blending ratio on RCCI combustion with different low reactivity fuels”. *Energy Conversion and Management*, Vol. 99, pp. 193–209, 2015. (cited in p. 92)
- Benajes J., Novella R., De Lima D., Tribotté P., Quechon N., Obernesser P. and Dugue V.** “Analysis of the combustion process, pollutant emissions and efficiency of an innovative 2-stroke HSDI engine designed for automotive applications”. *Applied Thermal Engineering*, Vol. 58 n^o 1-2, pp. 181–193, 2013. (cited in p. 162)
- Benajes J., Pastor J. V., García A. and Boronat V.** “A RCCI operational limits assessment in a medium duty compression ignition engine using an adapted compression ratio”. *Energy Conversion and Management*, Vol. 126, pp. 497–508, 2016. (cited in pp. 42 and 92)
- Benajes J., Pastor J. V., García A. and Monsalve-Serrano J.** “An experimental investigation on the influence of piston bowl geometry on RCCI performance and emissions in a heavy-duty engine”. *Energy Conversion and Management*, Vol. 103, pp. 1019–1030, 2015. (cited in p. 92)
- Benajes J., Pastor J. V., García A. and Monsalve-Serrano J.** “The potential of RCCI concept to meet EURO VI NO_x limitation and ultra-low soot emissions in a heavy-duty engine over the whole engine map”. *Fuel*, Vol. 159, pp. 952–961, 2015. (cited in pp. 42 and 92)
- Benson JD and Stebar Russell Ford.** “Effects of charge dilution on nitric oxide emission from a single-cylinder engine”. *SAE Technical Paper*, 1971. (cited in p. 60)
- Betta Giovanni, Capriglione Domenico, Pietrosanto Antonio and Sommella Paolo.** “ANN-based sensor fault accommodation techniques”. In *Diagnostics for Electric Machines, Power Electronics & Drives (SDEMPED), 2011 IEEE International Symposium on*, pp. 517–524, 2011. (cited in p. 59)
- Blanco-Rodríguez D.** *Modelling and observation of exhaust gas concentrations for diesel engine control*. PhD Thesis, Universitat Politècnica de València. Departamento de Máquinas y Motores Térmicos, 2013. (cited in pp. 68, 172, and 174)
- Bo T., Li G., Palaniyandi J., Hunt R. and Rowe C.** “Multiple-cylinder diesel engine CFD simulation using VECTIS”. *SAE Technical Papers*, 2009. (cited in p. 60)
- Bodisco T., Reeves R., Situ R. and Brown R.** “Bayesian models for the determination of resonant frequencies in a di diesel engine”. *Mechanical Systems and Signal Processing*, Vol. 26 n^o 1, pp. 305–314, 2012. (cited in p. 39)

- Bordjane Mustapha and Chalet David.** “Numerical Investigation Of Throttle Valve Flow Characteristics For Internal Combustion Engines”. *Journal of Multidisciplinary Engineering Science and Technology*, Vol. 2 n° 12, pp. 3532–3541, 2015. (cited in p. 65)
- Boretti A.** “Improving the Efficiency of Turbocharged Spark Ignition Engines for Passenger Cars through Waste Heat Recovery”. *SAE Paper 2012-01-0388*, 2012. (cited in p. 9)
- Borg J. M. and Alkidas A. C.** “Characterization of autoignition in a knocking si engine using heat release analysis”. *SAE Technical Papers*, 2006. (cited in p. 41)
- Bowman C. T.** “Kinetics of pollutant formation and destruction in combustion”. *Progress in Energy and Combustion Science*, Vol. 1 n° 1, pp. 33–45, 1975. (cited in pp. 36 and 37)
- Bradley D.** “Autoignitions and detonations in engines and ducts”. *Philosophical Transactions of the Royal Society A: Mathematical, Physical and Engineering Sciences*, Vol. 370 n° 1960, pp. 689–714, 2012. (cited in p. 33)
- Brands M.C., Werner J. and Hoehne J.L.** “Vehicle testing of Cummins turbocompound Diesel engine”. *SAE paper 810073*, 1981. (cited in p. 9)
- Brasseur G.** “Robust automotive sensors”. In *Conference Record - IEEE Instrumentation and Measurement Technology Conference*, volume 2, pp. 1278–1283, 1997. (cited in p. 59)
- Brecq G., Bellettre J. and Tazerout M.** “A new indicator for knock detection in gas SI engines”. *International Journal of Thermal Sciences*, Vol. 42 n° 5, pp. 523–532, 2003. (cited in p. 41)
- Brecq G. and Le Corre O.** “Modeling of in-cylinder pressure oscillations under knocking conditions: Introduction to pressure envelope curve”. *SAE Technical Papers*, 2005. (cited in p. 41)
- Brijesh P. and Sreedhara S.** “Exhaust emissions and its control methods in compression ignition engines: A review”. *International Journal of Automotive Technology*, Vol. 14 n° 2, pp. 195–206, 2013. (cited in pp. 9 and 216)
- Broatch A., Margot X., Gil A. and Donayre C.** “Computational study of the sensitivity to ignition characteristics of the resonance in di diesel engine combustion chambers”. *Engineering Computations (Swansea, Wales)*, Vol. 24 n° 1, pp. 77–96, 2007. (cited in pp. 39 and 119)
- Brooker AD, Ward J and Wang L.** “Lightweighting Impacts on Fuel Economy, Cost, and Component Losses”. *SAE paper 2013-01-0381*, 2013. (cited in p. 8)
- Brunt M. F. J. and Emtage A. L.** “Evaluation of burn rate routines and analysis errors”. *SAE Technical Papers*, 1997. (cited in p. 32)
- Brunt M. F. J. and Pond C. R.** “Evaluation of techniques for absolute cylinder pressure correction”. *SAE Technical Papers*, 1997. (cited in pp. 30, 168, and 183)
- Buehler P. J., Franchek M. A. and Makki I.** “Mass air flow sensor diagnostics for adaptive fueling control of internal combustion engines”. In *Proceedings of the American Control Conference*, volume 3, pp. 2064–2069, 2002. (cited in p. 59)
- Burkhard J. F.** “Individual cylinder fuel control for a turbocharged engine”. *SAE Technical Papers*, Vol. 1, 2014. (cited in p. 58)
- Butts K and Jaikamal V.** “Model-Based Verification and Validation of Electronic Engine Controls”. *SAE paper 2012-01-0961*, 2012. (cited in p. 13)
- Cains T., Pates D. and Warth M.** “Improving speed and accuracy of gasoline and diesel engine testing via closed-loop combustion control”. *SAE Technical Papers*, 2012. (cited in p. 27)

- Cairns Alasdair and Blaxill Hugh.** “The effects of combined internal and external exhaust gas recirculation on gasoline controlled auto-ignition”. Technical report, SAE Technical Paper, 2005. (cited in p. 192)
- Carrabine E and Longhurst B.** “Consuming the car: anticipation, use and meaning in contemporary youth culture”. *The Sociological Review*, Vol. 50 n° 2, pp. 181–196, 2002. (cited in p. 1)
- Cary M., Ebrahimi M., Ffrench K. and Sbaschnig R.** “Throttle body: Modelling and identification”. *Proceedings of the Institution of Mechanical Engineers, Part D: Journal of Automobile Engineering*, Vol. 215 n° 7, pp. 813–825, 2001. (cited in p. 65)
- Castillo F., Witrant E., Talon V. and Dugard L.** “Simultaneous air fraction and low-pressure EGR mass flow rate estimation for diesel engines”. In *IFAC Proceedings Volumes (IFAC-PapersOnline)*, pp. 731–736, 2013. (cited in pp. 70 and 71)
- Catania A. E., Ferrari A., Manno M. and Spessa E.** “Experimental investigation of dynamics effects on multiple-injection common rail system performance”. *Journal of Engineering for Gas Turbines and Power*, Vol. 130 n° 3, 2008. (cited in p. 67)
- Catania A. E., Ferrari A. and Spessa E.** “Numerical-experimental study and solutions to reduce the dwell-time threshold for fusion-free consecutive injections in a multijet solenoid-type CR system”. *Journal of Engineering for Gas Turbines and Power*, Vol. 131 n° 2, 2009. (cited in p. 67)
- Cavina N., Corti E., Minelli G., Moro D. and Solieri L.** “Knock indexes normalization methodologies”. *SAE Technical Papers*, 2006. (cited in p. 41)
- Cavina Nicolo, Cerofolini Alberto, Corti Enrico, Ponti Fabrizio, De Cesare Matteo and Stola Federico.** “Innovative Techniques for On-Board Exhaust Gas Dynamic Properties Measurement”. *SAE International Journal of Engines*, Vol. 6 n° 2013-01-0305, pp. 217–227, 2013. (cited in p. 58)
- Chaize E., Webster D. E., Krutzsch B., Wenninger G., Weibel M., Hodjati S., Petit C., Pitchon V., Kiennemann A., Loenders R., Monticelli O., Jacobs P. A., Martens J. A. and Kasemo B.** “Reduction of NOx in lean exhaust by selective NOx-Recirculation (SNR-Technique) part II: NOx storage materials”. *SAE Technical Papers*, 1998. (cited in p. 36)
- Chang C., Amstutz A. and Powell J. D.** “Air-Fuel Ratio Control in Spark-Ignition Engines Using Estimation Theory”. *IEEE Transactions on Control Systems Technology*, Vol. 3 n° 1, pp. 22–31, 1995. (cited in p. 58)
- Chauvin J., Corde G., Petit N. and Rouchon P.** “Motion planning for experimental airpath control of a diesel homogeneous charge-compression ignition engine”. *Control Engineering Practice*, Vol. 16 n° 9, pp. 1081–1091, 2008. (cited in pp. 70, 71, and 205)
- Chen L., Li T., Yin T. and Zheng B.** “A predictive model for knock onset in spark-ignition engines with cooled EGR”. *Energy Conversion and Management*, Vol. 87, pp. 946–955, 2014. (cited in pp. 34 and 199)
- Chen L. and Mehregany M.** “A silicon carbide capacitive pressure sensor for in-cylinder pressure measurement”. *Sensors and Actuators, A: Physical*, Vol. 145-146 n° 1-2, pp. 2–8, 2008. (cited in pp. 13 and 88)
- Chen P. and Wang J.** “Control-oriented model for integrated diesel engine and aftertreatment systems thermal management”. *Control Engineering Practice*, Vol. 22 n° 1, pp. 81–93, 2014. (cited in p. 205)

- Chen S. K. and Chen S.** “Engine diagnostics by dynamic shaft measurement: A progress report”. *SAE Technical Papers*, 1993. (cited in p. 43)
- Chen Z., Yao C., Wang Q., Han G., Dou Z., Wei H., Wang B., Liu M. and Wu T.** “Study of cylinder-to-cylinder variation in a diesel engine fueled with diesel/methanol dual fuel”. *Fuel*, Vol. 170, pp. 67–76, 2016. (cited in p. 58)
- Chevalier A., Müller M. and Hendricks E.** “On the validity of mean value engine models during transient operation”. *SAE Technical Papers*, 2000. (cited in p. 64)
- Chi J and DaCosta H.** “Modeling and Control of a Urea-SCR Aftertreatment System”. *SAE paper 2005-01-0966*, 2005. (cited in pp. 9 and 216)
- Chiang CJ and Stefanopoulou AG.** “Stability analysis in homogeneous charge compression ignition (HCCI) engines with high dilution”. *IEEE Trans. Control Syst. Technol.*, Vol. 15, pp. 209–219, 2007. (cited in p. 11)
- Cho H., Song H., Lee J. and Kauh S.** “Simulation of a transient torque response for engine performance in a spark ignition engine”. *Proceedings of the Institution of Mechanical Engineers, Part D: Journal of Automobile Engineering*, Vol. 215 n° 1, pp. 127–141, 2001. (cited in p. 65)
- Choi H. and Williams W. J.** “Improved time-frequency representation of multicomponent signals using exponential kernels”. *IEEE Transactions on Acoustics, Speech, and Signal Processing*, Vol. 37 n° 6, pp. 862–871, 1989. (cited in p. 109)
- Choi Y. and Chen J. .** “Fast prediction of start-of-combustion in HCCI with combined artificial neural networks and ignition delay model”. *Proceedings of the Combustion Institute*, Vol. 30 II, pp. 2711–2718, 2005. (cited in p. 34)
- Chung J., Oh S., Min K. and Sunwoo M.** “Real-time combustion parameter estimation algorithm for light-duty diesel engines using in-cylinder pressure measurement”. *Applied Thermal Engineering*, Vol. 60 n° 1-2, pp. 33–43, 2013. (cited in p. 30)
- Cohen L.** *Time-Frequency Analysis*. Prentice-Hall, New York, 1995. (cited in p. 109)
- Continental.** *Fuel quality sensor helps to protect the engine and the environment*. Continental, press release, 2011. (cited in p. 13)
- Copp D. G., Burnham K. J. and Lockett F. P.** “Model comparison for feedforward air/fuel ratio control”. In *IEE Conference Publication*, pp. 670–675, 1998. (cited in p. 58)
- Corti E. and Solieri L.** “Rapid control prototyping system for combustion control”. *SAE Technical Papers*, 2005. (cited in p. 88)
- Dabroom Ahmed and Khalil Hassan K.** “Numerical differentiation using high-gain observers”. In *Proceedings of the IEEE Conference on Decision and Control*, volume 5, pp. 4790–4794, 1997. (cited in p. 73)
- Daham B, Li H, Andrews GE, Ropkins K, Tate JE and Bell MC.** “Comparison of Real World Emissions in Urban Driving for Euro 1-4 Vehicles Using a PEMS”. *SAE Paper 2009-01-0941*, 2009. (cited in p. 6)
- D’Ambrosio S. and Ferrari A.** “Effects of exhaust gas recirculation in diesel engines featuring late PCCI type combustion strategies”. *Energy Conversion and Management*, Vol. 105, pp. 1269–1280, 2015. (cited in p. 11)
- Dargay J and Gately D.** “Income’s effect on car and vehicle ownership, worldwide: 1960-2015”. *Transportation Research Part A: Policy and Practice*, Vol. 33 n° 2, pp. 101–138, 1999. (cited in p. 1)

- Das P., Subbarao P. M. V. and Subrahmanyam J. P.** “Study of Combustion Behavior and Combustion Stability of HCCI-DI Combustion for a Wide Operating Range using a Low Cost Novel Experimental Technique”. *SAE Technical Papers*, Vol. 2014-October, 2014. (cited in p. 42)
- Das P., Subbarao P. M. V. and Subrahmanyam J. P.** “Control of combustion process in an HCCI-DI combustion engine using dual injection strategy with EGR”. *Fuel*, Vol. 159, pp. 580–589, 2015. (cited in p. 58)
- Dec J. E.** “A conceptual model of DI diesel combustion based on laser-sheet imaging”. *SAE Technical Papers*, 1997. (cited in p. 36)
- Dempsey A. B., Walker N. R., Gingrich E. and Reitz R. D.** “Comparison of low temperature combustion strategies for advanced compression ignition engines with a focus on controllability”. *Combustion Science and Technology*, Vol. 186 n° 2, pp. 210–241, 2014. (cited in p. 31)
- Desantes J. M., Bermúdez V., López J. J. and López-Pintor D.** “Experimental validation of an alternative method to predict high and low-temperature ignition delays under transient thermodynamic conditions for PRF mixtures using a Rapid Compression-Expansion Machine”. *Energy Conversion and Management*, Vol. 129, pp. 23–33, 2016. (cited in p. 34)
- Desantes J. M., López J. J., Molina S. and López-Pintor D.** “Validity of the Livengood & Wu correlation and theoretical development of an alternative procedure to predict ignition delays under variable thermodynamic conditions”. *Energy Conversion and Management*, Vol. 105, pp. 836–847, 2015. (cited in p. 34)
- Desantes J. M., López J. J., Molina S. and López-Pintor D.** “Theoretical development of a new procedure to predict ignition delays under transient thermodynamic conditions and validation using a Rapid Compression-Expansion Machine”. *Energy Conversion and Management*, Vol. 108, pp. 132–143, 2016. (cited in p. 34)
- Desantes J. M., López J. J., Redón P. and Arrègle J.** “Evaluation of the thermal NO formation mechanism under low-temperature diesel combustion conditions”. *International Journal of Engine Research*, Vol. 13 n° 6, pp. 531–539, 2012. (cited in p. 37)
- Desantes J. M., Luján J. M., Pla B. and Soler J. A.** “On the combination of high-pressure and low-pressure exhaust gas recirculation loops for improved fuel economy and reduced emissions in high-speed direct-injection engines”. *International Journal of Engine Research*, Vol. 14 n° 1, pp. 3–11, 2013. (cited in p. 58)
- Desantes JM, Galindo J, Guardiola C and Dolz V.** “Air mass flow estimation in turbocharged diesel engines from in-cylinder pressure measurement”. *Experimental Thermal and Fluid Science*, Vol. 34 n° 1, pp. 37–47, 2010. (cited in p. 65)
- Devarakonda M, Parker G, Johnson J and Strots V et al.** “Model-Based Estimation and Control System Development in a Urea-SCR Aftertreatment System”. *SAE Int. J. Fuels Lubr.*, Vol. 1 n° 1, pp. 646–661, 2009. (cited in pp. 9 and 216)
- Dimitriou P., Burke R., Copeland C. and Akehurst S.** “Study on the Effects of EGR Supply Configuration on Cylinder-to-Cylinder Dispersion and Engine Performance Using 1D-3D Co-Simulation”. *SAE Technical Papers*, 2015. (cited in p. 60)
- Diop S., Grizzle J. W., Moraal P. E. and Stefanopoulou A.** “Interpolation and numerical differentiation for observer design”. In *Proceedings of the American Control Conference*, volume 2, pp. 1329–1333, 1994. (cited in p. 73)

- Docquier N. and Candel S.** “Combustion control and sensors: A review”. *Progress in Energy and Combustion Science*, Vol. 28 n° 2, pp. 107–150, 2002. (cited in p. 58)
- Dolz V., Novella R., García A. and Sánchez J.** “HD Diesel engine equipped with a bottoming Rankine cycle as a waste heat recovery system. Part 1: Study and analysis of the waste heat energy”. *Applied Thermal Engineering*, Vol. 36, pp. 269–278, 2012. (cited in p. 9)
- Douaud A. M. and Eyzat P.** “Four-octane-number method for predicting the anti-knock behavior of fuels and engines”. *SAE Technical Papers*, 1978. (cited in pp. 34, 199, and 204)
- Doyle E., Dinanno L. and Kramer S.** “Installation of a Diesel Organic-Rankine Compound engine in a class 8 truck for a single-vehicle test”. *SAE paper 790646*, 1979. (cited in p. 9)
- Draper C. S.** “The physical effects of detonation in a closed cylindrical chamber”. Technical report, National Advisory Committee for Aeronautics, 1938. (cited in pp. 37, 38, and 114)
- Dueker H., Friese K. and Haecker W.** “Ceramic aspects of the bosch lambda-sensor”. *SAE Technical Papers*, 1975. (cited in p. 62)
- Dutka A., Javaherian H. and Grimble M. J.** “State-dependent Kalman filters for robust engine control”. In *Proceedings of the American Control Conference*, volume 2006, pp. 1185–1190, 2006. (cited in p. 72)
- DYTRAN.** “Introduction to Piezoelectric Pressure Sensors”. <http://www.dytran.com/>. Accessed: 2016-12-14. (cited in p. 69)
- EC.** *Energy, transport and environment indicators*. Publications Office of the European Union, 2011. (cited in p. 1)
- EC.** *A Roadmap for moving to a competitive low carbon economy in 2050*. Communication from the Commission to the European Parliament, the Council, the European Economic and Social Committee and the Committee of the Regions, 2011. (cited in p. 4)
- ECE.** *Proposal for a new UN Global Technical Regulation on Worldwide harmonized Light vehicles Test Procedures (WLTP)*. United Nations. Economic commission for Europe. Inland Transport Committee. World Forum for Harmonization of Vehicle Regulations, ece/trans/wp29/grpe/2013/13 edition, 2013. (cited in p. 6)
- Edenhofer R., Lucka K. and Köhne H.** “Low temperature oxidation of diesel-air mixtures at atmospheric pressure”. *Proceedings of the Combustion Institute*, Vol. 31 II, pp. 2947–2954, 2007. (cited in p. 35)
- EEA.** *The European environment - state and outlook 2015: synthesis report*. European Environment Agency, Copenhagen, 2015. (cited in p. 3)
- Egnell R.** *On Zero-dimensional Modelling of Combustion and NO_x Formation in Diesel Engines*. PhD Thesis, Lund Institute of Technology, 2001. (cited in p. 35)
- El Hadeif J., Colin G., Talon V. and Chamailard Y.** “Neural model for real-time engine volumetric efficiency estimation”. *SAE Technical Papers*, Vol. 6, 2013. (cited in p. 64)
- Emiliano P.** “Spark ignition feedback control by means of combustion phase indicators on steady and transient operation”. *Journal of Dynamic Systems, Measurement and Control, Transactions of the ASME*, Vol. 136 n° 5, 2014. (cited in p. 31)

- Eng J. A.** “Characterization of pressure waves in HCCI combustion”. *SAE Technical Papers*, 2002. (cited in pp. 42 and 116)
- Eng G. T. and Wallman S.** “Development of the volvo lambda-sond system”. *SAE Technical Papers*, 1977. (cited in p. 62)
- EPA.** *Light-duty automotive technology, carbon dioxide emissions, and fuel economy trends: 1975 through 2016*. EPA-420-R-12-001a. Transportation and Climate Division. Office of Transportation and Air Quality. US Environmental Protection Agency, 2016. (cited in pp. 5 and 12)
- Eriksson L.** “Mean value models for exhaust system temperatures”. *SAE Technical Papers*, 2002. (cited in pp. 31 and 208)
- Ettefagh M. M., Sadeghi M. H., Pirouzpanah V. and Arjmandi Tash H.** “Knock detection in spark ignition engines by vibration analysis of cylinder block: A parametric modeling approach”. *Mechanical Systems and Signal Processing*, Vol. 22 n° 6, pp. 1495–1514, 2008. (cited in p. 42)
- EU.** *Regulation (EC) No 443/2009 of the European Parliament and of the Council of 23 April 2009 setting emission performance standards for new passenger cars as part of the Community’s integrated approach to reduce CO₂ emissions from light-duty vehicles*. Official Journal of the European Union, 2009. (cited in p. 6)
- Fanelli I., Camporeale S. M. and Fortunato B.** “Efficient On-Board Pegging Calculation from Piezo-Electric Sensor Signal for Real Time In-Cylinder Pressure Offset Compensation”. *SAE International Journal of Engines*, Vol. 5 n° 2, pp. 672–682, 2012. (cited in pp. 30, 168, and 183)
- Fenimore C. P.** “Formation of nitric oxide in premixed hydrocarbon flames”. *Symposium (International) on Combustion*, Vol. 13 n° 1, pp. 373–380, 1971. (cited in p. 37)
- Ferrari A, Chiodi M, Bargende M and Roberti P et al.** “Virtual Set-up of a Racing Engine for the Optimization of Lap Performance through a Comprehensive Engine-Vehicle-Driver Model”. *SAE paper 2011-24-0141*, 2011. (cited in p. 13)
- Finesso R. and Spessa E.** “A control-oriented approach to estimate the injected fuel mass on the basis of the measured in-cylinder pressure in multiple injection diesel engines”. *Energy Conversion and Management*, Vol. 105, pp. 54–70, 2015. (cited in p. 67)
- Fitzgerald R. P., Steeper R., Snyder J., Hanson R. and Hessel R.** “Determination of cycle temperatures and residual gas fraction for HCCI negative valve overlap operation”. *SAE International Journal of Engines*, Vol. 3 n° 1, pp. 124–141, 2010. (cited in p. 193)
- Fons M., Muller M., Chevalier A., Vigild C., Hendricks E. and Sorenson S. C.** “Mean Value Engine Modelling of an SI engine with EGR”. *SAE Technical Papers*, 1999. (cited in p. 69)
- Fontaras G., Franco V., Dilara P., Martini G. and Manfredi U.** “Development and review of Euro 5 passenger car emission factors based on experimental results over various driving cycles”. *Science of the Total Environment*, Vol. 468-469, pp. 1034–1042, 2014. (cited in p. 7)
- Forte C., Corti E. and Bianchi G. M.** “Combined experimental and numerical analysis of knock in spark ignition engines”. In *Proceedings of the ASME Internal Combustion Engine Division Fall Technical Conference 2009*, pp. 473–488, 2009. (cited in pp. 40 and 41)
- Fox J. W., Cheng W. K. and Heywood J. B.** “A model for predicting residual gas fraction in spark-ignition engines”. *SAE Technical Papers*, 1993. (cited in pp. 65, 66, and 159)

- Frobert A., Raux S., Creff Y. and Jeudy E.** “About cross-sensitivities of NO_x sensors in SCR operation”. *SAE Technical Papers*, Vol. 2, 2013. (cited in p. 63)
- Fuenmayor F. J., Denia F. D., Albelda J. and Giner E.** “H-adaptive refinement strategy for acoustic problems with a set of natural frequencies”. *Journal of Sound and Vibration*, Vol. 255 n° 3, pp. 457–479, 2002. (cited in p. 120)
- Fulton B., Van Nieuwstadt M., Petrovic S. and Roettger D.** “Exhaust manifold temperature observer model”. *SAE Technical Papers*, Vol. 1, 2014. (cited in p. 216)
- Galindo J., Climent H, Guardiola C and Doménech J.** “Strategies for improving the mode transition in a sequential parallel turbocharged automotive diesel engine”. *International Journal of Automotive Technology*, Vol. 10 n° 2, pp. 141–149, 2009. (cited in p. 8)
- Galindo J, Climent H, Guardiola C, Tiseira A and Portalier J.** “Assessment of a sequentially turbocharged diesel engine on real-life driving cycles”. *International Journal of Vehicle Design*, Vol. 49 n° 1-3, pp. 214–234, 2009. (cited in p. 6)
- Galindo J., Serrano J. R., Guardiola C., Blanco-Rodriguez D. and Cuadrado I. G.** “An on-engine method for dynamic characterisation of NO_x concentration sensors”. *Experimental Thermal and Fluid Science*, Vol. 35 n° 3, pp. 470–476, 2011. (cited in pp. 63 and 69)
- Galloni E.** “Analyses about parameters that affect cyclic variation in a spark ignition engine”. *Applied Thermal Engineering*, Vol. 29 n° 5-6, pp. 1131–1137, 2009. (cited in p. 40)
- Galloni E.** “Dynamic knock detection and quantification in a spark ignition engine by means of a pressure based method”. *Energy Conversion and Management*, Vol. 64, pp. 256–262, 2012. (cited in p. 41)
- Galloni E.** “Knock-limited spark angle setting by means of statistical or dynamic pressure based methods”. *Energy Conversion and Management*, Vol. 116, pp. 11–17, 2016. (cited in p. 41)
- Gan S., Ng H. K. and Pang K. M.** “Homogeneous Charge Compression Ignition (HCCI) combustion: Implementation and effects on pollutants in direct injection diesel engines”. *Applied Energy*, Vol. 88 n° 3, pp. 559–567, 2011. (cited in p. 11)
- Gao J. B. and Harris C. J.** “Some remarks on Kalman filters for the multisensor fusion”. *Information Fusion*, Vol. 3 n° 3, pp. 191–201, 2002. (cited in p. 68)
- Gatowski J. A., Balles E. N., Chun K. M., Nelson F. E., Ekchian J. A. and Heywood J. B.** “Heat release analysis of engine pressure data”. *SAE Technical Papers*, 1984. (cited in p. 31)
- Gerardin R. C., Huallpa B. R. N., Alves M. A. F. and De França Arruda J. R.** “Analysis of spark ignition engine knock signals using fourier and discrete wavelet transform”. *SAE Technical Papers*, 2009. (cited in p. 38)
- Germann H., Tagliaferri S. and Geering H. P.** “Differences in pre-and post-converter lambda sensor characteristics”. *SAE Technical Papers*, 1996. (cited in p. 63)
- Gerow M. S., Shingne P. S., Triantopoulos V., Bohac S. V. and Martz J. B.** “A comparison of valving strategies appropriate for multi-Mode combustion within a downsized boosted automotive engine part b: Mid load operation within the SACI combustion regime”. In *ASME 2013 Internal Combustion Engine Division Fall Technical Conference, ICEF 2013*, volume 1, 2013. (cited in p. 12)

- Ghaffarpour M. R. and Noorpoor A. R.** “A numerical study of the use of pilot or split rate injection to reduce diesel engine noise”. *Proceedings of the Institution of Mechanical Engineers, Part D: Journal of Automobile Engineering*, Vol. 221 n° 4, pp. 457–464, 2007. (cited in p. 32)
- Giglio V., Iorio B., Police G. and Rispoli N.** “In-cylinder Pressure Measurement for Control and Diagnostics in Spark Ignition Engines”. *SAE Technical Papers*, 2005. (cited in p. 32)
- Goudarzi K., Moosaei A. and Gharaati M.** “Applying artificial neural networks (ANN) to the estimation of thermal contact conductance in the exhaust valve of internal combustion engine”. *Applied Thermal Engineering*, Vol. 87, pp. 688–697, 2015. (cited in p. 205)
- Gu F., Jacob P. J. and Ball A. D.** “RBF neural network model for cylinder pressure reconstruction in internal combustion engines”. In *IEE Colloquium (Digest)*, pp. 4/1–4/11, 1996. (cited in p. 43)
- Guardiola C., Climent H., Pla B. and Blanco-Rodriguez D.** “ECU-oriented models for NOx prediction. Part 2: Adaptive estimation by using an NOx sensor”. *Proceedings of the Institution of Mechanical Engineers, Part D: Journal of Automobile Engineering*, Vol. 229 n° 10, pp. 1345–1360, 2015. (cited in p. 35)
- Guardiola C., Dolz V., Pla B. and Mora J.** “Fast estimation of diesel oxidation catalysts inlet gas temperature”. *Control Engineering Practice*, Vol. 56, pp. 148–156, 2016. (cited in pp. 69, 174, and 216)
- Guardiola C., López J. J., Martín J. and García-Sarmiento D.** “Semiempirical in-cylinder pressure based model for NOx prediction oriented to control applications”. *Applied Thermal Engineering*, Vol. 31 n° 16, pp. 3275–3286, 2011. (cited in pp. 36, 217, 219, and 220)
- Guardiola C., Pla B., Bares P. and Waschl H.** “Adaptive calibration for reduced fuel consumption and emissions”. *Proceedings of the Institution of Mechanical Engineers, Part D: Journal of Automobile Engineering*, Vol. 230 n° 14, pp. 2002–2014, 2016. (cited in p. 13)
- Guardiola C., Pla B., Blanco-Rodriguez D. and Calendini P. O.** “ECU-oriented models for NOx prediction. Part 1: A mean value engine model for NOx prediction”. *Proceedings of the Institution of Mechanical Engineers, Part D: Journal of Automobile Engineering*, Vol. 229 n° 8, pp. 992–1015, 2015. (cited in p. 35)
- Guardiola C, Pla B, Blanco-Rodriguez D and Reig A.** “Modelling driving behaviour and its impact on the energy management problem in hybrid electric vehicles”. *International Journal of Computer Mathematics*, 2013. (cited in p. 13)
- Guzzella L. and Onder C.** *Introduction to modeling and control of internal combustion engine systems*. Springer, Berlin Heidelberg, 2010. (cited in p. 64)
- Hamann E., Manger H. and Steinke L.** “Lambda-sensor with Y2O3-stabilized zro2-ceramic for application in automotive emission control systems”. *SAE Technical Papers*, 1977. (cited in p. 62)
- Hamedović H., Raichle F. and Böhme J. F.** “In-cylinder pressure reconstruction for multicylinder SI-engine by combined processing of engine speed and one cylinder pressure”. In *ICASSP, IEEE International Conference on Acoustics, Speech and Signal Processing - Proceedings*, volume V, pp. V677–V680, 2005. (cited in p. 43)
- Hansen J, Ruedy R, Sato M and Lo K.** “Global surface temperature change”. *Reviews of Geophysics*, Vol. 48 n° 4, 2010. (cited in p. 3)

- Harris F. J.** “On the Use of Windows for Harmonic Analysis with the Discrete Fourier Transform”. *Proceedings of the IEEE*, Vol. 66 n° 1, pp. 51–83, 1978. (cited in p. 108)
- Haskara I. and Wang Y. .** “Closed-loop combustion noise limit control for modern diesel combustion modes”. *IEEE Transactions on Control Systems Technology*, Vol. PP n° 99, 2016. (cited in p. 27)
- Hendricks E., Chevalier A., Jensen M., Sorenson S. C., Trumpy D. and Asik J.** “Modelling of the intake manifold filling dynamics”. *SAE Technical Papers*, 1996. (cited in p. 69)
- Hendricks E., Vesterholm T. and Sorenson S. C.** “Nonlinear, closed loop, SI engine control observers”. *SAE Technical Papers*, 1992. (cited in p. 71)
- Hendricks Elbert.** “Isothermal vs. adiabatic mean value SI engine models”. In *Advances in Automotive Control 2001. Proceedings of the 3rd IFAC Workshop*, 2001. (cited in p. 70)
- Henningsson M.** *Data Rich Multivariable Control of Heavy-Duty Engines*. PhD Thesis, University of Lund, 2012. (cited in p. 68)
- Hernández J. J., Pérez-Collado J. and Sanz-Argent J.** “Role of the chemical kinetics on modeling NOx emissions in diesel engines”. *Energy and Fuels*, Vol. 22 n° 1, pp. 262–272, 2008. (cited in p. 37)
- Hernández López Leonor.** *Desarrollo de una metodología para la predicción y optimización de emisiones contaminantes y consumo en motores diesel de automoción mediante redes neuronales artificiales*. PhD Thesis, Universitat Politècnica de València. Departamento de Máquinas y Motores Térmicos, 2004. (cited in p. 2)
- Heywood J.B.** *Internal Combustion engine fundamentals*. McGraw-Hill, New York, 1988. (cited in p. 64)
- Hickling R., Feldmaier D. A., Chen F. H. and Morel J. S.** “Cavity resonances in engine combustion chambers and some applications”. *Journal of the Acoustical Society of America*, Vol. 73 n° 4, pp. 1170–1178, 1983. (cited in p. 39)
- Hickling R., Hamburg J. A., Feldmaier D. A. and Chung J.** “Method of measurement of bulk temperatures of gas in engine cylinders”, 1979. (cited in p. 39)
- Hiroyasu H., Kadota T. and Arai M.** “Development and use of a spray modelling to predict diesel engine efficiency and pollutant emissions (part 1 combustion modelling)”. *Bulletin of the JSME*, Vol. 26 n° 214, pp. 569–575, 1983. (cited in p. 35)
- Hofmann L., Rusch K., Fischer S. and Lemire B.** “Onboard emissions monitoring on a HD truck with an SCR system using Nox sensors”. *SAE Technical Papers*, 2004. (cited in p. 63)
- Homsy S. C. and Atreya A.** “An experimental heat release rate analysis of a diesel engine operating under steady state conditions”. *SAE Technical Papers*, 1997. (cited in p. 30)
- Hopmann U.** “Diesel engine waste heat recovery utilizing electric turbocompound technology”. *2004 Diesel Engine-Efficiency and Emissions Research (DEER) Conference*, 2004. (cited in p. 9)
- Hountalas D.T., Katsanos C.O., Kouremenos D.A. and Rogdakis E.D.** “Study of available exhaust gas heat recovery technologies for HD Diesel engine applications”. *International Journal of Alternative Propulsion*, Vol. 1, pp. 228–249, 2007. (cited in p. 9)
- Hsieh M, Canova M and Wang J.** “Model Predictive Control Approach for AFR Control during Lean NO_x Trap Regeneration”. *SAE Int. J. Engines*, Vol. 2 n° 1, pp. 149–157, 2009. (cited in p. 10)

- Hubbard M., Dobson P. D. and Powell J. D.** “Closed loop control of spark advance using a cylinder pressure sensor”. *Journal of Dynamic Systems, Measurement and Control, Transactions of the ASME*, Vol. 98 Ser G n° 4, pp. 414–420, 1976. (cited in p. 115)
- Hunicz J. and Kordos P.** “An experimental study of fuel injection strategies in CAI gasoline engine”. *Experimental Thermal and Fluid Science*, Vol. 35 n° 1, pp. 243–252, 2011. (cited in p. 11)
- Husted HL, Piock W and Ramsay G.** “Fuel Efficiency Improvements from Lean, Stratified Combustion with a Solenoid Injector”. *SAE Paper 2009-01-1485*, 2009. (cited in p. 10)
- IEA.** *Energy Technology Perspectives*. OECD International Energy Agency, 2010. (cited in p. 5)
- IEA.** *Energy balances of non-OECD countries*. OECD International Energy Agency, 2015. (cited in p. 3)
- IEO.** *International Energy Outlook 2016*. US Energy Information Administration, 2016. (cited in p. 4)
- Iglesias I, Isasi L, Larburu M and Martin A et al.** “Networked Clean Vehicles, How the Environment Information will Improve Fuel Efficiency and CO₂ Emissions”. *SAE Int. J. Fuels Lubr.*, Vol. 2 n° 1, pp. 167–171, 2009. (cited in p. 13)
- IPCC.** *The Science of Climate Change*. Joint national science academies’ statement, 2001. (cited in p. 2)
- Jankovic M. and Magner S. W.** “Cylinder air-charge estimation for advanced intake valve operation in variable cam timing engines”. *JSAE review*, Vol. 22 n° 4, pp. 445–452, 2001. (cited in p. 58)
- JCGM.** “Evaluation of Measurement Data - Guide to the Expression of Uncertainty in Measurement”. Technical report, Joint Committee for Guides in Metrology (JCGM), 2008. (cited in p. 147)
- Jia L., Naber J. D. and Blough J. R.** “Review of Sensing Methodologies for Estimation of Combustion Metrics”. *Journal of Combustion*, Vol. 2016, 2016. (cited in pp. 13 and 27)
- Johnson T.** “Vehicular Emissions in Review”. *SAE International Journal of Engines*, Vol. 7 n° 3, 2014. (cited in p. 8)
- Johnson TV.** “Review of CO₂ Emissions and Technologies in the Road Transportation Sector”. *SAE paper 2010-01-1276*, 2010. (cited in p. 2)
- Johnsson R. and Ågren A.** “Cylinder pressure reconstruction from vibration and speed measurements on IC engines”. In *Proceedings of the 2004 International Conference on Noise and Vibration Engineering, ISMA*, pp. 965–974, 2004. (cited in p. 43)
- Johri R., Salvi A. and Filipi Z.** “Real-time transient soot and NO_x virtual sensors for diesel engine using neuro-fuzzy model tree and orthogonal least squares”. *Journal of Engineering for Gas Turbines and Power*, Vol. 134 n° 9, 2012. (cited in p. 35)
- Julier Simon J. and Uhlmann Jeffrey K.** “New extension of the Kalman filter to non-linear systems”. In *Proceedings of SPIE - The International Society for Optical Engineering*, volume 3068, pp. 182–193, 1997. (cited in p. 72)
- Jung D. and Iida N.** “Closed-loop control of HCCI combustion for DME using external EGR and rebreathed EGR to reduce pressure-rise rate with combustion-phasing retard”. *Applied Energy*, Vol. 138, pp. 315–330, 2015. (cited in p. 31)

- Jung I., Jin J., Lee D., Lee S., Yang S. and Min K.** “Closed-Loop Control Method for Monitoring and Improving the Diesel Combustion Noise”. *SAE Technical Papers*, Vol. 2016-June n° June, 2016. (cited in p. 27)
- Jurgen R.K.** *Automotive electronics handbook*. New York: McGraw-Hill, 1995. (cited in p. 58)
- Kalman Rudolph Emil.** “A new approach to linear filtering and prediction problems”. *Journal of basic Engineering*, Vol. 82 n° 1, pp. 35–45, 1960. (cited in pp. 71 and 177)
- Kamalanathsharma R.K. and Rakha H.** “Agent-based modeling of eco-cooperative adaptive cruise control systems in the vicinity of intersections”. *IEEE Conference on Intelligent Transportation Systems, Proceedings, ITSC*, pp. 840–845, 2012. (cited in p. 13)
- Kao Minghui and Moskwa John J.** “Turbocharged diesel engine modeling for nonlinear engine control and state estimation”. *Journal of Dynamic Systems, Measurement and Control, Transactions of the ASME*, Vol. 117 n° 1, pp. 20–30, 1995. (cited in p. 69)
- Karaky H., Mauviot G., Tauzia X. and Maiboom A.** “Development and Validation of a New Zero-Dimensional Semi-Physical NOx Emission Model for a D.I. Diesel Engine Using Simulated Combustion Process”. *SAE International Journal of Engines*, Vol. 8 n° 4, 2015. (cited in p. 36)
- Karthikeya Sharma T., Amba Prasad Rao G. and Madhu Murthy K.** “Control of peak pressures of an HCCI engine under varying swirl and operating parameters”. *Frontiers in Energy*, Vol. 10 n° 3, pp. 337–346, 2016. (cited in p. 31)
- Karthikeya Sharma T., Amba Prasad Rao G. and Madhu Murthy K.** “Control of peak pressures of an HCCI engine under varying swirl and operating parameters”. *Frontiers in Energy*, Vol. 10 n° 3, pp. 337–346, 2016. (cited in p. 58)
- Kato N., Hamada Y. and Kurachi H.** “Performance of thick film NOx sensor on diesel and gasoline engines”. *SAE Technical Papers*, 1997. (cited in p. 63)
- Kato N., Kokune N., Lemire B. and Walde T.** “Long term stable NOx sensor with integrated in-connector control electronics”. *SAE Technical Papers*, 1999. (cited in p. 63)
- Kato N., Nakagaki K. and Ina N.** “Thick film ZrO₂ NOx sensor”. *SAE Technical Papers*, 1996. (cited in p. 63)
- Kato S., Tsugawa S., Tokuda K., Matsui T. and Fujii H.** “Vehicle Control Algorithms for Cooperative Driving with Automated Vehicles and Intervehicle Communications”. *IEEE Transactions on Intelligent Transportation Systems*, Vol. 3 n° 3, pp. 155–160, 2002. (cited in p. 13)
- Kawahara N., Tomita E. and Sakata Y.** “Auto-ignited kernels during knocking combustion in a spark-ignition engine”. *Proceedings of the Combustion Institute*, Vol. 31 II, pp. 2999–3006, 2007. (cited in pp. 40 and 197)
- Khaleghi B., Khamis A., Karray F. O. and Razavi S. N.** “Multisensor data fusion: A review of the state-of-the-art”. *Information Fusion*, Vol. 14 n° 1, pp. 28–44, 2013. (cited in p. 68)
- Kiencke U. and Nielsen L.** *Automotive control system for engine, driveline, and vehicle*. New York: Springer, 2005. (cited in p. 40)
- Kihlas D. and Uchanski M. R.** “Engine-Out NOx Models for on-ECU Implementation: A Brief Overview”. *SAE Technical Papers*, Vol. 2015-April n° April, 2015. (cited in p. 35)
- Kirchen P.** *Steady-State and Transient Diesel Soot Emissions: Development of a Mean Value Soot Model and Exhaust-Stream and In-Cylinder Measurements*. PhD Thesis, ETH Zurich, 2008. (cited in p. 35)

- Kirsten M., Pirker G., Redtenbacher C., Wimmer A. and Chmela F.** “Advanced Knock Detection for Diesel/Natural Gas Engine Operation”. *SAE International Journal of Engines*, Vol. 9 n° 3, 2016. (cited in p. 27)
- Klein M.** *A Specific Heat Ratio Model and Compression Ratio Estimation*. PhD Thesis, Linköping University, 2004. (cited in p. 32)
- Klett S., Piesche M., Heinzelmann S., Weyl H., Wiedenmann H. ., Schneider U., Diehl L. and Neumann H.** “Numerical and experimental analysis of the momentum and heat transfer in exhaust gas sensors”. *SAE Technical Papers*, 2005. (cited in p. 62)
- Kocher L., Koeberlein E., Van Alstine D. G., Stricker K. and Shaver G.** “Physically based volumetric efficiency model for diesel engines utilizing variable intake valve actuation”. *International Journal of Engine Research*, Vol. 13 n° 2, pp. 169–184, 2012. (cited in p. 64)
- Kokjohn S. L., Hanson R. M., Splitter D. A. and Reitz R. D.** “Fuel reactivity controlled compression ignition (RCCI): A pathway to controlled high-efficiency clean combustion”. *International Journal of Engine Research*, Vol. 12 n° 3, pp. 209–226, 2011. (cited in p. 12)
- Kolewe B., Haghani A., Beckmann R., Noack R. and Jeansch T.** “Data-driven estimation of air mass using Gaussian mixture regression”. In *IEEE International Symposium on Industrial Electronics*, pp. 2433–2438, 2014. (cited in p. 64)
- Kolmanovsky I., Sivergina I. and Sun J.** “Simultaneous input and parameter estimation with input observers and set-membership parameter bounding: Theory and an automotive application”. *International Journal of Adaptive Control and Signal Processing*, Vol. 20 n° 5, pp. 225–246, 2006. (cited in p. 65)
- Kolmanovsky I. and Siverguina I.** “Adaptive identification schemes in presence of bounded disturbances: An automotive case study”. In *Proceedings of the IEEE Conference on Decision and Control*, volume 1, pp. 508–513, 2001. (cited in pp. 65 and 71)
- Kolmanovsky Ilya, Sun Jing, Druzhinina Maria and van Nieuwstadt Michiel.** “Charge control for direct injection spark ignition engines with EGR”. In *Proceedings of the American Control Conference*, volume 1, pp. 34–38, 2000. (cited in pp. 65 and 71)
- Komninou N. P. and Rakopoulos C. D.** “Heat transfer in HCCI phenomenological simulation models: A review”. *Applied Energy*, Vol. 181, pp. 179–209, 2016. (cited in pp. 29 and 32)
- König D. and Böhme J. F.** “Wigner-Ville spectral analysis of automotive signals captured at knock”. *Applied Signal Processing*, Vol. 3 n° 1, pp. 54–64, 1996. (cited in p. 38)
- König G., Maly R. R., Bradley D., Lau A. K. C. and Sheppard C. G. W.** “Role of exothermic centres on knock initiation and knock damage”. *SAE Technical Papers*, 1990. (cited in p. 40)
- König G. and Sheppard C. G. W.** “End gas autoignition and knock in a spark ignition engine”. *SAE Technical Papers*, 1990. (cited in p. 41)
- Krüger U., Edwards S., Pantow E., Lutz R., Dreisbach R. and Glensvig M.** “High Performance Cooling and EGR Systems as a Contribution to Meeting Future Emission Standards”. *SAE paper 2008-01-1199*, 2008. (cited in p. 12)
- Krutzsch B., Wenninger G., Weibel M., Stapf P., Funk A., Webster D. E., Chaize E., Kasemo B., Martens J. and Kiennemann A.** “Reduction of NO_x in lean exhaust by selective NO_x-Recirculation (SNR-Technique) Part I: System and decomposition process”. *SAE Technical Papers*, 1998. (cited in p. 36)

- Kumar Maurya R., Pal D. D. and Kumar Agarwal A.** “Digital signal processing of cylinder pressure data for combustion diagnostics of HCCI engine”. *Mechanical Systems and Signal Processing*, Vol. 36 n° 1, pp. 95–109, 2013. (cited in p. 88)
- Kushch A.S., Bass J.C., Ghamaty S. and Elsner N.B.** “Thermoelectric development at Hi-Z Technology”. *2002 Diesel Engine-Efficiency and Emissions Research (DEER) Conference*, 2002. (cited in p. 9)
- Lähde T., Rönkkö T., Virtanen A., Solla A., Kytö M., Söderström C. and Keskinen J.** “Dependence between nonvolatile nucleation mode particle and soot number concentrations in an EGR equipped heavy-duty diesel engine exhaust”. *Environmental Science and Technology*, Vol. 44 n° 8, pp. 3175–3180, 2010. (cited in p. 58)
- Lamping M., Körfer T., Schnorbus T., Pischinger S and Chen Y.** “Tomorrows Diesel Fuel Diversity - Challenges and Solutions”. *SAE Paper 2008-01-1731*, 2008. (cited in pp. 12 and 27)
- Lancaster David R., Krieger Roger B. and Lienesch John H.** “Measurement and analysis of engine pressure data”. *SAE Prepr*, n° 750026, 1975. (cited in p. 30)
- Lang D., Stanger T. and Del Re L.** “Opportunities on fuel economy utilizing V2V based drive systems”. *SAE paper 2013-01-0985*, 2013. (cited in p. 13)
- Lapuerta M., Armas O. and Hernández J. J.** “Diagnosis of DI Diesel combustion from in-cylinder pressure signal by estimation of mean thermodynamic properties of the gas”. *Applied Thermal Engineering*, Vol. 19 n° 5, pp. 513–529, 1999. (cited in pp. 32, 116, 117, 147, 149, and 209)
- Lee H., Park Y. and Sunwoo M.** “Observer design for exhaust gas recirculation rate estimation in a variable-geometry turbocharger diesel engine using a model reference identification scheme”. *Proceedings of the Institution of Mechanical Engineers, Part D: Journal of Automobile Engineering*, Vol. 228 n° 14, pp. 1688–1699, 2014. (cited in p. 73)
- Lee J., Hwang S., Lim J., Jeon D. and Cho Y.** “A new knock-detection method using cylinder pressure, block vibration and sound pressure signals from a SI engine”. *SAE Technical Papers*, 1998. (cited in p. 41)
- Lee J., Lee S., Park W., Min K., Song H. H., Choi H., Yu J. and Cho S. H.** “The development of real-time NOx estimation model and its application”. *SAE Technical Papers*, Vol. 2, 2013. (cited in p. 36)
- Lee K., Yoon M. and Sunwoo M.** “A study on pegging methods for noisy cylinder pressure signal”. *Control Engineering Practice*, Vol. 16 n° 8, pp. 922–929, 2008. (cited in pp. 30, 168, and 183)
- Leonhardt S, Müller N and Isermann R.** “Methods for engine supervision and control based on cylinder pressure information”. *IEEE/ASME Transactions on Mechatronics*, Vol. 4 n° 3, pp. 235–245, 1999. (cited in pp. 13 and 30)
- Leppard W. R.** “Individual-cylinder knock occurrence and intensity in multicylinder engines”. *SAE Technical Papers*, 1982. (cited in p. 40)
- Leroy T., Chauvin J., Le Sollic G. and Corde G.** “Air path estimation for a turbocharged SI engine with variable valve timing”. In *Proceedings of the American Control Conference*, pp. 5088–5093, 2007. (cited in p. 71)
- Levant A.** “Robust Exact Differentiation via Sliding Mode Technique”. *Automatica*, Vol. 34 n° 3, pp. 379–384, 1998. (cited in p. 73)

- Li H., Guo Y., Cheng P., Liu F. and Jiang E.** “Study on cycle-to-cycle variations of CAI combustion using NVO strategy”. In *2010 International Conference on Logistics Engineering and Intelligent Transportation Systems, LEITS2010 - Proceedings*, pp. 47–50, 2010. (cited in p. 65)
- Li H. and Stone B. J.** “Time domain modelling of a reciprocating engine”. *Mechanical Systems and Signal Processing*, Vol. 13 n° 1, pp. 169–178, 1999. (cited in pp. 43 and 90)
- Li J., Yang W. and Zhou D.** “Review on the management of RCCI engines”. *Renewable and Sustainable Energy Reviews*, Vol. 69, pp. 65–79, 2017. (cited in p. 12)
- Liang L. and Reitz R. D.** “Spark Ignition engine combustion modeling using a level set method with detailed chemistry”. *SAE Technical Papers*, 2006. (cited in p. 35)
- Lin W., Sterniak J. and Bohac S. V.** “NO_x emissions characterization during transient spark assisted compression ignition (SACI) engine operation”. In *ASME 2013 Internal Combustion Engine Division Fall Technical Conference, ICEF 2013*, volume 1, 2013. (cited in p. 11)
- Lindenkamp N, Stöber-Schmidt C and Eilts P.** “Strategies for Reducing NO_x- and Particulate Matter Emissions in Diesel Hybrid Electric Vehicles”. *SAE Paper 2009-01-1305*, 2009. (cited in p. 5)
- Liu C.** “Simultaneous unknown state and input estimation with application to virtual air charge and egr sensors for automotive engines”. In *ASME 2010 Dynamic Systems and Control Conference, DSCC2010*, volume 1, pp. 727–734, 2010. (cited in p. 71)
- Liu H., Zhang J., Guo P., Bi F., Yu H. and Ni G.** “Sound quality prediction for engine-radiated noise”. *Mechanical Systems and Signal Processing*, Vol. 56, pp. 277–287, 2015. (cited in p. 39)
- Liu Y., Li L., Lu H., Deng J. and Hu Z.** “In-Cycle Knocking Detection and Feedback Control Based on In-Cylinder Pressure and Ion Current Signal in a GDI Engine”. *SAE Technical Papers*, Vol. 2016-April n° April, 2016. (cited in p. 28)
- Liu Y. and Zhangsaifei.** “Measurement and diagnostic system for crankshaft of diesel engine”. In *ICCASM 2010 - 2010 International Conference on Computer Application and System Modeling, Proceedings*, volume 13, pp. V13370–V13371, 2010. (cited in p. 43)
- Liu Zhiyuan and Wang Changhui.** “An LPV adaptive observer for updating a map applied to an MAF sensor in a diesel engine”. *Sensors*, Vol. 15 n° 10, pp. 27142–27159, 2015. (cited in p. 59)
- Livengood J. C. and Wu P. C.** “Correlation of autoignition phenomena in internal combustion engines and rapid compression machines”. *Symposium (International) on Combustion*, Vol. 5 n° 1, pp. 347–356, 1955. (cited in pp. 34, 131, and 199)
- Lopez J. J., Novella R., Valero-Marco J., Coma G. and Justet F.** “Evaluation of the Potential Benefits of an Automotive, Gasoline, 2-Stroke Engine”. *SAE Technical Papers*, 2015. (cited in p. 93)
- Lu P., Han J., Lai M., Henein N. A. and Bryzik W.** “Combustion visualization of diesel spray combustion inside a small-bore cylinder under different EGR and swirl ratios”. *SAE Technical Papers*, 2001. (cited in p. 58)
- Lu X., Han D. and Huang Z.** “Fuel design and management for the control of advanced compression-ignition combustion modes”. *Progress in Energy and Combustion Science*, Vol. 37 n° 6, pp. 741–783, 2011. (cited in p. 11)

- Luján J. M., Bermúdez V., Guardiola C. and Abbad A.** “A methodology for combustion detection in diesel engines through in-cylinder pressure derivative signal”. *Mechanical Systems and Signal Processing*, Vol. 24 n° 7, pp. 2261–2275, 2010. (cited in p. 27)
- Luján J. M., Climent H., Pla B., Rivas-Perea M. E., François N., Borges-Alejo J. and Soukeur Z.** “Exhaust gas recirculation dispersion analysis using in-cylinder pressure measurements in automotive diesel engines”. *Applied Thermal Engineering*, Vol. 89, pp. 459–468, 2015. (cited in p. 60)
- Luján J. M., Galindo J., Serrano J. R. and Pla B.** “A methodology to identify the intake charge cylinder-to-cylinder distribution in turbocharged direct injection Diesel engines”. *Measurement Science and Technology*, Vol. 19 n° 6, 2008. (cited in p. 60)
- Luján J. M., Guardiola C., Pla B. and Cabrera P.** “Considerations on the low-pressure exhaust gas recirculation system control in turbocharged diesel engines”. *International Journal of Engine Research*, Vol. 15 n° 2, pp. 250–260, 2014. (cited in pp. 12 and 61)
- Luján JM, Bermúdez V, Tormos B and Pla B.** “Comparative analysis of a DI diesel engine fuelled with biodiesel blends during the European MVEG-A cycle: Performance and emissions (II)”. *Biomass and Bioenergy*, Vol. 33 n° 6-7, pp. 948–956, 2009. (cited in p. 12)
- Ma X., Xia Z., Wu H. and Huang X.** “Combined Frequency Domain Analysis and Fuzzy Logic for Engine Misfire Diagnosis”. *SAE Technical Papers*, Vol. 2015-April n° April, 2015. (cited in p. 43)
- Macek J. and Vitek O.** “Determination and Representation of Turbocharger Thermodynamic Efficiencies”. *SAE Technical Papers*, 2016. (cited in p. 205)
- Macián V., Luján J. M., Guardiola C. and Perles A.** “A comparison of different methods for fuel delivery unevenness detection in Diesel engines”. *Mechanical Systems and Signal Processing*, Vol. 20 n° 8, pp. 2219–2231, 2006. (cited in p. 67)
- Macián V., Luján J. M., Guardiola C. and Yuste P.** “DFT-based controller for fuel injection unevenness correction in turbocharged diesel engines”. *IEEE Transactions on Control Systems Technology*, Vol. 14 n° 5, pp. 819–827, 2006. (cited in p. 43)
- Malaczynski G. W., Mueller M., Pfeiffer J., Cabush D. and Hoyer K.** “Replacing volumetric efficiency calibration look-up tables with Artificial Neural Network-based algorithm for variable valve actuation”. *SAE Technical Papers*, 2010. (cited in p. 64)
- Malikopoulos A.A. and Aguilar J.P.** “Optimization of driving styles for fuel economy improvement”. *IEEE Conference on Intelligent Transportation Systems, Proceedings, ITSC*, pp. 194–199, 2012. (cited in p. 13)
- Malte P. C. and Pratt D. T.** “Measurement of atomic oxygen and nitrogen oxides in jet-stirred combustion”. *Symposium (International) on Combustion*, Vol. 15 n° 1, pp. 1061–1070, 1975. (cited in p. 37)
- Manchur T. B. and Checkel M. D.** “Time resolution effects on accuracy of real-time NOx emissions measurements”. *SAE Technical Papers*, 2005. (cited in pp. 35 and 63)
- Manofsky L., Vavra J., Assanis D. and Babajimopoulos A.** “Bridging the gap between HCCI and SI: Spark-assisted compression ignition”. *SAE Technical Papers*, 2011. (cited in p. 11)
- Martín Jaime.** *Aportación al diagnóstico de la combustión en motores Diesel de inyección directa*. PhD Thesis, Universitat Politècnica de València. Departamento de Máquinas y Motores Térmicos - Departament de Màquines i Motors Tèrmics, 2007. (cited in p. 31)

- Maurya R. K.** “Estimation of optimum number of cycles for combustion analysis using measured in-cylinder pressure signal in conventional CI engine”. *Measurement: Journal of the International Measurement Confederation*, Vol. 94, pp. 19–25, 2016. (cited in p. 88)
- McKenzie J. and Cheng W. K.** “The Anatomy of Knock”. *SAE Technical Papers*, Vol. 2016-April, 2016. (cited in p. 40)
- Meszler D, German J, Mock P and Bandivadekar A.** “Summary of mass reduction impacts on EU cost curves”. Technical report, The International Council on Clean Transportation, 2013. (cited in p. 8)
- Millo F. and Ferraro C. V.** “Knock in S.I. Engines: A comparison between different techniques for detection and control”. *SAE Technical Papers*, 1998. (cited in p. 41)
- Milovanovic N, Blundell D, Gedge S and Turner J.** “SI-HCCI-SI Mode Transition at Different Engine Operating Conditions”. *SAE paper 2005-01-0156*, 2005. (cited in p. 12)
- Mladek M. and Onder C. H.** “A model for the estimation of inducted air mass and the residual gas fraction using cylinder pressure measurements”. *SAE Technical Papers*, 2000. (cited in p. 31)
- Mocanu F. and Taraza D.** “Estimation of main combustion parameters from the measured instantaneous crankshaft speed”. *SAE Technical Papers*, Vol. 2, 2013. (cited in p. 43)
- Mock P.** “EU vehicle technology study: Development of preliminary cost curves for the EU market”. In *27 April 2012 workshop for regulators, manufacturers, and others working on these issues in the EU in the 2020-25 time frame. GHG reduction potential and costs of LDV technologies, II*. The International Council on Clean Transportation, 2012. (cited in p. 5)
- Mock P.** “European CO₂ Emission Performance Standards for Passenger Cars and Light Commercial Vehicles”. Technical report, The International Council on Clean Transportation, 2012. (cited in pp. 6 and 7)
- Mock P.** “European Vehicle Market Statistics: Pocketbook 2015/16”. Technical report, The International Council on Clean Transportation, 2016. (cited in p. 5)
- Mock P, German J, Bandivadekar A and Riemersma I.** “Discrepancies between type-approval and real-world fuel consumption and CO₂ values in 2001-2011 European passenger cars”. Technical report, The International Council on Clean Transportation, 2012. (cited in p. 6)
- Molina S., García A., Pastor J. M., Belarte E. and Balloul I.** “Operating range extension of RCCI combustion concept from low to full load in a heavy-duty engine”. *Applied Energy*, Vol. 143, pp. 211–227, 2015. (cited in p. 92)
- Moos R.** “A brief overview on automotive exhaust gas sensors based on electroceramics”. *International Journal of Applied Ceramic Technology*, Vol. 2 n^o 5, pp. 401–413, 2005. (cited in pp. 9 and 63)
- Moroz S, Bourgoin G, Luján JM and Pla B.** “A 2.0 litre Diesel Engine with Low Pressure Exhaust Gas Recirculation and Advanced Cooling System”. *The Diesel Engine Conference, Proceedings of the SIA 2008 Conference, Rouen, France*, 2008. (cited in p. 12)
- Mrosek M., Sequenz H. and Isermann R.** “Identification of emission measurement dynamics for Diesel engines”. In *IFAC Proceedings Volumes (IFAC-PapersOnline)*, volume 18, pp. 11839–11844, 2011. (cited in pp. 35 and 68)
- Müller N. and Isermann R.** “Control of mixture composition using cylinder pressure sensors”. *SAE Technical Papers*, 2001. (cited in p. 28)

- Muller R, Hart M, Truscott A, Noble A, Krotz G, Eickhoff M, Cavalloni C and Gnielka M.** “Combustion Pressure Based Engine Management System”. *SAE Paper 2000-01-0928*, 2000. (cited in p. 13)
- Najt P. M. and Foster D. E.** “Compression-ignited homogeneous charge combustion”. *SAE Technical Papers*, 1983. (cited in p. 11)
- Nakagawa S, Hori T and Nagano M.** “A New Feedback Control of a Lean NO_x Trap Catalyst”. *SAE paper 2004-01-0527*, 2004. (cited in p. 9)
- Nakanouchi Y., Kurosawa H., Hasei M., Yan Y. and Kunimoto A.** “New type of NO_x sensors for automobiles”. *SAE Technical Papers*, 1996. (cited in p. 63)
- NASA.** “GISS Surface Temperature Analysis”. <http://data.giss.nasa.gov/gistemp/>. Accessed: 2016-12-05. (cited in pp. 3 and 4)
- Nates R. J. and Yates A. D. B.** “Knock damage mechanisms in spark-ignition engines”. *SAE Technical Papers*, 1994. (cited in p. 39)
- Negrean M., Schliecker S. and Ernst R.** “Timing implications of sharing resources in multicore real-time automotive systems”. *SAE International Journal of Passenger Cars - Electronic and Electrical Systems*, Vol. 3 n° 1, pp. 27–40, 2010. (cited in p. 13)
- Nelson-Gruel D., Chamailard Y. and Aljarbouh A.** “Modeling and estimation of the pollutants emissions in the Compression Ignition diesel engine”. In *2016 IEEE Conference on Control Applications, CCA 2016*, pp. 317–322, 2016. (cited in p. 35)
- Nicol A. J., Such C. and Sarnbratt U.** “Investigation of fuel injection strategies on a low emission heavy-duty diesel engine with high EGR rates”. In *Institution of Mechanical Engineers: Combustion Engines and Fuels Group - Internal Combustion Engines: Performance, Fuel Economy and Emissions*, pp. 173–183, 2008. (cited in p. 58)
- Nieuwstadt M. and Upadhyay D.** “Diagnosis of a urea scr catalytic system”, 2005. (cited in p. 63)
- Núesch S., Hellström E., Jiang L. and Stefanopoulou A. G.** “Mode switches among SI, SACI, and HCCI combustion and their influence on drive cycle fuel economy”. In *Proceedings of the American Control Conference*, pp. 849–854, 2014. (cited in p. 12)
- Ogata K.** *Modern control engineering*. Prentice Hall, 2001. (cited in p. 68)
- Ohyama Y.** “Engine control using combustion model”. *International Journal of Automotive Technology*, Vol. 2 n° 2, pp. 53–62, 2001. (cited in p. 34)
- OICA.** “Worldwide Vehicles in use”. <http://www.oica.net/category/vehicles-in-use/>. Accessed: 2016-12-02. (cited in p. 1)
- Olmeda P., Dolz V., Arnau F. J. and Reyes-Belmonte M. A.** “Determination of heat flows inside turbochargers by means of a one dimensional lumped model”. *Mathematical and Computer Modelling*, Vol. 57 n° 7-8, pp. 1847–1852, 2013. (cited in p. 207)
- Onishi S., Jo S. H., Shoda K., Jo P. D. and Kato S.** “Active Thermo-Atmosphere Combustion (ATAC) - A new combustion process for internal combustion engines”. *SAE Technical Papers*, 1979. (cited in p. 11)
- OPEC.** *World Oil Outlook*. OPEC Secretariat, 2015. (cited in pp. 4 and 5)
- Ortiz-Soto E. A., Vavra J. and Babajimopoulos A.** “Assessment of residual mass estimation methods for cylinder pressure heat release analysis of HCCI engines with negative valve overlap”. *Journal of Engineering for Gas Turbines and Power*, Vol. 134 n° 8, 2012. (cited in p. 66)

- Ostrowski G, Neely GD, Chadwell CJ, Mehta D and Wetzel P.** “Downspeeding and Supercharging a Diesel Passenger Car for Increased Fuel Economy”. *SAE Paper 2012-01-0704*, 2012. (cited in p. 8)
- Pace L and Presti M.** “An Alternative Way to Reduce Fuel Consumption During Cold Start: The Electrically Heated Catalyst”. *SAE paper 2011-24-0178*, 2011. (cited in p. 10)
- Palma A, D Del Core and Esposito C.** “The HCCI Concept and Control, Performed with MultiAir Technology on Gasoline Engines”. *SAE paper 2011-24-0026*, 2011. (cited in p. 12)
- Parizet E., Brocard J. and Piquet B.** “Influence of noise and vibration to comfort in diesel engine cars running at idle”. *Acta Acustica united with Acustica*, Vol. 90 n° 5, pp. 987–993, 2004. (cited in p. 32)
- Paykani A., Kakaee A., Rahnama P. and Reitz R. D.** “Progress and recent trends in reactivity-controlled compression ignition engines”. *International Journal of Engine Research*, Vol. 17 n° 5, pp. 481–524, 2016. (cited in p. 12)
- Payri F., Arrègle J., Javier López J. and Mocholí E.** “Diesel NOx modeling with a reduction mechanism for the initial NOx coming from EGR or re-entrained burned gases”. *SAE Technical Papers*, 2008. (cited in p. 36)
- Payri F., Broatch A., Margot X. and Monelletta L.** “Sound quality assessment of Diesel combustion noise using in-cylinder pressure components”. *Measurement Science and Technology*, Vol. 20 n° 1, 2009. (cited in pp. 33, 39, 65, 66, and 159)
- Payri F., Broatch A., Tormos B. and Marant V.** “New methodology for in-cylinder pressure analysis in direct injection diesel engines - Application to combustion noise”. *Measurement Science and Technology*, Vol. 16 n° 2, pp. 540–547, 2005. (cited in p. 28)
- Payri F. and Desantes J.M.** *Motores de combustión interna alternativos*. Universitat Politècnica de València, 2011. (cited in p. 3)
- Payri F., Luján J., Climent H. and Pla B.** “Effects of the intake charge distribution in HSDI engines”. *SAE Technical Papers*, 2010. (cited in p. 60)
- Payri F., Luján J. M., Guardiola C. and Pla B.** “A challenging future for the IC engine: New technologies and the control role”. *Oil and Gas Science and Technology*, Vol. 70 n° 1, pp. 15–30, 2015. (cited in p. 8)
- Payri F., Luján J. M., Guardiola C. and Rizzoni G.** “Injection diagnosis through common-rail pressure measurement”. *Proceedings of the Institution of Mechanical Engineers, Part D: Journal of Automobile Engineering*, Vol. 220 n° 3, pp. 347–357, 2006. (cited in p. 67)
- PCBPiezotronics.** “Introduction to Dynamic Pressure Sensors”. <http://www.pcb.com/>. Accessed: 2016-12-14. (cited in p. 88)
- Peng Z. and Jia M.** “An investigation and evaluation of variable-valve-timing and variable-valve-actuation strategies in a diesel homogeneous charge compression ignition engine using three-dimensional computational fluid dynamics”. *Proceedings of the Institution of Mechanical Engineers, Part D: Journal of Automobile Engineering*, Vol. 222 n° 6, pp. 1047–1064, 2008. (cited in p. 58)
- Peyton Jones J. C., Frey J. and Shayestehmanesh S.** “Stochastic Simulation and Performance Analysis of Classical Knock Control Algorithms”. *IEEE Transactions on Control Systems Technology*, Vol. PP n° 99, 2016. (cited in pp. 40 and 197)

- Peyton Jones J. C., Spelina J. M. and Frey J.** “Likelihood-based control of engine knock”. *IEEE Transactions on Control Systems Technology*, Vol. 21 n° 6, pp. 2169–2180, 2013. (cited in p. 40)
- Peyton Jones J. C., Spelina J. M. and Frey J.** “An optimal cumsum-based knock controller”. In *IFAC Proceedings Volumes (IFAC-PapersOnline)*, volume 7, pp. 372–377, 2013. (cited in p. 40)
- Peyton Jones J. C., Spelina J. M. and Frey J.** “Optimizing knock thresholds for improved knock control”. *International Journal of Engine Research*, Vol. 15 n° 1, pp. 123–132, 2014. (cited in p. 41)
- Pflueger M., Hoeldrich R., Brandl F. K. and Biermayer W.** “Subjective assessment of roughness as a basis for objective vehicle interior noise quality evaluation”. *SAE Technical Papers*, 1999. (cited in p. 39)
- Pierpont D. A., Montgomery D. T. and Reitz R. D.** “Reducing particulate and nox using multiple injections and egr in a D.I. diesel”. *SAE Technical Papers*, 1995. (cited in p. 60)
- Pipitone E.** “A comparison between combustion phase indicators for optimal spark timing”. *Journal of Engineering for Gas Turbines and Power*, Vol. 130 n° 5, 2008. (cited in p. 115)
- Pipitone E. and Beccari A.** “Determination of TDC in internal combustion engines by a newly developed thermodynamic approach”. *Applied Thermal Engineering*, Vol. 30 n° 14-15, pp. 1914–1926, 2010. (cited in pp. 28 and 30)
- Pischinger S.** “Current and Future Challenges for Automotive Catalysis: Engine Technology Trends and Their Impact”. *Topics in Catalysis*, Vol. 59 n° 10-12, pp. 834–844, 2016. (cited in pp. 8 and 10)
- Polóni T., Rohál-Ilkiv B. and Arne Johansen T.** “Mass flow estimation with model bias correction for a turbocharged Diesel engine”. *Control Engineering Practice*, Vol. 23 n° 1, pp. 22–31, 2014. (cited in p. 72)
- Pöschl M. and Sattelmayer T.** “Influence of temperature inhomogeneities on knocking combustion”. *Combustion and Flame*, Vol. 153 n° 4, pp. 562–573, 2008. (cited in p. 40)
- Potter MA.** “The Road to Math: The General Motors Approach to an Efficient Diesel Engine Technology Development”. In *Thiesel Conference*, 2012. (cited in p. 13)
- Powell J. D.** “Engine control using cylinder pressure: Past, present, and future”. *Journal of Dynamic Systems, Measurement and Control, Transactions of the ASME*, Vol. 115 n° 2 B, pp. 343–350, 1993. (cited in p. 13)
- Prucka R. G.** *An Experimental Characterization of a High Degree of Freedom Spark-Ignition Engine to Achieve Optimized Ignition Timing Control*. PhD Thesis, University of Michigan, 2008. (cited in p. 65)
- Prucka R. G., Filipi Z. S., Assanis D. N., Kramer D. M. and Ohl G. L.** “An evaluation of residual gas fraction measurement techniques in a high degree of freedom spark ignition engine”. *SAE International Journal of Engines*, Vol. 1 n° 1, pp. 71–84, 2009. (cited in p. 65)
- Przybyla G., Szlek A., Haggith D. and Sobiesiak A.** “Fuelling of spark ignition and homogenous charge compression ignition engines with low calorific value producer gas”. *Energy*, Vol. 116, pp. 1464–1478, 2016. (cited in p. 32)
- Quérel C, Grondin O and Letellier C.** “State of the Art and Analysis of Control Oriented NOx Models”. *SAE paper 2012-01-0723*, 2012. (cited in pp. 9 and 35)

- Quérel C., Grondin O. and Letellier C.** “Semi-physical mean-value NO_x model for diesel engine control”. *Control Engineering Practice*, Vol. 40, pp. 27–44, 2015. (cited in p. 36)
- Rausen D. J., Stefanopoulou A. G., Kang J., Eng J. A. and Kuo T.** “A mean-value model for control of Homogeneous Charge Compression Ignition (HCCI) engines”. *Journal of Dynamic Systems, Measurement and Control, Transactions of the ASME*, Vol. 127 n° 3, pp. 355–362, 2005. (cited in p. 34)
- Regitz S. and Collings N.** “Study of cycle-by-cycle air-to-fuel ratio determined from the exhaust gas composition and a novel fast response device based on a wide band lambda sensor”. *SAE Technical Papers*, 2008. (cited in p. 62)
- Reijnders J., Boot M. and de Goey P.** “Impact of aromaticity and cetane number on the soot-NO_x trade-off in conventional and low temperature combustion”. *Fuel*, Vol. 186, pp. 24–34, 2016. (cited in p. 10)
- Reitz R. D. and Duraisamy G.** “Review of high efficiency and clean reactivity controlled compression ignition (RCCI) combustion in internal combustion engines”. *Progress in Energy and Combustion Science*, Vol. 46, pp. 12–71, 2015. (cited in p. 12)
- Rezaei R., Dinkelacker F., Tilch B., Delebinski T. and Brauer M.** “Phenomenological modeling of combustion and NO_x emissions using detailed tabulated chemistry methods in diesel engines”. *International Journal of Engine Research*, Vol. 17 n° 8, pp. 846–856, 2016. (cited in p. 35)
- Riegel J, Neumann H and Wiedenmann H-M.** “Exhaust gas sensors for automotive emission control”. *Solid State Ionics*, Vol. 152-153, pp. 783–800, 2002. (cited in pp. 9, 35, 61, and 62)
- Rizzoni G, Guzzella L and Baumann BM.** “Unified modeling of hybrid electric vehicle drivetrains”. *IEEE/ASME Transactions on Mechatronics*, Vol. 4 n° 3, pp. 246–257, 1999. (cited in p. 5)
- Rubino L, Bonnel P, Hummel R, Krasenbrink A, Manfredi U and Santi G De.** “On-road Emissions and Fuel Economy of Light Duty Vehicles using PEMS: Chase-Testing Experiment”. *SAE Paper 2008-01-1824*, 2008. (cited in p. 6)
- Russell M. F. and Haworth R.** “Combustion noise from high speed direct injection diesel engines”. *SAE Technical Papers*, 1985. (cited in p. 33)
- Samimy B. and Rizzoni G.** “Engine knock analysis and detection using time-frequency analysis”. *SAE Technical Papers*, 1996. (cited in p. 27)
- Samimy B. and Rizzoni G.** “Mechanical Signature Analysis Using TimeFrequency Signal Processing: Application to Internal Combustion Engine Knock Detection”. *Proceedings of the IEEE*, Vol. 84 n° 9, pp. 1330–1343, 1996. (cited in p. 38)
- Santos A, McGuckin N, Nakamoto HY, Gray D and Liss S.** *Summary of travel trends: 2009 National Household Travel Survey*. US Department of Transportation. Federal Highway Administration, 2011. (cited in p. 1)
- Saracino R., Gaballo M. R., Mannal S., Motz S., Carlucci A. and Benegiamo M.** “Cylinder Pressure-Based Closed Loop Combustion Control: A Valid Support to Fulfill Current and Future Requirements of Diesel Powertrain Systems”. *SAE Technical Papers*, Vol. 2015, 2015. (cited in pp. 13 and 31)
- Saraswati S. and Chand S.** “Reconstruction of cylinder pressure for SI engine using recurrent neural network”. *Neural Computing and Applications*, Vol. 19 n° 6, pp. 935–944, 2010. (cited in p. 43)

- Sarnes B. and Schrüfer E.** “Determination of the time behaviour of thermocouples for sensor speedup and medium supervision”. *Proceedings of the Estonian Academy of Sciences: Engineering*, Vol. 13 n° 4, pp. 295–309, 2007. (cited in pp. 68, 69, and 210)
- Saxena S. and Bedoya I. D.** “Fundamental phenomena affecting low temperature combustion and HCCI engines, high load limits and strategies for extending these limits”. *Progress in Energy and Combustion Science*, Vol. 39 n° 5, pp. 457–488, 2013. (cited in p. 12)
- Schaub J., Koerfer T., Pischinger S. and Schnorbus T.** “Cylinder Pressure Based Fuel Path Control for Non-Conventional Combustion Modes”. *SAE International Journal of Engines*, Vol. 8 n° 5, 2015. (cited in p. 31)
- Schiefer D., Maennel R. and Nardoni W.** “Advantages of diesel engine control using in-cylinder pressure information for closed loop control”. *SAE Technical Papers*, 2003. (cited in p. 31)
- Schießl R. and Maas U.** “Analysis of endgas temperature fluctuations in an SI engine by laser-induced fluorescence”. *Combustion and Flame*, Vol. 133 n° 1-2, pp. 19–27, 2003. (cited in p. 40)
- Schilling A.** *Model-Based Detection and Isolation of Faults in the Air and Fuel Paths of Common-rail DI Diesel Engines Equipped with a Lambda and a Nitrogen Oxides Sensor*. PhD Thesis, ETH Zurich, 2008. (cited in pp. 62 and 69)
- Schmid U. and Seidel H.** “Study on an injection quantity sensor. I: Evaluation of the integration procedure”. *Journal of Micromechatronics*, Vol. 3 n° 1, pp. 15–32, 2005. (cited in p. 67)
- Schmid U. and Seidel H.** “Study on an injection quantity sensor. II: Evaluation of the sensing element”. *Journal of Micromechatronics*, Vol. 3 n° 1, pp. 33–50, 2005. (cited in p. 67)
- Schmitt J. and Parmentier M.** “Exhaust temperature predictor : an alternative approach to predictive control applied to diesel aftertreatment”. In *IFAC Proceedings Volumes*, volume 7, pp. 730–731, 2013. (cited in p. 205)
- Schnorbus T., Pischinger S., Körfer T., Lamping M., Tomazic D. and Tatur M.** “Diesel combustion control with closed-loop control of the injection strategy”. *SAE Technical Papers*, 2008. (cited in p. 31)
- Scholl D., Davis C., Russ S. and Barash T.** “The volume acoustic modes of spark-ignited internal combustion chambers”. *SAE Technical Papers*, 1998. (cited in pp. 38 and 120)
- Senecal P. K., Xin J. and Reitz R. D.** “Predictions of residual gas fraction in IC engines”. *SAE Technical Papers*, 1996. (cited in pp. 65, 66, and 159)
- Serrano J. R., Olmeda P., Arnau F. J., Reyes-Belmonte M. A. and Tartoussi H.** “A study on the internal convection in small turbochargers. Proposal of heat transfer convective coefficients”. *Applied Thermal Engineering*, Vol. 89, pp. 587–599, 2015. (cited in p. 208)
- Shaver G. M. and Gerdes J. C.** “Cycle-to-cycle control of HCCI engines”. In *American Society of Mechanical Engineers, Dynamic Systems and Control Division (Publication) DSC*, volume 72, pp. 403–412, 2003. (cited in p. 31)
- Sheesley R. J., Schauer J. J., Garshick E., Laden F., Smith T. J., Blicharz A. P. and Deminter J. T.** “Tracking personal exposure to particulate diesel exhaust in a diesel freight terminal using organic tracer analysis”. *Journal of Exposure Science and Environmental Epidemiology*, Vol. 19 n° 2, pp. 172–186, 2009. (cited in p. 3)

- Simon D.** *Optimal State Estimation: Kalman, H Infinity, and Nonlinear Approaches*. John Wiley & Sons, 2006. (cited in p. 71)
- Sjöberg M. and Dec J. E.** “Effects of engine speed, fueling rate, and combustion phasing on the thermal stratification required to limit HCCI knocking intensity”. *SAE Technical Papers*, 2005. (cited in p. 42)
- Smith J.A.** “Demonstration of a fast response on-board NO_x sensor for heavy-duty diesel vehicles”. Technical report, California Environmental Protection Agency, 2000. (cited in p. 63)
- Smith L. A., Fickenscher T. and Osborne R. P.** “Engine breathing - Steady speed volumetric efficiency and its validity under transient engine operation”. *SAE Technical Papers*, 1999. (cited in p. 64)
- Song X., Johnson J. H. and Naber J. D.** “A review of the literature of selective catalytic reduction catalysts integrated into diesel particulate filters”. *International Journal of Engine Research*, Vol. 16 n° 6, pp. 738–749, 2015. (cited in p. 10)
- Spelina J. M., Peyton Jones J. C. and Frey J.** “Characterization of knock intensity distributions: Part 2: Parametric models”. *Proceedings of the Institution of Mechanical Engineers, Part D: Journal of Automobile Engineering*, Vol. 227 n° 12, pp. 1650–1660, 2013. (cited in p. 40)
- Spelina J. M., Peyton Jones J. C. and Frey J.** “Characterization of knock intensity distributions: Part 1: Statistical independence and scalar measures”. *Proceedings of the Institution of Mechanical Engineers, Part D: Journal of Automobile Engineering*, Vol. 228 n° 2, pp. 117–128, 2014. (cited in pp. 40 and 197)
- Stanglmaier R. H. and Roberts C. E.** “Homogeneous charge compression ignition (HCCI): Benefits, compromises, and future engine applications”. *SAE Technical Papers*, 1999. (cited in p. 11)
- Stanković L. and Böhme J. F.** “Time-frequency analysis of multiple resonances in combustion engine signals”. *Signal Processing*, Vol. 79 n° 1, pp. 15–28, 1999. (cited in p. 38)
- Stas M. J.** “An universally applicable thermodynamic method for TDC determination”. *SAE Technical Papers*, 2000. (cited in pp. 28 and 30)
- statistics collector team 2011 ChartistBin.** “Worldwide Total Motor Vehicles (per 1,000 people)”. ChartistBin.com. Accessed: 2016-12-02. (cited in pp. 1 and 2)
- Stiller C., Puente León F. and Kruse M.** “Information fusion for automotive applications - An overview”. *Information Fusion*, Vol. 12 n° 4, pp. 244–252, 2011. (cited in p. 68)
- Stotsky A., Hedrick J. K. and Yip P. P.** “Use of sliding modes to simplify the backstepping control method”. In *Proceedings of the American Control Conference*, volume 3, pp. 1703–1708, 1997. (cited in p. 73)
- Stotsky A. and Kolmanovsky I.** “Simple unknown input estimation techniques for automotive applications”. In *Proceedings of the American Control Conference*, volume 5, pp. 3312–3317, 2001. (cited in p. 73)
- Stotsky A. and Kolmanovsky I.** “Application of input estimation techniques to charge estimation and control in automotive engines”. *Control Engineering Practice*, Vol. 10 n° 12, pp. 1371–1383, 2002. (cited in p. 73)
- Straif K., Cohen A. and Samet J.** *Air pollution and cancer: IARC scientific publication no. 161*. International Agency for Research on Cancer, 2013. (cited in p. 2)

- Strandh P., Bengtsson J., Johansson R., Tunestål P. and Johansson B.** “Cycle-to-cycle control of a dual-fuel HCCI engine”. *SAE Technical Papers*, 2004. (cited in p. 31)
- Szybist J. P., Dean Edwards K., Foster M., Confer K. and Moore W.** “Characterization of engine control authority on HCCI combustion as the high load limit is approached”. *SAE International Journal of Engines*, Vol. 6 n° 1, pp. 553–568, 2013. (cited in p. 42)
- Tagliatalata F., Cesario N. and Lavorgna M.** “Soft computing mass air flow estimator for a single-cylinder SI engine”. *SAE Technical Papers*, 2006. (cited in p. 59)
- Tagliatalata F., Lavorgna M., Mancaruso E. and Vaglieco B. M.** “Determination of combustion parameters using engine crankshaft speed”. *Mechanical Systems and Signal Processing*, Vol. 38 n° 2, pp. 628–633, 2013. (cited in p. 43)
- Tan C., Xu H., Ma H., Tian J. and Ghafourian A.** “A Study of Methodology for the Investigation of Engine Transient Performance”. *SAE Technical Papers*, Vol. 2014-October, 2014. (cited in p. 31)
- Thangaraja J. and Kannan C.** “Effect of exhaust gas recirculation on advanced diesel combustion and alternate fuels - A review”. *Applied Energy*, Vol. 180, pp. 169–184, 2016. (cited in p. 58)
- Thomasson A., Shi H., Lindell T., Eriksson L., Shen T. and Peyton Jones J. C.** “Experimental Validation of a Likelihood-Based Stochastic Knock Controller”. *IEEE Transactions on Control Systems Technology*, Vol. 24 n° 4, pp. 1407–1418, 2016. (cited in p. 40)
- Torregrosa A. J., Broatch A., Margot X., Marant V. and Beauge Y.** “Combustion chamber resonances in direct injection automotive diesel engines: A numerical approach”. *International Journal of Engine Research*, Vol. 5 n° 1, pp. 83–91, 2004. (cited in pp. 39 and 119)
- Torregrosa A. J., Broatch A., Martín J. and Monelletta L.** “Combustion noise level assessment in direct injection Diesel engines by means of in-cylinder pressure components”. *Measurement Science and Technology*, Vol. 18 n° 7, pp. 2131–2142, 2007. (cited in pp. 33, 34, and 39)
- Tschanz F., Amstutz A., Onder C. H. and Guzzella L.** “A real-time soot model for emission control of a diesel engine”. In *IFAC Proceedings Volumes (IFAC-PapersOnline)*, pp. 222–227, 2010. (cited in p. 35)
- Tschanz F., Amstutz A., Onder C. H. and Guzzella L.** “Feedback control of particulate matter and nitrogen oxide emissions in diesel engines”. *Control Engineering Practice*, Vol. 21 n° 12, pp. 1809–1820, 2013. (cited in p. 35)
- Tsugawa S.** “An overview on an automated truck platoon within the energy ITS project”. *IFAC Proceedings Volumes (IFAC-PapersOnline)*, Vol. 7, pp. 41–46, 2013. (cited in p. 13)
- Tunestål P.** “Self-tuning gross heat release computation for internal combustion engines”. *Control Engineering Practice*, Vol. 17 n° 4, pp. 518–524, 2009. (cited in p. 29)
- Turin R. C., Zhang R. and Chang M.** “Volumetric efficiency model for variable cam-phasing and variable valve lift applications”. *SAE Technical Papers*, 2008. (cited in p. 64)
- Urry J.** *Sociology beyond societies: Mobilities for the twenty first century*. Routledge, 2000. (cited in p. 1)
- Vanzuilen D., Mouaici G., Bernard F. and McKenzie I.** “Fuel sensor”. *US patent 7170303*, 2007. (cited in p. 13)
- Varnier O.** *Trends and limits of two-stage boosting systems for automotive diesel engines*. Universitat Politècnica de València. Departamento de Máquinas y Motores Térmicos, 2012. (cited in p. 8)

- Vashishtha A., Rathinam B., Delahaye L., Ravet F. and Justet F.** “Study of intake ports design for Ultra Low Cost (ULC) Gasoline Engine using STAR-CD”. *SAE Technical Papers*, 2012. (cited in p. 93)
- VDO Siemens.** “Integrated mass airflow sensor (SIMAF)”. Technical report, Siemens VDO, 2005. (cited in pp. 59 and 69)
- Vitale G, Siebenbrunner P, Hülser H, Bachler J and Pfahl U.** “OBD Algorithms: Model-based Development and Calibration”. *SAE Paper 2007-01-4222*, 2007. (cited in p. 13)
- Von Berg J., Ziermann R., Reichert W., Obermeier E., Eickhoff M., Krötz G., Thoma U., Boltshausen Th, Cavalloni C. and Nendza J. P.** “High temperature piezoresistive B-SiC-on-SOI pressure sensor for combustion engines”. *Materials Science Forum*, Vol. 264-268 n° PART 2, pp. 1101–1104, 1998. (cited in pp. 13 and 88)
- Walker AP.** “Controlling particulate emissions from diesel vehicles”. *Topics in Catalysis*, Vol. 28, pp. 165–170, 2004. (cited in p. 12)
- Wan E. A. and Van Der Merwe R.** “The unscented Kalman filter for nonlinear estimation”. In *IEEE 2000 Adaptive Systems for Signal Processing, Communications, and Control Symposium, AS-SPCC 2000*, pp. 153–158, 2000. (cited in p. 72)
- Wang D. Y.** “Real-time dynamics of amperometric exhaust oxygen sensors”. *Sensors and Actuators, B: Chemical*, Vol. 126 n° 2, pp. 551–556, 2007. (cited in p. 68)
- Wang J., Zhang Y., Xiong Q. and Ding X.** “Data acquisition of cylinder combustion pressure oriented to diesel engine control”. In *2009 IEEE Circuits and Systems International Conference on Testing and Diagnosis, ICTD09*, 2009. (cited in p. 88)
- Wang S., Prucka R., Prucka M. and Dourra H.** “Control-oriented residual gas mass prediction for spark ignition engines”. *International Journal of Engine Research*, Vol. 16 n° 7, pp. 897–907, 2015. (cited in p. 67)
- Wang X.** “Parameter determination of dynamic sensor model with particle swarm optimization technique”. In *2009 International Conference on Measuring Technology and Mechatronics Automation, ICMTMA 2009*, volume 1, pp. 43–46, 2009. (cited in p. 59)
- Wang Z., Zhu Q. and Prucka R.** “A Review of Spark-Ignition Engine Air Charge Estimation Methods”. *SAE Technical Papers*, Vol. 2016-April n° April, 2016. (cited in p. 64)
- Wattanapanichaporn O., Jantaradac W., Wannatong K. and T. Aroonsrisopon.** “Cylinder-to-Cylinder Variations in Diesel Dual Fuel Combustion under Low-load Conditions”. *Journal of Research and Applications in Mechanical Engineering*, Vol. 1 n° 4, 2012. (cited in p. 58)
- Weerasinghea W.M.S.R., Stobarta R.K. and Hounshama S.M.** “Thermal efficiency improvement in high output diesel engines a comparison of a Rankine cycle with turbo-compounding”. *Applied Thermal Engineering*, Vol. 30, pp. 2253–2256, 2010. (cited in p. 9)
- Westlund A.** *Simplified models for emission formation in diesel engines during transient operation*. PhD Thesis, Kungliga Tekniska Högskolan (KTH), 1998. (cited in p. 35)
- Westlund A., Lindström M. and Ångström H.** “A one-dimensional model for heat release rate and emission formation in diesel engines based on correlations for entrainment rate, lift-off length and ignition delay: Validation for transient conditions”. *Proceedings of the Institution of Mechanical Engineers, Part D: Journal of Automobile Engineering*, Vol. 226 n° 9, pp. 1243–1258, 2012. (cited in p. 35)

- Wheeler Jennifer, Polovina Dusan, Frasinél Vasile, Miersch-Wiemers Oliver, Mond Alan, Sterniak Jeff and Yilmaz Hakan.** “Design of a 4-cylinder GTDI engine with part-load HCCI capability”. *SAE International Journal of Engines*, Vol. 6 n° 2013-01-0287, pp. 184–196, 2013. (cited in p. 192)
- Willems F, Cloudt R, van den Eijnden E and et al. M van Genderen.** “Is Closed-Loop SCR Control Required to Meet Future Emission Targets?”. *SAE paper 2007-01-1574*, 2007. (cited in pp. 9 and 35)
- Win Z., Gakkhar R. P., Jain S. C. and Bhattacharya M.** “Investigation of diesel engine operating and injection system parameters for low noise, emissions, and fuel consumption using Taguchi methods”. *Proceedings of the Institution of Mechanical Engineers, Part D: Journal of Automobile Engineering*, Vol. 219 n° 10, pp. 1237–1251, 2005. (cited in p. 32)
- Witwit A.R., Yasinb A., Abasc M.A. and Gitanod H.** “Modern Methods in Engine Knock Signal Detection”. *Procedia Technology (ICEEI 2013)*, Vol. 11, pp. 40–50, 2013. (cited in p. 41)
- Worm J.** “An evaluation of several methods for calculating transient trapped air mass with emphasis on the delta P approach”. *SAE Technical Papers*, 2005. (cited in p. 65)
- Worret R., Bernhardt S., Schwarz F. and Spicher U.** “Application of different cylinder pressure based knock detection methods in spark ignition engines”. *SAE Technical Papers*, 2002. (cited in p. 40)
- Woschni G.** “A universally applicable equation for the instantaneous heat transfer coefficient in the internal combustion engine”. *SAE Technical Papers*, 1967. (cited in p. 29)
- Wu B., Filipi Z., Assanis D., Kramer D. M., Ohl G. L., Prucka M. J. and Divalentin E.** “Using artificial neural networks for representing the air flow rate through a 2.4 liter VVT engine”. *SAE Technical Papers*, 2004. (cited in p. 64)
- Xiaofeng G., Stone R., Hudson C. and Bradbury I.** “The detection and quantification of knock in spark ignition engines”. *SAE Technical Papers*, 1993. (cited in p. 42)
- Xie H, Stobart R, Tunestal P, Eriksson L, and Leteinturier Y Huangand P.** “Future Engine Control Enabling Environment Friendly Vehicle”. *SAE paper 2011-01-0697*, 2011. (cited in p. 13)
- Xu K., Zhang J., Wang X., Teng Q., Tan J. and Zhang Y.** “Improvements of nonlinear dynamic modeling of hot-film MAF sensor”. *Sensors and Actuators, A: Physical*, Vol. 147 n° 1, pp. 34–40, 2008. (cited in p. 59)
- Yang L., Franco V., Mock P., Kolke R., Zhang S., Wu Y. and German J.** “Experimental Assessment of NOx Emissions from 73 Euro 6 Diesel Passenger Cars”. *Environmental Science and Technology*, Vol. 49 n° 24, pp. 14409–14415, 2015. (cited in pp. 6 and 7)
- Yang Z., Winward E. and Stobart R. K.** “Improve Cylinder-to-Cylinder Consistency and Reduce Cycle-to-Cycle Variations of a Diesel Engine Using Closed-loop Control of Fuel Path Input Variables”. *IFAC-PapersOnLine*, Vol. 49 n° 11, pp. 239–244, 2016. (cited in p. 58)
- Yao M., Zhang Q., Liu H., Zheng Z. ., Zhang P., Lin Z., Lin T. and Shen J.** “Diesel engine combustion control: Medium or heavy EGR?”. *SAE Technical Papers*, 2010. (cited in p. 58)
- Yar A. and Bhatti A. I.** “Control of Air-to-Fuel ratio of spark ignited engine using super twisting algorithm”. In *Proceedings - 2012 International Conference on Emerging Technologies, ICET 2012*, pp. 71–75, 2012. (cited in p. 58)

- Yates A. D. B., Swarts A. and Viljoen C. L.** “Correlating auto-ignition delays and knock-limited spark-advance data for different types of fuel”. *SAE Technical Papers*, 2005. (cited in p. 35)
- Yoon P, Park S, Sunwoo M, Ohm I and Yoon KJ.** “Closed-loop Control of Spark Advance and Air-fuel Ratio in SI Engines using Cylinder Pressure”. *SAE Paper 2000-01-0933*, 2000. (cited in pp. 13 and 31)
- You-cheng S., Min X., Yong G., Yi C., Lei S. and Kang-yao D.** “Effects of injection pressure, exhaust gas recirculation and intake pressure on the cycle-to-cycle variations of HCCI combustion”. *Journal of the Energy Institute*, Vol. 89 n° 2, pp. 293–301, 2016. (cited in p. 58)
- Yu Robert C and Shahed Syed M.** “Effects of injection timing and exhaust gas recirculation on emissions from a DI diesel engine”. *SAE Preprints*, Vol. 811234, 1981. (cited in p. 60)
- Yun H., Wermuth N. and Najt P.** “Extending the high load operating limit of a naturally-aspirated gasoline HCCI combustion engine”. *SAE Technical Papers*, pp. 681–699, 2010. (cited in p. 42)
- Yun H. J. and Mirsky W.** “Schlieren-streak measurements of instantaneous exhaust gas velocities from a spark-ignition engine”. *SAE Technical Papers*, 1974. (cited in pp. 66 and 193)
- Zechnall R., Baumann G. and Eisele H.** “Closed-loop exhaust emission control system with electronic fuel injection”. *SAE Technical Papers*, 1973. (cited in p. 62)
- Zehni A., Khoshbakhti Saray R. and Poorghasemi K.** “Numerical comparison of PCCI combustion and emission of diesel and biodiesel fuels at low load conditions using 3D-CFD models coupled with chemical kinetics”. *Applied Thermal Engineering*, Vol. 110, pp. 1483–1499, 2017. (cited in p. 11)
- Zeldovich Y.B.** “The oxidation of nitrogen on combustion and explosions”. *Acta Physicochim URSS*, 1946. (cited in pp. 36 and 37)
- Zhan R, Huang Y and Khair M.** “Methodologies to Control DPF Uncontrolled Regenerations”. *SAE paper 2006-01-1090*, 2006. (cited in p. 10)
- Zhao J. and Wang J.** “Engine mass airflow sensor fault detection via an adaptive oxygen fraction observer”. In *2014 American Control Conference*, pp. 1517–1522. IEEE, 2014. (cited in p. 59)
- Zhao J. and Wang J.** “Adaptive observer for joint estimation of oxygen fractions and blend level in biodiesel fueled engines”. *IEEE Transactions on Control Systems Technology*, Vol. 23 n° 1, pp. 80–90, 2015. (cited in pp. 65, 70, 71, and 205)
- Zhao Y., Atlas L. E. and Marks R. J.** “Use of cone-shaped kernels for generalized time-frequency representations of nonstationary signals”. *IEEE Transactions on Acoustics, Speech, and Signal Processing*, Vol. 38 n° 7, pp. 1084–1091, 1990. (cited in p. 109)
- Zhao Y., Shen T. and Jiao X.** “Air-fuel ratio transient control design for gasoline engines based on individual cylinder air charge estimation”. *SAE Technical Papers*, Vol. 1, 2013. (cited in p. 58)
- Zhen X., Wang Y., Xu S., Zhu Y., Tao C., Xu T. and Song M.** “The engine knock analysis - An overview”. *Applied Energy*, Vol. 92, pp. 628–636, 2012. (cited in pp. 11, 40, and 41)

- Zheng Ming, Reader Graham T and Hawley J Gary.** “Diesel engine exhaust gas recirculation—a review on advanced and novel concepts”. *Energy conversion and management*, Vol. 45 n° 6, pp. 883–900, 2004. (cited in p. 58)
- Zhu H., Bohac S. V., Nakashima K., Hagen L. M., Huang Z. and Assanis D. N.** “Effect of fuel oxygen on the trade-offs between soot, NO_x and combustion efficiency in premixed low-temperature diesel engine combustion”. *Fuel*, Vol. 112, pp. 459–465, 2013. (cited in p. 58)
- Zhuiykov S.** *Electrochemistry of Zirconia gas sensors*. Taylor & Francis, 2010. (cited in p. 68)
- Zhuiykov S. and Miura N.** “Development of zirconia-based potentiometric NO_x sensors for automotive and energy industries in the early 21st century: What are the prospects for sensors?”. *Sensors and Actuators, B: Chemical*, Vol. 121 n° 2, pp. 639–651, 2007. (cited in p. 63)
- Zienkiewicz O. C., Taylor R. L. and Zhu J. Z.** *The Finite Element Method: its basis and fundamentals*. Oxford: Elsevier Butterworth-Heinemann, 2005. (cited in p. 120)
- Ziesmer D. A., Chuey M. D. and Hazelton L.** “Frequency domain characterization of mass airflow sensors”. *SAE Technical Papers*, 1993. (cited in p. 59)
- Zweiri Y. H. and Seneviratne L. D.** “Diesel engine indicated and load torque estimation using a non-linear observer”. *Proceedings of the Institution of Mechanical Engineers, Part D: Journal of Automobile Engineering*, Vol. 220 n° 6, pp. 775–785, 2006. (cited in p. 43)